

# Lawrence Berkeley National Laboratory

## Recent Work

### Title

BONDING AND SPECTRA OF METAL CHELATES: ULTRAVIOLET, VISIBLE, INFRARED, AND ELECTRON RESONANCE ABSORPTION NEAR-INFRARED SPECTRA OF ALCOHOLS

### Permalink

<https://escholarship.org/uc/item/5xc8j1bq>

### Author

Belford, R. Linn.

### Publication Date

1955-06-01

UNIVERSITY OF  
CALIFORNIA

*Radiation  
Laboratory*

BERKELEY, CALIFORNIA

## **DISCLAIMER**

This document was prepared as an account of work sponsored by the United States Government. While this document is believed to contain correct information, neither the United States Government nor any agency thereof, nor the Regents of the University of California, nor any of their employees, makes any warranty, express or implied, or assumes any legal responsibility for the accuracy, completeness, or usefulness of any information, apparatus, product, or process disclosed, or represents that its use would not infringe privately owned rights. Reference herein to any specific commercial product, process, or service by its trade name, trademark, manufacturer, or otherwise, does not necessarily constitute or imply its endorsement, recommendation, or favoring by the United States Government or any agency thereof, or the Regents of the University of California. The views and opinions of authors expressed herein do not necessarily state or reflect those of the United States Government or any agency thereof or the Regents of the University of California.

UNIVERSITY OF CALIFORNIA

Radiation Laboratory  
Berkeley, California

Contract No. W-7405-eng-48

BONDING AND SPECTRA OF METAL CHELATES:  
Ultraviolet, Visible, Infrared, and Electron Resonance Absorption  
NEAR-INFRARED SPECTRA OF ALCOHOLS

R. Linn Belford  
(Thesis)

June 1955

CONTENTS

ABSTRACT . . . . .	4
<b>I. EFFECT OF FLUORINE SUBSTITUTION UPON SPECTRA OF Cu(II) CHELATES</b>	
Introduction . . . . .	6
Experimental . . . . .	8
Results . . . . .	13
Discussion . . . . .	13
Preparations . . . . .	13
Ultraviolet and Visible Spectra . . . . .	28
Infrared Spectra . . . . .	33
<b>II. BONDING IN Cu(II) CHELATES: SOLVENT EFFECTS IN THEIR VISIBLE ABSORPTION SPECTRA</b>	
Introduction . . . . .	38
Experimental . . . . .	43
Results and Discussion . . . . .	44
Analysis of Spectra . . . . .	44
Identification of Transitions . . . . .	55
Crystal Field Results . . . . .	58
Allowance for Covalency . . . . .	61
Other Remarks Concerning the Data . . . . .	64
Summary . . . . .	67
<b>III. DEVELOPMENT OF THEORETICAL TREATMENTS FOR COPPER CHELATE COMPOUNDS</b>	
A. LCAO-MO Cu <sup>++</sup> Scheme . . . . .	68
B. LCAO-MO Treatment of the Ligand Pi-System. . . . .	84
1. General Method of Calculation . . . . .	84
2. Trial RE Calculations . . . . .	85
3. Electron Distribution for Acetylacetonate. . . . .	87
4. Predicting a Spectral Shift . . . . .	90
5. Restriction upon Use of Our MO Parameters . . . . .	91
C. Crystal Field Splitting . . . . .	93
1. Number and Degeneracy of Levels . . . . .	93
2. Derivation of Energy Level Formulae . . . . .	96

3.	a. Square Bonding . . . . .	99
	b. Axial Bonding . . . . .	101
	c. Specific Models. . . . .	103
	d. Overlapping Ligand and $\text{Cu}^{++}$ Charge . . . . .	122
D.	Bonding Information from Paramagnetic Resonance. . . . .	123
IV. ELECTRON-SPIN RESONANCE IN TRANSITION METAL CHELATES		
	Introduction . . . . .	131
	Experimental. . . . .	131
	Results. . . . .	133
	Discussion. . . . .	136
V. METAL-METAL BONDING: NICKEL (II) BISDIMETHYL-GLYOXIME		
	Introduction . . . . .	149
	Experimental. . . . .	149
	Discussion. . . . .	157
VI. NEAR-INFRARED SPECTRA OF ALCOHOLS		
	Purification . . . . .	160
	Instrumental Conditions . . . . .	161
	Results and Discussion . . . . .	163
ACKNOWLEDGMENT . . . . .		189
REFERENCES . . . . .		190

BONDING AND SPECTRA OF METAL CHELATES:  
Ultraviolet, Visible, Infrared, and Electron Resonance Absorption  
NEAR-INFRARED SPECTRA OF ALCOHOLS

R. Linn Belford

Radiation Laboratory and Department of Chemistry  
University of California, Berkeley, California

June 1955

ABSTRACT

Optical spectra of six  $\beta$ -diketones and their cupric chelates are presented and discussed in relation to the structures of the molecules. Infrared assignments are made. The 300  $\mu$  bands of the metal chelates are shown to be shifted enolate ion absorptions. The order of magnitude and direction of the shifts are predicted correctly by a simple molecular orbital and electrostatic calculation. Visible spectra are correlated with the nature of the chelating agent. Preparations of most substances studied are described, as are some problems arising from attempted preparation of others.

Absorption spectra, in the visible red and near infrared, are reported for solutions of bis-acetylacetonate-Cu(II) and its 3-ethyl variant in various media. The spectra could arise from a set of three Gaussian components whose positions and intensities are shown to depend primarily upon solvent basicity. These component bands are identified with three  $3d^1-3d^1$  transitions predicted from crystal field and molecular orbital theories. The behavior of these bands upon alteration of solvent and of chelate ring substituents appears consistent with the postulate that pi-bonding changes are energetically of less importance than changes in crystal field splitting and in sigma-bonding.

An exploratory study of electron spin resonance in solutions of transition metal chelates in organic solvents has yielded promise of future application of the resonance technique to chemical problems.

A visible absorption band unique to the solid state of nickel dimethylglyoxime is reported. Attempts to find other nickel chelates

displaying the same feature failed. A search for electrical semiconductivity or photoconductivity in the nickel dimethylglyoxime crystals was unsuccessful.

During a program of testing the instrument used to obtain the visible-region spectra mentioned above, near-infrared spectra of a number of specially purified alcohols were observed. They showed the first three harmonics of the hydroxyl stretch frequency. The extreme sensitivity of these bands to hydrogen bonding permits one to distinguish between primary, secondary, and tertiary alcohols because of their different degrees of steric hindrance to such bonding. The near-infrared range seems promising as a "fingerprint" analysis region.



BONDING AND SPECTRA OF METAL CHELATES:  
Ultraviolet, Visible, Infrared, and Electron Resonance Absorption  
NEAR-INFRARED SPECTRA OF ALCOHOLS

R. Linn Belford

Radiation Laboratory and Department of Chemistry  
University of California, Berkeley, California

June 1955

I. EFFECT OF FLUORINE SUBSTITUTION  
UPON SPECTRA OF CUPRIC CHELATE COMPOUNDS

Introduction

The work presented in this part is the first unit of a series of studies designed to investigate the properties, particularly spectra, of metal chelates of fluorinated ligands. The logical starting point for the investigation was the preparation and spectral study of the simplest and best-known chelates together with similar examination of the same chelates differing only by substitution of fluorine for hydrogen. Accordingly, the copper (II) chelates of bidentate ligands seemed appropriate substances. The ligands selected for this study are represented by Formula I, and the corresponding metal chelate compounds by Formula II. The names and structures of the metal chelate compounds prepared are given in Table I by defining the substituent groups R and R' in each case.

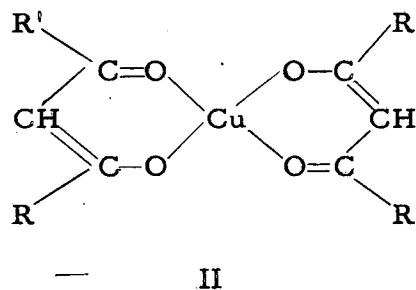
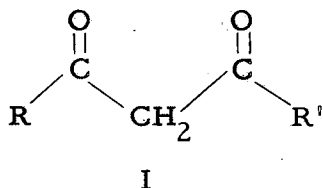


Table I

Bidentate Ligands and Cu(II) Chelates				
Name of Ligand	Formula <sup>a</sup>		References <sup>b</sup>	
	R	R'	Ligand	Cu(II) Chelate
Acetylacetone	CH <sub>3</sub>	CH <sub>3</sub>	--	4, 5, 6
Trifluoroacetylacetone	CF <sub>3</sub>	CH <sub>3</sub>	7, 8	8, 9, 10
Hexafluoroacetylacetone	CF <sub>3</sub>	CF <sub>3</sub>	10	10
Ethylacetoacetate	CH <sub>3</sub>	OC <sub>2</sub> H <sub>5</sub>	12	9, 12
Ethyl trifluoroacetoacetate	CF <sub>3</sub>	OC <sub>2</sub> H <sub>5</sub>	--	9, 10
Acetoacetic acid diethylamide	CH <sub>3</sub>	N(C <sub>2</sub> H <sub>5</sub> ) <sub>2</sub>	11	11

(a) R and R' refer to the corresponding groups in Formulas I and II.  
(b) Reference numbers refer to Bibliography.

Although bisacetylacetonone-Cu(II) was first studied early in the development of coordination chemistry,<sup>4, 5, 6</sup> the fluoro derivatives of acetylacetonone and similar ligands have not been available until recently, and relatively little has been done with the corresponding metal chelates. Trifluoroacetylacetonone has been studied by a number of investigators.<sup>7, 8</sup> Although the stability of bis-(trifluoroacetylacetonone)-Cu(II) was reported in 1945,<sup>9</sup> the first reports of the preparation of the compound appeared somewhat later.<sup>7, 8</sup> Some reactions of hexafluoroacetylacetonone have been studied by Haszeldine et al.<sup>10</sup>

Of the remaining substances listed in Table I, the diethylamide of acetoacetic acid and its copper (II) chelate have been investigated by Utzinger.<sup>11</sup> Also, the stability of the copper chelate of ethylacetoacetate has been reported by Calvin and Wilson,<sup>9</sup> and an absorption maximum in the ultraviolet has been reported by Morton and Rasney.<sup>12</sup>

#### Experimental

Bis(trifluoroacetylacetonone)-Cu(II). To 10.0 g (0.050 mole) of cupric acetate monohydrate dissolved in 150 ml of warm water was added a solution of 15.4 g (0.010 mole) of trifluoroacetylacetonone in 25 ml of ethanol. The reaction mixture was warmed and stirred, 1.2 g of anhydrous sodium carbonate was added, and the heating was continued for 15 minutes more. The blue precipitate which had first appeared when the solutions were mixed was filtered off and recrystallized from 50% aqueous ethanol. The hot solution was green, but turned greenish-blue on cooling, and a robin's-egg-blue alcoholate crystallized out. The product was filtered and air-dried, whereupon it became blue-lavender in appearance. The final yield was 17.1 g, or 92% of the theoretical amount. The compound was found to be soluble in cold chloroform, toluene, and benzene to give blue solutions, and is very soluble in hot chloroform, toluene, and benzene to give green solutions. It is not readily recovered from these solutions by cooling, but it may be recrystallized easily by cooling a hot carbon tetrachloride solution. It sublimes readily; a relatively large sample was obtained in one hour at 100° and 0.1 mm pressure. An attempt to determine the melting

point resulted in slow sublimation above  $140^{\circ}$  C. The melting point obtained is  $189^{\circ}$ , in agreement with that reported by Reid and Calvin<sup>8</sup> and by Park et al.<sup>2</sup>

Anal. Calcd. for  $C_{10}H_8O_4F_6Cu$ : C, 32.5; H, 2.2. Found: C, 32.3; H, 2.5.

Hexafluoroacetylacetone. A 50.0-g sample (approximately 0.20 mole) of hexafluoroacetylacetone dihydrate, obtained from the Caribou Chemical Company, was shaken with approximately three times its volume of 98% sulfuric acid until the material was completely dispersed. The heat evolved during the initial stages of dehydration was removed by immersion of the flask in cold water for a short time. After the mixture had been allowed to stand overnight, the anhydrous hexafluoroacetylacetone was seen to separate as a colorless liquid over the sulfuric acid, which was deeply colored by decomposed organic material. Dehydration of the product was repeated with a fresh batch of sulfuric acid. The final product was siphoned off and distilled. It was found that about 98% of the liquid distilled between  $70.0$  and  $70.2^{\circ}$  C. Qualitative observation indicated that the liquid has a low viscosity, low surface tension, and high vapor pressure, and that it hydrates rapidly when exposed to the atmosphere. Its density, measured by weighing the liquid delivered from a 0.02-ml micro-pipette, was found to be 1.46 g/ml.

Anal. Calcd. for  $C_5H_2O_2F_6$ : C, 28.82; H, 0.97. Found: C, 28.81, H, 1.13.

Acidic Hydrogen: Calcd. mol. wt = 208. Found: 205.

Bis(hexafluoroacetylacetonato)-Cu II.

Method I. To 10.0 g (0.05 mole) of cupric acetate dissolved in 150 ml of water, 25 g (0.1 mole) of hexafluoroacetylacetone dihydrate was added with stirring. The solution turned green, and pale green crystals gradually appeared. Upon the slow addition of 25 ml of 4.0-molar sodium hydroxide, the solution deepened in color and the amount of crystalline precipitate increased. After the reaction mixture was heated on a steam bath for an hour, it was cooled and the product was

filtered off. When it was recrystallized from 50% aqueous ethanol, a greenish-yellow solvate consisting of long, flat, radiating needles was obtained. On standing in air, the solvate decomposed and the needles crumbled, forming a green finely divided solid. The product weighed 14.0 g, or 55% of the theoretical amount, calculated as the dihydrate. It was found to be insoluble in water, but soluble in ethanol, dioxane, and organic solvents containing polar groups. It sublimed readily onto a cold finger in a drying pistol heated by boiling chloroform; a moderate-sized sample was collected in five hours. Its melting point was found to be 135°.

Anal. Calcd. for  $C_{10}H_2O_4F_{12}Cu \cdot 2H_2O$ : C, 23.4; H, 1.17. Found: C, 23.16; H, 1.16.

Method II. A 2.0-g sample of cupric acetate monohydrate was dissolved in 10 ml of anhydrous hexafluoroacetylacetone by boiling for five minutes. The excess reagent was evaporated off, and the residue was recrystallized from carbon tetrachloride. The resulting grass-green crystalline product weighed 4.5 g, or 80% of the theoretical amount.

Bisethylacetoacetato-Cu(II). To 10 g (0.05 mole) of cupric acetate dissolved in 100 ml of hot 50% aqueous ethanol was added 13 g (0.1 mole) of ethyl acetoacetate dissolved in 25 ml of ethanol. The mixture was heated on a steam bath until most of the alcohol had been expelled, then was cooled. The green-blue powder obtained upon filtration and air-drying was likely a hydrate. It was recrystallized twice successively from hot ligroin-chloroform mixture, the first time yielding a bluish powder, the second, large green plates. They melt at 193° C, with decomposition.

Anal. Calcd. for  $C_{12}H_{18}O_6Cu$ : C, 44.8; H, 5.64; Cu, 19.8. Found: C, 44.94; H, 5.78; Cu, 19.9.

Bis(ethyltrifluoroacetoacetato)-Cu(II). To a solution of 2.0 g (0.010 mole) copper (II) acetate monohydrate in 100 ml of dioxane was added 3.68 g (0.02 mole) of ethyltrifluoroacetoacetate. The blue color of the copper acetate quickly changed to deep green. The reaction mixture

was warmed for 15 minutes with 1.0 g of potassium carbonate, the excess base was filtered off, and the solution was diluted with an equal volume of water. After the light-green crystalline product that separated was filtered, washed, and air-dried, it was found to weigh 3.7 g, which corresponds to 86% of the theoretical yield. This product was recrystallized from 150 ml of carbon tetrachloride; it was obtained in the form of deep green crystals. It was found to be very soluble in acetone, chloroform, and dioxane, but insoluble in ligroin and water. Its melting point was 188°.

Anal. Calcd. for  $C_{12}H_{12}O_6F_6Cu$ : C, 33.5; H, 2.8; Cu, 14.8.  
Found: C, 31.2; H, 2.9; Cu, 15.0.

Reaction of diethylamine with ethyl trifluoroacetoacetate. To 50 ml of anhydrous diethylamine was added dropwise, with stirring, 15 g (0.08 mole) of ethyl trifluoroacetoacetate. To the reaction mixture was added 100 ml i-octane, and the solution was reduced to 20% of its original volume by low-pressure distillation. Upon cooling to 0° C, it yielded 12g of white crystals. They were washed with ice-cold i-pentane, recrystallized from i-octane, and dried in vacuo. The product is soluble in all organic solvents tried--from saturated hydrocarbons to ketones and alcohols--at room temperature. M. p. 82° C.

Anal. Calcd. for  $C_8H_{12}NO_2F_3$  (N,N-diethyl trifluoroacetoacetamide): C, 45.5; H, 5.69; N, 6.64. Calcd. for  $C_{10}H_{16}NO_2F_3$  ( $\beta$ -diethylamino ethyl trifluorocrotonate): C, 50.0; H, 6.76; N, 5.84. Found: C, 51.7; H, 6.97; N, 5.55.

Basic groups: Calcd. for  $CF_3C[N(C_2H_5)_2]CHCO_2C_2H_5$ : 1 basic amino group per 239 g. Found: 1 basic group per 238 g.

Reaction of  $\beta$ -diethylamino ethyltrifluorocrotonate with Cu(II). To 21.1 g (0.10 mole) of the above product dissolved in 100 ml of warm absolute ethanol was added 10.0 g (0.05 mole) of cupric acetate monohydrate. The metal salt gradually dissolved when the reaction mixture was boiled for 10 minutes, and a deep green solution was formed. After the solution had been cooled and diluted with an equal volume of water, a deep green crystalline precipitate was isolated. The weight of product obtained

was 21 g or 86% of the theoretical yield based on the expected copper (II) chelate. The product was recrystallized from a small amount of chloroform by adding n-heptane. After further recrystallization from carbon tetrachloride, it was obtained in the form of deep greenish-blue crystals, very soluble in chloroform, acetone and alcohols, sparingly soluble in carbon tetrachloride and in ligroin, and nearly insoluble in cold n-heptane.

Anal. Found: N, 0.0; Cu, 15.1.

Titrations. All titration curves were measured with a glass electrode in conjunction with a Beckman pH meter. Frequent checks were made against standard buffer solutions.

Hexafluoroacetylacetone was pipetted and the weight was calculated from the measured density (1.46 g/ml). It was titrated with 0.100 N NaOH.

One sample of  $\beta$ -diethylamino ethyl trifluorocrotonate was titrated with 0.385 N HCl. The resulting solution, at pH 1.9, was allowed to stand on a steam bath for 2 hours. A titration with 0.83 N KOH showed that no reaction had occurred in the hot acidic solution.

Absorption spectra. The infrared absorption spectra were measured with a Model 21 Perkin-Elmer Recording Double-Beam Spectrophotometer with NaCl optics. The liquid ligands were measured as thin films while the solid ligands, hexafluoroacetylacetone dihydrate and  $\beta$ -diethylamino ethyl trifluorocrotonate, as well as all the metal chelate compounds, were measured in the form of nujol mulls. Frequencies are estimated accurate to  $10 \text{ cm}^{-1}$ .

Some of the absorption spectra in the visible and ultraviolet were measured with a Cary Model 11 recording spectrophotometer; the others in the near infrared, visible, and ultraviolet were measured with a prototype of the Beckman DK recording spectrophotometer at fast speed in the ultraviolet and at medium speed in the visible and infrared. Quartz cells of 1 cm thickness were employed. The solutions were first made up by weight to 0.01 M, and these solutions were then successively diluted by syringe-type pipettes until absorption of the sample could be accurately measured. With few exceptions, the spectroscopic solvent employed was Eastman Kodak No. S337 spectro grade

chloroform. Sodium-dried B&A reagent-grade ether, distilled water, Phillips spectro grade cyclohexane, and absolute methanol were used in the special cases.

### Results

Figure 1 shows the ultraviolet absorption spectra of  $\beta$ -diethylamino ethyl trifluorocrotonate in a variety of solvents. The ultraviolet absorption spectra of the ligands are given in Figs. 2 and 3, and the corresponding spectra of the copper (II) chelate compounds are given in Figs. 3 and 4. Figures 5 and 6 illustrate the visible absorption spectra of the six copper (II) chelate compounds reported in this investigation. In each case molar extinction coefficient, based on the presumed formula weight, is plotted vs. wave length in  $\mu$ . The wave lengths of the maxima of the absorption bands found in the visible and ultraviolet regions of the spectrum are listed in Table II, along with the corresponding approximate molar extinction coefficients. In certain cases the irregular shape of a shoulder on the absorption band indicated probable additional bands adjacent to and partly obscured by the primary band. Such subsidiary bands are indicated in parentheses in Table II, if it was possible to estimate approximate frequencies.

The infrared absorption frequencies are listed in Table IIIa for the ligands, and in Table IIIb for the corresponding metal chelate compounds. Here, also, frequencies of very weak or doubtful bands are enclosed in parentheses.

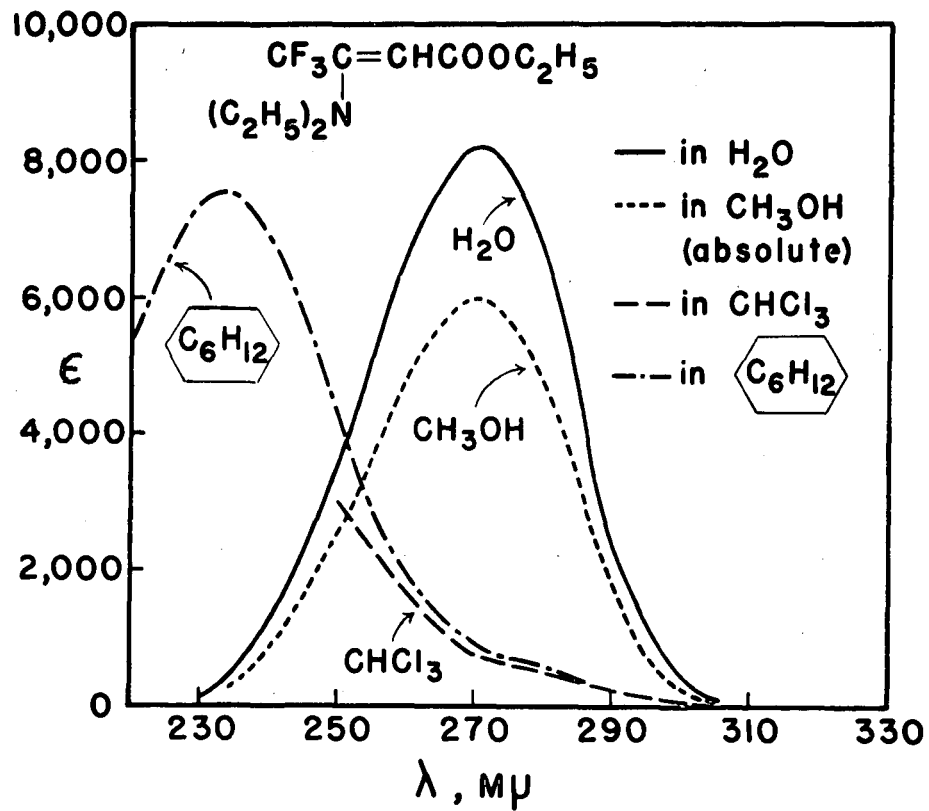
Titration curves are given in Figs. 7 and 8. From Figs. 7 and 8 we estimate the  $pK_A$  for hexafluoroacetylacetone to be about 4.6; for ethyl trifluorocrotonate  $\beta$ -diethylammonium ion, about 8.1.

### Discussion

#### Preparation of Ligands and Cu(II) Chelate Compounds.

All the ligands excepting N, N-diethylacetoacetamide and  $\beta$ -diethylamino ethyl trifluorocrotonate were available from commercial sources. The former compound, and its Cu(II) chelate, were kindly donated by Dr. G. E. Utzinger.<sup>11</sup> The product obtained from the reaction





MU-9269

Fig. 1. Ultraviolet spectra of  $\beta$ -diethylamino ethyl trifluorocrotonate,  $10^{-4}$  M in water, methanol, chloroform and cyclohexane.

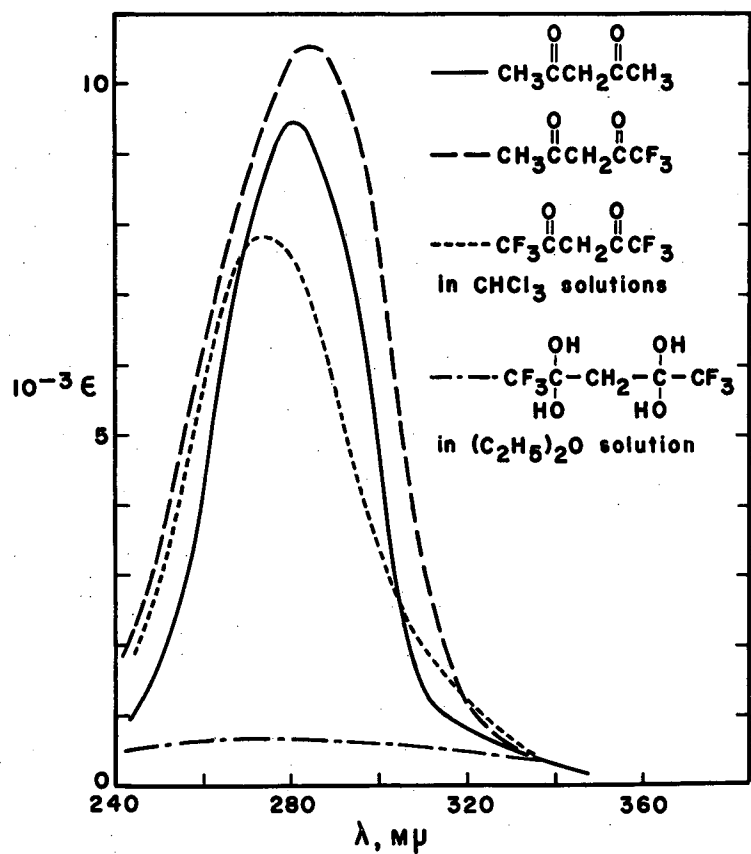


Fig. 2. Ultraviolet absorption spectra of acetylacetone, ———; trifluoroacetylacetone, — — —; and hexafluoroacetylacetone, - - - - -,  $4.0 \times 10^{-5}$  M in  $\text{CHCl}_3$ ; of hexafluoroacetylacetone dihydrate, — · — ·;  $4.0 \times 10^{-5}$  M in ether.

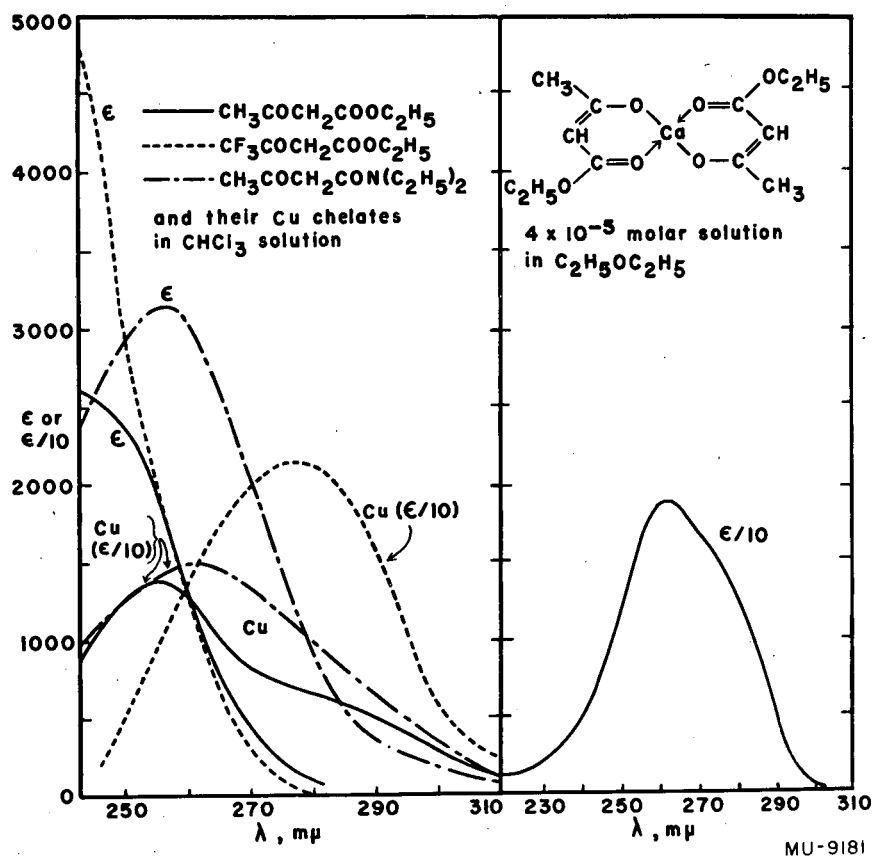


Fig. 3. Ultraviolet absorption spectra of (left): ethyl acetoacetate, —; ethyl trifluoroacetoacetate, - - - -; and N,N-diethyl acetoacetamide, - · - ·;  $2 \times 10^{-4}$  M in  $\text{CHCl}_3$ . The corresponding Cu chelates,  $2 \times 10^{-5}$  M in  $\text{CHCl}_3$ , are labeled "Cu." (right): bis-ethyl acetoacetato-Ca (II),  $4 \times 10^{-5}$  M in absolute ether.

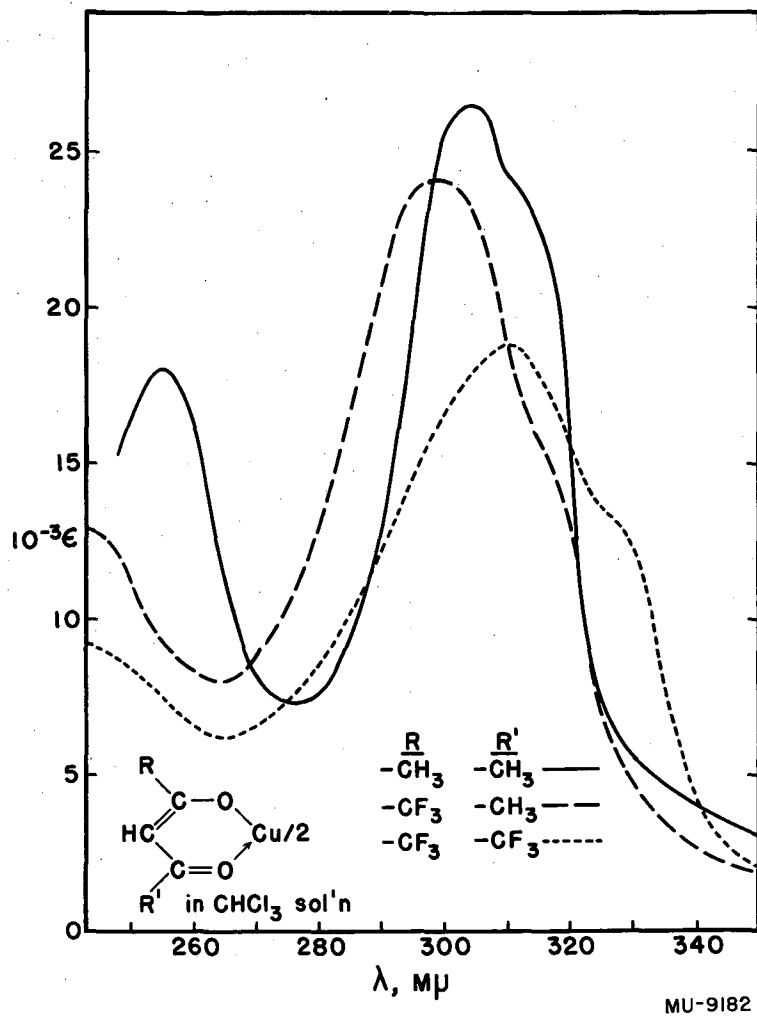


Fig. 4. Ultraviolet absorption spectra of  $2 \times 10^{-5}$  M bis-acetylacetonone-Cu(II), ———;  $2 \times 10^{-5}$  M bis-trifluoroacetylacetonone-Cu(II), - - -; and  $1 \times 10^{-5}$  M bis-hexafluoroacetylacetonone-Cu(II), ·····, in  $\text{CHCl}_3$ .

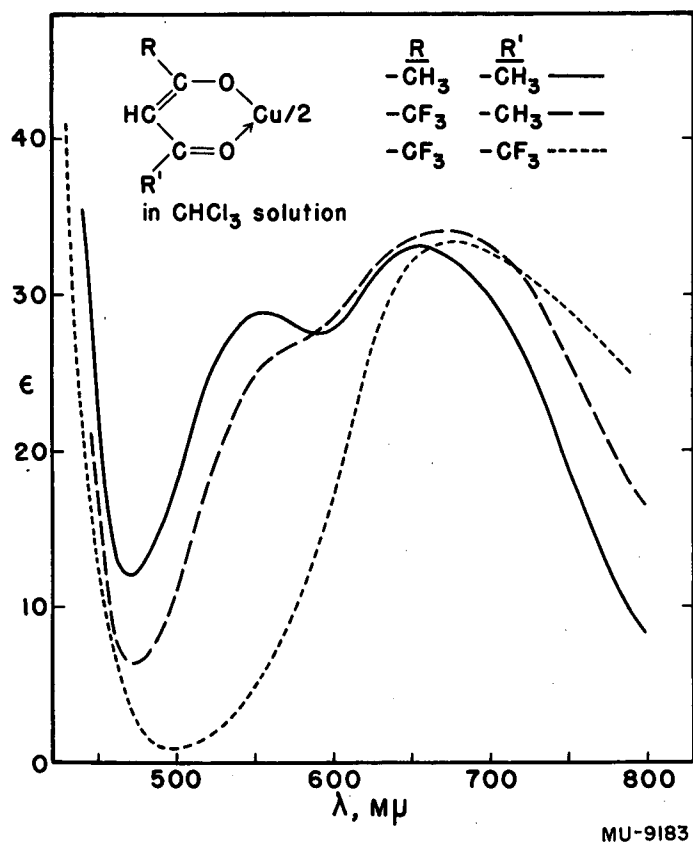


Fig. 5. Visible absorption spectra of bis-acetylacetonato-Cu(II), —; bis-trifluoroacetylacetonato-Cu(II), - - -; and bis-hexafluoroacetylacetonato-Cu(II), - - - - -; 0.010 M in  $\text{CHCl}_3$ .

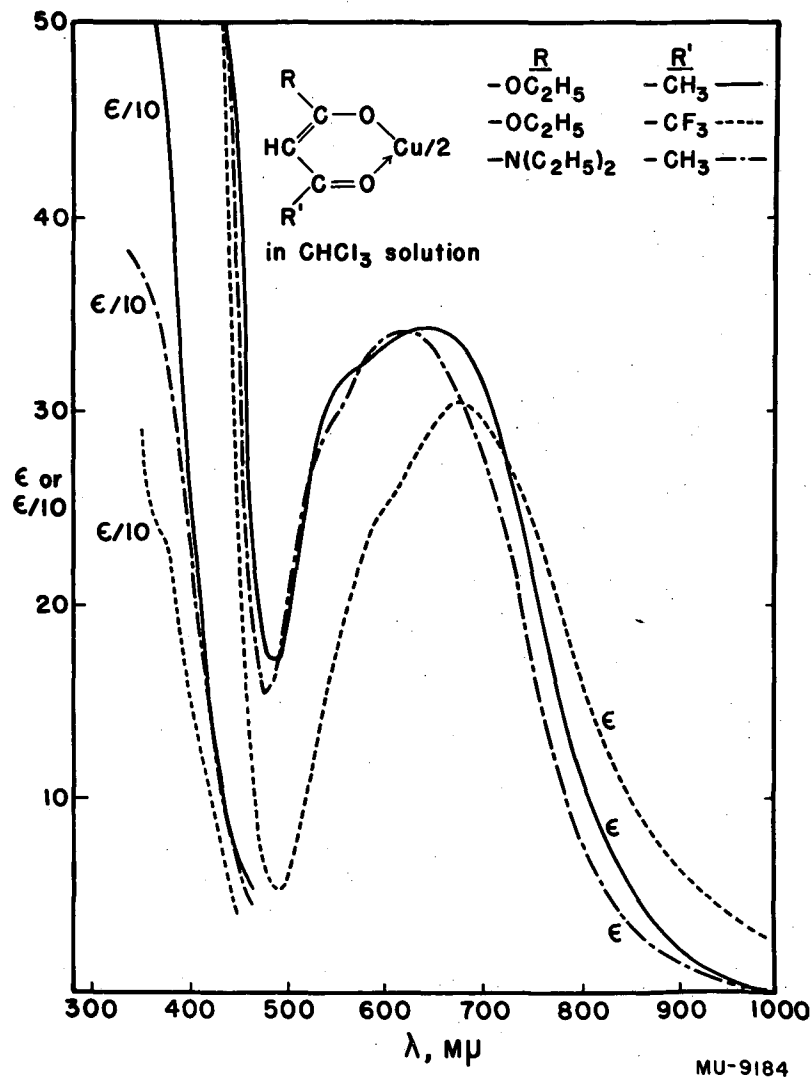


Fig. 6. Visible absorption spectra of bis-ethylacetoacetato-Cu(II), ———; bis-ethyl trifluoroacetoacetato-Cu(II), - - -; and bis-N,N-diethylacetoacetamido-Cu(II), - · - ·; 0.010 M in  $\text{CHCl}_3$ . Left-hand curves obtained with 0.0010 M solutions.

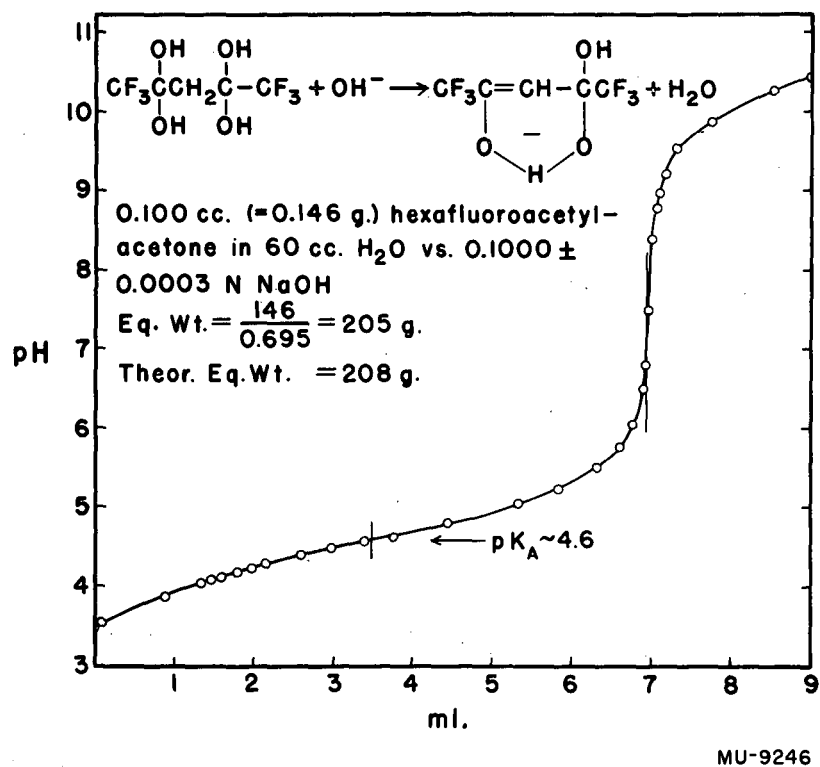
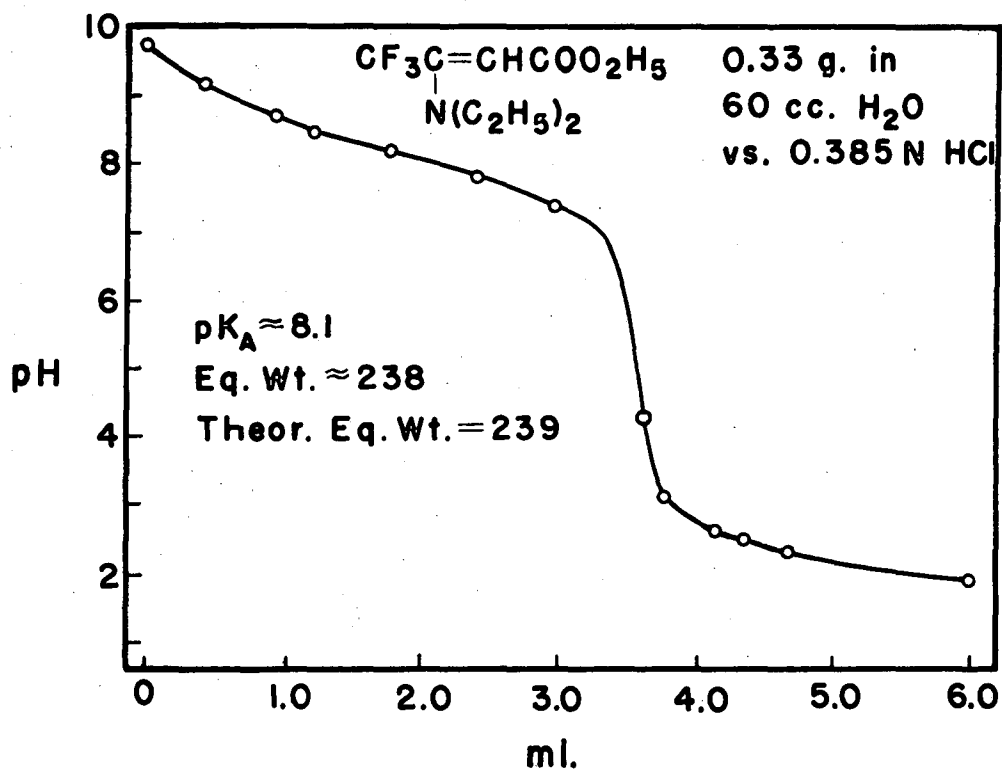


Fig. 7. Titration of aqueous hexafluoroacetylacetone with sodium hydroxide solution.



MU-9268

Fig. 8. Titration of aqueous  $\beta$ -diethylamino ethyl trifluorocrotonate with hydrochloric acid.



Table II

Absorption Bands of $\text{CHCl}_3$ Solutions in the Visible and Ultraviolet Regions			
Compound	Molarity	$\lambda_{\text{max}}$	$\epsilon_{\text{max}}$
<u>I</u> Acetylacetone	$4 \times 10^{-5}$	280	9,500
<u>II</u> Trifluoroacetylacetone	$4 \times 10^{-5}$	284	10,500
<u>III</u> Hexafluoroacetylacetone dihydrate <sup>a</sup>	$4 \times 10^{-5}$	none	--
<u>IIIa</u> Hexafluoroacetylacetone	$4 \times 10^{-5}$	273	7,800
<u>IV</u> Ethylacetoacetate	$2 \times 10^{-4}$	<246	~2,600
<u>V</u> Ethyltrifluoroacetoacetate		<246 (~290)	~4,900
<u>VI</u> N,N-diethylacetoacetamide	$2 \times 10^{-4}$	256	3,200
		(Utzinger gives $\lambda_{\text{max}} = 253, \log \epsilon = 4.0$ ) <sup>a</sup>	
<u>I-Cu</u> bisacetylacetonato-Cu(II)	$2 \times 10^{-5}$	254 304 (313) (390) 552 660	18,000 26,000 -- -- 29 33
<u>II-Cu</u> bistrifluoroacetylacetonato-Cu(II)	$2 \times 10^{-5}$	298 (316)	24,000 --
	$1 \times 10^{-2}$	(566) 680	-- 34
<u>III-Cu</u> bishexafluoroacetylacetonato-Cu(II)	$1 \times 10^{-4}$	310 (329)	18,700 --
	$1 \times 10^{-2}$	710	40
<u>IV-Cu</u> bisethylacetoacetato-Cu(II)	$2 \times 10^{-5}$	254 (281)	14,000 --
	$1 \times 10^{-2}$	(560) 650	-- 34
<u>V-Cu</u> bisethyltrifluoroacetoacetato-Cu(II)	$2 \times 10^{-5}$	277 (590)	22,000
	$1 \times 10^{-2}$	680	30
<u>VI-Cu</u> bis-N,N-diethylacetoacetamido-Cu(II)	$1 \times 10^{-5}$	260	~16,000
	$1 \times 10^{-2}$	(540) 620	-- 34

<sup>a</sup>Dissolved in diethyl ether rather than  $\text{CHCl}_3$ .

Table IIIa

Infrared Absorption Bands of Bidentate Ligands								
Region	I	II	III	IIIa	IV	V	VI	VII*
OH str.	3550	3360 (3120)	3330	3120	3550	3360 (3100)	3480	((3500)) ((3100))
CH str.	2960 (2620) (2350)	2980 (2350)	(2500) (2330) (2160)	2950 (2580) 2420 (2200) 2000	3050	2920  2340	2960  (2350)	((2520)) ((2430))
C=O and C=C str.	(1725) 1708 1620	1775 1745 (1713) 1680 1680  (1475)		1790 1765 1680 1625	1735 1720 1650 (1640)  1470	1650 1608 (1562) 1545 (1525) (1510) (1475)	1720 1640 (1595) (1560) (1545) 1495 1440	1688  1635 1560 (1545)
CH <sub>2</sub> and CH <sub>3</sub> deform; C-C str.	1425 1365 1305 1252	1455 (1430) 1375 1350 1282 1230 1200 1160 1095 1030 (990)  900	1340  1278 1212  1188 1138 990 970 910	1450 (1350)  1270 1220  1160 1085  1096 1037 913	(1265)  1235  1190 1150 (1115)  (928)	1285  1207  1157 1112  1096 (1030) (895)	1280 1223  1205 1142 1100 1080 1038 1010 963 943 920 826 790 775 725 670	1275 1190  1165 1130 1110 1098 (1065) 1030 963  913 863 837 790  725 675
*β-diethylamino ethyl trifluorocrotonate.								

Table IIIb

Infrared Absorption Bands of Bidentate Cu(II) Chelates					
I-Cu	II-Cu	III-Cu	IV-Cu	V-Cu	VI-Cu
(2360)	(2350)	(2350)	(2340)	(3110)	(2340)
1582	1615	1643	(1645)	1635	1565
(1560)	1535	(1615)	1600	1612	(1550)
1530		1565	1555	1564	1525
		1540	1538	(1550)	1500
		1490		1495	
(1425)	(1422)	(1450)	(1425)	(1432)	(1440)
(1362)	1312	1360	1290	1375	1398
1278	1230	(1340)	(1270)	1312	1363
1193	1198	(1300)	(1225)	1248	1343
	1157	1260	1180	1230	1302
	1142	1210		1228	(1280)
		1150		1188	1212
		1110		1155	1167
					1102
1020	1030	1080	1070	1092	1085
940	1015	1044	1022	1013	1075
(720)	952	(955)	985	985	1050
682	870	(895)	973	967	(1030)
	800	871	(865)	925	1000
	738	802	778	862	970
		746	(758)	842	960
		679		815	928
				802	830
				755	785
				732	728
				722	670
				698	

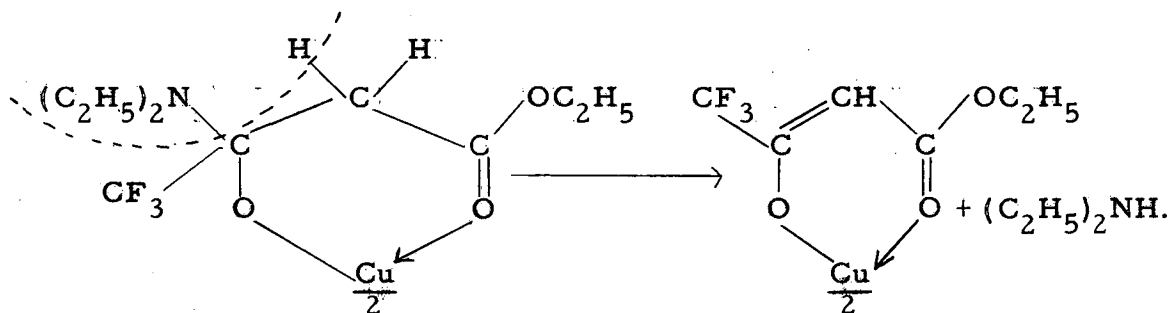
of diethylamine with ethyl trifluoroacetoacetate always contained less nitrogen than that calculated for the desired product, N,N-diethyl trifluoroacetoacetamide, but corresponded quite closely to the value calculated for  $\beta$ -diethylamino ethyltrifluorocrotonate. This structure for the product was confirmed by titration curves, absorption spectra, and failure to obtain a nitrogen-containing copper chelate.

The method described for the preparation and purification of hexafluoroacetylacetone from the dihydrate has not been reported previously and seems to be an improvement over the method given by Haszeldine et al.,<sup>10</sup> which involves the treatment of an ether solution of the hydrate with metallic sodium. The boiling range of the product is quite narrow, and differs somewhat from the values reported by Haszeldine et al. ( $54^{\circ}$ - $85^{\circ}$ ) and by Henne et al.<sup>7</sup> ( $63^{\circ}$ - $65^{\circ}$ ).

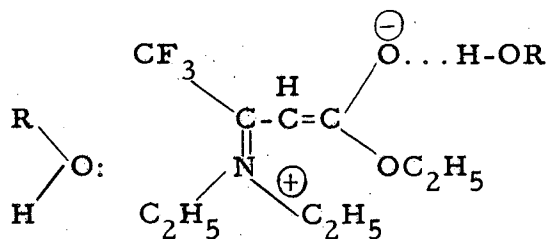
The procedures used for the preparation of the copper (II) chelates of trifluoroacetylacetone, ethylacetoacetate, and ethyltrifluoroacetoacetate are sufficiently different from the procedures previously reported<sup>7, 8, 10, 11</sup> to warrant a brief description here. The preparation of the copper (II) chelate compounds of trifluoroacetylacetone given above has not been described previously although it has apparently been carried out by Henne et al.<sup>7</sup> In the preparation of bishexafluoroacetylacetonate-Cu(II), the results of this investigation indicate that, contrary to the findings of Haszeldine et al.,<sup>10</sup> the metal chelate is formed in the presence of water. On the other hand, there is general agreement in that the yield of metal chelate seems much higher in nonaqueous media.

The reaction of copper (II) acetate monohydrate with  $\beta$ -diethylamino ethyl trifluorocrotonate in boiling ethanol resulted in a product free of nitrogen. The analytical results checked the theoretical values of bisethyltrifluoroacetoacetate-Cu(II), and except for some rather minor differences, the infrared and ultraviolet spectra of the latter compound also corresponded very closely to those of the reaction product. It seems, therefore, that the diethylamino group was replaced by a hydroxy group. That this process of hydrolysis (or alcoholysis) must be metal-catalyzed is shown by the previously mentioned titration experiments; one should certainly observe hydrolysis products by titration, since the  $pK_A$  of the liberated diethylamine would be  $> 11$ . However,

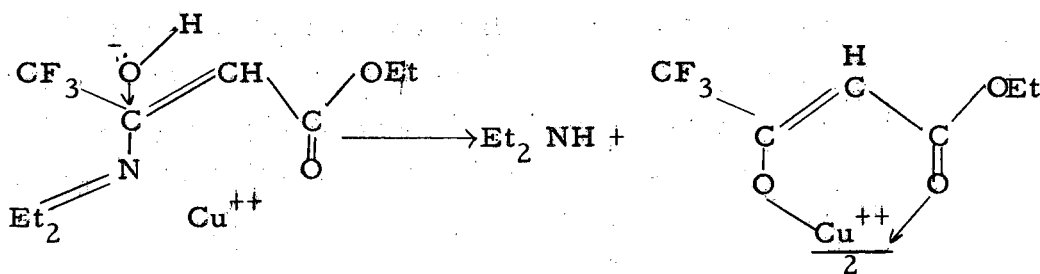
prolonged heating of the free amino crotonic ester in aqueous solutions ranging from neutral to quite acid yielded quantitatively the initial undecomposed amine,  $pK_A \sim 8.1$ . A likely mechanism for metal-catalyzed hydrolysis would involve the hydrate either in the transition state or as stable intermediate:



Accordingly, ultraviolet spectra of the crotonate (Fig. 1) were examined for that disappearance of high-intensity bands which would mark extensive conversion of the crotonate to a solvent addition product (across the double bond). No such evidence is to be seen; indeed, in the hydroxylated solvents not only is the principal band quite as strong as in cyclohexane or chloroform, but it also has undergone a shift from 234 to 270  $m\mu$ . This indicates that the hydroxylated solvents must assist excitation of the conjugated system, perhaps through forms such as



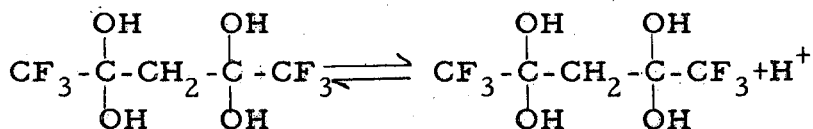
The question that this interpretation leaves unanswered is why chloroform, a hydrogen-bonding agent, does not exhibit a similar effect. Perhaps the steric hindrance would be sufficient to prevent useful approach of chloroform, or perhaps its ability to H-bond is too small to be observed here. At any rate, we have found no evidence against such a  $Cu^{++}$  catalysis of amine elimination as



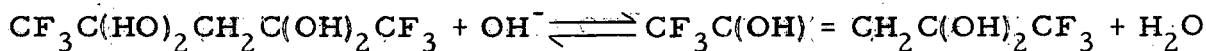
which invokes the polarizing power of the dipositive ion to weaken the carbon-nitrogen bond.

The low metal and carbon analyses of bishexafluoroacetylacetonocopper(II), and a high hydrogen analysis, indicate the possibility of a dihydrate, but this chelate compound sublimed very readily without change in color or composition. Also, there were no hydroxyl bands in the infrared. Since it is unlikely that a hydrate of any kind could be produced without the retention of O-H bonds, the conclusion is inevitable that the analytical results are in error and that the chelate is anhydrous with a structure corresponding to Formula I.

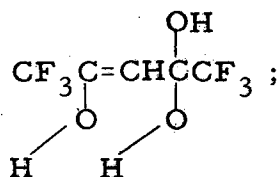
Another experience would indicate that hexafluoroacetylacetonate anion is indeed no more than monohydrated. The titration with 0.100 N base (Fig. 7) shows hexafluoroacetylacetonate to be an acid slightly stronger than acetic acid. However, the equilibrium



would probably have a much higher  $pK_A$ ; other known alcohols very highly substituted with trifluoromethyl groups have acid  $pK$  values no smaller than about ten (e. g.:  $(\text{C}_3\text{F}_7)_2\text{CHOH}$ ,  $pK_A = 10.66$ ;  $(\text{C}_3\text{F}_7)_3\text{COH}$ ,  $pK_A = 10.0$ ).<sup>13</sup> The alternative reaction would seem to be one involving dehydration,



The  $pK_A$  value observed should then correspond to the acid structure

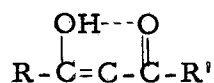


in fact, 4.6 would be a reasonable value for this enol.

Morgan and Moss<sup>14</sup> have pointed out that metal chelate compounds of type II, in which two betadiketonic residues are bound to a transition metal, form stable addition compounds with two other donors to give complexes in which the metal coordinate linkages are presumed to have an octahedral arrangement. In this investigation no addition compounds were obtained under the conditions employed in the production of bisacetylacetonone-Cu(II). However, this tendency was apparent in the case of bistrifluoroacetylacetonone-Cu(II), for which an unstable solvate formed in cold 50% aqueous ethanol and gradually decomposed to the anhydrous form when exposed to air over the period of a few hours. It is perhaps surprising that we did not obtain addition compounds of greater stability for the hexafluoroacetylacetonone chelate, since the tendency of the trifluoromethyl groups to decrease stability<sup>9</sup> would be expected to enhance the affinity of the metal ion for additional donor groups. However, an unstable solvate, perhaps also an alcoholate, was first isolated when the chelate was recrystallized from aqueous ethanol. Samples of bishexafluoroacetylacetonone-Cu(II) prepared from the dihydrate of the ligand in aqueous media, and from the diketonic form of the ligand in anhydrous media, both gave products with identical properties and spectra.

#### Ultraviolet and Visible Absorption Spectra.

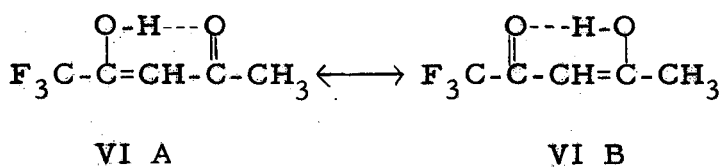
All the ultraviolet absorption bands of ligands in Figs. 2 and 3 are high-intensity bands arising from electronic transitions in the conjugated system



IV

Such bands are sometimes called "K" transitions.<sup>1</sup> This enolic system-- in which R may be methyl or trifluoromethyl, and R' may be methyl, trifluoromethyl, ethoxy, or diethylamino--is common to all the ligands investigated.

In Fig. 2, a simple comparison may be made between the spectra of acetylacetone and its trifluoro and hexafluoro derivatives. The maximum of the intense absorption band of acetylacetone is shifted to longer wave lengths and further intensified by the substitution of an electron-attracting trifluoromethyl group at one end of the conjugated system. In this case two isomeric enol forms are possible,



The influence of the trifluoromethyl group increases enolization;<sup>8</sup> one may surely suppose that A has greater acidity than B and therefore that B is likely present in higher concentration than A. The absorption band of hexafluoroacetylacetone, on the other hand, is considerably decreased in intensity, while its frequency is also decreased. A rough quantitative comparison of these spectra on the basis of relative intensities is possible even though the relative degrees of enolization are not known exactly. From published data on the absorption intensity of the pure enol of acetylacetone, one would guess it to be approximately 50% enolized in the solvent used in this investigation. Meyer<sup>15</sup> reports the enol content of acetylacetone to be 79% at 20° C in chloroform. Assuming this to be correct, and making reasonable estimations for the enol contents of trifluoro-<sup>8</sup> and hexafluoroacetylacetone of ~95% and ~100% respectively, one obtains the values given below.

enol of	Approx. % enol	$\lambda_{\text{max}}$	Approx. $\epsilon_{\text{max}}$ for enol
acetylacetone	73-79	280	12,500 ± 500
trifluoroacetylacetone	90-100	284	11,100 ± 600
hexafluoroacetylacetone	100	273	7,800



Although these values are not precise, one can safely draw from them the conclusion that an increase in the electron-donating power of the groups R and R' produces a corresponding increase in the intensity of K-absorption. This point is borne out by other substitutions as well. Taking the degree of enolization into account, one finds that when R is -CH<sub>3</sub>, the K-band intensities for various R' groups increase in the order -CF<sub>3</sub> < -CH<sub>3</sub> < -OC<sub>2</sub>H<sub>5</sub> < -N(C<sub>2</sub>H<sub>5</sub>)<sub>2</sub>.

The wave-length shifts with fluorine substitution are what one would expect: an increase when a strong electron-attracting group is placed on one end of a conjugated system, and a decrease when such electron-attracting groups are placed on both ends of the system.

The spectrum of acetylacetone given in Fig. 2 is in rough agreement with those given by Haszeldine et al.<sup>10</sup> and by Acly and French<sup>16</sup> for alcohol solutions. Close agreement would not be expected in view of the wide variation with solvent of both frequency and intensity of β-dicarbonyl compounds reported by Haszeldine et al.<sup>10</sup> Subject to the same qualification, the absorption curves of ethyl acetoacetate and of ethyltrifluoroacetoacetate given in Fig. 3 and in Table II agree with the values reported previously.<sup>10</sup> In this work, however, no secondary absorption band at higher wave length was observed for ethyltrifluoroacetoacetate, as was reported for this substance in cyclohexane.<sup>10</sup> It is of interest to note that an increase in intensity is produced by a modification of the structure of ethylacetoacetate. In the trifluoromethyl analogue, the effect is probably due to an increase in the degree of enolization of the compound. On the other hand the intensity increase, accompanied by an increase in λ<sub>max</sub>, observed for N,N-diethylacetamide is due to the effect on a conjugated system of replacing an electron-donating group, - $\overset{\text{O}}{\parallel}$ -C<sub>2</sub>H<sub>5</sub>, by a stronger electron-donating group,  $\text{N} \begin{matrix} \diagup \text{C}_2\text{H}_5 \\ \diagdown \text{C}_2\text{H}_5 \end{matrix}$ .

The ultraviolet absorption spectra of bisacetylacetonato-Cu(II), and of its two fluoro analogues, represented in Fig. 4, show some resemblance to those of the ligands themselves. The main absorption band of the ketoenol seems to be considerably intensified in the chelates, and to be split more clearly into double bands. Furthermore, there seems to be a weaker K-type band at lower wave length, although the maxima are below the range of the measurements for the fluorinated chelates.

For the copper (II) chelates of the  $\beta$ -keto esters and amide illustrated in Fig. 3, the spectra resemble those of the ligands much more closely than do those of the  $\beta$ -diketones. Here, also, the effect of the metal is to intensify the absorption bands of the ligand and to shift them to longer wave lengths.

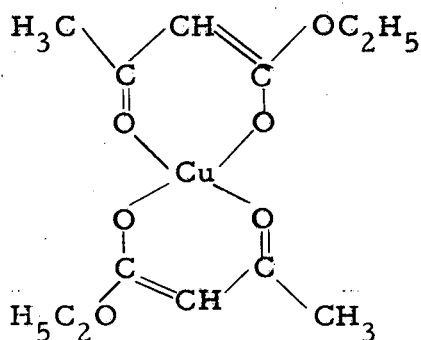
It is interesting to observe the spectrum, in this range, of the calcium chelate of ethylacetoacetate (Fig. 3). It resembles, both in intensity and band placement, that of the corresponding Cu chelate. This unmistakably points to the origin of the ultraviolet bands of the chelates as transitions in the enolate ions; charge-transfer spectra would surely exhibit drastic changes upon the replacement of  $\text{Cu}^{++}$  by  $\text{Ca}^{++}$ . The theoretical reasonableness of these points is partially shown in Part IIIB.

The absorption spectra of the copper (II) chelates in the visible region, shown in Figs. 5 and 6, clearly indicate that the influence of substitution by trifluoromethyl groups in the ligand is to shift the absorption bands to longer wave lengths, thus passing more light in the low-wave-length region and accounting for the typically green color of copper chelates of fluorinated ligands. This shift of the absorption bands increases as the number of trifluoromethyl groups increases, and thus correlates with a decrease in the stability of the metal chelate.\*

Another interesting inference may be drawn from the similarity of the spectra of the copper (II) chelates of ethylacetoacetate and N, N-diethylacetoacetamide. The fact that these curves are almost superimposable indicates that the copper (II) ion is bound only through the oxygen atoms of both ligands as indicated by formulas V A and V B.

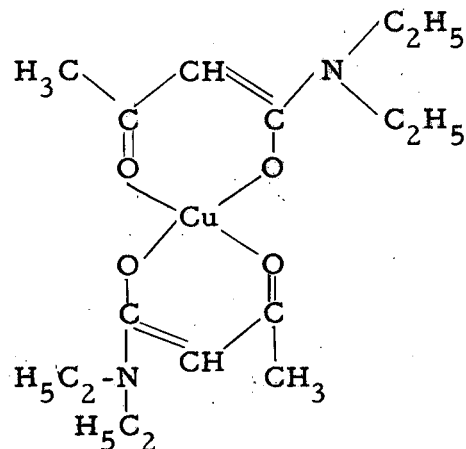
---

\*An increase in the acidity of the ligand and a decrease in the affinity for  $\text{Cu(II)}$  ion was demonstrated by Calvin and Wilson<sup>9</sup> to accompany the replacement of one methyl group of acetylacetone by a strongly electron-attracting  $\text{CF}_3$  group. It is believed that the replacement of the second methyl group will further decrease the donor power of the ligand.



V A

Bisethylacetoacetato-Cu(II)



V B

Bis-N, N-diethylacetoacetamido-Cu(II)

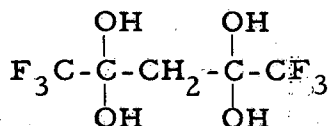
It is seen that all the copper chelate spectra in the visible region consist of at least two overlapping absorption bands. We believe that these are transitions between d-orbitals of the Cu(II) ion; the strong molecular field of the ligands partially removes the 3d orbital degeneracy, permitting transitions in the visible. The two strong bands that appear for chloroform solutions of the molecules reported in this paper are likely the transitions of the hole in configuration  $3d^9$  from the ground state, the  $d_{xy}$ -orbital (if we consider ligands to be centered near the lines  $x = y$  and  $x = -y$ ), to the higher-energy d-orbitals,  $d_{xz}$ ,  $d_{yz}$ , and  $d_{x^2-y^2}$ . The supposition that such transitions are responsible for the visible and near-infrared absorption bands of the transition metal hydrates as well as of some complex ions has been under investigation by several workers very recently.<sup>17, 18, 21, 22, 23, 24</sup>

It will be shown in Parts II and III that if the visible chelate absorption is of this sort, a decrease in donor base strength and covalent bonding tendency such as one expects from the series acetylacetonone-trifluoroacetylacetonone-hexafluoroacetylacetonone should cause a shift of both bands to the red and a slight increase in the ratio of wave length of the higher-wave-length band to that of the lower. For the acetylacetonone series this seems to hold true. Upon passing from ethylacetoacetato-Cu(II) to the corresponding trifluoro derivative, one notes the proper shift of both bands to the red; their ratio appears to be little changed.

We have noticed that the visible absorption spectra of some of the Cu(II) chelates exhibit interesting solvent effects. These will be reported in Part II.

### Infrared Spectra.

For the free ligands, acetylacetone and the corresponding trifluoro and hexafluoro analogues, there is an OH stretching vibration indicating strong enolization of one of the carbonyl groups. It is interesting that the influence of one trifluoromethyl group results in a shift of the OH band from  $3550\text{ cm}^{-1}$  in acetylacetone to  $3360\text{ cm}^{-1}$  in the trifluoromethyl derivative. This correlates with the fact that the enol of trifluoroacetylacetone is more acidic than that of acetylacetone itself. The further shift of the OH band in anhydrous hexafluoroacetylacetone to  $3120\text{ cm}^{-1}$  is then just as one should expect. In the dihydrate of hexafluoroacetylacetone there are four hydroxyl groups, as indicated by formula VI, which result in a very intense broad band at  $3330\text{ cm}^{-1}$ .



### VI. Hexafluoroacetylacetone dihydrate

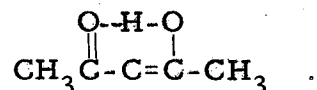
Other bidentate ligands show a similar effect of the trifluoromethyl group in displacing the OH bond vibration to longer wave lengths. Thus the enol band of ethylacetoacetate ( $3550\text{ cm}^{-1}$ ) is displaced to  $3360\text{ cm}^{-1}$  in the trifluoromethyl derivatives.

Additional evidence for the assignment of these absorption bands to OH stretching vibrations may be found in the complete absence of these bands in the spectra of the corresponding metal chelate compounds. Since all the enolic hydrogens are replaced by metal ions in the chelates, as is indicated by Formula II, it is apparent that all the OH bands should disappear.

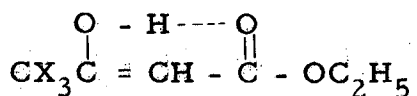
All the ligands have absorption frequencies that may be assigned to free carbonyl groups, with shifts to higher (or lower) frequencies when a  $\text{CF}_3$  group is present. Thus the normal carbonyl

frequencies, 1708 and 1725  $\text{cm}^{-1}$ , of acetylacetone are shifted to 1775  $\text{cm}^{-1}$  and to 1745  $\text{cm}^{-1}$  in trifluoroacetylacetone; to 1790  $\text{cm}^{-1}$  and to 1765  $\text{cm}^{-1}$  in hexafluoroacetylacetone.

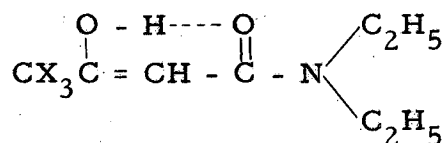
For all three ligands there is a strong, broad band, 70 to 90  $\text{cm}^{-1}$  below the free carbonyl bands, which must be due to the conjugated, hydrogen-bonded carbonyl group characteristic of the enolic form of the  $\beta$ -diketone:



Since the free carbonyl frequencies of ethylacetoacetate and the corresponding amide should be close to that of acetylacetone, the 1720  $\text{cm}^{-1}$  bands may be given this assignment. In ethylacetoacetate, the band found at 1735  $\text{cm}^{-1}$ , 15  $\text{cm}^{-1}$  above the free carbonyl band, has been assigned to the ester carbonyl. The highest carbonyl frequency of ethyltrifluoroacetoacetate, found at 1650  $\text{cm}^{-1}$ , may possibly be assigned to the ester carbonyl group, and the next lower frequency, 1608  $\text{cm}^{-1}$ , to the free-carbonyl vibration. In acetoacetic acid diethylamide, there can be no ester carbonyl bands, in agreement with the observed spectra. The frequency observed at 1640  $\text{cm}^{-1}$  may be assigned to the typical Amide I frequencies (tertiary amide). The lowest of the three carbonyl frequencies observed for each ester and amide may be assigned to the H-bonded (chelated) form of the ester or amide carbonyl, according to formulas VII and VIII, where X may be H or F.



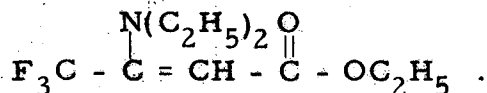
VII



VIII

These frequencies appear at about 100  $\text{cm}^{-1}$  lower than for the corresponding ester carbonyl, and from 120 to 140  $\text{cm}^{-1}$  below the frequency assigned to the amide carbonyl group. Our assignments for acetylacetone and ethylacetoacetate agree with those of Bellamy and Beecher.<sup>3</sup>

Note: In the ethylester of diethylamino trifluoro crotonic acid, the  $1688\text{ cm}^{-1}$  line may be assigned to ester carbonyl (reduced by  $-\text{CF}_3$  group and conjugation from normal position), and the  $1638\text{ cm}^{-1}$  line to a C=C stretch of the crotonyl structure, corresponding to the formula



An apparent anomaly, if these tentative assignments be assumed correct, is the influence of  $\text{CF}_3$  substitution on the carbonyl frequencies. In acetylacetone, a shift to higher frequencies is observed, whereas in ethylacetoacetate there is a very strong shift to lower frequencies. The corresponding shifts of the H-bonded (chelated) carbonyl frequencies, resulting from fluorine substitution, occur in the same direction as the shifts in the free carbonyl frequencies, and are of similar magnitude.

It is interesting that no C=C stretching frequencies have been assigned for the ligands, in analogy with the assignment of the  $1633\text{ cm}^{-1}$  line of acetylacetone to this group. In all cases, however, other strong bands have appeared where this band would normally be expected, and the observed absorption bands may therefore be considered as combinations of the two component bands.

The bands observed in the  $1300$  to  $1500\text{ cm}^{-1}$  region of the spectrum must be due to  $\text{CH}_3$  and  $\text{CH}_2$  deformation vibrations, in accordance with the observed frequencies of other compounds.

Cu Chelate Spectra\*. The metal chelate spectra given in Table IIIa are characterized by the absence of normal carbonyl, ester carbonyl and amide carbonyl absorptions. In each case the carbonyl spectrum of the ligand is replaced by metal-chelated carbonyl absorptions at much lower frequencies. The absorption bands of bisacetylacetonate-Cu(II) at  $1582$  and  $1530\text{ cm}^{-1}$  have been assigned to chelated carbonyl and C=C stretch, respectively, by Lecompte et al.<sup>19,20</sup> Thus the chelate

---

\*Attention is called to the work of Bellamy and Branch<sup>26</sup> on infrared spectra of  $\text{CHCl}_3$  solutions of some metal chelates. We feel that the solution spectra are not directly comparable with solid spectra.

carbonyl absorptions of bisacetylacetonato-Cu(II), bistrifluoroacetylacetonato-Cu(II), and of bishexafluoroacetylacetonato-Cu(II), occur at 1582, 1615, and 1643  $\text{cm}^{-1}$ , respectively. There seems to be an increase in frequency of the carbonyl band as the stability of the metal chelate decreases. Thus, decreased interaction of the metal with the carbonyl groups results from increased fluorine substitution in the molecule. The frequencies of the C=C stretch vibrations, on the other hand, are increased only slightly as methyl groups are replaced by trifluoromethyl groups. In the case of bishexafluoroacetylacetonato-Cu(II) there is an additional band at 1565  $\text{cm}^{-1}$  which is difficult to assign; it also is likely due to C=C stretch.

The ester and amide chelate compounds, IV-Cu, V-Cu, and VI-Cu, seem to have double chelate carbonyl bands, corresponding to the ketonic carbonyl and the ester or amide carbonyl of the ligands. The 1600  $\text{cm}^{-1}$  band of the ethylacetoacetate chelate has been assigned to the ester carbonyl chelated to the Cu(II) ion, and the lower-frequency band at 1555  $\text{cm}^{-1}$  must correspond to the chelated ketonic carbonyl group. The frequencies of both these bands are therefore strongly shifted ( $\sim 150 \text{ cm}^{-1}$ ) to lower frequencies by coordination with the metal ion. Another band at 1538  $\text{cm}^{-1}$  is assigned to a C=C stretch vibration, analogous to the corresponding bands in the acetylacetonate derivatives.

The frequency assignments made for bisethyltrifluoroacetoacetato-Cu(II) are completely analogous, with the exception that all the frequencies are somewhat higher than those of the ethylacetoacetate chelate. The shift to higher frequencies is much greater for the chelated ketonic carbonyl than for the chelated ester carbonyl, as would be expected from the position of the trifluoromethyl group. The C=C stretch frequency undergoes the smallest shift. The carbonyl frequencies of the N,N-diethylacetoacetamide chelate are considerably lower than the corresponding values for the esters, and coordination with the metal ion results in a smaller frequency decrease (75  $\text{cm}^{-1}$ ) for the amide than was observed for the corresponding esters.

As for the free ligands, a number of the absorption bands in the 1300 to 1500  $\text{cm}^{-1}$  region must be due to  $\text{CH}_2$  and  $\text{CH}_3$  deformations. Many of these bands are missing, however, because of the interference of two strong nujol bands in this region of the spectrum.

It must be emphasized that some of the assignments of infrared frequencies may be in error; especially where two or more bands lie fairly close together, it is often impossible to decide how the likely assignments for that region should be distributed among them. It is felt, however, that the general features of these spectra and the structure inferences drawn from them cannot be gross misinterpretations. The assignments have been examined quite carefully for consistency with known spectra whose interpretations are clear. A parallel infrared spectral study of the ligands and their chelates with appropriate isotopic substitutions might prove valuable in making assignments.



## II. BONDING IN COPPER (II) CHELATES: SOLVENT EFFECTS IN THEIR VISIBLE ABSORPTION SPECTRA

### Introduction

The detailed electronic structures--that is to say, the nature of the bonds--in most of the chelate compounds of the transition metal ions are still undetermined. It has been the practice of many workers in the field, therefore, to assume one extreme picture for bonding, e. g., completely covalent or completely ionic, and to ignore totally the other viewpoints. On the other hand, some of us have chosen to accept often flimsy criteria to classify a particular chelate either as covalent or as ionic. That these criteria provide no distinction at all is easily demonstrated. The solubility of a complex in organic solvents, for instance, and conjugately its insolubility in water, is extensively regarded as evidence of the covalent bond type. However, it is in reality only evidence that strong intermolecular ionic forces do not exist. For example, to dissolve sodium chloride as NaCl molecules one must break five  $\text{Na}^+ \text{Cl}^-$  nearest-neighbor lattice bonds; to dissolve cobalt (III) trisacetylacetonate, regardless of whether the molecule is held together by ionic or covalent linkages, one need only overcome Van der Waal attraction between virtual hydrocarbons. Only for those (comparatively few) anions which would surely bridge two or more metal ions if covalency were not important can solubilities furnish a clue as to the nature of the bonds.

Likewise, the magnetic criterion for bond type, so confidently invoked by nearly all co-ordination chemists until recently, has been shown by Orgel<sup>18</sup> to be invalid. An intuitive picture of why this last should be true can be obtained from the following line of thought: Suppose we have a transition metal ion with, say, seven (three unpaired) electrons in the d shell, and we chelate it with four ligands. The Pauling valence bond picture presents us with the following bonding alternatives, with their corresponding magnetic result:

(a) Ionic bonds may be formed, with little or no electron exchange energy. Here the customary line of reasoning has been to suppose that the ligands orient themselves with the greatest possible ligand spacing;

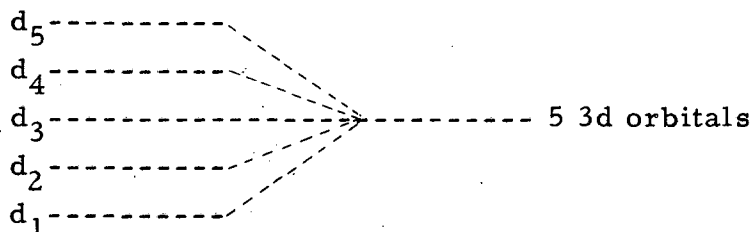
namely, in a tetrahedral configuration around the central ion. Interaction of ligand charge with d-orbital charge is completely ignored; any exchange interactions that might occur are assumed to take place by  $sp^3$  hybridization of the central ion's empty orbitals. Of course, with the unaffected d orbitals containing still three unpaired electrons, the magnetic susceptibility is given as that for the free ion.

(b) Covalent bonds may be formed. Here it is supposed (by Pauling's "maximum extension" or "maximum angular strength" criterion<sup>31</sup>) that covalent bonding is strongest for square-planar arrangement of ligands about the central atom, for which case  $dsp^2$  hybridization of the central metal atom is assumed. The ligand donors are supposed to provide eight electrons, two apiece, for the bonds, and any electrons residing in the metal's 3d, 4s, or two 4p orbitals used in bonding have to move to another atomic orbital of the metal to make room for the donor electrons. One supposes that, for our example, two of the unpaired d electrons would have to pair and share a single d orbital, so that the magnetic susceptibility of the complex shows only the value for a single unpaired electron per molecule.

The Orgel picture, however, is as follows: Supposing all the complexes to be ionic, we first seek the geometrical arrangement of most favorable energy. If the central ion has only closed shells, its charge distribution has approximately spherical symmetry. Accordingly, the ligands will occupy positions of least mutual repulsion--a situation determined by electrostatic, steric, and strain considerations. On the other hand, if the outer shell (3d shell for the first transition element series) is partially filled, there will in general be a nonspherical charge distribution for the central ion. Obviously, for any given surrounding charge configuration, the nonspherical electron charge cloud will arrange or orient itself, so far as it is able, in such a way that its greatest density is as far as possible from surrounding negative charges. More precisely, it is required that the expectation value for electrostatic repulsion energy between central ion and ligand electrons be minimized. This ligand-to-central ion charge-cloud repulsion energy then becomes a fourth factor in determining the most energetically favorable arrangement of ligands. Generally this factor would favor a

square-planar arrangement of four charges about the central ion rather than a tetrahedral one. Thus we have an explanation for square-planar ligand configuration which involves no covalency.

Now let us consider the magnetism of our  $3d^7$  ion. First we notice that a nonspherical  $3d$  charge distribution means that the five  $3d$  orbitals are no longer spatially degenerate. Whether the magnetism corresponds to three unpaired electrons or to one will depend upon whether Hund's rule is still obeyed. As we shall proceed to show, Hund's rule applies for weak ligand charge but fails for strong. Let us suppose that, in the presence of the ligands, the energy levels of our five  $d$  orbitals are as follows:



Now we ask into which of these orbitals each electron goes as we start filling that  $3d$  shell. The first goes into orbital  $d_1$ . The second may go into either  $d_1$  or  $d_2$ . (It will not go into higher-energy orbitals, since it seeks the position of least energy.) If the energy separation between orbitals  $d_1$  and  $d_2$  is greater than the repulsion energy between two electrons in  $d_1$ , then the second electron will go into  $d_1$  and we will have a spin singlet. Hund's rule does not apply, and the complex is diamagnetic. If, however, the surrounding ligand charges were so weak that the separation between  $d_1$  and  $d_2$  energy levels were less than the mutual repulsion energy between two electrons in orbital  $d_1$ , then the second electron would be forced to go into  $d_2$  for the ground state. Then one should observe two-free-electron magnetic susceptibility, and Hund's rule is obeyed.

The same considerations apply to seven electrons. If our surrounding charges are weak or distant ones, Hund's rule is obeyed. Then  $d_1$  and  $d_2$  each have two electrons;  $d_3$ ,  $d_4$ , and  $d_5$ , one electron. Now let us increase the ligand charges so as to separate the energy levels of  $d_3$  and  $d_4$  farther and farther. When this separation passes

the repulsion energy of two electrons both in orbital  $d_3$ , the ground state will be a spin doublet, having two electrons in each of  $d_1$ ,  $d_2$ ,  $d_3$ ; one electron in  $d_4$ ; and  $d_5$  unoccupied. Therefore the magnetic susceptibility of the ground-state complex passes from that corresponding to three unpaired electrons per molecule to that corresponding to only one. No covalency need be postulated for this to happen.

Other examples could be cited, but the above will illustrate the fact that most of the tools used by co-ordination chemists for the past quarter century to investigate electronic structure and bond type in metal chelate compounds are guilty of indeterminacy. Fortunately, the need for rebuilding almost an entire major branch of chemistry is stimulating theoretical and experimental advances, and is causing many experimentalists who have at their disposal recently developed kinds of apparatus to become interested in these problems. The paramagnetic-resonance technique is one of the most promising of the newer methods. The way in which paramagnetic-resonance data can be used to examine bonding is discussed in Part III. This section (Part II) gives results of measurements of Cu(II) chelate absorption spectra, both in the visible region, which has long been available to experimentalists everywhere, and in the near-infrared region, for which instruments comparable in operation with visible spectrophotometers have been available for about two years only. Until recently no interpretation that is even qualitatively satisfactory has been realized for visible and near-infrared absorption bands; however, the moderate success that a number of workers have had during the past few years<sup>18, 25, 21, 22, 24</sup> suggests that the most recent attempts have been in the right direction. Accordingly, this section offers a tentative explanation for the spectra based on the treatment just mentioned (crystal field theory), plus a molecular orbital bonding scheme (which has not, as far as the author knows, been heretofore applied to such spectra, although such a scheme has been employed to explain paramagnetic resonance results<sup>23, 33</sup>).

A brief history of the most recent work on visible spectra of transition metal ions is in order. Orgel<sup>18</sup> has discussed the application of the crystal field theory to these complexes in a general way. Hartmann and Ilse<sup>25</sup> have applied crystal field theory to the electronic spectrum of  $Ti^{+++} \cdot 6H_2O$  and of  $V^{+++}$  with some success. They assumed

a simple set of parameters and attempted direct numerical calculation of the transition frequencies. Ballhausen<sup>21</sup>, and Bjerrum, Ballhausen, and Jørgensen<sup>22</sup> made similar calculations for the absorption spectra of complexes of Cu(II) with water and with ammonia. They consider the results quantitatively meaningful and attach significance to discrepancies between the observed spectra and their calculations for certain models.

Holmes and McClure<sup>17</sup> have studied the absorption spectra of single crystals of transition-metal ion hydrates and have been quite successful in explaining the experiments in terms of the crystal field treatment; their assumptions are fewer than those of the Danish authors.<sup>21,22</sup> They have not attempted to obtain absolute numerical values from the calculations but have instead treated every quantity not determined by the symmetry of the model alone as an undetermined parameter, to be fixed by experiment. For  $\text{Cu}^{++} \cdot 4\text{H}_2\text{O} \cdot 2\text{H}_2\text{O}$ , in which four water molecules form a plane containing the  $\text{Cu}^{++}$  in the middle of an approximate square and the remaining two are axially situated about 20% farther from the  $\text{Cu}^{++}$  than are the first four, they have analyzed the spectral envelope into three Gaussian bands, two of which they attribute to the transition  $\omega_1$  (see Section III), split into two components by the rhombic part of the crystal field, and the other to  $\omega_2$ . They have attempted to obtain the cubic splitting parameter (which they call  $Dq$ )<sup>17</sup> by extrapolating the values for it determined from the spectra of  $\text{Ni}^{++} \cdot 6\text{H}_2\text{O}$ , etc. However, since crystallographic evidence shows the  $\text{Ni}^{++} \cdot 6\text{H}_2\text{O}$  and other hexaquo ions used for the extrapolation to have six very nearly equal ion-water molecule distances, and since  $Dq$  depends upon the position and charge of the axial molecules--becoming smaller as the axial molecules move farther away--the extrapolation is of doubtful value. It probably sets an upper limit on  $Dq$ .

For this study, two molecules were chosen:  $\text{Cu}^{++}$  bisacetylacetone ( $\text{CuA}_2$ ) and  $\text{Cu}^{++}$  bis-3-ethylacetylacetone ( $\text{CuE}_2$ ).  $\text{CuA}_2$  seemed a good choice for the study for a number of reasons: First, it is stable and easy to prepare. Second, it is one of the very few metallo-organic chelates whose complete x-ray structure determination (crystal) has been worked out.<sup>27</sup> Third, its red absorption bands are

not obscured by tail-off from the strong blue and ultraviolet absorption. Fourth, it is a molecule of as high a symmetry as could be found. It is true that there exist  $\text{Cu}^{++}$  chelate molecules possessing true  $D_{4h}$  symmetry--copper phthalocyanines, for example--but they do not meet the third criterion.

### Experimental

Measurements. The visible and near-infrared absorption spectra of  $\text{CuA}_2$  and of  $\text{CuE}_2$  were measured with a prototype of the Beckman DK recording spectrophotometer in the range 450 to 2000  $\mu$ . The lead sulfide detector was used throughout the whole range; small slit widths were maintained. (The slit was always less than 0.1 mm, usually near 0.01 mm.) Scanning was at medium or slow speed. Wave lengths were marked on each spectrum at frequent intervals by tapping a micro-switch which shorted the sample circuit when a desired wave length was seen to pass under the indicator hairline. This technique gives the same result as flicking the shutter in the sample beam but allows much better precision and saves wear and tear on the operator's fingers, eyes, and nerves. Immediately prior to each spectral run, a base line was run on the same chart with pure solvent in both cells.

Preparation and source of materials. The solutes employed were freshly recrystallized from toluene and were desiccated. The  $\text{CuA}_2$  was in the form of blue needles; the  $\text{CuE}_2$ , gray-green crystals.

Sources of the spectroscopic solvents were as follows:

Chloroform--Merck Reagent Grade.

Nitrobenzene--Eastman. It was distilled at aspirator pressure, bp  $89.2 \pm 0.05^\circ \text{C}$ .

Benzene--Baker's "Analyzed".

Acetone--Baker and Adamson No. 1004.

Pyridine--Baker and Adamson No. 2165.

1,4-Dioxane--Eastman White Label grade, dried and stored over sodium.

Piperidine--Eastman, purified by low-pressure distillation. The distillate was crystal-clear.

Methanol--Eastman Spectro Grade, No. S467.

n-Pentanol--Baker's "Analyzed" n-Amyl Alcohol, refluxed with sodium metal and Eastman No. 2362 n-amyl butyrate, and distilled, bp 136.5°-137° C.

To make up each solution,  $1.00 \times 10^{-4}$  mols of solute were weighed to the nearest 0.1 mg and were placed in a 10-ml volumetric flask. Solvent was added to make 10 ml of  $10^{-2}$  M solution. Most spectra were taken for that solution; in the case of  $\text{CuE}_2$  in methanol, insolubility demanded dilution of the  $10^{-2}$  M solution to  $4.0 \times 10^{-3}$  M. This was done by transferring the entire contents of the 10-ml flask to a 25 ml flask and adding washings from the 10-ml flask to make up 25 ml. This procedure was also used for the  $\text{CuA}_2$  piperidine solution, because its absorption in the red was too strong for reliable spectral intensity measurement.  $\text{CuA}_2$  in pentanol required  $10^{-3}$  M because of poor solubility. The colors of the various solutions as they appeared to the eye are listed below:

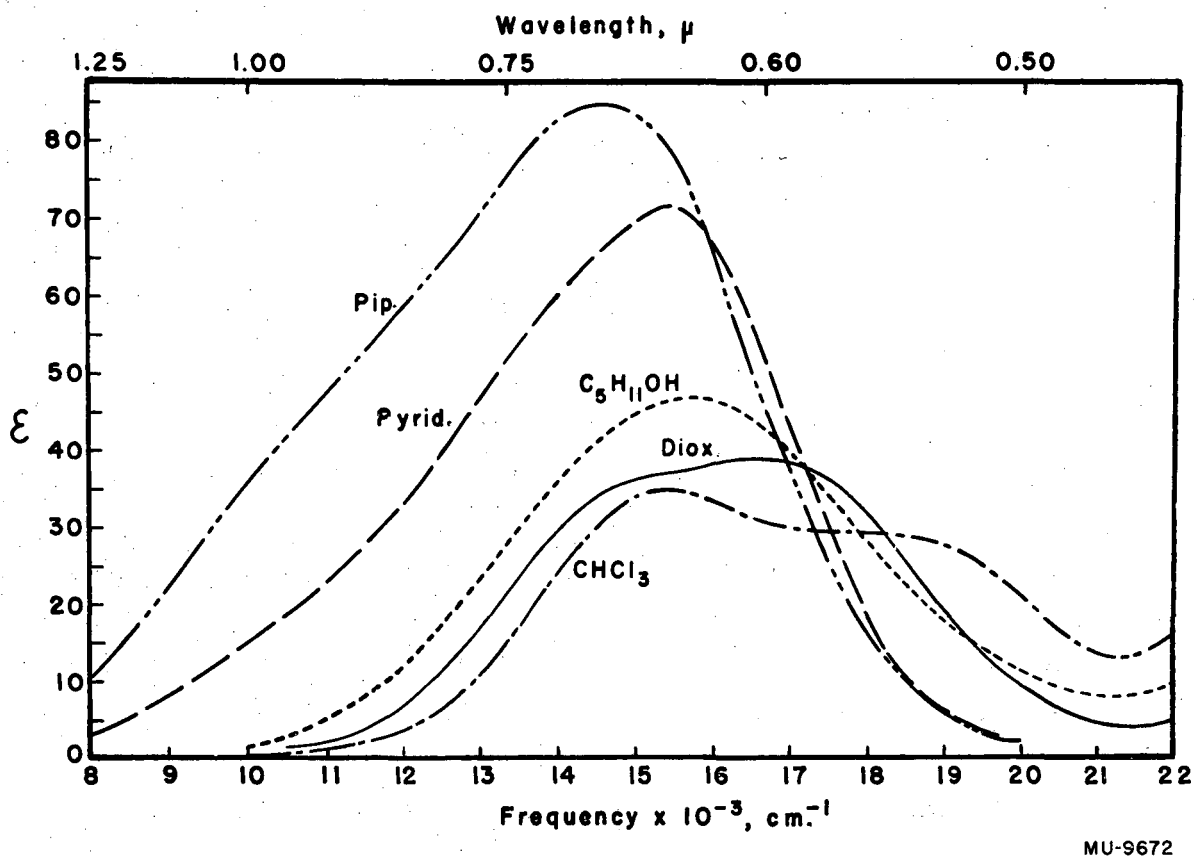
<u>Solvent</u>	<u>CuA<sub>2</sub></u>	<u>CuE<sub>2</sub></u>
Chloroform	Steel blue (grayish)	Yellow-green (grayish)
Benzene	Steel blue (grayish)	Yellow-green (grayish)
Nitrobenzene	Yellow-green (grayish)*	
Dioxane	Clear blue	Aquamarine
Acetone		Olive green
Methanol		Blue-green (grayish)
Pentanol	Blue (green tint)	
Pyridine	Clear green	Emerald green
Piperidine	Clear green	Bright (olive) green

\*Yellow color due to tinge of color in the nitrobenzene.

### Results and Discussion

#### Analysis of Spectra

Figures 9 and 10 give the spectra of  $\text{CuA}_2$  and  $\text{CuE}_2$ , respectively, in the above series of solvents. (The benzene and nitrobenzene solution spectra were not sufficiently different from the chloroform



MU-9672

Fig. 9.  $\text{Cu}^{++} (\text{Acetylacetonate})_2$  in solvents of varying basicity.



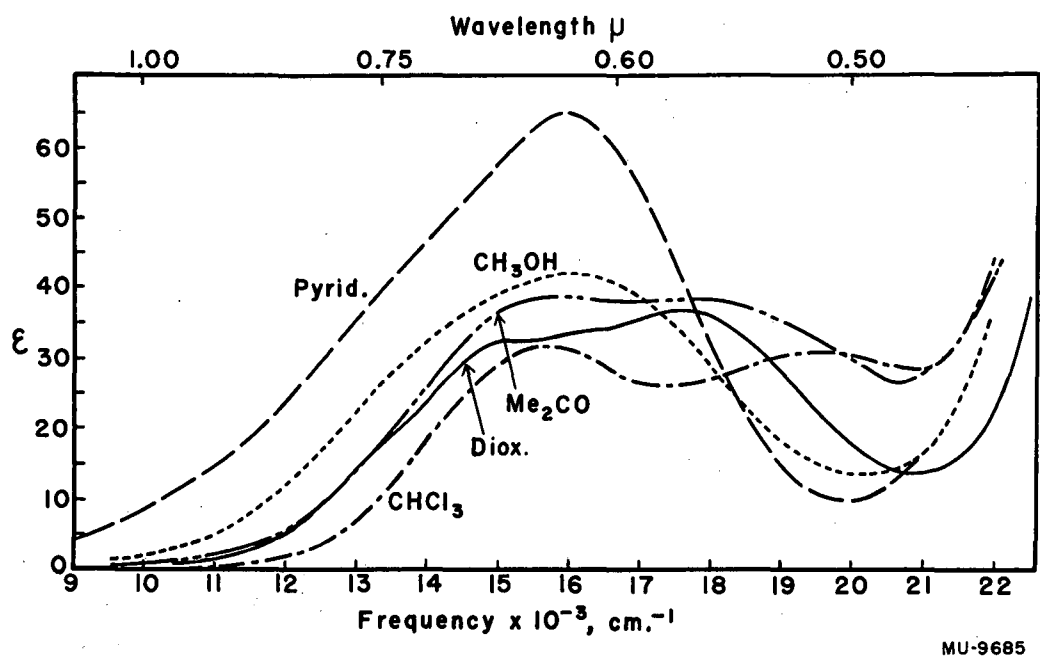


Fig. 10. Cu II 3-Ethyl Acetylacetonate in solvents of varying basicity.

MU-9685

solution spectra to be worth showing here.) It seems apparent from casual examination of these spectra that they vary smoothly (that is, the entire character of the spectrum is not changed) as one passes from chloroform to acetone to dioxane to alcohols to pyridine to piperidine. Towards the first of the series, each solute shows at least two peaks, well separated, in the visible--one in the green, one in the red. Towards the end of the series the total absorption intensity is much higher, and absorption in the green is missing. Instead, there is absorption in the red and near infrared. One notices further that the order of the above series is just what one would expect to be the order of local solvent basicities or coordinating strength.

It seemed that it might be possible to analyze the individual experimental curves into component bands. Symmetric Gaussian error curves were chosen for this purpose. \* The possibility of applying the method of least squares to fit each experimental envelope by three such curves, involving nine parameters, was examined. (An analysis into more than three curves would be of very little significance, being somewhat like approximating a function by the first four or more terms of a power series.) For the pyridine solution of  $\text{CuA}_2$ , thirteen points were taken from the envelope (experimental spectrum) and were worked up in such a least-squares analysis. Needless to say, the work was laborious and time-consuming--every step had to be checked. Furthermore, the required manipulations decreased the number of significant figures to the point where none were left at all by the time answers were in sight. Therefore a trial-and-error procedure was adopted. It might be noted at this point that the analyses were obtained in this way before the theory which has been invoked to explain their results was considered. The author pleads "not guilty" to charges that he might have analyzed these curves with the shadow of bias of theory lurking in his mind. The individual breakdowns for each solution of

---

\*The Gaussian error curve is one of the form

$$\epsilon = \epsilon_{\max} e^{-(\omega - \omega_{\max})^2 / a^2}$$
$$\text{or } \epsilon = \epsilon_{\max} 2^{-(\omega - \omega_{\max})^2 / \delta_{1/2}^2}$$

where  $\delta_{1/2}^2 = a^2 \ln 2$ , and  $\delta_{1/2}$  is the half width at half maximum.

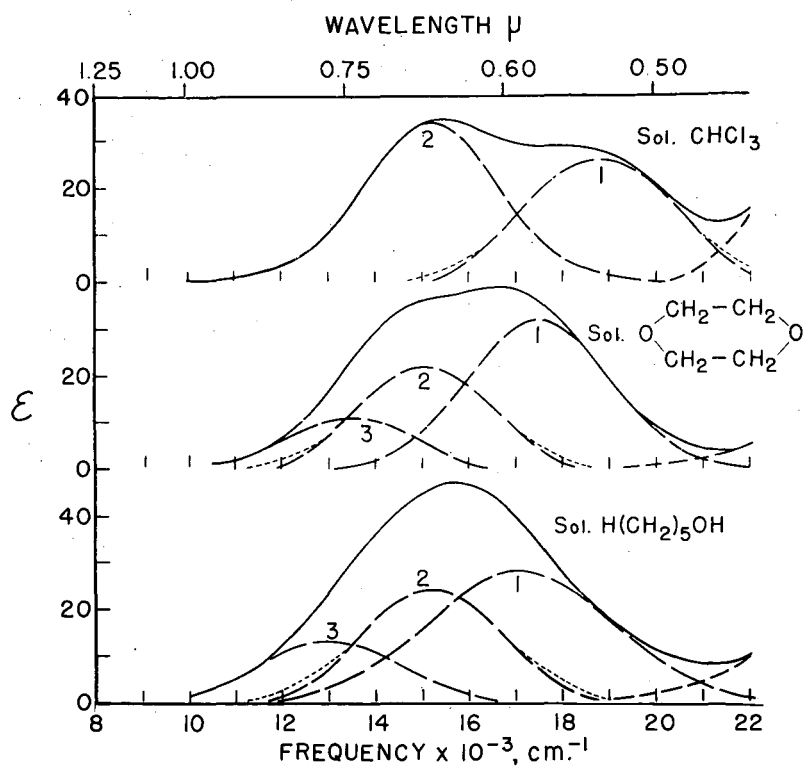
$\text{CuA}_2$  are shown in Figs. 11 a, b, c; for  $\text{CuE}_2$ , in Figs. 12 a, b. A panoramic view of all the breakdowns for both  $\text{CuA}_2$  and  $\text{CuE}_2$  is afforded by Fig. 13. It was interesting to find that rather small deviations from the given component curves usually made the fit to the observed envelope quite poor. While totally different Gaussian analyses seemed to be possible for certain individual curves, no other could be found that seemed to display any sort of pattern throughout the series of solvents. Also, although certain (though not most) of the envelopes that are taken as arising from three components might conceivably fit a very different analysis into only two, it cannot be assumed that a two-component analysis might fit all the experimental curves. It is obvious, for example, that the long flat tops which some of the experimental curves display do not arise merely from a sum of two Gaussian bands; it would be impossible to fit only two Gaussian curves to the spectra of  $\text{CuA}_2$  in dioxane, or to that of  $\text{CuE}_2$  in acetone or dioxane. For these reasons it is felt that the pattern of breakdown given here is the best that one can hope to obtain.

Jørgensen<sup>28</sup> has proposed that absorption curves be fitted to semi-Gaussian distributions, any absorption band being represented by the left side of one Gaussian curve combined with the right side of another. In other words, he has taken a function of the form

$$\epsilon = \epsilon_{\max} \left[ \delta_{(\omega - \omega_0), |\omega - \omega_0|} e^{-(\omega - \omega_0)^2 / a^2} + \delta_{(\omega_0 - \omega), |\omega - \omega_0|} e^{-(\omega - \omega_0)^2 / b^2} \right].$$

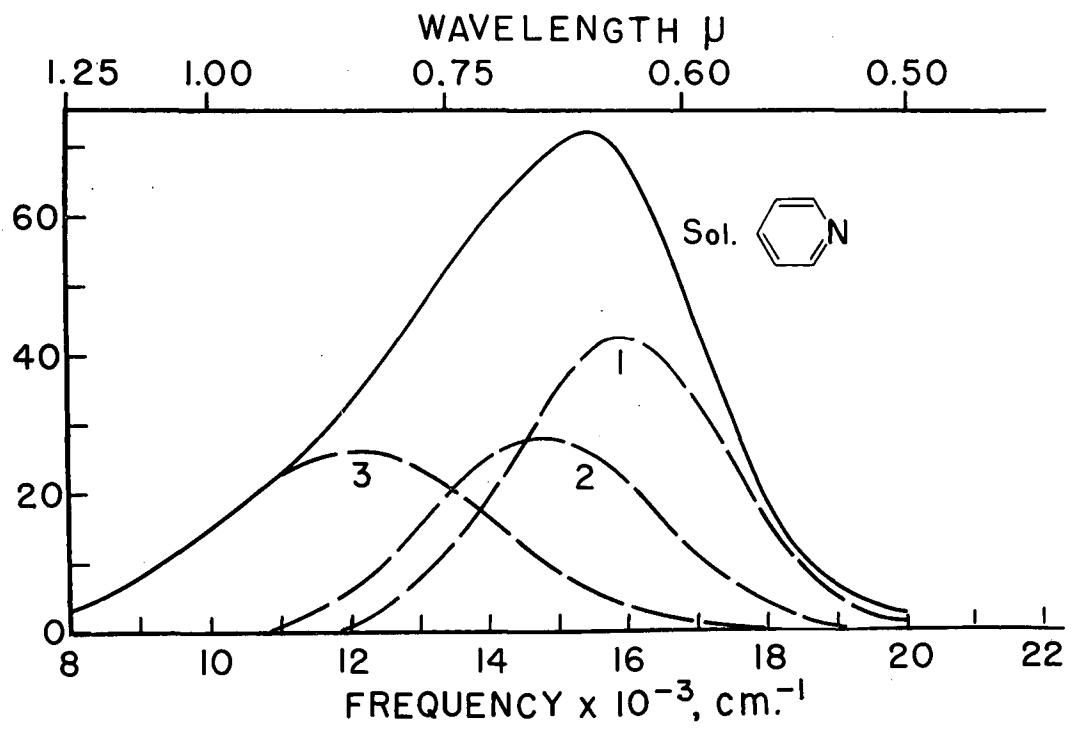
Just what virtue there is in using such a peculiar function escapes us, so we have chosen to ignore Jørgensen's proposal. There is no obvious reason why absorption bands which may indeed be asymmetric should be any sort of Gaussian distribution.

Our breakdowns indicate that the postulating of three important absorption bands is consistent with the experimental spectra. We label the bands 1, 2, and 3, as shown in Fig. 13. Their peak positions,



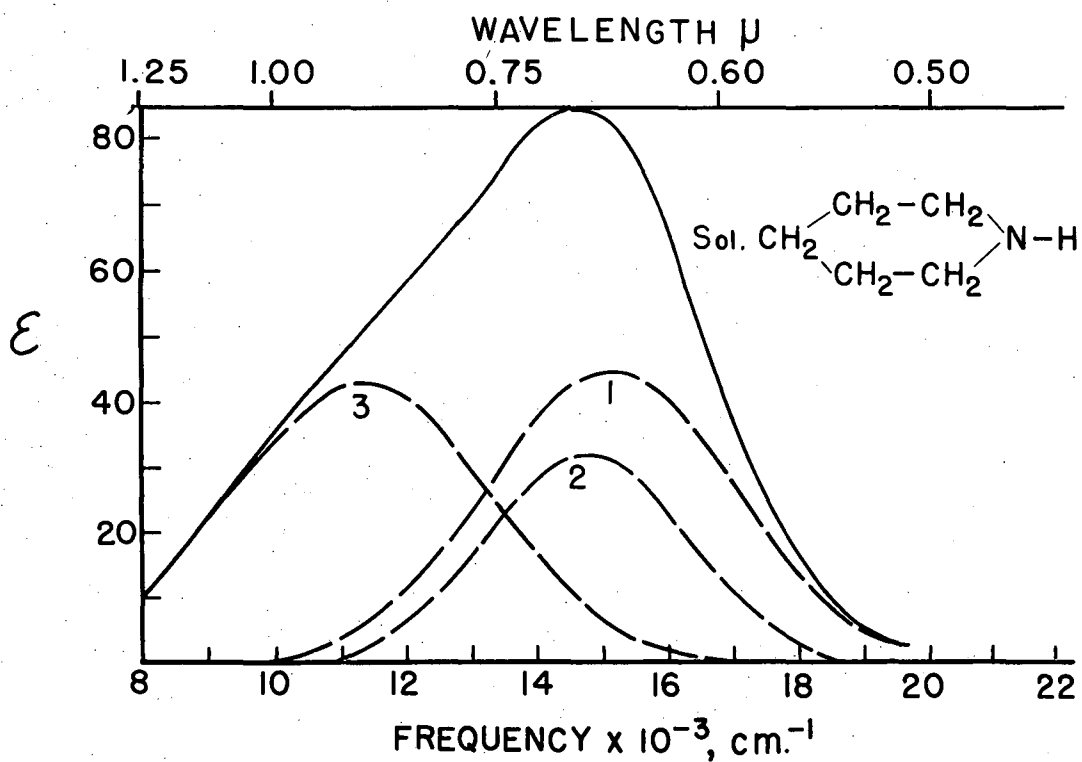
MU-9634-A

Fig. 11a.  $\text{Cu}(\text{II})$  bisacetylacetonate in various solvents. Dotted curves are true Gaussian, where the best fit, the symmetric dashed curve, deviates.



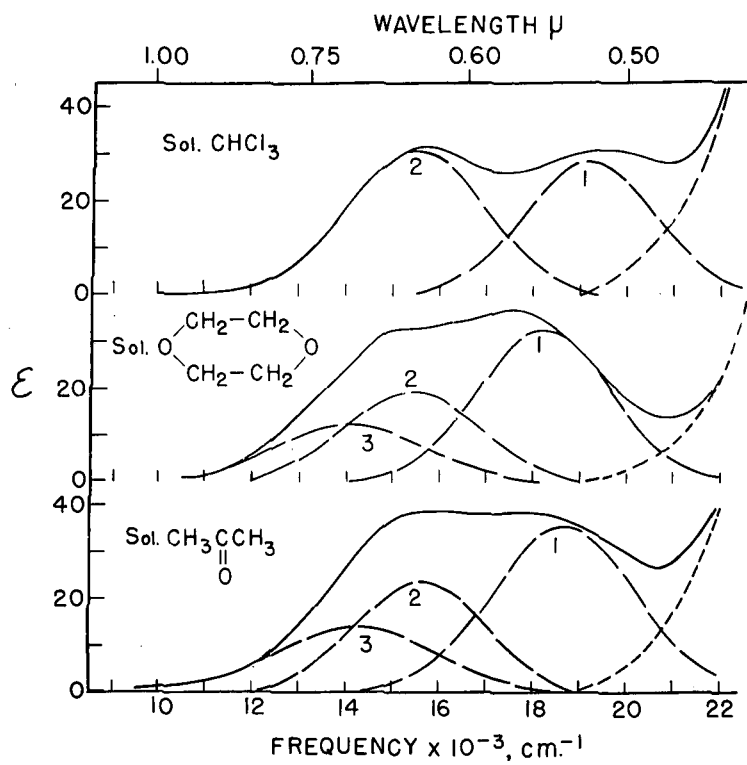
MU-9634-B

Fig. 11b. Cu(II) bisacetylacetonate dissolved in pyridine.



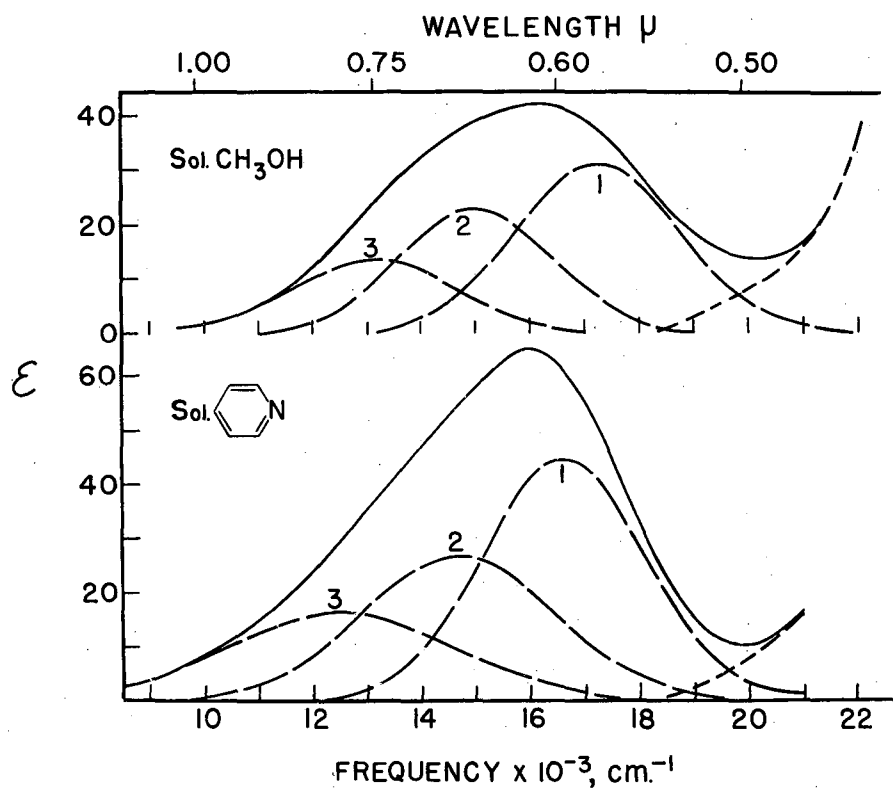
MU-9634-C

Fig. 11c. Cu(II) bisacetylacetonate dissolved in piperidine.



MU-9634-D

Fig. 12a. Cu(II) bis-3-ethyl acetylacetonate dissolved in various solvents.



MU-9634-E

Fig. 12b. Cu(II) bis-3-ethyl acetylacetonate dissolved in methanol and in pyridine.



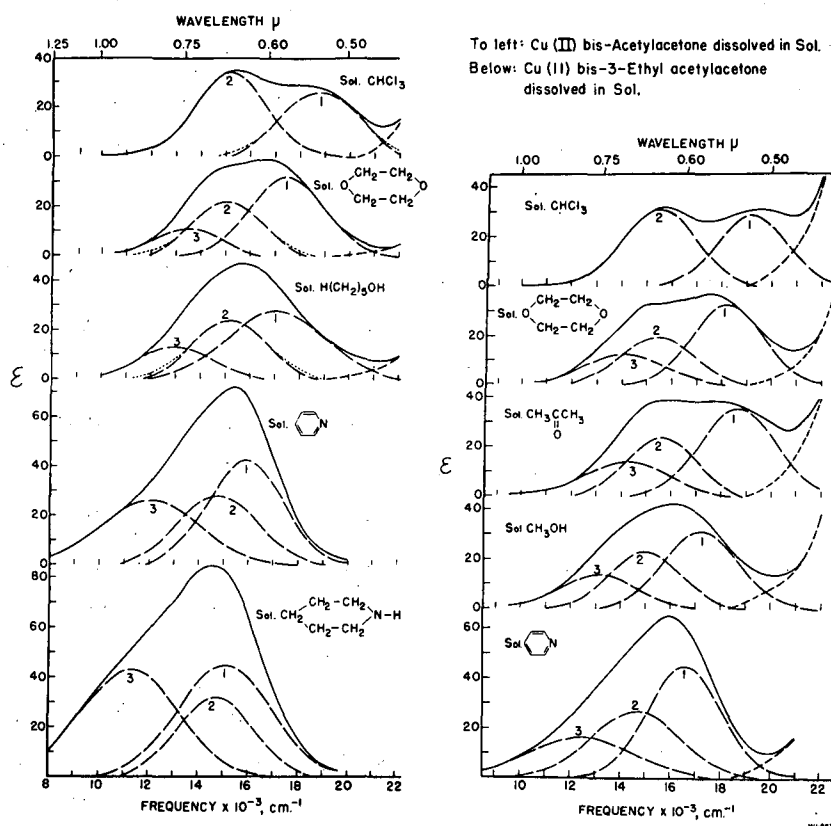


Fig. 13. Visible and near-infrared spectra with breakdowns into Gaussian Components. Where true Gaussian did not fit, symmetric curve that fit well is  $\text{---}$  ; Gaussian is  $\text{- - - - -}$ .

half widths, maximum extinction coefficients, and integrated intensities\* are presented in Tables IV and V.

We can see that these bands are characterized by extinction coefficients in the neighborhood of 30 and by their breadth (3200 to 4700  $\text{cm}^{-1}$  width at half height). The bands are seemingly of the same sort as those found for  $\text{Cu}^{++}$  ion hydrates, both in the solid crystal<sup>17</sup> and in solution, and for aqueous ammonia solutions of  $\text{Cu}^{++}$ .<sup>22</sup> Such absorptions are not observed for  $\text{Cu}^{++}$  free ion (gaseous). The idea that these are transitions between the different 3d orbitals of the  $\text{Cu}^{++}$  ion perturbed by the electric field of the ligands is quite reasonable. It seems to be the only one in agreement with the observations just mentioned and so is now shared by those workers who have recently considered transition-metal-ion visible spectra in any detail.<sup>18, 25, 21, 17, 24</sup>

#### Identification of transitions

In order to correlate the observed spectra with this theory, we must examine how the  $\text{Cu}^{++}$  3d orbital levels are split by the molecular electric field of the surrounding ligands. In Part III of this thesis there is an account of those molecular field calculations necessary to this examination. Now, we must also have a geometrical model for the molecules at hand. X-ray structure analysis indicates the  $\text{CuA}_2$  molecule to be planar; the metal-oxygen distances are given as all equal within experimental error.<sup>27</sup> For noninteracting solvent, which chloroform and benzene probably approach, we need consider only the molecular symmetry. Let us approximate this symmetry as  $D_{4h}$ . (Although in each of these cases the entire molecule has only  $D_{2h}$  symmetry, it will be supposed that the nearly square arrangement of the four oxygen

---

\*The area under a Gaussian curve is proportional to its height-width product. This is easily shown by integrating the function

$$\begin{aligned} \text{Area} &= \int_{-\infty}^{\infty} \epsilon \, d\omega = a \epsilon_{\text{max}} \int_{-\infty}^{\infty} e^{-(\omega - \omega_0)^2/a^2} d\left(\frac{\omega - \omega_0}{a}\right) \\ &= a \epsilon_{\text{max}} \int_{-\infty}^{\infty} e^{-x^2} dx \\ &= \sqrt{\pi} a \epsilon_{\text{max}} = \sqrt{\pi/lm^2} \delta_{1/2} \epsilon_{\text{max}} \end{aligned}$$

Table IV

Component bands of Cu(II) bis-acetylacetonone in the visible and near infrared. *												
Solvent**	$\omega_{01}$	$\epsilon_{\max 1}$	$1\delta_{1/2}$	$(\epsilon\delta)_1$	$\omega_{02}$	$\epsilon_{\max 2}$	$2\delta_{1/2}$	$(\epsilon\delta)_2$	$\omega_{03}$	$\epsilon_{\max 3}$	$3\delta_{1/2}$	$(\epsilon\delta)_3$
Chloroform	18810	26.3	1910	50233	15190	34.1	1690	57629				
1,4-Dioxane	17500	32	1750	56000	15100	22	1700	37400	13500	11	1600	17600
n-Pentanol	17100	28	2300	64400	15200	24	1800	43200	13000	13	1750	22750
Pyridine	15900	42.5	1750	74375	14800	28	1900	53200	12100	26	2330	60580
Piperidine	15100	45	2200	99000	14800	32	1800	57600	11300	43	2300	98900

\*All frequencies and half widths given in  $\text{cm}^{-1}$ .  $\delta_{1/2}$  = half width at  $\epsilon = \epsilon_{\max}/2$ .

\*\*Nitrobenzene and benzene were also used as solvents but gave spectra insufficiently different from the chloroform solution to make analysis worth while.

Table V.

Component visible and near-infrared bands of Cu(II) bis-3-Et-acetylacetonate. <sup>a, c</sup>												
Solvent <sup>b</sup>	$\omega_{01}$	$\epsilon_{\max 1}$	$1\delta_{1/2}$	$(\epsilon\delta)_1$	$\omega_{02}$	$\epsilon_{\max 2}$	$2\delta_{1/2}$	$(\epsilon\delta)_2$	$\omega_{03}$	$\epsilon_{\max 3}$	$3\delta_{1/2}$	$(\epsilon\delta)_3$
Chloroform	19200	29	1650	47850	15500	(31)	1750	54250				
Acetone	18700	36	1800	64800	15600	24	1650	39600	14300	14	2000	28000
Dioxane	18250	33	1650	54450	15450	19.5	1700	33150	14100	12.5	1900	23750
Methanol	17250	31	1750	54250	15000	23	1650	37950	13150	13.5	1750	23625
Pyridine	16600	44.5	1700	75650	14650	26.5	2050	54325	12500	16	2450	39200

<sup>a</sup> All frequencies and half widths given in  $\text{cm}^{-1}$ .  $\delta_{1/2}$  = half width at  $\epsilon = \epsilon_{\max}/2$ .

<sup>b</sup> The results with benzene as solvent were quite similar to those with chloroform.

<sup>c</sup> Because of the interference of the strong blue absorption tail, the separation of these bands, especially as to half width and intensity, is less precise than for  $\text{CuA}_2$ .

donors, copper's nearest neighbors, is most important and thus that the  $\text{Cu}^{++}$  sees a potential not very distorted from  $D_{4h}$  symmetry. The molecular field treatment in Part III gives the energy levels for this case. Transitions take place from the  $xz$ ,  $yz$  orbitals to the  $xy$ ; from the  $x^2 - y^2$  to the  $xy$ ; and from the  $2z^2 - x^2 - y^2$  to the  $xy$ . These will be called, respectively,  $\omega_1$ ,  $\omega_2$ , and  $\omega_3$ . First, we ask whether these might be correlated with our experimental component bands in the visible and near infrared. The analysis gives three bands; so does the theory. The theoretical result predicts the following behavior for  $\omega_1$ ,  $\omega_2$ , and  $\omega_3$  as two axial ligands are added to a square-planar complex to complete an axially elongated octahedron: For invariant square-planar ligand position, increasing strength (that is, increasing effective negative charge) on the axial ligands will cause the  $xz$ ,  $yz$  level to approach the  $x^2 - y^2$  level, will cause the  $2z^2 - x^2 - y^2$  level to approach the  $xy$  level, and will cause the  $xy$  and  $x^2 - y^2$  levels to undergo identical shifts. Thus  $\omega_1$  and  $\omega_3$  should decrease but  $\omega_2$  remain constant if one were to replace the two axial ligands in such a tetragonal hexacoordinated  $\text{Cu}^{++}$  chelate with more strongly basic ones. Furthermore, as the axial ligands approach the planar ones in basicity,  $\omega_1$  should approach  $\omega_2$ ;  $\omega_3$  should approach 0.

Now let us suppose that the solvents, which are bases approximately in the order previously mentioned, furnish an axial field of a strength which increases as the solvent local base strength increases. Then to correlate an experimental band with  $\omega_2$ , we would have to find one that displays little movement from solvent to solvent. For both  $\text{CuA}_2$  and  $\text{CuE}_2$ , one such does exist-- $\omega_{02}$ . Then to identify  $\omega_1$ , we would look for an experimental band lying at higher frequency than  $\omega_{02}$  and approaching it as solvent basicity is increased. Again, there is one such for  $\text{CuA}_2$  and for  $\text{CuE}_2$ -- $\omega_{01}$ . Finally,  $\omega_3$  would be identified with the remaining band, provided that the remaining band decreased in frequency with increasing solvent basicity. The test is met by  $\omega_{03}$ . We may presume, then, that  $\omega_2 = \omega_{02}$ ,  $\omega_1 = \omega_{01}$ , and  $\omega_3 = \omega_{03}$ .

#### Crystal field results

Now let us examine the bands a little more closely with the assumption that the crystal field treatment should explain all the observed

behavior. Since the  $\text{CuA}_2$  molecule is surely planar in solution, and since chloroform and hydrocarbons furnish very little axial coordinating power, we look at the square-planar case of Part III. The expressions (III-32) or (III-37, 38) apply; from (III-38) we take the ratios of transition frequencies as

$$\frac{\omega_1}{\omega_2} = (5/7) + (18/35) \left( \frac{\overline{r^2}}{r_1^2} \frac{r_1^2}{\overline{r^4}} \right),$$

and

$$\frac{\omega_3}{\omega_2} = (2/7) + (24/35) \left( \frac{\overline{r^2}}{r_1^2} \frac{r_1^2}{\overline{r^4}} \right).$$

If we take from Table IV the values  $\omega_{01} = 18,810 \text{ cm}^{-1}$  and  $\omega_{02} = 15,190 \text{ cm}^{-1}$  for  $\text{CuA}_2$  in chloroform, we find

$$\omega_{01}/\omega_{02} = \omega_1/\omega_2 = 1.24.$$

Then  $\left( \frac{\overline{r^2}}{r_1^2} \frac{r_1^2}{\overline{r^4}} \right) = 1.02$ . From this result we would predict an  $\omega_3$  as follows:

$$\omega_3 \text{ (predicted)}/\omega_2 = 0.99, \text{ or } \omega_3 \text{ (pred.)} = 15,040 \text{ cm}^{-1}.$$

Thus a predicted third band would lie just under the second ( $\omega_2 = 15,190 \text{ cm}^{-1}$ ). This very interesting result apparently agrees with experiment, for the  $\omega_{02}$  for chloroform solution seems to be a combination band. If one looks at the intensities for band No. 2 (Table IV) one notices that there is a very regular monotonic increase of both maximum extinction coefficient and integrated absorption intensity with increase in solvent basicity except for the chloroform solution, which has a band No. 2 as intense as that for the piperidine solution. It would be hard to explain this extreme reversal on any other basis than the supposition that for chloroform solution band No. 2 has a large contribution from band No. 3. Thus the simple point-charge molecular field treatment would indicate just what we appear to see.  $\text{CuE}_2$  yields the same result, based on data in Table V:

$$\begin{aligned} \omega_{01}/\omega_{02} &= 1.24; \omega_3 \text{ (predicted)}/\omega_{02} = 0.99; \\ \omega_3 \text{ (pred.)} &= 15350, \\ \omega_3 \text{ (found)} &= 15500. \end{aligned}$$

However, the conclusions of the previous paragraph must be taken with a grain of salt; the assumptions and approximations involved are much too crude to warrant such agreement. Particularly, the value of 1.02 for  $(r^2 r_1^2 / r^4)$  is highly artificial, since it is untenable under our assumption that the ligand and  $\text{Cu}^{++}$  3d charge clouds do not appreciably overlap. Obviously they do overlap, so that the equations (III-37, 38) are not realistic. The expressions (III-32) are better, but cannot be used because they contain as many parameters as the experiments furnish and hence cannot provide useful quantitative predictions.

Be that as it may, expressions (III-32) and (III-37, 38) should both be useful for qualitative predictions. We see that the effect of increasing base strength ( $q$  in (III-37, 38)) of the planar ligands should be that of increasing the over-all splitting and thus of shifting all three absorption bands to higher frequencies. For  $\text{CuA}_2$  and  $\text{CuE}_2$  this prediction is borne out--all three bands of  $\text{CuE}_2$  are at higher frequencies than those of  $\text{CuA}_2$ , as we should expect from the fact that the 3-ethyl group is an electron donor and so should increase the electron density on the four planar ligand oxygen atoms (increase the effective ligand charge). Part I illustrates the same effect for a series of five other variants upon the  $\text{CuA}_2$  molecule, and other examples are to be found in the literature. It is easy to see why chelate stability should be related to the position of the visible absorption bands and so to the color of the complex.<sup>32</sup> In every case observed, the more stable chelates--those formed from the more basic ligand ions--produce absorption farther towards the blue. It must be pointed out here, however, that the base strength of the ligands is only one of several factors affecting complex stability. Strain considerations and other similar variables will also play a part, so that one must be careful even in this correlation.

On the other hand, theory predicts that for a given ligand-metal ion distance the ratios  $\omega_1/\omega_2$  and  $\omega_2/\omega_3$  will be independent of effective ligand charge. It has been shown in a previous paragraph that such is the case for  $\text{CuA}_2$  and  $\text{CuE}_2$ ; the data in Part I seem to indicate that this prediction holds up fairly well for a more varied series of ligands. Of course, one might argue that we do not know the metal-oxygen distances to be the same in all cases. That argument may be answered

by pointing to the  $\text{Cu}^{++} - \text{O}$  distances in hydrated copper salts and in  $\text{CuA}_2$  (as determined by x-ray crystal diffraction). Beever and Lipson<sup>34</sup> determined the  $\text{Cu}^{++} - \text{O}_e$  distance (in the equatorial plane) for  $\text{CuSO}_4 \cdot 5\text{H}_2\text{O}$  to be 1.96 Å, while Koyama, Saito, and Kuroya<sup>27</sup> have determined the  $\text{Cu}^{++} - \text{O}$  distance in acetylacetonato-Cu(II) ( $\text{CuA}_2$ ) to be 1.96 Å. It seems likely, therefore, that where ring strain does not forbid, the  $\text{Cu}^{++} - \text{O}$  distance in any such complex, at least in the crystalline state, may be assumed to have the same value. (The near equality of  $\text{Cu}^{++} - \text{O}$  distances in complexes that have heretofore been considered so widely different as have the hydrates and the acetylacetonates is strongly suggestive that they are after all likely not so different. Professor Connick<sup>35</sup> has pointed out that the energy differences between the various complexes and chelates of a given transition metal ion never cover a very wide range.)

#### Allowance for covalency: LCAO-MO treatment

Now it should be worth while to consider what covalent binding may be admitted and how such bonding will affect the spectral predictions previously made. The Pauling valence bond ideas, which have been discussed in the introductory section of this part, could be adapted for this purpose. It seems to me, however, that a clearer picture might be obtained from a treatment that has received little attention in the consideration of metal chelate compounds (some examples of its application, however, will be found in works by Seely,<sup>36</sup> Owen,<sup>33</sup> and McGarvey<sup>37</sup>)--namely, the LCAO-MO (Linear Combination of Atomic Orbitals--Molecular Orbital) treatment. Here we will consider the crystal field splitting as already accomplished and simply graft the LCAO-MO treatment onto the crystal field results. Since no accurate quantitative results can be expected from the treatment in any case, the question of which is the dominant interaction and which the perturbation upon that principal effect can be dispensed with. The development of the required molecular orbital treatment is traced in Part III, and Fig. 17 will be most useful to the present discussion. It will illustrate the following points.

The position of the odd electron is not determined by the type of bonding, but instead by the separation between atomic energy levels



and subsequently by the magnitude of bonding energy. The Pauling picture, as was previously noted, claims that when a bond is formed from two atomic orbitals, there can be accommodation for only two electrons. The bonding scheme in Part III shows, however, that when the xy orbital of  $\text{Cu}^{++}$  and a four-oxygen orbital combine, there are two resulting orbitals--one antibonding and one bonding. Now, two electrons may be accommodated in the bonding orbital, but a third electron may be placed in the antibonding one. (If a fourth electron were available, it could reside there also.) In the simple treatment, the net bonding energy is the same as for a one-electron bond. The four oxygen orbitals ( $\sigma$ -type) may also combine with a  $\text{Cu}^{++}$  4s and two 4p orbitals to complete a total set of four bonding and four antibonding orbitals-- $2E_u$ ,  $A_{1g}$ ,  $B_{2g}$ . The four bonding ones, which can accommodate eight electrons, are equivalent to the four  $dsp^2$  hybrid bonds in the Pauling formulation. But the odd electron is still in the xy orbital, which forms the major part of the  $B_{2g}$ -a orbital. The transition to the Pauling picture occurs if the bond formed between the xy orbital and the oxygens has so much stabilization energy that its antibonding level,  $B_{2g}$ -a, is raised above the  $p_z$  (or  $A_{2u}$ -a) level. When this happens, the odd electron will of course go into the lowest-energy orbital available, the  $A_{2u}$ -a. However, it is interesting to note that if pi-bonding to the  $p_z$  orbital is important energywise, the Pauling picture is even harder to attain, since the  $A_{2u}$ -a level will itself be raised above the original  $p_z$  energy.

In fact, one can at the present time state with certainty that for  $\text{CuA}_2$  the unpaired electron is in a d orbital with its maximum extension in the x, y plane. This fact has been experimentally established by the paramagnetic resonance measurements performed by Dr. B. R. McGarvey with  $\text{CuA}_2$  samples supplied by the writer. From Part IIID we see that for the odd electron to be in the  $p_z$  orbital, it must display  $g_{\parallel} < g_{\perp}$ . However, McGarvey's values for  $\text{CuA}_2$  single crystal at room temperature are  $g_{\parallel} = 2.25 \pm 0.02$ ;  $g_{\perp} = 2.071 \pm 0.002$ . As the account of resonance interpretation shows, for the electron in the xy orbital,  $(g_{\parallel} - 2)/(g_{\perp} - 2) = 4\omega_1/\omega_2$  in the case of a purely ionic bond to surrounding ligands. Greater or smaller values for that ratio are obtained if one allows bonding via the molecular orbital scheme here described.

Then, knowing that the unpaired electron resides where it is shown in our MO scheme, we can ask what should happen to transitions  $\omega_1$ ,  $\omega_2$ , and  $\omega_3$  as the coordinating tendency of various ligands becomes greater.

1. Sigma bonding to the xy orbital. The  $B_{2g}$ -a level is raised as base strength (coordinating tendency) of the four planar ligands increases. If the remaining three levels remain unaffected,  $\omega_1$ ,  $\omega_2$ , and  $\omega_3$  all increase. This agrees with the crystal field result and with experiment. As the axial ligands become better bases, there is no effect upon the  $B_{2g}$ -a level, so that  $\omega_1$ ,  $\omega_2$ , and  $\omega_3$  would be unaffected.

2. Sigma bonding to the  $2z^2 - x^2 - y^2$  orbital. The  $A_{1g}^*$ -a level is raised as growing base strength of planar ligands increases sigma bonding with the "charge doughnut" of this orbital, and  $\omega_3$  should be a little less than it would if this effect could not occur. However, since the doughnut is quite diffuse, overlap and exchange energy must certainly be much smaller than for the xy sigma bonding, so that the effect of Item 1 should not be overpowered. As axial ligands become better covalent coordinators, on the other hand, the  $A_{1g}^*$ -a level is raised and  $\omega_3$  decreases,  $\omega_1$  and  $\omega_2$  remaining unaltered. This does not contradict experimental findings.

3. Pi bonding to the xz, yz orbitals. Increasing pi-bonding tendency of the planar ligands would serve to raise the  $E_g$ -a level, producing a decrease in  $\omega_1$  and no change in  $\omega_2$ ,  $\omega_3$ . (Increasing axial pi-bonding tendency, which I feel cannot be important enough to be included in the bonding scheme, would give the same result.)

4. In-plane pi bonding to the  $x^2 - y^2$  orbital. This would be unaffected by axial changes. Planar ligands, as they increased in tendency to form such bonds, would cause the  $B_{1g}$ -a level (on the scheme called  $B_{1g}$ -n because the in-plane pi bonding was omitted altogether in development of the ideas) to increase, and so cause a decrease in  $\omega_2$  and no change in  $\omega_1$ ,  $\omega_3$ .

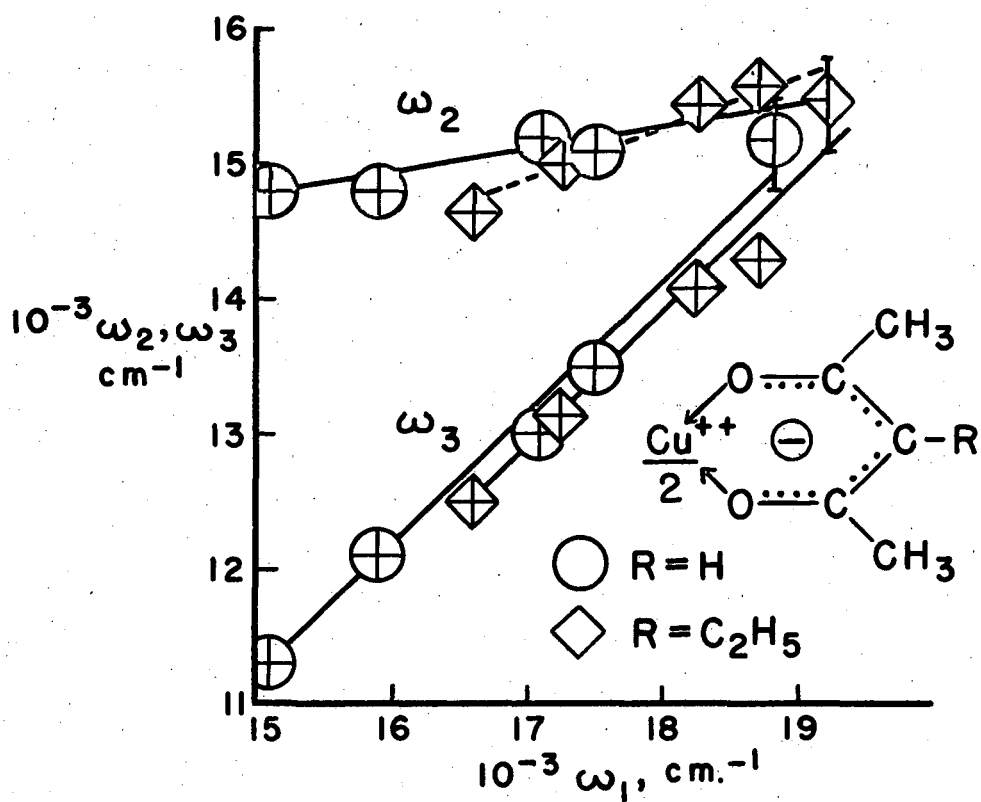
Experimental results are in real conflict only with the supposition that Items 3 and 4 are important effects energywise. We may conclude that various ligands attached to a  $Cu^{++}$  ion affect its d-orbital energy levels differently primarily because of differences in crystalline field interaction and in sigma bonding rather than in pi bonding.

Other remarks regarding the data of Part II

Various correlations between half widths, intensities, and positions of component bands can be made. The fact that most of these show smooth variation of one property with respect to another, although no such variation was sought during execution of the analyses, is possible evidence that the three bands obtained are real ones. Two such plots are shown in Figs. 14 and 15.

Figure 14 illustrates for  $\text{CuA}_2$  and for  $\text{CuE}_2$  the correlation of the positions of Band 2 and of Band 3 with that of Band 1. The first point to be noted is that, while  $\omega_2$  in each case shows only a small change as solvents become more basic, that change is generally towards lower frequencies. This effect may be attributed to the repulsion of square-planar ligand electrons by the incoming highly polarized axial groups; such repulsion would cause a decrease in over-all crystal field splitting and in the  $B_{2g}$ -a level. Again, the fact that  $\omega_3$  is apparently a very smooth function of  $\omega_1$  shows that the analyses into components yielded smooth variation of properties where little was demanded.

Figure 15 illustrates one of many plots that could be made of band intensities vs positions. Such correlations are generally better for  $\text{CuA}_2$  than for  $\text{CuE}_2$ , in line with footnote (c) to Table V. In the correlation shown, the total integrated intensity of Bands 2 and 3 is plotted vs Band 3 position. A sum of intensities was used so that the chloroform points could be included. Here I have no explanation why the points follow the form of curve shown. It does seem reasonable, however, that as the chelate molecules are subjected to stronger and stronger solvent electric fields, the probabilities for the 3d-3d transitions may increase. Holmes and McClure<sup>17</sup> suppose that the transitions, formally forbidden ones, are made allowed by vibrations of the surroundings. On this assumption, one would expect higher transition probabilities as more ligands able to execute such vibrations are added. This argument, of course, is merely in the nature of a reasonable speculation. At any rate, it is here again apparent that there are correlations where none were sought in the actual work of analysis.



MU-9666

Fig. 14. Correlation of positions of Bands 2 and 3 with that of Band 1.  $\bigcirc$  = CuA<sub>2</sub>;  $\diamond$  = CuE<sub>2</sub>.

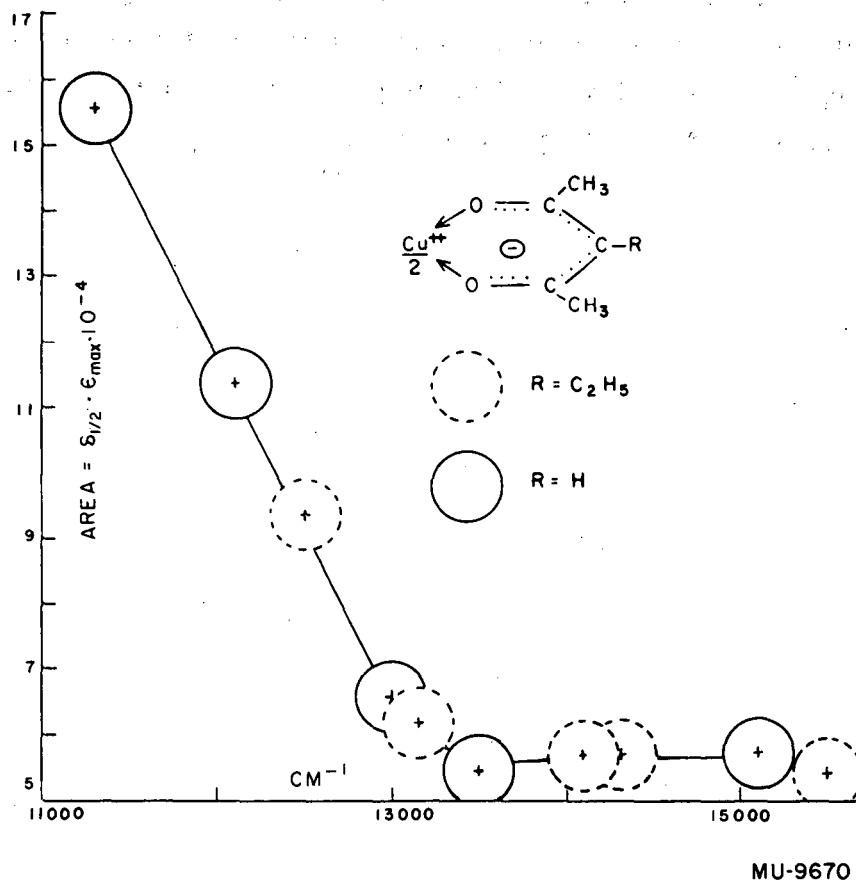


Fig. 15. Area under Bands 2 and 3 vs. Band 3 absorption maxima.

Summary of Part II

Absorption spectra of Cu(II) bisacetylacetonate and its 3-ethyl variant are reported for solutions in solvents ranging from low to high effectiveness as Lewis bases. The spectra could arise from a set of three Gaussian component bands whose positions and intensities are shown to depend primarily upon the solvent basicity. The bands are identified with three transitions predicted from the crystal field and molecular orbital theories described in Part III. The behavior of these transitions upon changing solvent and upon changing chelate ring substituents is shown to be consistent with the postulate that crystal field splitting changes and sigma-bonding changes are energetically more important than pi-bonding changes.

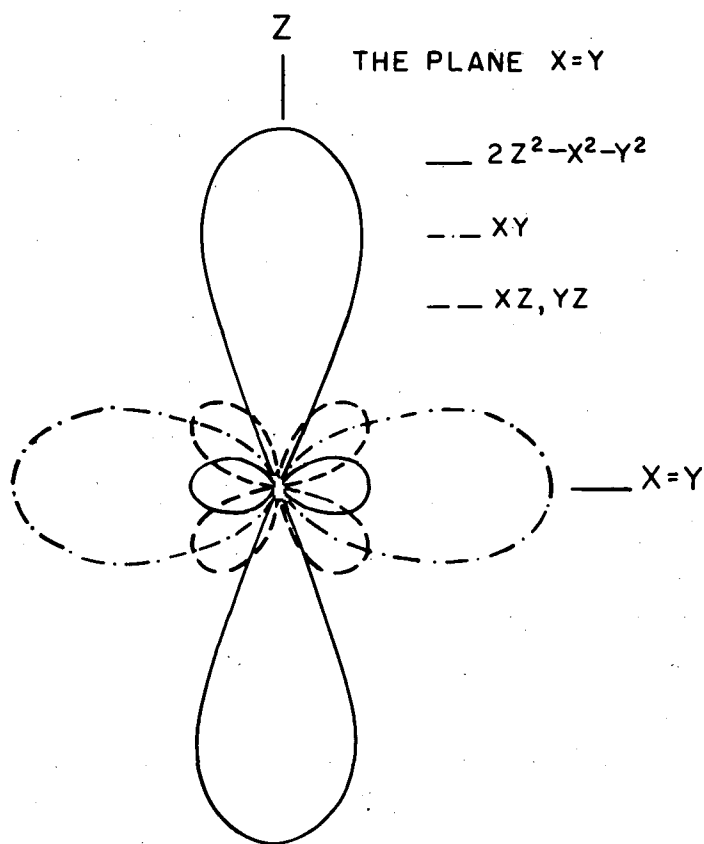
### III. DEVELOPMENT OF THEORETICAL TREATMENTS FOR COPPER CHELATE COMPOUNDS

In this part are (A) an account of a molecular orbital scheme for copper chelate binding, (B) a record of some attempts to treat the ligand pi system by the molecular orbital method (with one successful calculation regarding the ultraviolet absorption of acetylacetonate enol and its divalent cation chelates), (C) a demonstration of the crystal (molecular) field treatment of  $\text{Cu}^{++}$  chelates, with calculations for some simple point-charge and finite dipole models, and (D) an account of calculations showing the possible use of paramagnetic resonance results as an aid in interpreting  $\text{Cu}^{++}$  chelate binding.

#### A. LCAO-MO $\text{Cu}^{++}$ Chelate Scheme

The theory of groups and their application to the classification of molecular orbitals as to symmetry and to factoring the secular determinant are found in a number of books.<sup>38, 39, 40, 41, 43</sup> The notations and concepts given there are assumed throughout the following discussions. Also, the ideas and approximations behind a simple LCAO-MO treatment are well known<sup>40, 41, 42, 44</sup> and are, for the most part, assumed.

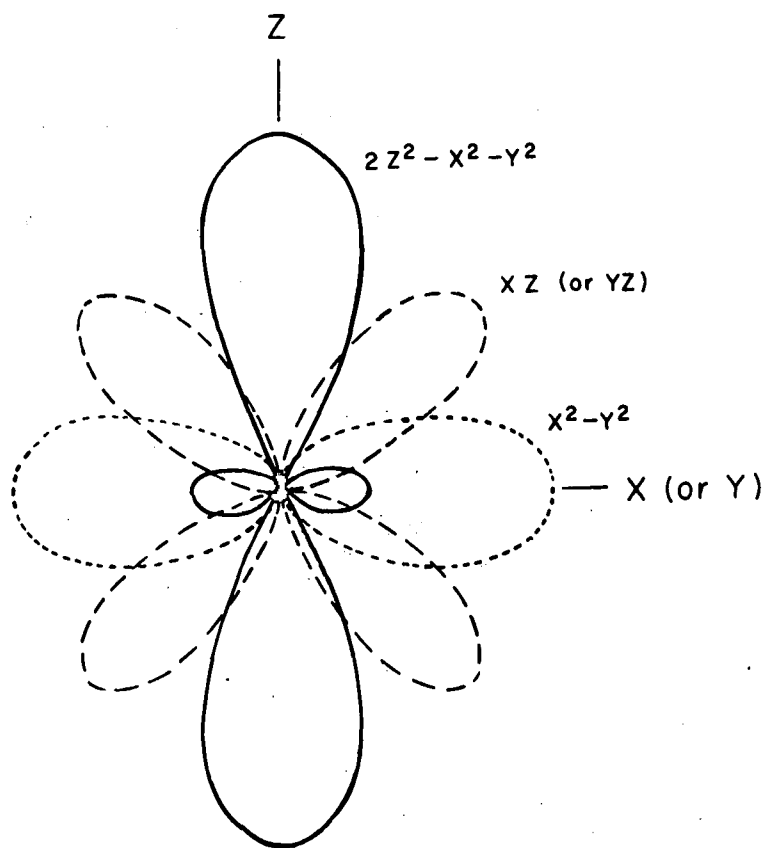
We consider a  $\text{Cu}^{++}$  ion with the following set of orbitals that might be available for bonding:  $d(xy)$ ,  $d(x^2 - y^2)$ ,  $d(xz)$ ,  $d(yz)$ ,  $d(2z^2 - x^2 - y^2)$ --also called  $d_0$  or  $d_{z^2}$  for convenience--,  $s$ ,  $p(x)$ ,  $p(y)$ , and  $p(z)$ . Each function has the angular variation given by the argument; that variation is shown for the five d-orbitals in Fig. 16 a, b, c. (Note that the radial distance for those figures represents not radial distance in space,  $r$ , but rather the magnitude of electron density for fixed  $r$ .) Now we take a set of fourteen orbitals which might be furnished by six surrounding ligands placed as shown.



MU-9673

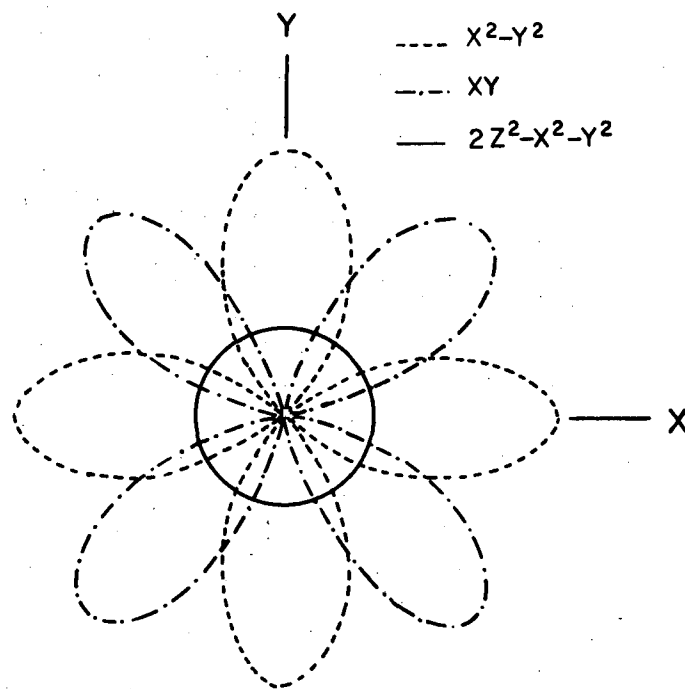
Fig. 16a. Angular variation of electron density in 3d orbitals.





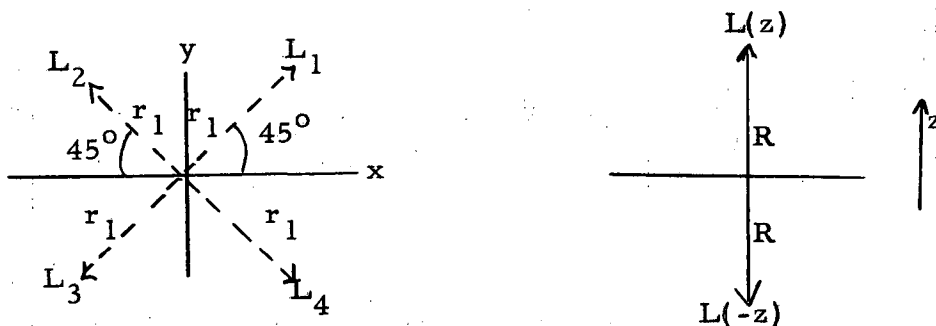
MU-9675

Fig. 16b. Angular variation of electron density in 3d orbitals.



MU-9674

Fig. 16c. Angular variation of electron density in 3d orbitals.



The Cu nucleus is here taken as the center of the coordinate system. Twelve of the ligand orbitals would arise from L<sub>1</sub>, L<sub>2</sub>, L<sub>3</sub>, and L<sub>4</sub> thus: For each, there would be an orbital directed along the internuclear axis (45° line), called  $\sigma_1, \sigma_2, \sigma_3, \sigma_4$ ; one p orbital directed perpendicular to the 45° line, having a node perpendicular to the xy plane and containing the 45° line, called  $t_1, t_2, t_3, t_4$ ; and one p<sub>z</sub> orbital with the xy plane as node, called  $\pi_1, \pi_2, \pi_3, \pi_4$ . The remaining two ligands, L(z) and L(-z), are assumed to have orbitals directed along the z-axis toward the Cu nucleus; they are named  $\sigma(z)$  and  $\sigma(-z)$ .

Now we make use of an assumed symmetry for the complex: D<sub>4h</sub>. The transformation table for the orbitals listed above, under the symmetry operations of group D<sub>4h</sub>, is given in Table VI. The  $\chi$ -row gives the characters for the 23-dimensional reducible representation (of the group) having the original atomic orbital functions as basis. They are found by setting, for each position in a row of the table, "1" wherever the first element of that row is repeated, and "0" otherwise; these are then added columnwise. To reduce the 23-by-23 secular determinant we break the 23-dimensional representation into a sum of irreducible ones, using the relationships of Eqs. (III-1) and (III-2):

$$n_i = (1/g) \sum_{s=1}^g \chi_s \chi_{is} \quad \text{(III-1)}$$

$$\phi_r(\Gamma_i) = \sum_{s=1}^g \chi_{is} P_s \phi_r^0, \quad \text{(III-2)}$$

where i labels a particular irreducible representation,  $\Gamma_i$ ; s labels

Table VI

Transformations of Orbitals,  $D_{4h}$ 

E	$C_2$	$2C_4$	$2C_{2'}$	$2C_{2''}$	i	$\sigma_h$	$2S_4$	$2\sigma_{v'}$	$2\sigma_{v''}$
$d_{xy}$	$d_{xy}$	$-d_{xy}$	$-d_{xy}$	$d_{xy}$	$d_{xy}$	$d_{xy}$	$-d_{xy}$	$-d_{xy}$	$d_{xy}$
$d_{x^2-y^2}$	$d_{x^2-y^2}$	$-d_{x^2-y^2}$	$d_{x^2-y^2}$	$-d_{x^2-y^2}$	$d_{x^2-y^2}$	$d_{x^2-y^2}$	$-d_{x^2-y^2}$	$d_{x^2-y^2}$	$-d_{x^2-y^2}$
$d_{xz}$	$-d_{xz}$	$\mp d_{yz}$	$\mp d_{xz}$	$\mp d_{yz}$	$d_{xz}$	$-d_{xz}$	$\mp d_{yz}$	$\mp d_{xz}$	$\pm d_{yz}$
$d_{yz}$	$-d_{yz}$	$\pm d_{xz}$	$\pm d_{yz}$	$\pm d_{xz}$	$d_{yz}$	$-d_{yz}$	$\pm d_{xz}$	$\pm d_{yz}$	$\pm d_{xz}$
$d_0$	$d_0$	$d_0$	$d_0$	$d_0$	$d_0$	$d_0$	$d_0$	$d_0$	$d_0$
$p_x$	$-p_x$	$\mp p_y$	$\pm p_x$	$\pm p_y$	$-p_x$	$p_x$	$\pm p_y$	$\mp p_x$	$\pm p_y$
$p_y$	$-p_y$	$\pm p_x$	$\mp p_y$	$\pm p_x$	$-p_y$	$p_y$	$\mp p_x$	$\pm p_y$	$\pm p_x$
$p_z$	$p_z$	$p_z$	$-p_z$	$-p_z$	$-p_z$	$-p_z$	$-p_z$	$p_z$	$p_z$
s	s	s	s	s	s	s	s	s	s
$\sigma_1$	$\sigma_3$	$\sigma_{4,2}$	$\sigma_{4,2}$	$\sigma_{3,1}$	$\sigma_3$	$\sigma_1$	$\sigma_{2,4}$	$\sigma_{2,4}$	$\sigma_{3,1}$
$\sigma_2$	$\sigma_4$	$\sigma_{1,3}$	$\sigma_{3,1}$	$\sigma_{2,4}$	$\sigma_4$	$\sigma_2$	$\sigma_{3,1}$	$\sigma_{1,3}$	$\sigma_{2,4}$
$\sigma_3$	$\sigma_1$	$\sigma_{2,4}$	$\sigma_{2,4}$	$\sigma_{1,3}$	$\sigma_1$	$\sigma_3$	$\sigma_{4,2}$	$\sigma_{4,2}$	$\sigma_{1,3}$
$\sigma_4$	$\sigma_2$	$\sigma_{3,1}$	$\sigma_{1,3}$	$\sigma_{4,2}$	$\sigma_2$	$\sigma_4$	$\sigma_{1,3}$	$\sigma_{3,1}$	$\sigma_{4,2}$

Table VI (continued)

E	$C_2$	$2C_4$	$2C_2'$	$2C_2''$	i	$\sigma_h$	$2S_4$	$2\sigma_v'$	$2\sigma_v''$	
$\pi_1$	$\pi_3$	$\pi_{4,2}$	$-\pi_{4,2}$	$-\pi_{3,1}$	$-\pi_3$	$-\pi_1$	$-\pi_{2,4}$	$\pi_{2,4}$	$\pi_{3,1}$	
$\pi_2$	$\pi_4$	$\pi_{1,3}$	$-\pi_{3,1}$	$-\pi_{2,4}$	$-\pi_4$	$-\pi_2$	$-\pi_{3,1}$	$\pi_{1,3}$	$\pi_{2,4}$	
$\pi_3$	$\pi_1$	$\pi_{2,4}$	$-\pi_{2,4}$	$-\pi_{1,3}$	$-\pi_1$	$-\pi_3$	$-\pi_{4,2}$	$\pi_{4,2}$	$\pi_{1,3}$	
$\pi_4$	$\pi_2$	$\pi_{3,1}$	$-\pi_{1,3}$	$-\pi_{4,2}$	$-\pi_2$	$-\pi_4$	$-\pi_{1,3}$	$\pi_{3,1}$	$\pi_{4,2}$	
$t_1$	$t_3$	$t_{4,2}$	$-t_{4,2}$	$-t_{3,1}$	$t_3$	$t_1$	$t_{2,4}$	$-t_{2,4}$	$-t_{3,1}$	
$t_2$	$t_4$	$t_{1,3}$	$-t_{3,1}$	$-t_{2,4}$	$t_4$	$t_2$	$t_{3,1}$	$-t_{1,3}$	$-t_{2,4}$	
$t_3$	$t_1$	$t_{2,4}$	$-t_{2,4}$	$-t_{1,3}$	$t_1$	$t_3$	$t_{4,2}$	$-t_{4,2}$	$-t_{1,3}$	
$t_4$	$t_2$	$t_{3,1}$	$-t_{1,3}$	$-t_{4,2}$	$t_2$	$t_4$	$t_{1,3}$	$-t_{3,1}$	$-t_{4,2}$	
$\sigma(z)$	$\sigma(z)$	$\sigma(z)$	$\sigma(-z)$	$\sigma(-z)$	$\sigma(-z)$	$\sigma(-z)$	$\sigma(-z)$	$\sigma(z)$	$\sigma(z)$	
$\sigma(-z)$	$\sigma(-z)$	$\sigma(-z)$	$\sigma(z)$	$\sigma(z)$	$\sigma(z)$	$\sigma(z)$	$\sigma(z)$	$\sigma(-z)$	$\sigma(-z)$	
$\chi_s$	23	3	3	1	-1	3	7	-1	5	7

group elements;  $g$  is the number of group elements;  $P$  is a group element;  $\chi$  is a character;  $\phi_r^0$  is an initial orbital function; and  $\phi_r(\Gamma_i)$  is a linear combination of orbital functions which belongs to the  $i$ th irreducible representation.<sup>38, 39</sup> Using Herzberg's Table 23<sup>43</sup> together with our Table VI and the above, we obtain for the  $n_i$  and  $\phi_r(\Gamma_i)$  the groupings of Table VII.

Symbols for the usual LCAO-MO integrals are defined as follows:

$$Q_{\phi_r} = \int \overline{\phi_r} H \phi_r d\tau, \text{ the "Coulomb integral";} \quad (\text{III-3})$$

$$\beta_{\phi_r \phi_j} = \int \overline{\phi_r} H \phi_j d\tau, \text{ the "exchange integral",}$$

where  $H$  is the Hamiltonian for the problem. If the true wave functions,  $\psi(\Gamma_i)$ , are assumed to be linear variation functions of the  $\phi(\Gamma_i)$ ,

$$\psi_k(\Gamma_i) = \sum_{r=1}^{n_i} a_{kr} \phi_r(\Gamma_i); \quad (\text{III-4})$$

then if we (a) consider the  $\phi_r$  as an orthonormal set, (b) neglect overlap (except as it is corrected for in the choice of Coulomb and exchange integrals) and neglect all direct inter-ligand exchange and all other perturbations, (c) set  $\beta_{rj} = \beta_{jr}$ , and (d) take account of the equivalence of  $L_1 \dots L_4$ , of  $L(z)$  and  $L(-z)$ , of  $p(x)$  and  $p(y)$ , and of  $d_{xz}$  and  $d_{yz}$ , the energy levels for our simple system are the solutions  $W$  to the secular Equations (III-5 to III-12).

$$A_{1g} \begin{vmatrix} Q_s - W & 2\beta_{s, \sigma_1} & 0 & \sqrt{2}\beta_{s, \sigma(z)} \\ 2\beta_{s, \sigma_1} & Q_{\sigma_1} - W & 2\beta_{d_0, \sigma_1} & 0 \\ 0 & 2\beta_{d_0, \sigma_1} & Q_{d_0} - W & \sqrt{2}\beta_{d_0, \sigma(z)} \\ \sqrt{2}\beta_{s, \sigma(z)} & 0 & \sqrt{2}\beta_{d_0, \sigma(z)} & Q_{\sigma(z)} - W \end{vmatrix} = 0 \quad (\text{III-5})$$

Table VII

Reduction of the 23-Dimensional Representation into Irreducible Blocks, with New Basis		
Functions		
$\Gamma_i$	$n_i$	$\phi_r(\Gamma_i)$ --normalized
$A_{1g}$	4	$\begin{cases} s \\ d(2z^2 - x^2 - y^2) = d_0 \\ \Sigma_+ = (\sigma_1 + \sigma_2 + \sigma_3 + \sigma_4)/2 \\ Z_+ = [\sigma(z) + \sigma(-z)]/\sqrt{2} \end{cases}$
$A_{1u}$	0	
$A_{2g}$	1	$T_+ = (t_1 + t_2 + t_3 + t_4)/2$
$A_{2u}$	3	$\begin{cases} p(z) \\ \Pi_+ = (\pi_1 + \pi_2 + \pi_3 + \pi_4)/2 \\ Z_- = [\sigma(z) - \sigma(-z)]/\sqrt{2} \end{cases}$
$B_{1g}$	2	$\begin{cases} d(x^2 - y^2) \\ T_- = (t_1 - t_2 + t_3 - t_4)/2 \end{cases}$
$B_{1u}$	1	$\Pi_- = (\pi_1 - \pi_2 + \pi_3 - \pi_4)/2$
$B_{2g}$	2	$\begin{cases} d(xy) \\ \Sigma_- = (\sigma_1 - \sigma_2 + \sigma_3 - \sigma_4)/2 \end{cases}$
$B_{2u}$	0	
$E_g$	2	$\begin{cases} d(xz) \\ \Pi_1 = (\pi_1 - \pi_2 - \pi_3 + \pi_4)/2 \end{cases}$
		degenerate with
		$\begin{cases} d(yz) \\ \Pi_2 = (\pi_1 + \pi_2 - \pi_3 - \pi_4)/2 \end{cases}$

Table VII (continued)

$\Gamma_i$	$n_i$	$\phi_r(\Gamma_i)$ --normalized
$E_u$	3	$\begin{cases} p(x) \\ \Sigma_1 = (\sigma_1 - \sigma_2 - \sigma_3 + \sigma_4)/2 \\ T_1 = (t_1 + t_2 - t_3 - t_4)/2 \end{cases}$ <p style="text-align: center;">degenerate with</p> $\begin{cases} p(y) \\ \Sigma_2 = (\sigma_1 + \sigma_2 - \sigma_3 - \sigma_4)/2 \\ T_2 = (t_2 - t_1 + t_3 - t_4)/2 \end{cases}$



$$A_{2u} \begin{vmatrix} Q_{p(z)} - W & 2\beta_{p(z), \pi_1} & \sqrt{2}\beta_{p(z), \sigma(z)} \\ 2\beta_{p(z), \pi_1} & Q_{\pi_1} - W & 0 \\ \sqrt{2}\beta_{p(z), \sigma(z)} & 0 & Q_{\sigma(z)} - W \end{vmatrix} = 0 \quad (\text{III-7})$$

$$B_{1g} \begin{vmatrix} Q_{d(x^2-y^2)} - W & 2\beta_{d(x^2-y^2), t_1} \\ 2\beta_{d(x^2-y^2), t_1} & Q_{t_1} - W \end{vmatrix} = 0 \quad (\text{III-8})$$

$$A_{2g} \quad W = Q_{t_1} \quad (\text{III-6})$$

$$B_{1u} \quad W = Q_{\pi_1} \quad (\text{III-9})$$

$$B_{2g} \begin{vmatrix} Q_{d(xy)} - W & 2\beta_{d(xy), \sigma_1} \\ 2\beta_{d(xy), \sigma_1} & Q_{\sigma_1} - W \end{vmatrix} = 0 \quad (\text{III-10})$$

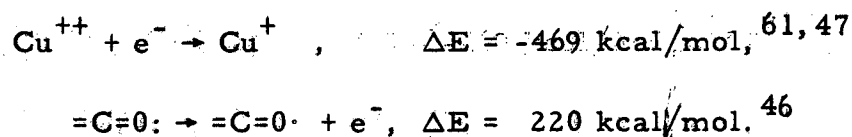
$$E_g \begin{vmatrix} Q_{d(yz)} - W & 2\beta_{d(yz), \pi_1} \\ 2\beta_{d(yz), \pi_1} & Q_{\pi_1} - W \end{vmatrix}^2 = 0 \quad (\text{III-11})$$

$$E_u \begin{vmatrix} Q_{p(y)} - W & 2\beta_{p(y), \sigma_1} & 2\beta_{p(y), t_1} \\ 2\beta_{p(y), \sigma_1} & Q_{\sigma_1} - W & 0 \\ 2\beta_{p(y), t_1} & 0 & Q_{t_1} - W \end{vmatrix}^2 = 0 \quad (\text{III-12})$$

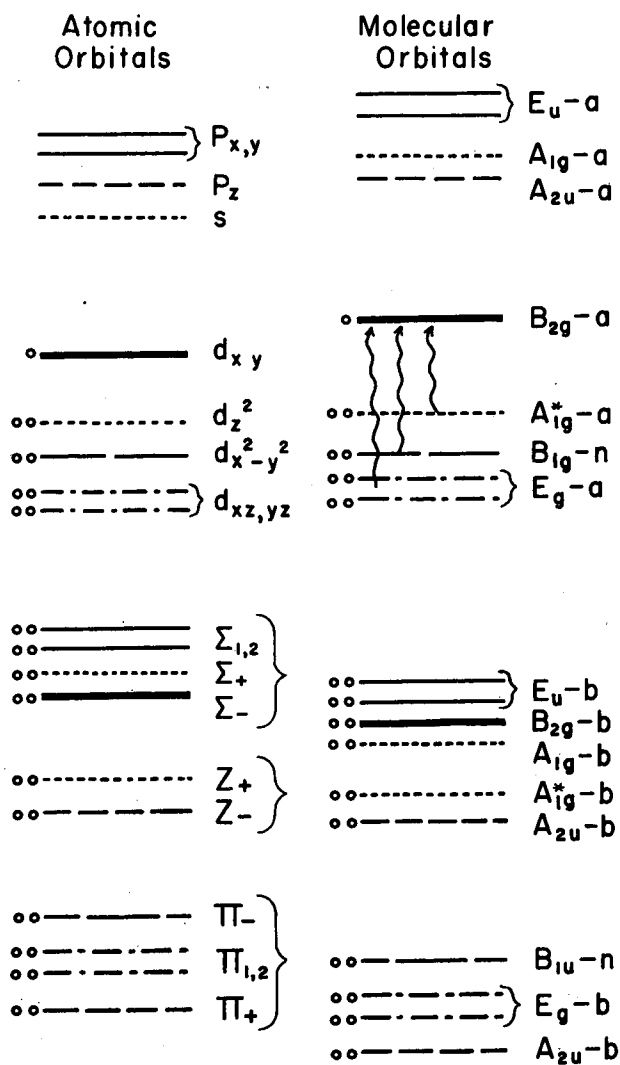
Without solving the secular equations specifically one can obtain an idea of how atomic energy levels should change upon entering into the above combinations. When two or more energy states perturb one another there is a general spreading of levels. Also, if two or more energy levels diverge because of molecular orbital formation, to preserve the center of symmetry of the energies the upper half, approximately, of atomic orbital levels increase their energy in forming anti-bonding molecular orbitals. The remainder decrease in energy and

form bonding orbitals. A molecular orbital is called nonbonding if its energy is unchanged from one of the atomic orbital levels; quite often it is just an atomic orbital itself. We already know what orbitals of our system can combine, so that if we can get a notion of how the atomic orbital energy levels lie (this amounts to approximations to the  $Q$ 's), then we can say how the molecular energy levels will diverge.

To obtain approximate values for  $Q(\text{Cu}^{++} 3d) - Q(\text{oxygen})$ -- lumping for the moment the d-orbitals together and the oxygen orbitals together--one can take the ionization potentials for  $\text{Cu}^+$  and for a keto compound and then correct for the electrostatic change in energy upon electron transfer:



Assume  $0.6 e^-$  charge per oxygen,  $1.9 \text{ \AA}$  Cu-O distance. Then the electrostatic energy change in the above transfer, including interligand repulsion, is, for four oxygens about the  $\text{Cu}^{++}$ ,  $\Delta E = 388 \text{ kcal/mol}$ . Thus the total energy of transfer is  $\Delta E = \text{ca } 140 \text{ kcal/mol}$ . Actually, the  $=\text{C}=\text{O}$  ionization potential, taken as the ethyl acetate value, would be expected to be somewhat smaller because of polarization by the dipositive cation.<sup>44</sup> It seems likely, then, that the  $Q_d$ 's should lie somewhere between 0 and  $160 \text{ kcal/mol}$  higher than the  $Q_{(\text{oxygen})}$ 's. Also, for resonating chelate anion chains or rings, the pi-type orbitals will probably be at somewhat lower energy than the  $\sigma$ 's and t's. With these points in mind, and taking the 4s and 4p levels as somewhat higher than the 3d levels and supposing the d's and p's are already split by the ligand crystalline electric field (see Part III. C), we would draw the molecular levels as shown in Fig. 17. (The contribution of the t orbitals has not been included. If it were,  $B_{1g} - n$  would become  $B_{1g} - a$  and would be a little raised. Also, the  $E_u - a$  level would be somewhat raised.) The kind of line used to indicate a molecular energy level relates it to its parent atomic orbitals. (The discussion of Part II is based on this diagram.)



MU-9378

Fig. 17. Energy level scheme in a tetragonal  $\text{Cu}^{++}$  chelate.  
 o : Location of an electron.  
 † : Three postulated transitions, invisible and infrared.  
 } : Bracket denotes one degenerate level.  
 a : "antibonding".                      b : "bonding".  
 n : "nonbonding".

It is possible to solve the secular equations, of course, if we have values for the parameters  $Q$  and  $\beta$ . Conjugately, if we know the  $a_{kr}$  of Eq. (III-4), then only one of the quantities  $W$ ,  $Q$ ,  $\beta$  is needed to find the others. For a discussion of the d-electrons of  $\text{Cu}^{++}$ , Expressions (III-6), (III-9), and (III-12) are of only secondary interest. If, for simplicity, we ignore the axial ligands and the s and p orbitals of  $\text{Cu}^{++}$ , then there are only quadratics remaining whose solutions are

$$W(A_{1g}) = \frac{(Q_{d_0} + Q_{\sigma_1}) \pm \sqrt{(Q_{d_0} - Q_{\sigma_1})^2 + 16\beta_{d_0, \sigma_1}^2}}{2}, \quad (\text{III-13})$$

$$W(B_{1g}) = \frac{(Q_{d(x^2-y^2)} + Q_{t_1}) \pm \sqrt{(Q_{d(x^2-y^2)} - Q_{t_1})^2 + 16\beta_{d(x^2-y^2), t_1}^2}}{2}, \quad (\text{III-14})$$

$$W(B_{2g}) = \frac{(Q_{d(xy)} + Q_{\sigma_1}) \pm \sqrt{(Q_{d(xy)} - Q_{\sigma_1})^2 + 16\beta_{d(xy), \sigma_1}^2}}{2}, \quad (\text{III-15})$$

$$W(E_g) = \frac{(Q_{d(yz)} + Q_{\pi_1}) \pm \sqrt{(Q_{d(yz)} - Q_{\pi_1})^2 + 16\beta_{d(yz), \pi_1}^2}}{2}. \quad (\text{III-16})$$

Now Eq. (III-4) becomes, for the antibonding combination of any particular d-function  $d_j$  with its proper oxygen function  $O_j$

$$\psi_{j-a} = c_j d_j - \sqrt{1 - c_j^2} O_j. \quad (\text{III-17})$$

We can define a "percent ionicity" for antibonding orbital  $j$  by choosing a function which is 100% for  $c^2 = 1$ , 0% for  $c^2 = 0.5$ , and 100% for  $c^2 = 0$ ; the simplest such function is

$$I = [c^2 - (1 - c^2)] \cdot 100 = \text{"\% Ionicity."} \quad (\text{III-18})$$

In Table VIII are given, for various values of  $(Q_{d_j} + Q_{O_j})$  and for various percent ionicities, the one-electron stabilization energy for the  $d_j, O_j$  bonding.

How might the magnitudes of the numbers in Table VIII yield some information about the spectra of Part II? First, if  $j$  is  $xy$ , the

Table VIII

Raising of the  $\psi_{j-a}$  level above its parent d-orbital level, in  $\text{cm}^{-1}$ .  
 Tabular entries are  $W_{j-a} - Q_{dj}$  (for  $Q_{0j}$  as zero point of energy).

I	c	$Q_{dj}$ , kcal/mol						
		15	30	45	60	90	120	150
100	% 1.00	0	0	0	0	0	0	0
80.5	% 0.95	634	1268	1902	2536	3804	5072	6340
62	% 0.90	1602	3204	4806	6408	9612	12816	16020
44.5	% 0.85	3300	6600	9900	13200	19800	26400	33000
28	% 0.80	6800	13600	20400	27200	40800	54400	68000
12.5	% 0.75	18500	37000	55500	74000	111000	148000	185000

entries give crudely calculated covalent contributions to the three transitions  $\omega_1$ ,  $\omega_2$ , and  $\omega_3$  ( $E_g - a \rightarrow B_{1g} - n \rightarrow$ , and  $A_{1g} - a \rightarrow B_{2g} - a$ ). For  $I = 80.5\%$ , the value  $Q = 120$  kcal/mol--our estimated value--gives a 5000 wavenumber contribution of sigma bonding to all three transitions, while the observed  $\omega_2$  is ca 15,000  $\text{cm}^{-1}$  for  $\text{CuA}_2$ . The covalent contribution to the spectra would be quite large (perhaps even larger than just mentioned); this is probably the chief reason why direct calculation of crystal field splitting has always yielded values apparently much too low, providing reasonable radial distribution functions were assumed for the central ion. (For example, see the very nice calculations of Kleiner<sup>48</sup> for  $\text{Cr} \cdot 6\text{H}_2\text{O}^{+++}$ , which yielded a splitting factor of 550  $\text{cm}^{-1}$  instead of the observed 1000-2000  $\text{cm}^{-1}$ . Kleiner used as radial function for  $\text{Cr}^{+++}$  that calculated for  $\text{Cr}^{++}$  by Mooney<sup>49</sup> using the SCF method.)

On the other hand, for very small  $Q_j$ , even considerable covalency could yield only minor energy effects. Professor Pitzer<sup>30</sup> has suggested that perhaps the t atomic levels lie somewhat higher in energy than the  $\sigma_{1...4}$  and  $\pi_{1...4}$ . Together with the crystal field splitting, which brings the  $d(x^2 - y^2)$  level lower than the  $d(xy)$ , there may be a situation such that  $Q_{t_1}$  is very near  $Q_{d(x^2 - y^2)}$ . This would explain why the spectra in Parts I and II seem to show pi bonding to be less important than sigma bonding for bidentate chelates of  $\text{Cu}^{++}$ , but the paramagnetic resonance spectra seem to show the reverse for  $\text{CuA}_2$  crystals.<sup>37</sup> (See also Part III. D.) The visible spectra show energy effects in bond formation, while the paramagnetic resonance results depend directly upon the coefficients  $c_j$ , regardless of whether or not there is any significant exchange energy.

As noted previously, the  $Q_n$  level will likely lie lowest of the ligand orbitals. Considering the statements of the previous paragraph, one might be tempted to assume for that reason higher ionicity for the  $\pi_{1...4}$  pi bonding than for the in-plane ( $t_{1...4}$ ) pi bonding. (Using the formulae developed in section D we have

$$\frac{\delta g_{||}}{\delta g_{\perp}} = 4 \frac{\omega_1}{\omega_2} \left[ \frac{c_{(x^2-y^2)}}{c_{(yz)}} \right]^2$$

Dr. McGarvey gives the ratio  $(\delta g_{||}/\delta g_{\perp})$  as 3.3, and  $(\omega_1/\omega_2)$  for  $\text{CuA}_2$  in chloroform solution (Part II) is 1.24, so that the  $c/c$  ratio is ca 0.816.)

## B. LCAO-MO Treatment of the Ligand Pi System

While investigating possible origins of the visible absorption bands of cupric acetylacetonate and related chelates, we desired molecular orbital calculations for the chelate-ring pi system. Although actual application to an entire metal chelate ring has not proved fruitful, use of the method has yielded an apparently satisfactory calculation for the metal chelation shift of ligand ultraviolet absorption bands. Methods were assumed for handling the problem; they were tried in the calculation of resonance energies of carboxylate ion and acetylacetonate ion. The following material presents the postulates and their applications.

### 1. General Method of Calculation

The LCAO-MO usages are given in Part III. A. When bonds and atoms are not all equivalent for an organic molecule, choosing the Q's and  $\beta$ 's presents considerable difficulty. Various ways have been proposed for handling the problem, none of which has been entirely satisfactory.<sup>44, 50, 51, 52, 53</sup> Here we postulate that the  $\beta$ 's can be taken as follows: We assume that the exchange integral is proportional to the "second bond" energy of a normal double bond joining the two atoms under discussion. For carbon-oxygen links, then, we take

$$\beta_0 = (E_{\text{C=O}} - E_{\text{C-O}})/(E_{\text{C=C}} - E_{\text{C-C}}),$$

where, as in the remainder of this section, all energies are based on the carbon-carbon aromatic  $\beta$  as unit. Landolt-Bornstein<sup>54</sup> gives a ratio of 1.8 for  $\beta_0$ .

For the Q's, we take a first guess,  $Q^0$ .  $Q_0^0$  is set as 2. (Various values have been proposed for  $Q_0$ --ranging as high as 4,<sup>53</sup> but more often assumed less than 1. Most workers have assumed  $\beta_0 = 1$ , so that the conclusions of others regarding the proper size of

$Q_0$  do not directly apply to our work.) Then we correct all  $Q^i$ 's for the inductive effect, using a method stated by Branch and Calvin<sup>55</sup> and used by Jaffe.<sup>50</sup> Let the final  $Q$  be given by

$$Q_i = \sum_j (1/3)^k Q_j^0,$$

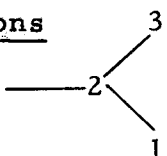
where  $k$  is the number of bond lengths connecting atoms  $i$  and  $j$ .

The normal simplifying approximations are made and the secular equations are then

$$\det (H_{ij} - \delta_{ij} W) = 0.$$

The resonance energy is obtained by placement of two electrons in each energy level (from the highest down until all have been placed) of the MO scheme and by comparison of the resultant total energy with that expected of the classical principal structure. The classical-structure energy may be found by deleting from the proper secular determinant all  $\beta$ 's connecting atoms not double-bonded in the formal structure and then placing the electrons just as before. The resonance energy "RE" is taken as the difference between the ground-state energies obtained from the ordinary and the deleted secular equation.

## 2. Trial RE Calculations

Carboxylate Ion.  , 4 electrons, The ion has symmetry

$D_{2h}$ ;  $C_2$  symmetry is sufficient to factor the secular determinant, 3 by 3, into a linear and a quadratic block whose solutions are

$$W_a = Q_1,$$

$$W_{b,c} = \left( Q_1 + Q_2 \pm \sqrt{(Q_1 - Q_2)^2 + 8 \beta_0^2} \right) / 2.$$

The deleted secular determinant gives

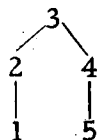
$$W'_a = Q_1$$

$$W'_{b,c} = \left( Q_1 + Q_2 \pm \sqrt{(Q_1 - Q_2)^2 + 4 \beta_0^2} \right) / 2.$$



Using the methods outlined previously, we find  $Q_1 = Q_3 = 0$ ;  $Q_2 = -(8/9)$ . Then the RE is  $2(W_b - W'_b)$ , or  $1.46 \beta$ . If we take the value 21 kcal for  $\beta$  (from the RE for benzene, quoted by Pitzer<sup>41</sup> as 42 kcal), the carboxylate resonance energy becomes 30.7 kcal, in fairly good agreement with the value of about 35 kcal (taken from Branch and Calvin,<sup>55</sup> pp. 219 and 283).

Acetylacetonate Anion. 6 electrons.



The symmetry is  $C_{2v}$ ; factoring of the fifth-order secular determinant into a cubic and a quadratic is made possible by this symmetry. The factored determinant is

$$\begin{vmatrix} Q_1 - W & \beta_0 & & & & \\ & & & & & 0 \\ \beta_0 & Q_2 - W & & & & \\ & & & & & \\ & & Q_3 - W & 2\beta_C & & 0 \\ & 0 & 2\beta_C & Q_2 - W & \beta_0 & \\ & & 0 & \beta_0 & Q_1 - W & \end{vmatrix} = 0$$

Using the guesses  $Q_1^0 = Q_5^0 = 2$  and  $Q_2^0 = Q_3^0 = Q_4^0 = 0$ , and correcting for the inductive effect, we obtain  $Q_3 = 0$ ,  $Q_1 = Q_5 = 1.8$ ,  $Q_2 = Q_4 = 0.52$ . Now, using the values  $\beta_0 = 1.8$ ,  $\beta_C = 1$ , we obtain the energy levels as 3.30, 3.07, 0.66, -0.75, -1.64.

The deleted secular determinant, corresponding to the structure  $O=C-C=C-O^-$ , is

$$\begin{vmatrix} Q_1 - W' & \beta_0 & 0 & 0 & 0 \\ \beta_0 & Q_2 - W' & 0 & 0 & 0 \\ 0 & 0 & Q_3 - W' & \beta_C & 0 \\ 0 & 0 & \beta_C & Q_4 - W' & 0 \\ 0 & 0 & 0 & 0 & Q_5 - W' \end{vmatrix} = 0$$

If we use the Q's and  $\beta$ 's as above, we obtain for W' the values 3.07, 1.8, 1.29, -0.75, -0.77. The RE is calculated as  $2(3.30 + 3.07 + 0.66 - 3.07 - 1.8 - 1.29)\beta_C$ , or  $1.74 \beta_C$ . For  $\beta_C = 21$  kcal, RE = 36.5 kcal. In view of the fact that the same calculation for carboxylate ion gave a value about 5 to 6 kcal too low, we would be inclined to put a RE value for acetylacetonate ion at about 42 kcal. This seems a quite reasonable value, considering the behavior of the molecule.

### 3. Electron Distribution for Acetylacetonate

Maps of charge distribution for the anion in its ground and excited states will be of interest. We compute the linear-variation molecular wave function by the relationship

$$\psi_k = \frac{\sum_i c_{ki} \phi_i}{\sum_i (c_{ki})^2},$$

where  $\psi_k$  is the kth proper variation function, the  $c_{ki}$  are constants, and the  $\phi_i$  are the original atomic functions. The c's are found by solution of the equations

$$\sum_i (H_{ji} - \delta_{ji} W_k) c_{ki} = 0.$$

At each atom, i, the fraction of electron charge for one electron in molecular orbital k is given as  $(c_{ki})^2$ . These points are well explained by Coulson<sup>44</sup> and others and need not be elaborated upon here. Suffice it to say that using the above relationships we have calculated for acetylacetonate anion the following set of molecular orbital functions:

a. For  $W = 3.30$

$$\psi_a = 0.524 \phi_1 + 0.436 \phi_2 + 0.264 \phi_3 + 0.436 \phi_4 + 0.524 \phi_5,$$

b. For  $W = 3.07$

$$\psi_b = 0.578 \phi_1 + 0.408 \phi_2 \quad -0.408 \phi_4 - 0.578 \phi_5,$$

c. For  $W = 0.66$

$$\psi_c = 0.392 \phi_1 - 0.249 \phi_2 - 0.754 \phi_3 - 0.249 \phi_4 + 0.392 \phi_5,$$

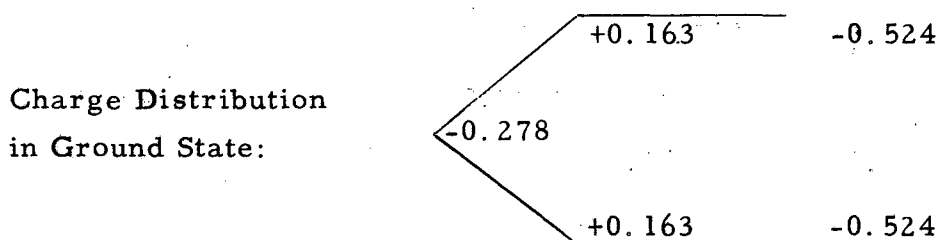
d. For  $W = -0.75$

$$\psi_d = 0.408 \phi_1 - 0.578 \phi_2 \quad + 0.578 \phi_4 - 0.408 \phi_5,$$

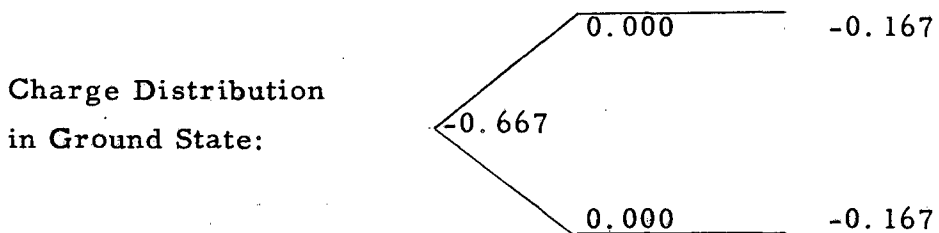
e. For  $W = -1.64$

$$\psi_e = 0.260 \phi_1 - 0.498 \phi_2 + 0.607 \phi_3 - 0.498 \phi_4 + 0.260 \phi_5.$$

The electron distribution for each orbital is given in Table IX. To obtain ground-state distribution one multiplies the electron distribution for each orbital by the number of electrons occupying that orbital. For the ground state we assume two electrons each in orbitals a, b, and c; none in d and e. Now, for each atom we take the charge on the core as + 1. To find the distribution of actual charge in excess of that required to neutralize the core charge one must subtract the total electron distribution at each atom from 1. The ion-charge distribution so found is:



It is interesting to compare this distribution with that calculated on the assumption that all  $\beta$ 's are equal and all  $Q$ 's equal--i. e., for pentadiene anion,



If we suppose that the first electronic excitation involves the transfer of one electron from orbital c to d, the distribution for the first excited state is found by altering the ground-state distribution by the difference between the c and d rows in Table IX. The result follows:

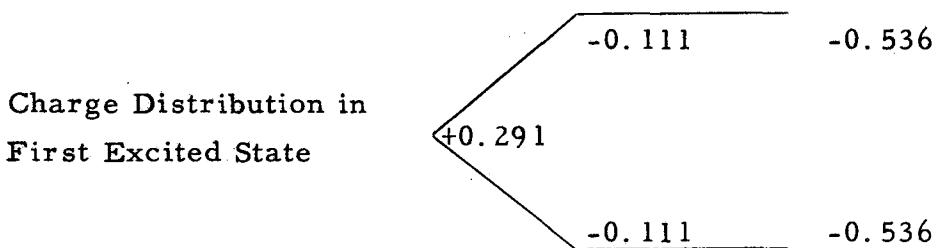
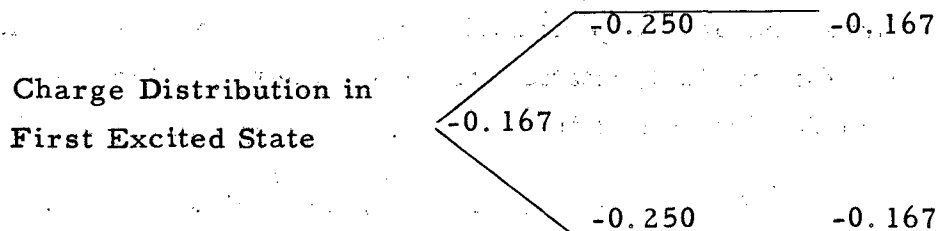


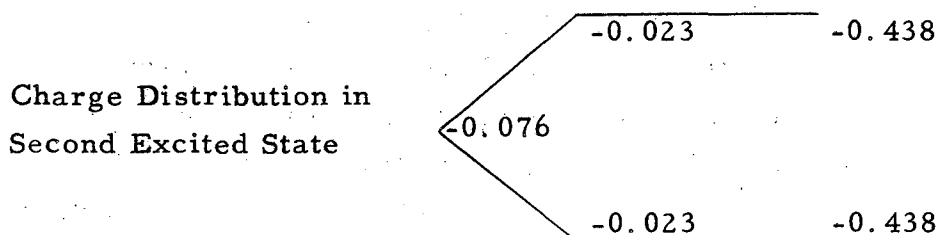
Table IX

One-Electron Distribution for Each Molecular Orbital of Acetylacetonone Anion					
Orbital	Electron Density on Atom				
	1	2	3	4	5
a	0.2742	0.1905	0.0697	0.1905	0.2742
b	0.334	0.166	0	0.166	0.334
c	0.154	0.062	0.5695	0.062	0.154
d	0.166	0.334	0	0.334	0.166
e	0.0676	0.248	0.368	0.248	0.0676

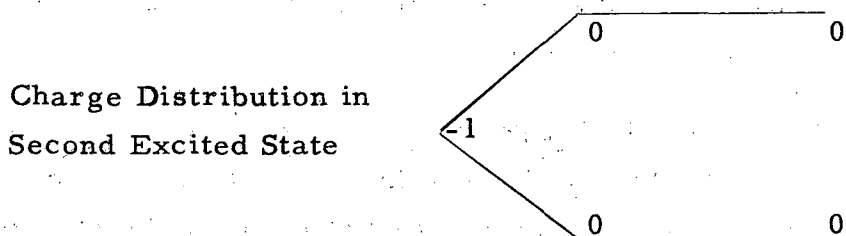
Again, we may contrast this with the corresponding values for penta-  
diene anion:



A second excited state occurs if the same electron goes into orbital  $e$   
instead. The charge distribution for that state is derived from the  
ground-state distribution and the difference between rows  $c$  and  $e$  of  
Table IX.



This can be contrasted with the corresponding distribution calculated  
for pentadiene anion:



#### 4. Predicting a Spectral Shift

Using the electron distribution found above for the ground and  
first excited states of acetylacetonate ion, we can calculate the shift  
of the principal (first) ultraviolet band of acetylacetonate when its labile  
proton is replaced with a dipositive cation. Let us suppose that the  
main effect of the change from monopositive to dipositive cation in the  
chelate ring is increased electrostatic interaction between central ion  
and ligand charges. Then a shift of the first absorption band of the

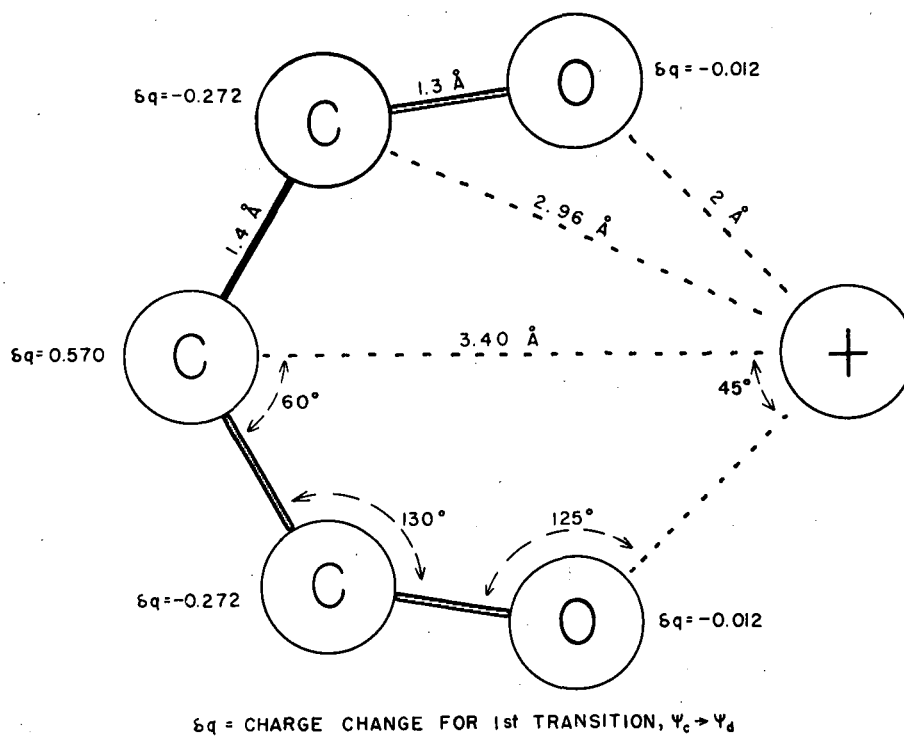
ligand upon chelation would be caused by the different Coulombic interaction of ligand with cation for the ground and first excited states. We adopt the geometrical model shown in Fig. 18. Also shown there is the increment of charge at each ring position for the transition  $\psi_c \rightarrow \psi_d$ . The direct electrostatic interaction energy of the extra cation charge with that increment is

$$\sum_{i=1}^5 (\delta q_i) e^2 / r_i = 2(-0.272e^2 / 2.96) - 0.012e^2 + 0.57e^2 / 3.4 .$$

This quantity has the value of  $-3200 \text{ cm}^{-1}$ . This is in very good agreement with the movement of the  $280\text{-m}\mu$  band of acetylacetone to  $304$  (or a little more)  $\text{m}\mu$  in the  $\text{Cu}^{++}$  chelate--a shift of about  $-2820 \text{ cm}^{-1}$ . The same calculations based on the pentadiene anion model, with the geometry as given in Fig. 18, yield ca  $-2500 \text{ cm}^{-1}$ . Thus we see that the calculation as outlined does give the correct direction and indeed even very close to the correct quantitative observed value for the shift, regardless of what values are chosen for the MO parameters (within reason, of course). The method just demonstrated, though a useful one, is not often utilized. It avoids direct molecular-orbital calculation of energy levels, yet obtains energy information through a quantity which the simple MO method usually predicts fairly well--electron distribution. It may be that this technique would be useful in the theoretical study of reactions.

##### 5. Restriction Upon Use of Our MO Parameters

The  $Q$ 's and  $\beta$ 's used in this section are useful only if the system under consideration has aromatic bond distances (the carbon-oxygen counterpart of an aromatic distance being that for carboxylate ion, about  $1.28 \text{ \AA}$ ). Both the systems discussed above--carboxylate ion and acetylacetonate ion--answer those requirements. If the distances diverge very far from the aromatic ones, however, the  $\beta$ 's must change drastically. Thus, for example, the quoted  $\beta$ 's would be worthless for furan or benzoquinone.



MU-9671

Fig. 18. Acetylacetonate skeleton.

### C. Crystal Field Splitting

We consider a  $\text{Cu}^{++}$  ion in a vacuum. It has spherically symmetric charge distribution. Its outer configuration is  $3d^9$ , which we shall henceforth consider as  $3d^1$  positron configuration. (That is, we think of  $\text{Cu}^+$  with a positron in the 3d shell. Of course, there is in actuality no positron, because it has coalesced with one of the electrons to form a hole.) Now if we place the ion into a position in a molecule or crystal, the potential field in which the electrons move will no longer be spherically symmetric but will instead allow the 3d electrons to know direction in space. Each individual 3d orbital does not have spherical symmetry; some will be, on the average, closer to surrounding negative charges than others. It is obvious that our positron will have lower energy if it resides in one of the former than if it is in one of the latter. Thus the original fivefold degeneracy of the d orbitals has been lifted. The effect just described is called "crystalline field splitting;" its calculation is the subject of this section.

#### 1. Number and Degeneracy of Levels

One need know only the symmetry of the surrounding nuclei as seen from the site of the  $\text{Cu}^{++}$  in order to determine into how many different energy levels the fivefold degenerate level will split and to determine just what degeneracy remains in each level. The determination is best accomplished through group theory; the principles and methods are just those that are used in Section III. A for classifying component atomic orbitals and determining number and degeneracy of levels in the LCAO-MO scheme. Bethe<sup>57</sup> has discussed the methods at great length. Let us apply his ideas to the  $d^1$  problem for a number of different environment symmetries. A set of five d-orbital functions are the functions

$$P_2^m(\cos \theta) \exp(im\phi), \quad (\text{III-19})$$

where m takes on the values 2, 1, 0, -1, -2; the P's are the associated Legendre polynomials. Bethe<sup>57</sup> has shown that with the above functions as basis, the reducible representation for a rotation operation about any axis, by any angle  $\alpha$ , is just



$$\chi(\alpha) = \sin(2.5\alpha)/\sin(0.5\alpha). \quad (\text{III-20})$$

Furthermore, the addition of the inversion operation and its product with all the rotation operations of the group adds nothing new, so that we need only consider the rotational subgroup of our full symmetry group. Equation (III-1) gives the number of times any irreducible representation appears in the reduction of our reducible one; we can find the number of levels for surroundings of any given symmetry by adding all the  $n$ 's. The degeneracy of each level is given by the dimension of the irreducible representation to which that level belongs. A variety of ligand arrangements about the central  $\text{Cu}^{++}$  ion are given below, together with the salient facts of the determination:

a. Tetrahedron. Point group  $T$  (see Herzberg<sup>43</sup> p. 123). Classes are  $I$ ,  $C_2$ ,  $C_3$ , for which Eq. (III-20) becomes respectively, 5, 1, -1. Using Eq. (III-1), we find  $(5 \times 1 - 1 \times 8 + 1 \times 3) = 0$ , so irreducible representation  $A$  does not appear;  $(5 \times 2 + 8 \times 1 - 2 \times 3)/12 = 1$ , so irreducible representation  $E$ , which is two-dimensional, appears once;  $(5 \times 3 - 0 \times 8 - 1 \times 3)/12 = 1$ , so irreducible representation  $F$ , which is three-dimensional, appears once. Thus for a tetrahedral environmental symmetry, the five 3d orbitals of a  $\text{Cu}^{++}$  will have two energy levels: one doubly and the other triply degenerate.

b. Trigonal Pyramid: Point group  $C_3$ . Since there are only one-dimensional representations in the group, there will be no degenerate levels. Therefore a  $\text{Cu}^{++}$  ion at a site of  $C_3$  symmetry will have, in general, five d-orbitals all of different energy.

c. Trigonal Bipyramid. Point group  $D_3$  or  $D_{3h}$ . Our ion is in the center of an equilateral triangle of atoms. There may be also atoms placed pairwise along the threefold axis at equal distances on each side of the plane (see Herzberg<sup>43</sup> p. 110). Classes are  $I$ ,  $C_3$ , and  $C_2$ , for which Eq. (III-20) becomes respectively 5, -1, -1. Using Eq. (III-1) we find  $(5 \times 1 - 1 \times 2 + 1 \times 3)/6 = 1$ , so irreducible representation  $A_1$  appears once;  $(5 \times 1 - 1 \times 2 - 1 \times 3) = 0$ , so irreducible representation  $A_2$  does not appear;  $(5 \times 2 + 1 \times 2 - 0)/6 = 2$ , so the two-dimensional representation  $E$  appears twice. Therefore a cupric ion at a molecular or crystal site of the type described will have three 3d energy levels--one nondegenerate and two each doubly degenerate.

d. Pentagonal Bipyramid. Point group  $D_5$  or  $D_{5h}$  (see Herzberg<sup>43</sup> p. 117). Classes are  $I$ ,  $2C_5$ ,  $2C_5^2$ , and  $5C_2$ , for which Eq. (III-20) becomes respectively 5, 0, 0, 1. From Eq. (III-1) we find  $(5x_1 + 1x_5)/10 = 1$ , so irreducible representation  $A_1$  appears once;  $(5x_1 - 1x_5) = 0$ , so irreducible representation  $A_2$  does not appear;  $(5x_2)/10 = 1$ , so irreducible representations  $E_1$  and  $E_2$ , each two-dimensional, appear once. The splitting, therefore, will yield the same number and degeneracy of 3d orbital levels as in the  $D_3$  case above.

e. Hexagonal Bipyramid. Point groups  $D_6$  or  $D_{6h}$  (see Herzberg<sup>43</sup> p. 114). Classes are  $I$ ,  $2C_6$ ,  $2C_3$ ,  $3C_2$ ,  $3C_2'$ , and  $C_2''$ , for which Eq. (III-20) becomes respectively 5, 1, -1, 1, 1, 1. Using Eq. (III-1) we find  $(5x_1 + 2x_1 - 1x_2 + 1x_3 + 1x_3 + 1x_1)/12 = 1$ , so irreducible representation  $A_1$  appears once;  $(5x_2 + 1x_2 + 1x_2 - 1x_2)/12 = 1$ , so the two-dimensional irreducible representation  $E_1$  appears once;  $(5x_2 - 1x_2 + 1x_2 + 1x_2)/12 = 1$ , so the two-dimensional irreducible representation  $E_2$  appears once. Thus when a cupric ion is placed at a crystal or molecular site of  $D_6$  or  $D_{6h}$  symmetry its five 3d orbital functions group into two pairs and a single, each of different energy.

f. Cube or Octahedron. Point group  $O$  or  $O_h$  (see Herzberg<sup>43</sup> p. 121). Classes are  $I$ ,  $8C_3$ ,  $6C_2$ ,  $6C_4$ ,  $3C_2''$ , for which Eq. (III-20) becomes respectively 5, -1, 1, -1, 1. Using (III-1), we obtain  $(5x_1 - 1x_8 + 1x_6 - 1x_6 + 1x_3)/24 = 0$ , so irreducible representation  $A_1$  does not appear;  $(5x_1 - 1x_8 - 1x_6 + 1x_6 + 1x_3) = 0$ , so  $A_2$  will not appear;  $(5x_2 + 1x_8 + 2x_3)/24 = 1$ , so the two-dimensional representation  $E$  appears once;  $(5x_3 + 1x_6 + 1x_6 - 1x_3)/24 = 1$ , so the three-dimensional representation  $F_2$  appears once. Accordingly, when a cupric ion is surrounded by eight equivalent atoms in a perfect cubic arrangement or by six in a perfect octahedral one, its five 3d orbitals split into two energy levels--one doubly and one triply degenerate.

g. Tetragonal Bipyramid. Point group  $D_4$  or  $D_{4h}$ . We have already seen how five d-orbitals transform under the appropriate symmetry operations; the transformations have been tabulated in Table VI. From Table VI we find that the three orbitals  $d(2z^2 - x^2 - y^2)$ ,  $d(x^2 - y^2)$ ,

and  $d(xy)$  each fall into a one-dimensional representation-- $A_1$ ,  $B_1$ , and  $B_2$ , respectively. Each of those functions describes a nondegenerate energy level. The remaining two orbitals,  $d(xz)$  and  $d(yz)$ --or any linear combinations of them--fall together into the two-dimensional representation  $E$ ; a doubly-degenerate level results.

h. Tetragonal Pyramid. Point group  $C_{4v}$  (see Herzberg<sup>43</sup> p. 113). Classes are  $I$ ,  $2C_4$ ,  $C_2$ ,  $2\sigma_v$ , and  $2\sigma_d$ . For the first three, Eq. (III-20) becomes respectively 5, -1, 1. For the reflection operations, we must see how the function (III-19) transforms. Now,  $\sigma_v$  transforms  $\phi$  into  $-\phi$ , so that each of the (III-19) functions transforms entirely into another member of the set, except for the function having  $m = 0$ ; it transforms into itself and so yields a character of 1. The other class of reflections has the same properties as the first; which one is denoted "v" and which "d" is purely arbitrary. Thus the character for  $\sigma_d$  is also 1. Using Eq. (III-1), we must obtain just the same result as for  $D_4$ , since the reducible representation has the same characters as for that case and since  $C_{4v}$  and  $D_4$  have the same abstract group. Therefore, our five d-orbitals have again formed three nondegenerate and one doubly-degenerate levels.

i. Orthorhombus. Point groups  $C_{2v}$ ,  $D_{2h}$ ,  $D_2$  (see Herzberg<sup>43</sup> p. 106). Classes for  $D_2$  ( $C_{2v}$  will yield identical results, just as  $C_{4v}$  yields the same result as does  $D_4$ ) are  $I$ ,  $C_2$ ,  $C_{2y}$ ,  $C_{2x}$ , for which Eq. (III-20) becomes respectively 5, 1, 1, 1. All irreducible representations of the group are one-dimensional; therefore each of the five proper 3d functions will in general have a unique energy level.

## 2. Derivation of Energy Level Formulae

It is possible to calculate approximately, by standard perturbation methods,<sup>60</sup> the degree to which the  $Cu^{++}$  3d energy levels are split by the crystalline electric field of surrounding ligands. The calculation for a limited number of cases is presented here. We first present the method of attack. The tacit assumption, unless we make a statement to the contrary, is that the entire copper charge is contained within a sphere outside of which is located the entire ligand charge.

It is assumed that the five 3d orbital functions of  $\text{Cu}^{++}$  can be written each as a one-electron function

$$U_i = [P(r)/r] d_i(\theta, \phi). \quad (\text{III-21})$$

Taking the  $d_i$  as the angular 3d wave functions for hydrogen, we have, in polar co-ordinates,

$$\left. \begin{aligned} d_{z^2} &= \sqrt{5/16\pi} (3 \cos^2 \theta - 1), \\ d_{xz} &= \sqrt{15/4\pi} \sin \theta \cos \theta \cos \phi, \\ d_{yz} &= \sqrt{15/4\pi} \sin \theta \cos \theta \sin \phi, \\ d_{x^2-y^2} &= \sqrt{15/16\pi} \sin^2 \theta \cos 2\phi, \\ d_{xy} &= \sqrt{15/16\pi} \sin^2 \theta \sin 2\phi. \end{aligned} \right\} \quad (\text{III-22})$$

The Cartesian co-ordinate expressions will also be useful.

$$\left. \begin{aligned} d_{z^2} &= \sqrt{5/16\pi} (2z^2 - x^2 - y^2)/r^2, \\ d_{xz} &= \sqrt{15/4\pi} xz/r^2, \\ d_{yz} &= \sqrt{15/4\pi} yz/r^2, \\ d_{x^2-y^2} &= \sqrt{15/16\pi} (x^2 - y^2)/r^2, \\ d_{xy} &= \sqrt{15/4\pi} xy/r^2. \end{aligned} \right\} \quad (\text{III-23})$$

The Dirac notation<sup>59</sup> will be used wherever possible. We take the effect of the molecular field to be the simple addition of an extra potential energy term  $V'$  to the unperturbed Hamiltonian  $H_0$  of  $\text{Cu}^{++}$ . Thus if we form a set of proper functions,

$$\psi_j = \sum_i c_{ij} d_i, \quad (\text{III-24})$$

we require that each satisfy the Schrodinger equation,

$$(H_0 + V')(P/r) \psi_j > = (E_0 + E_j')(P/r) \psi_j >, \quad (\text{III-25})$$

where  $E_0$  and  $(E_0 + E')$  are the unperturbed and perturbed energies respectively. Since the  $\psi_j$ , which we have normalized, are solutions to the unperturbed equation, we need only

$$V' (P/r) \psi_j > = E_j' (P/r) \psi_j >, \quad (\text{III-26})$$

and  $E_0$  may be taken as the reference zero of energy. Then

$$E_j' = \langle (P/r) \psi_j | V' (P/r) \psi_j \rangle, \quad (\text{III-27})$$

or for  $V$  which commutes with all  $(P/r) \psi_j$ ,

$$E_j' = \langle V' | (P/r) \psi_j |^2 \rangle. \quad (\text{III-28})$$

$V'$  is the electrostatic attraction energy between the positron and the charge cloud of the ligands; thus  $E'$  is the expectation value for this energy. It is seen that in general  $E'$  may be calculated exactly only if we know exactly the electron distribution for the surrounding ligands as well as the true radial distribution function for  $\text{Cu}^{++}$  in the environment of those ligands. Since these quantities are not known and are not likely to be known for a long time, we must assume models for them. Furthermore, the results are quite sensitive to the models chosen; although attempts have been made to find reasonable models, <sup>22, 24, 21, 48</sup> none of them has as yet yielded theoretical results in good agreement with experiment. A semi-empirical method, in which one makes as few assumptions as possible and attempts to fill in the missing quantities from experimental data, has proven more fruitful.

Least stringent of the necessary assumptions is the symmetry of the molecule. This information alone determines the degree to which the d-orbital degeneracy is lifted. Let us expand  $V'$  in a series of spherical surface harmonic polynomials:

$$V' = \sum_{n, m} C_n^m r^n L_n^m(\theta, \phi). \quad (\text{III-29})$$

The  $C$ 's are constants for any given molecule; they depend upon the exact ligand charge distribution. The  $L$ 's are trigonometric function polynomials in their arguments; they are precisely the trigonometric

solutions to the angular wave equation for hydrogen and are both orthogonal and normalized. Hereafter the L's will be denoted by their familiar hydrogen orbital names: i. e.,  $L_0 = s$ ;  $L_1 = p$ ;  $L_3 = f$ ;  $L_2 = d$ ;  $L_4 = g$ .

Now the functions  $d_i^2$  may be written each as a linear expression in the g's, d's, and s. They are

$$\begin{aligned}
 d_{z^2}^2 &= (3/7 \sqrt{\pi}) g_0 + (\sqrt{5}/7 \sqrt{\pi}) d_{z^2} + 1/4\pi, \\
 d_{xz}^2 &= (-\sqrt{5}/7 \sqrt{\pi}) g_2 - (2/7 \sqrt{\pi}) g_0 + (\sqrt{15}/14 \sqrt{\pi}) d_{x^2-y^2} \\
 &\quad + (\sqrt{5}/14 \sqrt{\pi}) d_{z^2} + 1/4\pi, \\
 d_{yz}^2 &= (\sqrt{5}/7 \sqrt{\pi}) g_2 - (2/7 \sqrt{\pi}) g_0 + (-\sqrt{15}/14 \sqrt{\pi}) d_{x^2-y^2} \\
 &\quad + (\sqrt{5}/14 \sqrt{\pi}) d_{z^2} + 1/4\pi, \\
 d_{x^2-y^2}^2 &= (\sqrt{35}/14 \sqrt{\pi}) g_4 + (1/14 \sqrt{\pi}) g_0 - (\sqrt{5}/7 \sqrt{\pi}) d_{z^2} + 1/4\pi, \\
 d_{xy}^2 &= -(\sqrt{35}/14 \sqrt{\pi}) g_4 + (1/14 \sqrt{\pi}) g_0 - (\sqrt{5}/7 \sqrt{\pi}) d_{z^2} + 1/4\pi.
 \end{aligned}
 \tag{III-30}$$

The p, f, and g functions are given in Table X.

### Square-Planar Bonding

We first treat the case of four ligands arranged symmetrically in the x-y plane around the central  $\text{Cu}^{++}$  ion. This arrangement belongs to point group  $D_{4h}$  and  $V^i$  must also exhibit the same symmetry. Such a criterion allows us to state immediately that most of the C's must be zero. If we situate the ligands along the lines  $x = y$  and  $x = -y$ , we have

$$V_{sq}^i = A_0 s + A_2^0 r^2 d_{z^2} + A_4^0 r^4 g_0 + A_4^4 r^4 g_4. \tag{III-31}$$

We need not consider terms of higher order since they are always orthogonal to every  $\bar{\psi}_j, \psi_j$ . Both symmetry arguments and brute force examination show that the matrix

$$\langle (P/r) d_i | V_{sq}^i | (P/r) d_j \rangle$$

Table X

Normalized Angular Wave Functions	
s	$1/2 \sqrt{\pi}$
$p_z$	$\sqrt{3/4\pi} \cos \theta$
$p_x$	$\sqrt{3/4\pi} \sin \theta \cos \phi$
$p_y$	$\sqrt{3/4\pi} \sin \theta \sin \phi$
$d_{z^2}$	$\sqrt{5/16\pi} (3 \cos^2 \theta - 1)$
$d_{xz}$	$\sqrt{15/4\pi} \sin \theta \cos \theta \cos \phi$
$d_{yz}$	$\sqrt{15/4\pi} \sin \theta \cos \theta \sin \phi$
$d_{x^2-y^2}$	$\sqrt{15/16\pi} \sin^2 \theta \cos 2\phi$
$d_{xy}$	$\sqrt{15/16\pi} \sin^2 \theta \sin 2\phi$
$f_0$	$\sqrt{7/16\pi} (5 \cos^3 \theta - 3 \cos \theta)$
$f_1$	$\sqrt{21/32\pi} (5 \cos^2 \theta - 1) \sin \theta \cos \phi$
$f_1'$	$\sqrt{21/32\pi} (5 \cos^2 \theta - 1) \sin \theta \sin \phi$
$f_2$	$\sqrt{105/16\pi} \sin^2 \theta \cos \theta \cos 2\phi$
$f_2'$	$\sqrt{105/16\pi} \sin^2 \theta \cos \theta \sin 2\phi$
$f_3$	$\sqrt{35/32\pi} \sin^3 \theta \cos 3\phi$
$f_3'$	$\sqrt{35/32\pi} \sin^3 \theta \sin 3\phi$
$g_0$	$(3/16\sqrt{\pi})(35 \cos^4 \theta - 30 \cos^2 \theta + 3)$
$g_1$	$(15/4\sqrt{10\pi})(7 \cos^3 \theta - 3 \cos \theta) \sin \theta \cos \phi$
$g_1'$	$(15/4\sqrt{10\pi})(7 \cos^3 \theta - 3 \cos \theta) \sin \theta \sin \phi$
$g_2$	$(-\sqrt{45/64\pi})(7 \cos^2 \theta - 1) \sin^2 \theta \cos 2\phi$
$g_2'$	$(-\sqrt{45/64\pi})(7 \cos^2 \theta - 1) \sin^2 \theta \sin 2\phi$
$g_3$	$(3\sqrt{35/32\pi}) \sin^3 \theta \cos \theta \cos 3\phi$
$g_3'$	$(3\sqrt{35/32\pi}) \sin^3 \theta \cos \theta \sin 3\phi$
$g_4$	$(3\sqrt{35/\pi/16}) \sin^4 \theta \cos 4\phi$
$g_4'$	$(3\sqrt{35/\pi/16}) \sin^4 \theta \sin 4\phi$

is diagonal and thus that the  $d_i$ 's are themselves the proper functions  $\psi$  for this potential. Multiplying each  $d_i^2$  by  $V_{sq}$  and integrating over all space, we obtain the energy level for each orbital:

$$\left. \begin{aligned} E_{z^2}^{sq} &= A_0/2\sqrt{\pi} + (\sqrt{5}/7\sqrt{\pi})A_2^0 \overline{r^2} + (3/7\sqrt{\pi}) A_4^0 \overline{r^4}, \\ E_{xz}^{sq} &= A_0/2\sqrt{\pi} + (\sqrt{5}/14\sqrt{\pi})A_2^0 \overline{r^2} - (2/7\sqrt{\pi}) A_4^0 \overline{r^4} = E_{yz}^{sq}, \\ E_{x^2-y^2}^{sq} &= A_0/2\sqrt{\pi} - (\sqrt{5}/7\sqrt{\pi})A_2^0 \overline{r^2} + [(1/14\sqrt{\pi}) A_4^0 + \\ &\quad (\sqrt{35}/14\sqrt{\pi}) A_4^4] \overline{r^4}, \\ E_{xy}^{sq} &= A_0/2\sqrt{\pi} - (\sqrt{5}/7\sqrt{\pi})A_2^0 \overline{r^2} + [(1/14\sqrt{\pi}) A_4^0 - \\ &\quad (\sqrt{35}/14\sqrt{\pi}) A_4^4] \overline{r^4}. \end{aligned} \right\} \text{(III-32)}$$

Here  $\overline{r^4}$  and  $\overline{r^2}$  are the positron's expectation values of  $r^4$  and  $r^2$ , respectively. Formally they are given by

$$\overline{r^n} = \int_0^{\infty} |P(r)|^2 r^n dr.$$

### Axial Bonding

The case of two ligands located along the  $z$  axis may be treated in the same way. The electric field created by these ligands has infinite rotational symmetry about the  $z$  axis, and the only surface spherical harmonic polynomials having this symmetry are those with  $m = 0$ . So  $V_{ax}$  is

$$V_{ax} = B_0 s + B_2^0 r^2 d_{z^2} + B_4^0 r^4 g_0. \quad \text{(III-33)}$$

Again the  $d_i$ 's turn out to be the proper functions, so that we obtain the energy levels as before. They are

$$\left. \begin{aligned} E_{z^2}^{ax} &= B_0/2\sqrt{\pi} + (\sqrt{5}/7\sqrt{\pi})B_2^0 \overline{r^2} + (3/7\sqrt{\pi})B_4^0 \overline{r^4}, \\ E_{xz}^{ax} &= B_0/2\sqrt{\pi} + (\sqrt{5}/14\sqrt{\pi})B_2^0 \overline{r^2} - (2/7\sqrt{\pi})B_4^0 \overline{r^4} = E_{yz}^{ax}, \\ E_{x^2-y^2}^{ax} &= B_0/2\sqrt{\pi} - (\sqrt{5}/7\sqrt{\pi})B_2^0 \overline{r^2} + (1/14\sqrt{\pi})B_4^0 \overline{r^4} = E_{x^2-y^2}^{ax} \end{aligned} \right\} \text{(III-34)}$$



The first case which we consider as a possible representation of an actual  $\text{Cu}^{++}$  chelate molecule is that of an axially distorted octahedron. This picture may fairly well describe those molecules such as cupric phthalocyanines in which four equivalent ligands are bound tightly to the central ion. The axial contribution is necessary to account for the effects of solvents and neighboring molecules in the crystal. (For the gaseous phase it might be possible to neglect axial terms.) Now for convenience we define some new molecular parameters in terms of those we have been using:

$$\left. \begin{aligned} W_0 &= (A_0 + B_0)/2\sqrt{\pi}, \\ W_2 &= -(A_2^0 + B_2^0)(\sqrt{5}/14\sqrt{\pi}) \overline{r^2}, \\ W_4 &= (A_4^0 + B_4^0)(1/14\sqrt{\pi}) \overline{r^4}, \\ W_{sq} &= -(\sqrt{35}/14\sqrt{\pi}) A_4^0 \overline{r^4}. \end{aligned} \right\} \text{(III-35)}$$

In terms of these quantities the energy levels for a chelate of tetragonal symmetry become

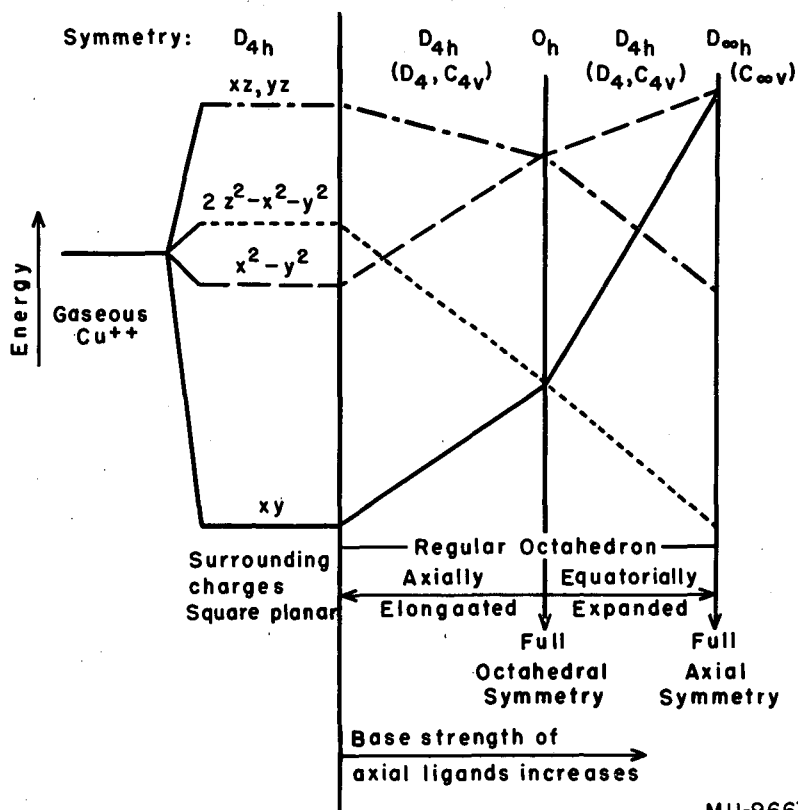
$$\left. \begin{aligned} E_{z^2}^{\text{tet}} &= W_0 - 2W_2 + 6W_4, \\ E_{xz}^{\text{tet}} &= W_0 - W_2 - 4W_4, \\ E_{yz}^{\text{tet}} &= W_0 - W_2 - 4W_4, \\ E_{x^2-y^2}^{\text{tet}} &= W_0 + 2W_2 + W_4 - W_{sq}, \text{ and} \\ E_{xy}^{\text{tet}} &= W_0 + 2W_2 + W_4 + W_{sq}. \end{aligned} \right\} \text{(III-36)}$$

For a tetragonal structure, then, the electric field theory predicts four distinct  $\text{Cu}^{++}$  3d energy levels, one of them being degenerate. Examination of the expressions obtained for them yields some useful information. First, the center of gravity of the levels is changed by an amount  $W_0$ . This represents the average or over-all gain in ionic

attraction upon removing one electron from  $\text{Cu}^+$  in the chelate. If all the orbitals were spherical in electron distribution  $W_0$  would be the only term in each expression. The remaining terms all are to account for the fact that in a given d orbital the positron is not on the average the same distance from attracting centers in the ligands as it would be for a spherical orbital. Since the orbital  $d_{xy}$  is directed along the bonds,  $W_{sq}$  must represent a gain energywise. The orbital  $d_{x^2-y^2}$  is then seen to lie just  $2 W_{sq}$  above  $d_{xy}$ . Also we see immediately that this separation is determined solely by the ligands involved in square-planar bonding and contains no contribution from the axially situated molecules. Similar arguments show that for a molecule in which the axial groups are farther from the central ion or weaker than the planar ones,  $W_2$ ,  $W_4$ ,  $W_0$ , and  $W_{sq}$  all represent energy gains (i. e., they are negative). When the axial groups are closer to the central ion than the planar ones, only  $W_2$  changes sign. Further scrutiny of the above equations and their predecessors reveals that for molecules which are predominantly square-planar the ground state should be  $d_{xy}$ . The splitting scheme, neglecting the constant term, is shown in Fig. 19. The orbitals involved are depicted in Figs. 16 a, b, c with plots of the angular distribution function as radius vs the angle for certain cross sections through the Cu nucleus.

#### Calculations for Specific Models

One can obtain a better intuitive picture of what the quantities  $W$  mean by carrying through more specific calculations with a simple model. We have discussed above, in general terms, the effect of a tetragonal ligand field. A specific example of such a situation would be four equivalent point charges situated at  $(r, \theta, \phi)$  values of  $(r_1, 90^\circ, 45^\circ)$ ,  $(r_1, 90^\circ, 135^\circ)$ ,  $(r_1, 90^\circ, 225^\circ)$ ,  $(r_1, 90^\circ, 315^\circ)$ . Letting each charge possess magnitude  $q$ , we must find the Coulombic attraction energy between the  $q$ 's and the positron (of charge + 1). To do so, we shall consider the potential along two specific directions in space where it is particularly easy to express the electrostatic energy between the four charges and the positron. By setting down the expression for this energy and then by comparing it with the equivalent expression obtained for those specific directions from Eq. (III-31), we shall be able to evaluate the  $A$  coefficients in Eq. (III-31).



MU-9667

Fig. 19. Positron energy levels of cupric ion in crystal fields of various strengths and symmetries.

Potential on z-Axis. First, one can easily set down the potential for any point  $z$  along the  $z$ -axis as  $4q/r_z$ , where  $r_z$  is the distance from each charge to the point  $z$ . But  $r_z$  is just  $\sqrt{r_1^2 + z^2}$  so that  $V'(z\text{-axis}) = 4q/\sqrt{r_1^2 + z^2}$ . Now we expand the inverse square root in a power series in  $z/r_1$ :

$$V'(z\text{-axis}) = (4q/r_1) \left( 1 - \frac{1}{2} \frac{z^2}{r_1^2} + \frac{3}{8} \frac{z^4}{r_1^4} - \dots \right).$$

Also, according to Eq. (III-31), when we substitute  $z$  for  $r$  and evaluate the  $d$  and  $g$  functions for  $(\theta = 0)$ , we find that the general expression for the potential reduces to

$$V'(z\text{-axis}) = A_0/2\sqrt{\pi} + A_2^0 z^2 \sqrt{5/4\pi} + A_4^0 z^4 \cdot 3/2\sqrt{\pi} + \dots.$$

Now when we set the coefficients of corresponding powers of  $z$  equal in our two expressions for  $V'$ , we obtain

$$A_0 = (4q/r_1) 2\sqrt{\pi};$$

$$A_2^0 = (4q/r_1) (-\sqrt{\pi/5}/r_1^2);$$

$$A_4^0 = (4q/r_1) \sqrt{\pi}/4r_1^4.$$

Along  $x = y$ . The coefficient  $A_4^0$  is still undetermined. It can be found by examination of the potential along the line  $x = y$ . The potential due to the two charges located along that line will just be

$$V'_{1,2}(x = y) = (q/\sqrt{r_1 + r''}) + (q/\sqrt{r_1 - r''}),$$

where  $r''$  is the radial distance along the line  $x = y$ . Also, the two charges situated along the line  $x = -y$  will contribute a potential of

$$V'_{3,4}(x = y) = 2q/\sqrt{r_1^2 + r''^2}.$$

By algebraic manipulation we can arrange each of these in form to be expanded in a power series in  $(r''/r_1)$ :

$$V'_{1,2}(x = y) = (2q/r_1) \left( 1 + (r''/r_1)^2 + (r''/r_1)^4 + \dots \right);$$

$$V'_{3,4}(x = y) = (2q/r_1) \left( 1 - \frac{r''^2}{2r_1^2} + \frac{3}{8} \frac{r''^4}{r_1^4} - \dots \right).$$

The total potential along  $x = y$  is just the sum of the two above,

$$V'(x = y) = (4q/r_1) \left( 1 + \frac{1}{4} \frac{r''^2}{r_1^2} + \frac{11}{16} \frac{r''^4}{r_1^4} + \dots \right).$$

Now when we evaluate Eq. (III-31) for  $r = r''$ ,  $\theta = 90^\circ$ , and  $\phi = 45^\circ$ , we obtain

$$V'(x = y) = (A_0/2\sqrt{\pi}) - (A_2^0 r''^2 \sqrt{5/16\pi}) + ([9A_4^0/16\sqrt{\pi}] - [A_4^4 \sqrt{315/256\pi}]) r''^4 - \dots$$

By setting the two expressions for  $V'(x = y)$  equal, we obtain the same values as previously found for  $A_0$  and  $A_2^0$ . But there also emerges the relationship

$$(9A_4^0/16\sqrt{\pi}) - (\sqrt{315/256\pi})A_4^4 = (11/16r_1^4) \frac{4q}{r_1},$$

which, taken together with the  $A_4^0$  value already determined, yields

$$A_4^4 = - (4q/r_1) (\sqrt{35\pi/12} r_1^4).$$

Energy Levels. Feeding the A coefficients we have just obtained into Eqs. (III-32), we find

$$\begin{aligned} E_{z^2}^{sq} &= \frac{4q}{r_1} \left( 1 - \frac{1}{7} \frac{r^2}{r_1^2} + \frac{3}{28} \frac{r^4}{r_1^4} \right), \\ E_{yz}^{sq} = E_{xz}^{sq} &= \frac{4q}{r_1} \left( 1 - \frac{1}{14} \frac{r^2}{r_1^2} - \frac{1}{14} \frac{r^4}{r_1^4} \right), \\ E_{x^2-y^2}^{sq} &= \frac{4q}{r_1} \left( 1 + \frac{1}{7} \frac{r^2}{r_1^2} - \frac{4}{21} \frac{r^4}{r_1^4} \right), \text{ and} \\ E_{xy}^{sq} &= \frac{4q}{r_1} \left( 1 + \frac{1}{7} \frac{r^2}{r_1^2} + \frac{19}{84} \frac{r^4}{r_1^4} \right). \end{aligned} \tag{III-37}$$

The separation in energy of each of the first three levels from the last, the  $xy$  level, will be denoted  $\omega$ . The three  $\omega$ 's for the above set of levels are

$$\begin{aligned}\omega_1^{sq} &\equiv E_{xz}^{sq} - E_{xy}^{sq} = (-4q/r_1) \left[ (3/14)(\overline{r^2}/r_1^2) \right. \\ &\quad \left. + (25/84)(\overline{r^4}/r_1^4) \right] \\ \omega_2^{sq} &\equiv E_{x^2-y^2}^{sq} - E_{xy}^{sq} = (-4q/r_1) (5/12)(\overline{r^4}/r_1^4) \quad (\text{III-38}) \\ \omega_3^{sq} &\equiv E_{z^2}^{sq} - E_{xy}^{sq} = (-4q/r_1) \left[ (2/7)(\overline{r^2}/r_1^2) \right. \\ &\quad \left. + (5/42)(\overline{r^4}/r_1^4) \right].\end{aligned}$$

Normally, if the charges surrounding the  $\text{Cu}^{++}$  are to be representatives of ligands in an actual molecule,  $q$  will be negative. Then, obviously, the  $d(xy)$  orbital will be the ground state for the positron, since all terms in the expressions (III-38) will be positive. This means that all three  $\omega$ 's are excitation energies for the positron from its ground state and thus are possible frequencies of absorption bands. (It is well to remember that a positron's jump from here to there is really, for our situation, an electron's jump from there to here. Accordingly, the three transitions may be thought of as the movement of a given hole from its ground-state orbital to four excited-state orbitals, or as the movement of electrons from the totally populated four lowest-energy orbitals to the vacancy in the half-populated highest-energy orbital.) It is interesting to note that expressions (III-38) specify that  $\omega_2$  is smaller than  $\omega_1$  but do not direct whether  $\omega_3$  is greatest or smallest of the three transitions: For very great Cu-to-ligand distance,  $r_1^4 \gg r_1^2$ : then  $\omega_3$  is greatest of the three. For very small  $r_1$ ,  $\omega_3$  is about the same as  $\omega_2$ . Likely, the cases most often met with are intermediate ones.

By assuming a radial distribution function for the  $\text{Cu}^{++}$  3d orbitals we can calculate  $\omega_1$ ,  $\omega_2$ , and  $\omega_3$ . Although Bjerrum, Ballhausen, and Jørgensen<sup>22, 21</sup> have assumed a hydrogenlike function with seemingly good results, such a distribution must be far from the truth. The SCF (self-consistent field) calculations of Hartree and Hartree<sup>29</sup> for  $\text{Cu}^+$ , which surely will not differ drastically from  $\text{Cu}^{++}$  in 3d radial distribution (a point specifically stated by Hartree and Hartree as well), are very much at variance with the hydrogenlike function having  $Z_{\text{eff}} = 7.85$  (the value assumed by the Danish workers). Both these functions are plotted

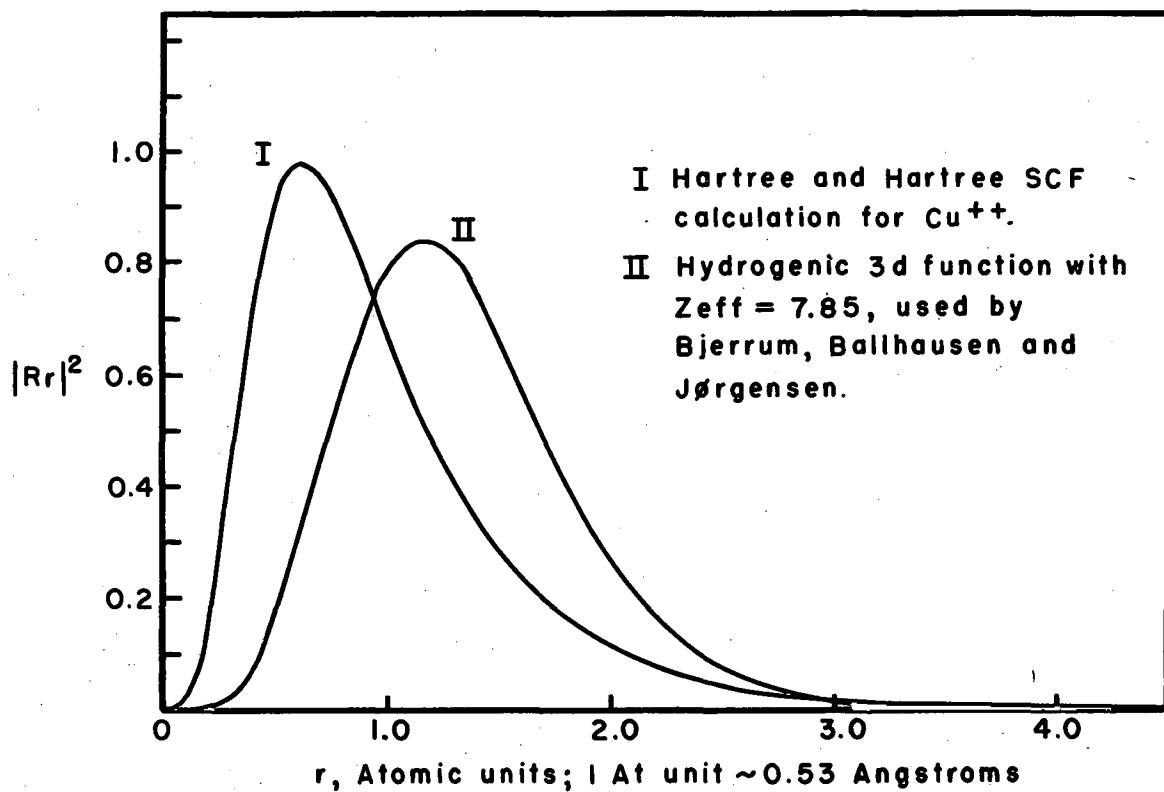
in Fig. 20. We can see that the hydrogenic radial function yields a maximum farther from the central ion than does the SCF function. In the environment of the negatively-charged ligands, the 3d orbitals might well suffer orbital contraction but expansion seems most unlikely. Furthermore, the loss of one electron from  $\text{Cu}^+$  to give  $\text{Cu}^{++}$  would further contract the tail of the distribution. On the other hand, this effect might be somewhat counterbalanced by some sharing of ligand electrons by the Cu. It is instructive to plot the actual quantities whose integrals over  $r$  ( $\overline{r^2}$  and  $\overline{r^4}$ ) appear in the calculations of orbital splitting. This has been done for the hydrogenlike function assumed by the Danish workers and for the Hartree SCF function; the results are shown in Fig. 21. We can see from this how poor an approximation the hydrogenlike function is. We feel that the SCF function, while not exactly correct for our atom in its ligand environment, would furnish a much better basis for attempts at quantitative calculation than would the hydrogenic function.

Using the Hartree radial distribution function,<sup>29</sup> then, and a numerical integration approximation, we find

$$\overline{r^2} \equiv \int_0^{2 \text{ \AA}} |P(r)|^2 r^2 dr = 0.3224 \text{ \AA}^2, \text{ and}$$

$$\overline{r^4} \equiv \int_0^{2 \text{ \AA}} |P(r)|^2 r^4 dr = 0.294 \text{ \AA}^4.$$

The quantities  $\overline{r^2}$  and  $\overline{r^4}$  are sufficient to establish magnitudes. To take account of the specific integration required for each different ligand position would entail more work but would tell us essentially nothing new. Using those fixed quantities, then, we have calculated  $\omega_1$ ,  $\omega_2$ , and  $\omega_3$  on the basis of Eq. (III-38) for a number of ligand charges and distances. The results are given in Table XI. Now, although we know the copper-oxygen internuclear distance in square-planar chelates to be ca  $2 \text{ \AA}$ , we must suppose that for any real chelate molecule the effective distance  $r_1$  that would best represent the ligand is surely smaller than  $2 \text{ \AA}$  owing to polarization of the electrons on the oxygen atoms, especially those in the p-orbitals directed approximately toward the



MU-9635

Fig. 20. Radial distribution functions for  $\text{Cu}^{++}$  3d  $R^2 r^2$  vs. r.



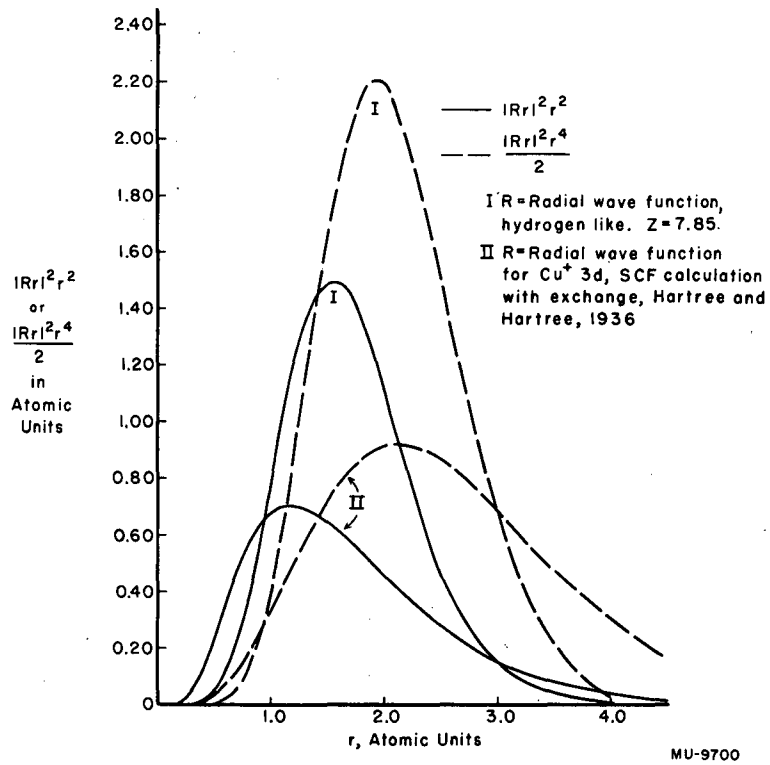


Fig. 21. Radial variation of the functions  $|Rr|^2 r^2$  and  $|Rr|^2 r^4$ .

Table XI

Calculated transitions for $\text{Cu}^{++}$ surrounded by 4 unit point charges <sup>a</sup> in square arrangement			
$r_1, \text{\AA}$	$\omega_2, \text{cm}^{-1}$	$\omega_1, \text{cm}^{-1}$	$\omega_3, \text{cm}^{-1}$
1.1	35,300	49,000	41,600
1.2	22,800	34,600	30,800
1.3	15,300	25,300	23,600
1.4	10,600	19,100	18,300
1.5	7,490	14,750	13,800
1.6	5,420	11,600	11,800
1.7	3,980	9,250	9,660
1.8	3,020	7,550	8,240
1.9	2,290	6,250	6,800
2.0	1,770	5,220	5,790

<sup>a</sup>To find the corresponding entries for any ligand charge, q, multiply entries in this table by q.

Cu nucleus. Also, the effective charge  $q$  should be greater than the formal charge,  $-1/2$  per oxygen, because of the greater electron affinity of oxygen than of carbon and because of the polarization of pi-conjugation electrons of the ligand chain or ring by the dipositive cupric ion. Reasonable upper limits on these effects would seem to be  $q = -1$  and  $r_1 = 1.5 \text{ \AA}$ . Taken together with the fact that we have used values of  $\overline{r^2}$  and  $\overline{r^4}$  too large for point charges located  $1.5 \text{ \AA}$  from the copper nucleus, these limits set probably upper bounds upon the magnitudes of the transitions that should be observed of approximately the values in the  $1.5 \text{ \AA}$  row of Table XI.

The upper limit set by the above procedure for  $\omega_2$  is ca  $7,500 \text{ cm}^{-1}$  ( $13,300 \text{ \AA}$ ), in the near infrared. As we have seen in Part II, the only observed absorption band that could reasonably be identified as  $\omega_2$  (for  $\text{CuA}_2$  as well as for a number of other chelates of  $\text{Cu}^{++}$ ) appears at ca  $15,000 \text{ cm}^{-1}$  ( $6,700 \text{ \AA}$ ), in the visible red. We are forced to conclude either that the process by which we obtained the results and the approximations we made were too crude even to allow us to set upper limits, or that there are important interactions which do not belong in the category of crystal or molecular field splitting. The obvious such interaction is electron exchange; we do feel that covalent bonding must play an important role in the cupric chelates. We have already considered the effect covalency would exert upon the spectra (Part III. A).

Axial Charges. Let us now place a charge  $p$  along the  $z$ -axis at  $(r, \theta, \phi)$  values of  $(Z, 0, --)$ . The potential along the  $x$ -axis due to this charge  $p$  is

$$V'(x\text{-axis}) = p/\sqrt{Z^2 + x^2}.$$

Expanding  $V'$  in a power series in  $(x/Z)$ , we have

$$V'(x\text{-axis}) = (p/Z)[1 - (3/2)(x^2/Z^2) + (3/8)(x^4/Z^4) \dots]$$

Also, Eq. (III-33) evaluated along the  $x$ -axis is

$$V'(x\text{-axis}) = (B_0/2\sqrt{\pi}) - (\sqrt{5} B_2^0 x^2/4\sqrt{\pi}) + (9B_4^0 x^4/16\sqrt{\pi}) \dots$$

Then  $B_0/2\sqrt{\pi} = p/Z$ ,

$\sqrt{5} B_2^0/7\sqrt{\pi} = (6/7)p/Z^3$ , and

$B_4^0/\sqrt{\pi} = (2/3)p/Z^5$ .

Then, from Eq. (III-34),

$$E_{z^2}^{ax} = (p/Z)[1 + (6/7)(\overline{r^2}/Z^2) + (2/7)(\overline{r^4}/Z^4)]$$

$$E_{xz}^{ax} = (p/Z)[1 + (3/7)(\overline{r^2}/Z^2) - (4/21)(\overline{r^4}/Z^4)] = E_{yz}^{ax}$$

$$E_{xy}^{ax} = (p/Z)[1 - (6/7)(\overline{r^2}/Z^2) + (1/21)(\overline{r^4}/Z^4)] = E_{x^2-y^2}^{ax}$$

If there are no other charges than the axial one(s), the ground-state orbital for the positron is obviously  $d_{z^2}$ . We have the relations

$$\left. \begin{aligned} E_{xz}^{ax} - E_{z^2}^{ax} &= (-p/Z)[(3/7)(\overline{r^2}/Z^2) + (10/21)(\overline{r^4}/Z^4)] , \\ -\omega_3^{ax} = E_{xy}^{ax} - E_{z^2}^{ax} &= (-p/Z)[(12/7)(\overline{r^2}/Z^2) + (5/21)(\overline{r^4}/Z^4)] , \\ \omega_1^{ax} = E_{xz}^{ax} - E_{xy}^{ax} &= (-p/Z)[(-9/7)(\overline{r^2}/Z^2) + (5/21)(\overline{r^4}/Z^4)] , \\ E_{x^2-y^2}^{ax} - E_{xy}^{ax} &= 0 = \omega_2^{ax} . \end{aligned} \right\} \text{(III-40)}$$

Thus if the  $\text{Cu}^{++}$  ion has as near neighbors only negative charges along a single line through the nucleus, the three positron energy levels will increase in the order  $E_{z^2} < E_{xz} = E_{yz} < E_{x^2-y^2} = E_{xy}$ . One can visualize why this should be so quite easily. A negative charge at some point along the z-axis will be on the average closest to the orbital which is directed towards it,  $d_{z^2}$ ; somewhat farther and equidistant from the two,  $d_{xz}$  and  $d_{yz}$ , directed  $45^\circ$  to the x, y plane; farthest and equidistant from the two,  $d_{x^2-y^2}$  and  $d_{xy}$ , directed in the x, y plane.

Both Axial and Square-Planar Charges. The same set of eigenfunctions,  $d$ , was used to describe both axial and planar bonding. Therefore, the results obtained for each can be simply added together for cases where both axial and planar ligands are present. The energy level formulae,

Eqs. (III-37) and (III-39), are to be taken as building blocks (with this restriction: that there be introduced no potential terms that upset the diagonalization for the d-functions as given). For example, a tetragonal bipyramidal arrangement formed from four square-planar charges arranged as previously noted and two charges  $p'$  and  $p''$  arranged along the z-axis at  $+Z'$  and  $-Z''$ , would give rise to energy levels obtained by adding to each term in Eq. (III-39) the corresponding term in Eq. (III-38) twice--once with  $p = p'$  and  $Z = Z'$ ; once with  $p = p''$  and  $Z = Z''$ :

$$E_{z^2}^{\text{tet bi}} = \left( \frac{4q}{r_1} + \frac{p'}{Z'} + \frac{p''}{Z''} \right) - \left( \frac{4q}{r_1^3} - \frac{6p'}{(Z')^3} - \frac{6p''}{(Z'')^3} \right) \frac{r^2}{7} + \left( \frac{3q}{r_1^5} + \frac{2p'}{(Z')^5} + \frac{2p''}{(Z'')^5} \right) \frac{r^4}{7},$$

and so on for the remaining four orbitals.

When axial charges are brought into the square-planar picture to an extent such that they do not upset the  $d_{xy}$  orbital's being the ground state for the positron, the three transitions  $\omega_1^{sq}$ ,  $\omega_2^{sq}$ , and  $\omega_3^{sq}$  are still the possible ones, but they must be modified by addition of  $\omega_1^{ax}$ ,  $\omega_2^{ax}$ , and  $\omega_3^{ax}$ . Thus addition of the axial charges will, according to Eq. (III-40), decrease  $\omega_1$  and  $\omega_3$  but leave  $\omega_2$  unaltered. This result is used in Part II as an aid in identifying Band 2.

Octahedron. The cubic field--with six point charges  $q$ , placed at the corners of a regular octahedron whose center is the Cu nucleus, at a distance  $r_1$  from the center--is a special case of the tetragonal bipyramid just discussed, with  $q = p' = p''$  and  $r_1 = Z' = Z''$ . Then the energy levels are

$$E_{z^2}^{\text{Oct}} = E_{xy}^{\text{Oct}} = \frac{6q}{r_1} \left( 1 + \frac{1}{6} \frac{r^4}{r_1^4} \right), \text{ and} \quad (III-41)$$

$$E_{x^2-y^2}^{\text{Oct}} = E_{xz}^{\text{Oct}} = E_{yz}^{\text{Oct}} = \frac{6q}{r_1} \left( 1 - \frac{1}{9} \frac{r^4}{r_1^4} \right).$$

Cis-Planar  $90^\circ$  Bonds. Now we consider the square-planar case but with two of the ligand charges removed, leaving two in cis-configuration, at  $(r, \theta, \phi)$  positions  $(r_1, 90^\circ, 45^\circ)$  and  $(r_1, 90^\circ, 135^\circ)$ . To find the proper set of orbitals with which to start, we set down the effects of the symmetry operations of group  $C_{2v}$  upon the d-functions:

	<u>I</u>	<u>C<sub>2</sub></u>	<u>σ<sub>yz</sub></u>	<u>σ<sub>xy</sub></u>
	d <sub>z</sub> <sup>2</sup>	d <sub>z</sub> <sup>2</sup>	d <sub>z</sub> <sup>2</sup>	d <sub>z</sub> <sup>2</sup>
	d(xz)	d(xz)	-d(xz)	-d(xz)
	d(yz)	-d(yz)	d(yz)	-d(yz)
	d(x <sup>2</sup> -y <sup>2</sup> )	d(x <sup>2</sup> -y <sup>2</sup> )	d(x <sup>2</sup> -y <sup>2</sup> )	d(x <sup>2</sup> -y <sup>2</sup> )
	d(xy)	-d(xy)	-d(xy)	d(xy)
χ	5	1	1	1

The functions may be classified into blocks of the matrix according to the irreducible representations to which they belong:

A: (1, 1, 1, 1). We have, as in the first section of this part,  $n_A = (1 \times 5 + 1 \times 1 + 1 \times 1 + 1 \times 1) / 4 = 2$ . The two functions  $d_{z^2}$  and  $d_{x^2-y^2}$  fall into irreducible representation A. Then we know that although there may be off-diagonal matrix elements connecting these two functions, there may be none connecting either of them with any of the other d-functions. (That is, we do not need to consider terms of the type  $\langle d_{z^2} \text{ or } d_{x^2-y^2} | V_{C_{2v}} | d_{xz} \text{ or } d_{yz} \text{ or } d_{xy} \rangle$ , but we must test the term  $\langle d_{z^2} d_{x^2-y^2} | V' \rangle$ .)

A': (1, 1, -1, -1);  $n_{A'} = 1$ . The  $d_{xz}$  function alone belongs to A' and so is an eigenfunction.

B: (1, -1, 1, -1);  $n_B = 1$ . The  $d_{yz}$  function alone belongs to B and so is an eigenfunction.

B': (1, -1, -1, 1);  $n_{B'} = 1$ . The  $d_{xy}$  function alone belongs to B' and so is an eigenfunction.

First, we should examine the possible matrix element of V' connecting the  $z^2$  and  $x^2-y^2$  functions. Their product is

$$d_{z^2} d_{x^2-y^2} = -\sqrt{5/49\pi} d_{x^2-y^2} - (\sqrt{15}/14\sqrt{\pi}) g_2.$$

The potential V' can have, because of its C<sub>2v</sub> symmetry, only terms involving the surface spherical harmonics s, p<sub>y</sub>, d<sub>z<sup>2</sup></sub>, d<sub>x<sup>2</sup>-y<sup>2</sup></sub>, f<sub>1</sub><sup>'</sup>, f<sub>3</sub><sup>'</sup>, g<sub>0</sub>, g<sub>2</sub>, g<sub>4</sub>, ... The potential can be written

$$V' = A_0 + A_1^1 p_y r + (A_2^0 d_{z^2} + A_2^2 d_{x^2-y^2}) r^2 + (A_3^1 f_1^1 + A_3^3 f_3^1) r^3 + (A_4^0 g_0 + A_4^2 g_2 + A_4^4 g_4) r^4 + \dots$$

If we expand the Coulomb potential along the z-axis, we find

$$V'(z\text{-axis}) = A_0 + A_2^0 z^2 \sqrt{5/4\pi} + 3A_4^0 z^4 / 2\sqrt{\pi} + \dots$$

and 
$$V'(z\text{-axis}) = (2q/r_1)(1 - z^2/2r_1^2 + 3z^4/8r_1^4 \dots)$$

Consequently, 
$$A_0 = 2q/r_1,$$

$$-A_2^0 = (2q/r_1)\sqrt{\pi/5}/r_1^2,$$

$$A_4^0 = (2q/r_1)\sqrt{\pi}/4r_1^4.$$

A similar evaluation of  $V'$  along the y-axis yields

$$\begin{aligned} V'(y\text{-axis}) &= (2q/r_1)(y^2/4r_1^2) - \sqrt{15/16\pi} A_2^2 y^2/r_1^2 \\ &+ [(2q/r_1)9/64r_1^4 - 3\sqrt{5/\pi} A_4^2/8r_1^4 + 3A_4^4\sqrt{35/\pi}/16r_1^4] y^4 \\ &+ \text{terms in } y^0, y, y^3, \text{ and higher powers than 4.} \end{aligned}$$

Also, expansion of the Coulomb potential due to the two charges along the y-axis gives

$$\begin{aligned} V'(y\text{-axis}) &= (2q/r_1)[(1 + y/\sqrt{2} r_1) + (1/4)(y/r_1)^2 \\ &- \sqrt{1/32} (y/r_1)^3 - (13/32)(y/r_1)^4 \dots] \end{aligned}$$

Setting the two expressions for  $V'(y\text{-axis})$  equal, one has

$$A_2^2 = 0, \text{ and}$$

$$\sqrt{7} A_4^4 - 2A_4^2 = (2q/r_1)(7\sqrt{5\pi}/12r_1^4).$$

To find  $A_4^4$  and  $A_4^2$  we need only examine the fourth-power term in the expansion of the potential along the line  $x = y$ . The coefficient of  $r^4$  along  $x = y$  is

$$[(9/64)(2q/r_1) - (3/16)\sqrt{35/\pi} A_4^4].$$

This corresponds to the coefficient of  $r^4$  in the actual electrostatic potential expansion,

$$(2q/r_1)(11/16 r_1^4).$$

Then 
$$A_4^4 = (2q/r_1) \sqrt{35\pi/12} r_1^4,$$

which we had previously stated to be the sum of  $A_4^4$  and  $A_4^2 \cdot \text{const.}$  Thus  $A_4^2 = 0$ . Since our possible off-diagonal matrix element is the integral over a combination of  $d_{x^2-y^2}$  and  $g_2$  times a potential function involving only terms orthogonal to those two, the element is zero. Then all the calculations are just the same as for the square-planar case, and the results are identical. In general, then, a cis-90° tetracoordination by 2 charges  $q_1$  at a distance  $r_1$  from the Cu nucleus and two charges  $q_2$  at a distance  $r_2$  from the nucleus results in the following set of levels:

$$E_{\text{any orbital}}^{\text{cis-1, 1;2, 2}} = (2q_1/r_1) \epsilon(r_1) + (2q_2/r_2) \epsilon(r_2),$$

where  $\epsilon(r)$  is defined by

$$E_{\text{same orbital}}^{\text{sq}} = (4q/r) \epsilon(r).$$

TransPlanar 90° Bonds. Let us now consider the effect of two pairs of charges arranged around the Cu ion in a trans-planar configuration. Charges  $q_1$  lie at  $(r_1, 90^\circ, 45^\circ)$  and  $(r_1, 90^\circ, 225^\circ)$ ;  $q_2$  at  $(r_2, 90^\circ, 135^\circ)$  and  $(r_2, 90^\circ, 315^\circ)$ . The symmetry group for this case is  $D_2$ . The operations of the group upon our initial orbital functions follow:

I	$C_2(z)$	$C_2(x = -y)$	$C_2(x = y)$
$d_{z^2}$	$d_{z^2}$	$d_{z^2}$	$d_{z^2}$
$d_{xy}$	$d_{xy}$	$d_{xy}$	$d_{xy}$
$d_{x^2-y^2}$	$d_{x^2-y^2}$	$-d_{x^2-y^2}$	$-d_{x^2-y^2}$
$d_{xz}$	$-d_{xz}$	$d_{yz}$	$-d_{yz}$
$d_{yz}$	$-d_{yz}$	$-d_{xz}$	$-d_{xz}$

In the same way as we have previously done, we find that  $d_{z^2}$  and  $d_{xy}$  both belong to the same irreducible representation and so may have a perturbation matrix element connecting them, while  $d_{x^2-y^2}$ ,  $(d_{xz} \pm d_{yz})/\sqrt{2}$  all belong to different irreducible representations and so are eigenfunctions.

First, we shall find the perturbation matrix element connecting  $d(z^2)$  and  $d(xy)$ . The product function is



$$d(z^2)d(xy) = -\sqrt{5/49\pi} d(xy) - (\sqrt{15/14\sqrt{\pi}}) g_2'$$

Of the surface spherical harmonics which appear in an expansion of the  $D_{2h}$  potential, only the s, d, and g functions need be considered. The general potential expression for  $D_{2h}$  symmetry is

$$V' = A_0 + r^2 A_2^0 d(z^2) + r^2 A_2^2 d(xy) + r^4 [A_4^0 g_0 + A_4^2 g_2' + A_4^4 g_4] + \dots$$

Now, along the z axis this reduces to

$$V'(z\text{-axis}) = A_0 + \sqrt{5/4\pi} A_2^0 z^2 + A_4^0 z^4 \frac{3}{2} \sqrt{\pi} + \dots$$

Expansion of the Coulomb potential along the z-axis yields

$$V'(z\text{ axis}) = \sum_{j=1}^2 \frac{2q_j}{r_j} \left[ 1 - \frac{1}{2} \left(\frac{z}{r_j}\right)^2 + \frac{3}{8} \left(\frac{z}{r_j}\right)^4 - \dots \right]$$

Equating coefficients, we find

$$A_0 = \frac{2q_1}{r_1} + \frac{2q_2}{r_2};$$

$$A_2^0 = -\sqrt{\pi/5} \left( \frac{2q_1}{r_1^3} + \frac{2q_2}{r_2^3} \right);$$

$$A_4^0 = (\sqrt{\pi}/4) \left( \frac{2q_1}{r_1^5} + \frac{2q_2}{r_2^5} \right).$$

Next, we examine the potential along  $x = y$ . There, at radial distance  $r''$ ,

$$V'(x = y) = A_0 + r''^2 \sqrt{5/16\pi} (\sqrt{3} A_2^2 - A_2^0) + r''^4 (9A_4^0/16\sqrt{\pi} + A_4^2 \sqrt{45/64\pi} - A_4^4 \sqrt{315/256\pi}) + \dots$$

The potential expansion there is just

$$V'(x = y) = (2q_1/r_1) \left[ 1 + \left(\frac{r''}{r_1}\right)^2 + \left(\frac{r''}{r_1}\right)^4 + \dots \right] + \left(\frac{2q_2}{r_2}\right) \left[ 1 - \frac{r''^2}{2r_2^2} + \frac{3}{8} \left(\frac{r''}{r_2}\right)^4 + \dots \right].$$

After equating equivalent terms in the two preceding series, we have

$$\sqrt{3}A_2^{2'} - A_2^0 = 4\sqrt{\pi/5} [(2q_1/r_1^3) - (1/2)(2q_2/r_2^3)] ;$$

$$3A_4^0 + 2\sqrt{5}A_4^{2'} - \sqrt{35}A_4^4 = (16\sqrt{\pi}/3)[(2q_1/r_1^5) + (3/8)(2q_2/r_2^5)] .$$

Using the values previously found for  $A_2^0$  and  $A_4^0$ , we can evaluate the following quantities,

$$A_2^{2'} = \sqrt{3\pi/5} [(2q_1/r_1^3) - (2q_2/r_2^3)] ,$$

$$2A_4^{2'} - \sqrt{7}A_4^4 = \sqrt{5\pi/16} [(11/3)(2q_1/r_1^5) + (2q_2/r_2^5)] .$$

Now the relationship between  $A_4^{2'}$  and  $A_4^4$  may be found by considering the fourth-power term in the potential expansion along the line  $x = -y$ . Here the general potential expression is the same as along the line  $x = y$  in the fourth-power term except that the  $A_2^{2'}$  term changes sign. Also, the electrostatic potential expansion is the same except that  $q_1$  and  $r_1$  interchange with  $q_2$  and  $r_2$ . Then we have

$$-2A_4^{2'} - \sqrt{7}A_4^4 = \sqrt{5\pi/16} [(11/3)(2q_2/r_2^5) + (2q_1/r_1^5)] .$$

Together with the previous relationship, this gives us

$$A_4^{2'} = (1/6) \sqrt{5\pi} [(2q_1/r_1^5) - (2q_2/r_2^5)]$$

$$\text{and } A_4^4 = (-\sqrt{35\pi}/12)[(2q_1/r_1^5) + (2q_2/r_2^5)] .$$

Then the off-diagonal matrix element,  $\langle d(z^2)d(xy)V' \rangle$ , is easily evaluated by the orthogonality of the functions in terms of which  $d(z^2)d(xy)$  and  $V'$  are expressed. Its value is

$$\begin{aligned} \langle xy|V'|z^2 \rangle &= \sqrt{3/49} [(2q_2/r_2^3) - (2q_1/r_1^3)] \overline{r^2} \\ &+ (5\sqrt{3}/84)[(2q_2/r_2^5) - (2q_1/r_1^5)] \overline{r^4} . \end{aligned}$$

The corresponding diagonal elements are easily evaluated:

$$\langle xy|V'|xy \rangle = \sum_{j=1}^2 \left( \frac{2q_j}{r_j} \right) \left( 1 + \frac{\overline{r^2}}{7r_j^2} - \frac{4}{21} \frac{\overline{r^4}}{r_j^4} \right) ,$$

$$\langle z^2|V'|z^2 \rangle = \sum_{j=1}^2 \left( \frac{2q_j}{r_j} \right) \left( 1 - \frac{\overline{r^2}}{7r_j^2} + \frac{3}{28} \frac{\overline{r^4}}{r_j^4} \right) .$$

Now, the energy levels arising from those two orbitals are given by

$$W_{\pm} = \sum_{j=1}^2 \left( \frac{2q_j}{r_j} \right) \left( 1 - \frac{5}{84} \frac{\overline{r_j^4}}{r_j^4} \right) \quad (\text{III-41})$$

$$\pm \sqrt{\left[ \sum_{j=1}^2 \left( \frac{q_j}{r_j} \right) \left( 1 - \frac{5}{84} \frac{\overline{r_j^4}}{r_j^4} \right) \right]^2 + \left[ \sum_{j=1}^2 (-1)^j \left( \frac{2q_j}{r_j} \right) \left( \sqrt{\frac{3}{49}} \frac{\overline{r_j^2}}{r_j^2} + \frac{5\sqrt{3}}{84} \frac{\overline{r_j^4}}{r_j^4} \right) \right]^2}$$

The proper orbital combinations are

$$\psi_{\pm} = \sqrt{\frac{\langle xy | V' | z^2 \rangle^2}{[\langle xy | V' | xy \rangle - W_{\pm}]^2 + \langle xy | V' | z^2 \rangle^2}} d(xy) \quad (\text{III-42})$$

$$\pm d(z^2) \sqrt{\frac{[\langle xy | V' | xy \rangle - W_{\pm}]^2}{[\langle xy | V' | xy \rangle - W_{\pm}]^2 + \langle xy | V' | z^2 \rangle^2}}$$

Of these orbitals,  $\psi_+$  will be the ground state of the positron in the  $\text{Cu}^{++}$  ion. The orbital will have the shape of a four-leaf clover in the  $xy$  plane, with the two lobes directed towards the strongest and closest ligand charges greater than the two lobes pointing toward the weaker and more distant charges, plus two small lobes directed along the  $z$  axis above and below the  $xy$  plane. The shape of such an orbital is pictured in Fig. 22.

The remaining three orbital levels are calculated quite easily. For the  $x^2 - y^2$  orbital, we find

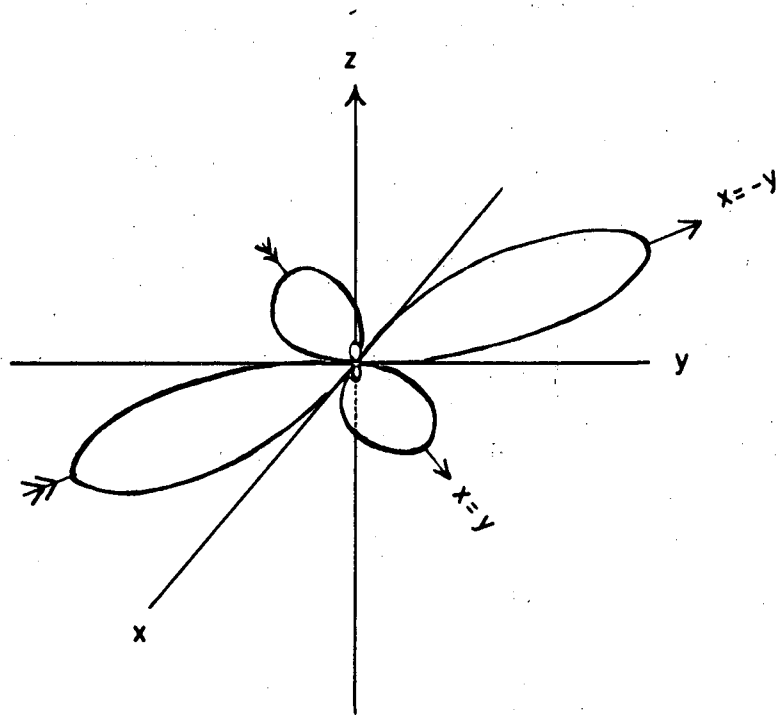
$$E_{x^2-y^2} = \sum_{j=1}^2 \frac{2q_j}{r_j} \left( 1 + \frac{\overline{r_j^2}}{7r_j^2} + \frac{19}{84} \frac{\overline{r_j^4}}{r_j^4} \right) \quad (\text{III-43})$$

To evaluate the levels for the two  $xz$ ,  $yz$  combinations one needs to know the squares of the functions. They are:

$$\left( \frac{d_{xz} \pm d_{yz}}{\sqrt{2}} \right)^2 = \frac{(d_{xz}^2 + d_{yz}^2)}{2} \pm d_{xz} d_{yz}$$

Now,  $d^2(xz)$  and  $d^2(yz)$  are the same except for a term in  $g_2$  (Eq. III-30), which does not appear in our potential. Thus we only need  $d(xz) \pm d(xz)d(yz)$ . The cross product is just

$$d(xz)d(yz) = (1/14)\sqrt{15\pi} d(xy) - (1/7)\sqrt{5/\pi} g_2'$$



MU-9874

Fig. 22. Sketch of angular variation of electron density for orbital ( $9d_{xy} + d_{z^2}$ ):

Knowing this, we evaluate the two orbital energies as

$$E_{(x\pm y)z} = \sum_{j=1}^2 \frac{2q_j}{r_j} \left[ \left( 1 - \frac{1}{14} \frac{r^2}{r_j^2} - \frac{19}{12} \frac{r^4}{r_j^4} \right) \mp (-1)^j \left( \frac{3r^2}{14r_j^2} - \frac{5}{42} \frac{r^4}{r_j^4} \right) \right]$$

Thus we see that in trans-90° bonding, as opposed to cis-90° bonding, there are five distinct energy levels, and only one of the proper orbitals is one of our original functions. The ground-state orbital is made up of the  $xy$  and  $2z^2 - x^2 - y^2$  orbitals, so combined as to allow the positron to spend more of its time nearest the strongest two ligand charges. The  $(x + y)z$  and  $(x - y)z$  orbitals are just the same as the  $xz$  and  $yz$  orbitals, but rotated 45° about the  $z$  axis, so that they extend over and under the bond axes. Naturally, that one which extends over the axis connecting the  $\text{Cu}^{++}$  nucleus with the two strongest ligand charges will have lower energy for a positron than will the other.

Overlapping ligand and  $\text{Cu}^{++}$  Charge. For the sake of completeness, we finish this section with a statement of the method of attack for calculating crystal field splittings where the ligand and central ion charge clouds may overlap. We take the symmetry of the ligand charge cloud as  $D_{4h}$ , for an example. Consider an infinitesimally thin spherical shell, centered at the  $\text{Cu}^{++}$  nucleus, of radius  $\gamma$  and thickness  $d\gamma$ , containing ligand charge. The potential expression, analogous to Eq. (III-31), is

$$\begin{aligned} dV_\gamma = & A_0(\gamma)d\gamma + d(x^2 - y^2) \left[ (A_2(\gamma)r^2)_{r<\gamma} + (A_2'(\gamma)/r^2)_{r>\gamma} \right] d\gamma \\ & + g_0 \left[ (A_4(\gamma)r^4)_{r<\gamma} + (A_4'(\gamma)/r^4)_{r>\gamma} \right] d\gamma \\ & + g_4 \left[ (A_{sq}(\gamma)r^4)_{r<\gamma} + (A_{sq}'(\gamma)/r^4)_{r>\gamma} \right] d\gamma. \end{aligned} \quad \text{(III-45)}$$

Now integration is carried out over  $\gamma$ . We multiply Eq. (III-45) by each of Eq. (III-30) in turn and integrate over  $r$ ,  $\phi$ ,  $\theta$  as before and then over to  $\gamma$  to obtain

$$\left. \begin{aligned}
 E_{z^2}^{\text{tet}} &= A_0 + 2\sqrt{5}A_2 + 6A_4, \\
 E_{xz}^{\text{tet}} &= E_{yz}^{\text{tet}} = A_0 + \sqrt{5}A_2 - 4A_4, \\
 E_{x^2-y^2}^{\text{tet}} &= A_0 - 2\sqrt{5}A_2 + A_4 + \sqrt{35} A_{\text{sq}}, \\
 E_{xy}^{\text{tet}} &= A_0 - 2\sqrt{5}A_2 + A_4 - \sqrt{35} A_{\text{sq}},
 \end{aligned} \right\} \text{(III-46)}$$

where

$$\begin{aligned}
 A_0 &= \int_0^\infty A_0(\gamma) d\gamma, \\
 A_{i \neq 0} &= (1/14\sqrt{\pi}) \int_0^\infty \left[ \int_0^\gamma A_i(\gamma) r^{n+2} R^2 dr \right. \\
 &\quad \left. + \int_\gamma^\infty A_i'(\gamma) r^{2-n} R^2 dr \right] d\gamma.
 \end{aligned}$$

(n = 2 for i = 2; n = 4 for i = 4, sq.)

The results are just the same as in Eq. (III-36), except that here the prescribed method for obtaining the coefficients is less restricted.

#### D. Bonding Information from Paramagnetic Resonance

The paramagnetic resonance technique is discussed in an excellent review article by Bleaney and Stevens.<sup>58</sup> Here will be given an account of how the results of the technique, together with the LCAO-MO scheme of Part III. A, may be used to obtain information about bond type in cupric chelates.

A brief description of the experiment follows: A sample to be examined is placed in a strong homogeneous magnetic field  $H_v$  (~3000 oersteds) along some crystal direction, let us say the v axis. Our  $\text{Cu}^{++}$  sample possesses unpaired electrons having spin  $S = 1/2$  and orbital angular momentum  $L$  (in units of  $\hbar$ ). The spin is quantized along the v axis; there are two possible orientations,  $\alpha$  and  $\beta$ , with resulting magnetic moments

$$\mu_v(\alpha) = (1 + L_v^\alpha)\mu_B \text{ and}$$

$$\mu_v(\beta) = (-1 + L_v^\beta)\mu_B ,$$

where  $\mu_B$  is the Bohr magneton and  $L_v$  is the orbital angular momentum projected on the  $v$  axis. Now transitions are caused to take place (by means of a microwave field) between the  $\alpha$  and the  $\beta$  states which have energies  $W = -\mu_v H_v$ . The transition energy,

$$\Delta W = W(\beta) - W(\alpha) = (2 + L_v^\alpha - L_v^\beta)\mu_B H_v , \quad (\text{III-47})$$

is measured.

The 3d orbitals that we are interested in are much affected by environment. As we have seen in the section immediately preceding this one, for tetragonal arrangement of ligands, the ground state of the unpaired electron is the  $d(xy)$  orbital. The  $d(xy)$  orbital is easily shown to have no quantized orbital momentum in any particular direction: the expectation value for the observable  $L_v$  is given by<sup>59, 60</sup>

$$\langle L_v \rangle = \langle d(xy) | L_v | d(xy) \rangle .$$

Now the  $L_x$ ,  $L_y$ , and  $L_z$  are given as the quantum-mechanical expressions:

$$\left. \begin{aligned} iL_x &= y(\partial/\partial z) - z(\partial/\partial y) = -\sin\phi(\partial/\partial\theta) - \cot\theta\cos\phi(\partial/\partial\phi) , \\ iL_y &= z(\partial/\partial x) - x(\partial/\partial z) = \cos\phi(\partial/\partial\theta) - \cot\theta\sin\phi(\partial/\partial\phi) , \\ iL_z &= x(\partial/\partial y) - y(\partial/\partial x) = \partial/\partial\phi . \end{aligned} \right\} (\text{III-48})$$

Therefore, the expected value for  $L_x$  is

$$\langle L_x \rangle_{\text{pr.}} = \langle xy | y(\partial xy/\partial z) - z(\partial xy/\partial y) \rangle = 0 ,$$

(where pr. denotes "proportional to"). Likewise, we have for  $v = z$  or  $y$ :

$$\langle L_y \rangle_{\text{pr.}} = \langle xy | z(\partial xy/\partial x) - x(\partial xy/\partial z) \rangle = 0 ,$$

and

$$\langle L_z \rangle_{\text{pr.}} = \langle xy | x(\partial xy/\partial y) - y(\partial xy/\partial x) \rangle = 0 .$$

Therefore, to that approximation in which the ground state is assumed to be  $d(xy)$ ,  $\Delta W$  will just be the spin-only value,  $2\mu_B H_V$ .

Now, it is customary to assume that a spin-orbit magnetic dipole coupling energy of magnitude  $\lambda L \cdot S$  exists, where  $\lambda$  is a constant characteristic of the particular orbital of the atom in question. This coupling energy introduces, by standard second-order perturbation theory, an admixture of excited orbital states into the ground-state function. For the corrected ground-state function, which we call  $\psi_0''$ , the expectation value of  $L_V$  will not be zero; thus the  $\lambda L \cdot S$  interaction will cause the measured transition energy to be different from the spin-only value. If we define the experimental value of  $\Delta W$  as

$$\Delta W \equiv g_V \mu_B H_V \equiv (2 + \delta g_V) \mu_B H_V ,$$

then  $\delta g_V$  measures the orbital contributions to resonance. It is this quantity that we shall calculate.

Let us use as first-approximation functions the following set (see Part III. A, especially Table VII and Eq. (III-17)):

$$\begin{aligned} \psi_{0\alpha} &= [a d(xy) - \sqrt{1 - a^2} \Sigma_-] \alpha , \\ \psi_{0\beta} &= [a d(xy) - \sqrt{1 - a^2} \Sigma_-] \beta , \\ \psi_{1\alpha} &= [b d(xz) - \sqrt{1 - b^2} \Pi_1] \alpha , \\ \psi_{1\beta} &= [b d(xz) - \sqrt{1 - b^2} \Pi_1] \beta , \\ \psi'_{1\alpha} &= [b d(yz) - \sqrt{1 - b^2} \Pi_2] \alpha , \\ \psi'_{1\beta} &= [b d(yz) - \sqrt{1 - b^2} \Pi_2] \beta , \\ \psi_{2\alpha} &= [c d(x^2 - y^2) - \sqrt{1 - c^2} \Gamma_-] \alpha , \\ \psi_{2\beta} &= [c d(x^2 - y^2) - \sqrt{1 - c^2} \Gamma_-] \beta , \\ \psi_{3\alpha} &= [e d_0 - f(\Sigma_+, Z_+)] \alpha , \text{ and} \\ \psi_{3\beta} &= [e d_0 - f(\Sigma_+, Z_+)] \beta . \end{aligned} \tag{III-49}$$

Now we feed the above set of functions into the standard second-order perturbation formulae,



$$\psi_{0\alpha}'' = \psi_{0\alpha} + \sum_j \psi_j (k_{j\alpha} \alpha + k_{j\beta} \beta), \quad (\text{III-50})$$

where the k's are given by

$$k_{js} = \lambda \langle \psi_{js} | L \cdot S | \psi_{0\alpha} \rangle / \omega_j, \quad (\text{III-51})$$

where s denotes either  $\alpha$  or  $\beta$ .

Now the  $\psi_0$  involve no spin coordinates and the  $\alpha$  and  $\beta$  no space coordinates; L components operate only on space coordinates while S components operate only on spin coordinates. Consequently, Eq. (III-51) may be written:

$$2\omega_j k_{js} = \lambda \langle j | L | 0 \rangle \cdot \langle s | \sigma | \alpha \rangle, \quad (\text{III-52})$$

where  $\sigma$  is the spin vector ( $= 2S$ ) defined by Dirac.<sup>59</sup> The  $2\omega_j k_{js}$  are easiest to find by considering the  $4 \times 3$  matrix  $(L_{jv})$  having for row j the x, y, z components of  $\langle j | L | 0 \rangle$  and the  $3 \times 2$  matrix  $(\sigma_{vs})_{\alpha}$  having for column s the x, y, z components of  $\langle s | \sigma | \alpha \rangle$ . Then the matrix

$$(2\omega_j k_{js} / \lambda)_{\alpha} = (L_{jv})(\sigma_{vs})_{\alpha}. \quad (\text{III-53})$$

The  $L_{jv}$  are obtained as before by application of the L components Eq. (III-48) to the functions (III-49), multiplying again by Eq. (III-49), and integrating. A sample calculation for the matrix element  $L_{1x}$  follows:

$$\begin{aligned} L_{1x} &= (1/i) \langle b | d(xz) | a [-\sin\phi (\partial d(xy)/\partial \theta) \\ &\quad - \cot\theta \cos\phi (\partial d(xy)/\partial \phi)] \rangle \\ &= (ab/i) \langle d(xz) | \sqrt{15/16\pi} (-2\sin\theta \cos\theta \sin\phi \sin 2\phi \\ &\quad - 2\sin\theta \cos\theta \cos\phi \cos 2\phi) \rangle \\ &= (-ab/i) \langle d(xz) | d(xz) \rangle = -ab/i. \end{aligned}$$

Here it should be noticed that we neglect the orbital moment of oxygen orbitals; the neglect probably introduces no error of measurable magnitude into the calculation. The entire  $(L_{jv})$  matrix is

$$(L_{jv}): \quad \begin{matrix} j=1 \\ 1' \\ 2 \\ 3 \end{matrix} \begin{bmatrix} \underline{x} & \underline{y} & \underline{z} \\ iab & 0 & 0 \\ 0 & -iab & 0 \\ 0 & 0 & -2iac \\ 0 & 0 & 0 \end{bmatrix}$$

The spin matrix,  $(\sigma_{vs})$ , is dependent upon the direction of spin quantization. We shall denote that direction, given by the direction of applied external magnetic field to a good approximation, by a left-hand subscript. Thus  $z(\sigma_{vs})_{\alpha}$  means the spin matrix for z-quantization. Since the x and y directions are perfectly equivalent for tetragonal symmetry, we need consider only one of them; we need, that is, only  $z(\sigma_{vs})_{\alpha}$  and  $y(\sigma_{vs})_{\alpha}$ . They are given below:

$$z(\sigma_{vs})_{\alpha}: \quad \begin{matrix} x \\ y \\ z \end{matrix} \begin{bmatrix} \underline{\alpha} & \underline{\beta} \\ 0 & 1 \\ 0 & -i \\ 1 & 0 \end{bmatrix}$$

$$y(\sigma_{vs})_{\alpha}: \quad \begin{matrix} x \\ y \\ z \end{matrix} \begin{bmatrix} 0 & -i \\ 1 & 0 \\ 0 & 1 \end{bmatrix}$$

Now, the  $(2\omega_{jjs}/\lambda)_{\alpha}$  are the matrix products:

$$z(2\omega_{jjs}/\lambda)_{\alpha} = \begin{matrix} 1 \\ 1' \\ 2 \\ 3 \end{matrix} \begin{bmatrix} \underline{\alpha} & \underline{\beta} \\ 0 & iab \\ 0 & ab \\ -2iac & 0 \\ 0 & 0 \end{bmatrix},$$

and

$$y(2\omega_{jjs}/\lambda)_{\alpha} = \begin{matrix} 1 \\ 1' \\ 2 \\ 3 \end{matrix} \begin{bmatrix} \underline{\alpha} & \underline{\beta} \\ 0 & ab \\ -iab & 0 \\ 0 & -2iac \\ 0 & 0 \end{bmatrix}.$$

Also, we are interested in the transition from the corrected  $\psi_{0\alpha} - \psi''_{0\alpha}$  to the corrected  $\psi_{0\beta} - \psi''_{0\beta}$ . Hence we need the  $\langle \beta | \sigma | s \rangle$  matrices, which we call  $(\sigma_{vs})_{\beta}$ :

$$z^{(\sigma_{vs})} \beta = \begin{matrix} & \underline{\alpha} & \underline{\beta} \\ x & \begin{bmatrix} 1 & 0 \\ i & 0 \\ 0 & -1 \end{bmatrix} \\ y & \\ z & \end{matrix} ,$$

and

$$y^{(\sigma_{vs})} \beta = \begin{matrix} & \underline{\alpha} & \underline{\beta} \\ x & \begin{bmatrix} i & 0 \\ 0 & -1 \\ 1 & 0 \end{bmatrix} \\ y & \\ z & \end{matrix} .$$

These result in:

$$z^{(2\omega_j k_{js}/\lambda)} \beta = \begin{matrix} 1 & \begin{bmatrix} iab & 0 \\ ab & 0 \\ 0 & 2iac \\ 0 & 0 \end{bmatrix} \\ 1' & \\ 2 & \\ 3 & \end{matrix}$$

and

$$y^{(2\omega_j k_{js}/\lambda)} \beta = \begin{matrix} & \underline{\alpha} & \underline{\beta} \\ 1 & \begin{bmatrix} -ab & 0 \\ 0 & iab \\ -2iac & 0 \\ 0 & 0 \end{bmatrix} \\ 1' & \\ 2 & \\ 3 & \end{matrix} .$$

Now it is possible to write down immediately the perturbed functions  $\psi''_0$ : For magnetic field along the z axis,

$$z \psi''_{0\alpha} = \psi_0 \alpha + (a\lambda/2) [(i\psi_1 + \psi'_1)(\beta b/\omega_1) - 2ic \psi_2 \alpha/\omega_2] ,$$

$$z \psi''_{0\beta} = \psi_0 \beta + (a\lambda/2) [(i\psi_1 + \psi'_1)(\alpha b/\omega_1) + 2ic \psi_2 \beta/\omega_2] .$$

For magnetic field along the y axis,

$$y \psi''_{0\alpha} = \psi_0 \alpha + (a\lambda/2) \{ [(b\psi_1/\omega_1) - (2ic \psi_2/\omega_2)] \beta - (ib \psi'_1/\omega_1) \alpha \} ,$$

$$y \psi''_{0\beta} = \psi_0 \beta + (a\lambda/2) \{ [-(b\psi_1/\omega_1) - (2ic \psi_2/\omega_2)] \alpha + ib \psi'_1 \beta/\omega_1 \} .$$

We need the expectation values of  $L_z$ ,

$$\langle L_z \rangle_{\alpha} = \langle z \psi''_{0\alpha} | L_z | z \psi''_{0\alpha} \rangle , \text{ and}$$

$$\langle L_z \rangle_\beta = \langle \overline{\psi''_{0\beta}} | L_z | \psi''_{0\beta} \rangle.$$

Using Eq. (III-48) and the above corrected functions, we obtain directly

$$iL_z \psi_0 = 2ad(x^2 - y^2), \quad iL_z \psi_1 = -bd(yz),$$

$$iL_z \psi'_1 = bd(xz), \quad \text{and} \quad iL_z \psi_2 = -2cd(xy).$$

Remembering that  $\alpha\beta$  products yield zero, we find

$$\langle L_z \rangle_\alpha = (4c^2 a^2 \lambda / \omega_2) - (b^4 \lambda^4 a^2 / 2\omega_1^2), \quad \text{and}$$

$$\langle L_z \rangle_\beta = -(4c^2 a^2 \lambda / \omega_2) - (b^4 \lambda^4 a^2 / 2\omega_1^2),$$

and therefore

$$\delta g_{||} = \langle L_z \rangle_\alpha - \langle L_z \rangle_\beta = 8\lambda c^2 a^2 / \omega_2.$$

(The mark || is a common notation meaning "magnetic field along the principal symmetry axis".  $\perp$  means "magnetic field perpendicular to that axis".)

To find  $\delta g_{\perp}$ , we need the expectation values of  $L_y$ ,

$$\langle L_y \rangle_\alpha = \langle \overline{\psi''_{0\alpha}} | L_y | \psi''_{0\alpha} \rangle \quad \text{and}$$

$$\langle L_y \rangle_\beta = \langle \overline{\psi''_{0\beta}} | L_y | \psi''_{0\beta} \rangle.$$

These are calculated as before; the values are

$$\langle L_y \rangle_\alpha = (a^2 b^2 \lambda / \omega_1) - (abc\lambda)^2 / \omega_1 \omega_2,$$

$$\langle L_y \rangle_\beta = -(a^2 b^2 \lambda / \omega_1) + (abc\lambda)^2 / \omega_1 \omega_2.$$

Neglecting the very small second term, we then have

$$\delta g_{\perp} = 2\lambda a^2 b^2 / \omega_1.$$

The ratio of the  $\delta g$ 's is then

$$(\delta g_{||} / \delta g_{\perp}) = (4c^2 \omega_1 / b^2 \omega_2).$$

Providing that the approximations we have made are not obscuring a very important effect, we may use the paramagnetic resonance results, in conjunction with optical spectra, to find the coefficients  $c_j$  in Eq. (III-17). (In this section, for convenience, we have used the letters  $a$ ,  $b$ , and  $c$  to denote the  $c_j$ 's.) The values obtained by McGarvey<sup>23, 37</sup> for  $g_{\parallel}$  and  $g_{\perp}$  of cupric acetylacetonate crystals,  $2.25 \pm 0.02$  and  $2.071 \pm 0.002$ , respectively, have already been used at the end of Part III. A to find  $c/b = 0.816$ , or  $c^2/b^2 = 2/3$ . The spin-orbit coupling constant  $\lambda$  is about  $830 \text{ cm}^{-1}$  for  $\text{Cu}^{++}$ ; from this and from the value for  $\omega_1$ ,  $15000 \text{ cm}^{-1}$ , given in Part II, we find

$$\delta g_{\parallel} = 0.25 = 6640a^2c^2/15000 \approx 0.443a^2c^2, \text{ or}$$

$$a^2c^2 \approx 0.565;$$

$$\delta g_{\perp} = 0.071 = 1660a^2b^2/18800 \approx 0.0883a^2b^2, \text{ or}$$

$$a^2b^2 \sim 0.80 .$$

Below are listed, for several possible values of  $b^2$ , the corresponding values of  $a^2$  and  $c^2$ :

$\underline{b^2}$	$\underline{c^2}$	$\underline{a^2}$	$\underline{b}$	$\underline{a}$	$\underline{c}$
1.00	0.666	0.80	1.00	0.894	0.816
0.96	0.64	0.834	0.98	0.913	0.80
0.92	0.613	0.87	0.96	0.933	0.782
0.88	0.587	0.91	0.938	0.954	0.766
0.84	0.56	0.952	0.916	0.976	0.748
0.80	0.533	1.00	0.894	1.00	0.73

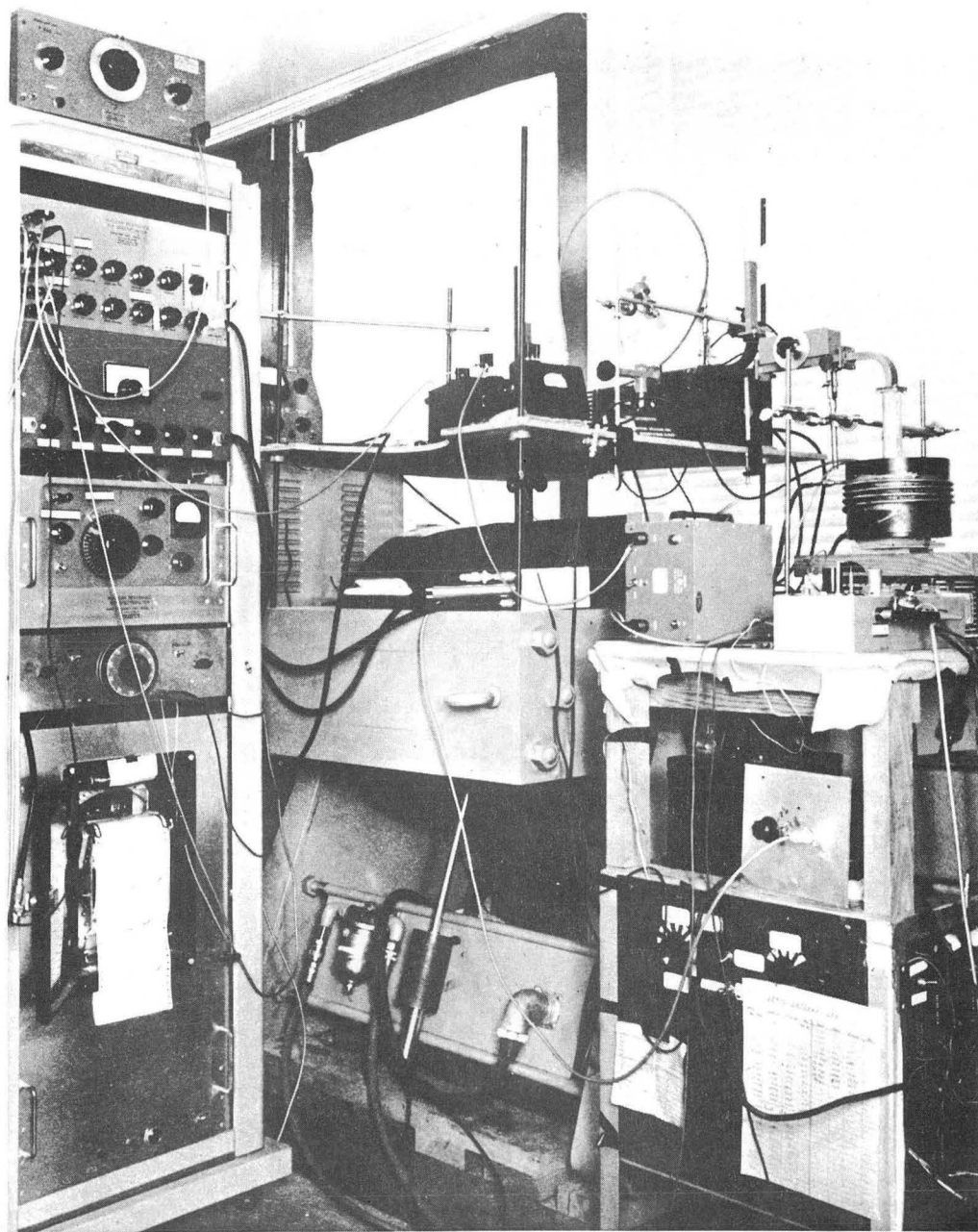
#### IV. ELECTRON-SPIN RESONANCE IN TRANSITION METAL CHELATES

##### Introduction

Although the paramagnetic resonance technique has been used extensively to investigate transition metal ions in solid salts, study of the large class of organic-soluble compounds of those ions has been largely neglected. The advantages that may be gained from such studies are numerous. Not only may one investigate molecular binding in single crystals (as sketched in Part III. D), but one may also be able to observe well-separated nuclear hyperfine structure for the dissolved complex or chelate. Single-crystal and solution work are complementary: neither may replace the other nor provide just the same information. Not only may binding be studied by the electron-spin resonance method applied to solutions, but also other facts important to chemists may be learned. For example, one might take advantage of the difference in resonance patterns between two or more chemical species to study kinetics and reaction equilibria. This last application has been made by Cohn and Townsend,<sup>68</sup> who studied the complexing of  $Mn^{++}$  ions in aqueous solution by observing the disappearance of the ion's resonance absorption as it complexed. Really, the example cited is just the reverse of the kind of observation in which we have been particularly interested--examination of ions in complexes directly. Two sorts of study are reported here, one a survey of resonance absorption in organic solutions of some chelate compounds of all the first-row transition metals in at least one oxidation state each, and the other a more careful study of resonance absorption in vanadyl acetylacetonate and related compounds.

##### Experimental

Measurements were taken with the electron-spin resonance equipment of Dr. Harry Weaver at Varian Associates, Palo Alto. A general view of the apparatus is shown in Fig. 23a. The magnet is seen in the center of the picture; at the upper right some of the microwave



ZN-1308

Fig. 23a. View of electron-spin resonance spectrometer used in this study. (Picture by courtesy of Dr. Harry Weaver and Varian Associates, Inc., Palo Alto, Cal.)

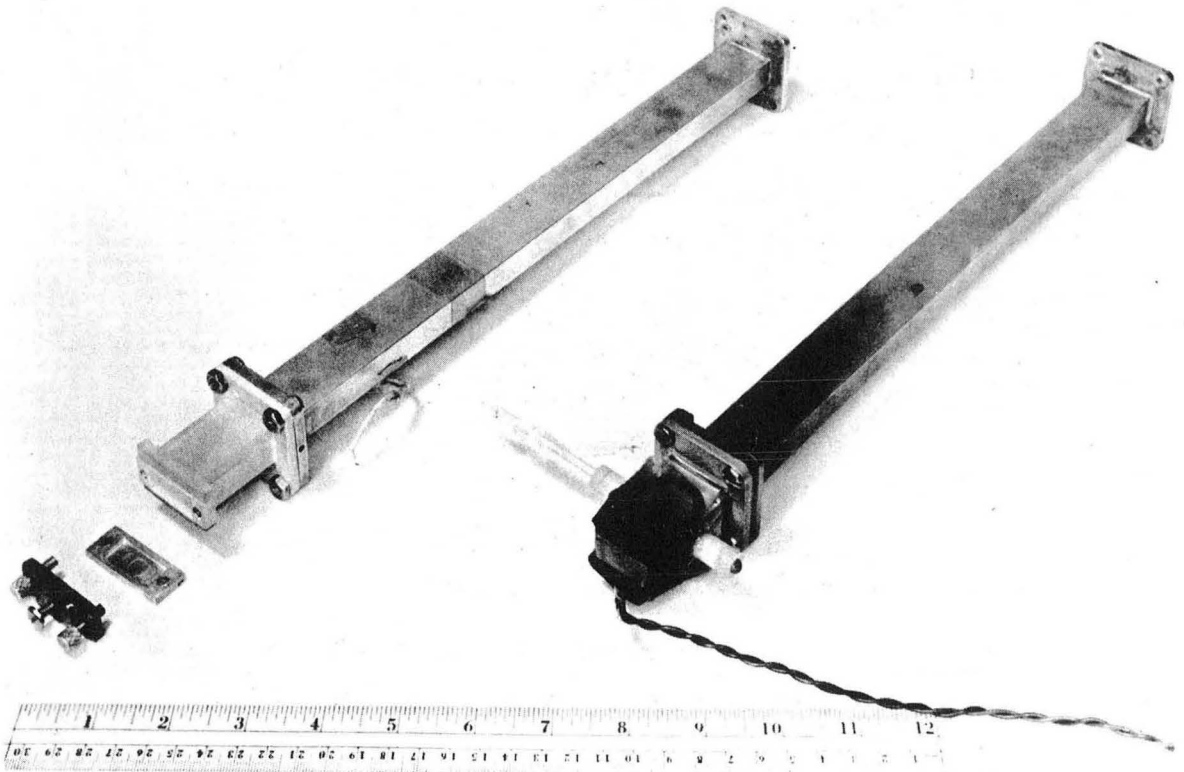
equipment is visible. At the lower right one sees the front of a large block of dry cells used to power the klystron--very good frequency stabilization results from the use of batteries. The small strip chart shown in the rack at the left was used for the survey study. Data for the quantitative work were taken with a large Bristol linear strip chart recorder. Magnetic field measurements were taken in the following manner: A nuclear-resonance head was mounted between the magnet pole pieces at a point where the field was, within the limits of desired accuracy, the same as at the electron-resonance sample position. To find the field, we measured the frequency at which nuclear resonance of protons in a water sample occurred. The numbers marked on all the figures in this part are the actual laboratory measurements--the frequency of which the proton resonance frequency was the fourth harmonic, in kc/sec. To find the field, in oersteds, from these laboratory numbers one must multiply by four times the field/frequency ratio characteristic of the proton resonance; the required factor is 0.975. Microwave frequency measurements were made by observation of the field at which paramagnetic resonance occurred for a bit of free radical, diphenylpicrahydrazyl. The microwave frequency, in mc/sec, is then just 2.80 times the field, in oersteds. The quantity observed was the first derivative of power absorbed in the sample with respect to field. Samples were mounted in two ways, as shown in Fig. 23b. For some of the earlier measurements, samples were placed in the recess in the bottom plate of the two-piece cavity, while all the later measurements were taken with the sample--powder or solution--in small-bore tubing passed through the walls of the other cavity.

## Results

### Survey Study

A number of transition-metal ion chelate compounds were surveyed for easily detectable paramagnetic resonance at room temperature, in powder and in solution wherever possible. The results are listed.





ZN-1309

Fig. 23b. The two waveguide terminating cavities with sample holders used in the electron spin-resonance experiments. Sample was placed in depression in removable bottom of left-hand cavity, in glass tube through center of right-hand one. (Picture courtesy of Dr. Harry Weaver and Varian Associates, Inc., Palo Alto, Cal.)

Vanadyl. 1. Vanadyl acetylacetonate. Broad resonance line in solid powder; eight narrow, well-spaced lines of varying intensity in toluene or dioxane solution.

2. Vanadyl salicylaldehyde bisethylenediimine. Same behavior as no. 1.

3. Vanadyl complex of the DuPont dye 1-amino 2-naphthol 4-sulfonic acid phenyl methyl pyrazolone. Same sort of broad resonance in solid, apparently asymmetric. Solubility was insufficient for solution measurements.

Chromium (III). Cr(III) trisacetylacetonate. No resonance observed, either in powder or in intense red benzene solution.

Manganese (III). Mn(III) trisacetylacetonate. No resonance observed in powder or in benzene solution.

Iron (II). 1. Ferrous complex of dye mentioned above. Very strong resonance over a wide range of field, with some narrow line structure. Insolubility prevented solution work.

2. Ferrous phthalocyanine. No resonance observed in powder or benzene solution.

3. Ferrous salicylaldehyde bisethylenediimine. Powder gave broad resonance centered at  $g = 2$ .

Iron (III). Ferric trisacetylacetonate. No resonance was observed for powder or concentrated orange solution in benzene.

Cobalt (II). 1. Cobaltous 8-oxyquinoline dihydrate. No resonance observed for powder.

2. Cobaltous acetylacetonate bisethylenediimine. No resonance observed for powder.

3. Cobaltous salicylaldehyde bispropylene triamine. No resonance observed for powder or solution in a benzene-dioxane mixture.

Cobalt (III). Cobaltic trisacetylacetonate. No resonance observed for powder or benzene solution.

Nickel (II). 1. Ni(II) salicylaldehyde bistetramethylene diimine. No signal observed for powder.

2. Ni(II) bis-salicylaldehyde methylimine. No resonance observed for benzene or dioxane solutions and suspensions.

3. Ni(II) bistrisfluoroacetylacetone. No resonance observed for powder or solution in dioxane.

Copper (II). Cupric bisacetylacetone, trifluoroacetylacetone, dibenzoyl methane, salicylaldehyde methyl imine, 3-benzyl acetylacetone, glycine, salicylaldehyde p-nitroanil, salicylaldehyde anisidil, and benzoylacetone all gave rather broad, somewhat asymmetric resonance bands in the powder. Those that would dissolve in dioxane or in benzene gave in those media four distinguishable but overlapping resonance bands whose character depended upon the ligand.

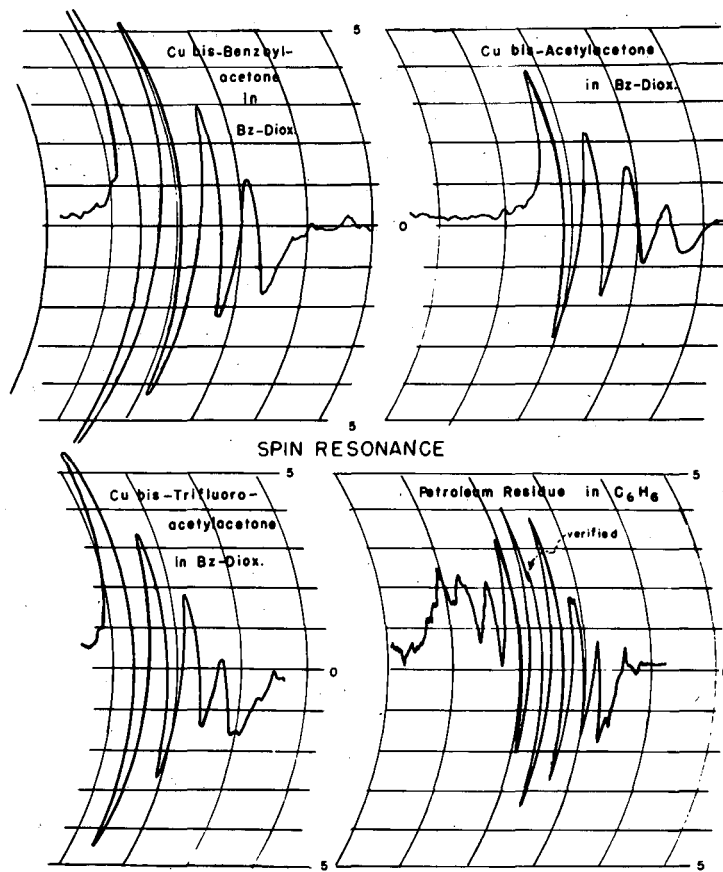
Four of the survey resonance spectra, with the first derivative of the absorption as ordinate and decreasing magnetic field as abscissa, are presented in Fig. 24. The petroleum residue we have not yet mentioned. This was a sample of tar or sludge from a refinery; analysis shows it to contain vanadium.

#### Quantitative Measurements

Figures 25, 26, 27, 28, 29, 30, and 31 show the first derivative of the resonance absorption with respect to magnetic field for various compounds tested. The numbers have been explained in the experimental section.

#### Discussion

The primary object of this exploratory investigation has been to find out whether the chemical environment of a metal ion would affect its resonance pattern sufficiently so that the resonance might be used as a tool in the identification of chemical species. For Cu(II) chelates, one has merely to look at Figs. 24, 25, and 26 to assure himself that the answer to our question is affirmative. In most cases, changing the nature of the chelating agent actually changed the qualitative appearance of the resonance pattern. When this was not the case, quantitative differences which were well-defined and reproducible distinguished one compound from another. The theoretical interpretation of these resonance



MU-9694

Fig. 24. Recordings of electron resonance.

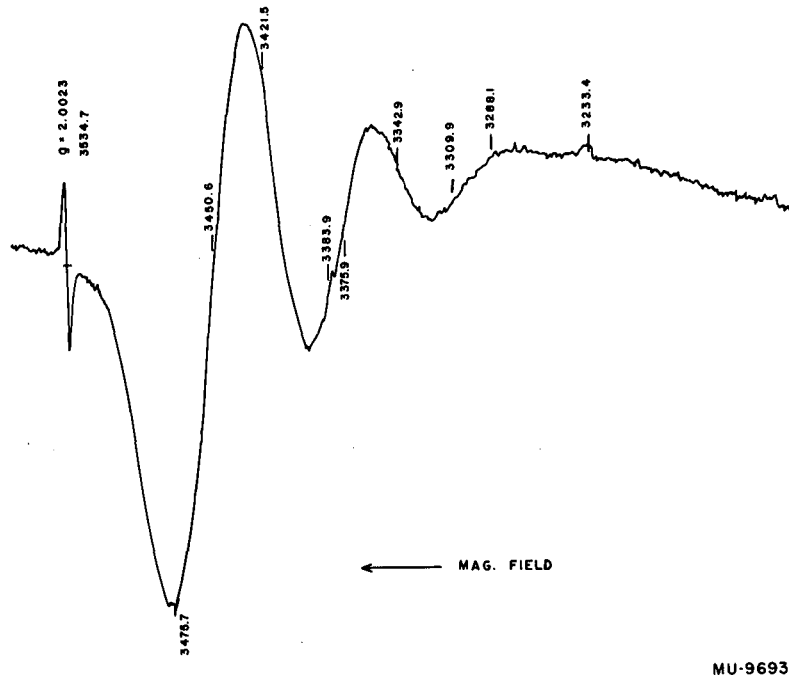


Fig. 25. Spin resonance of Cu Sal. Anisidil.

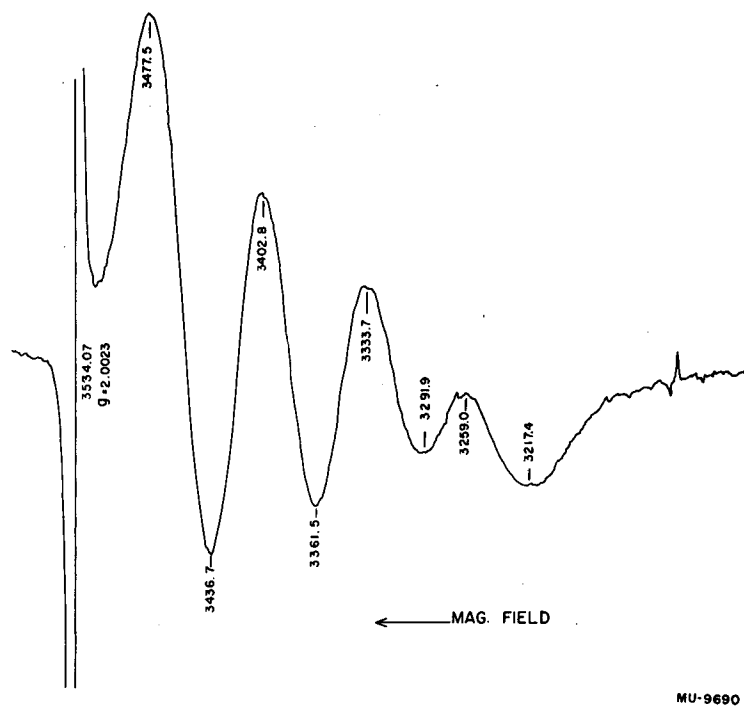
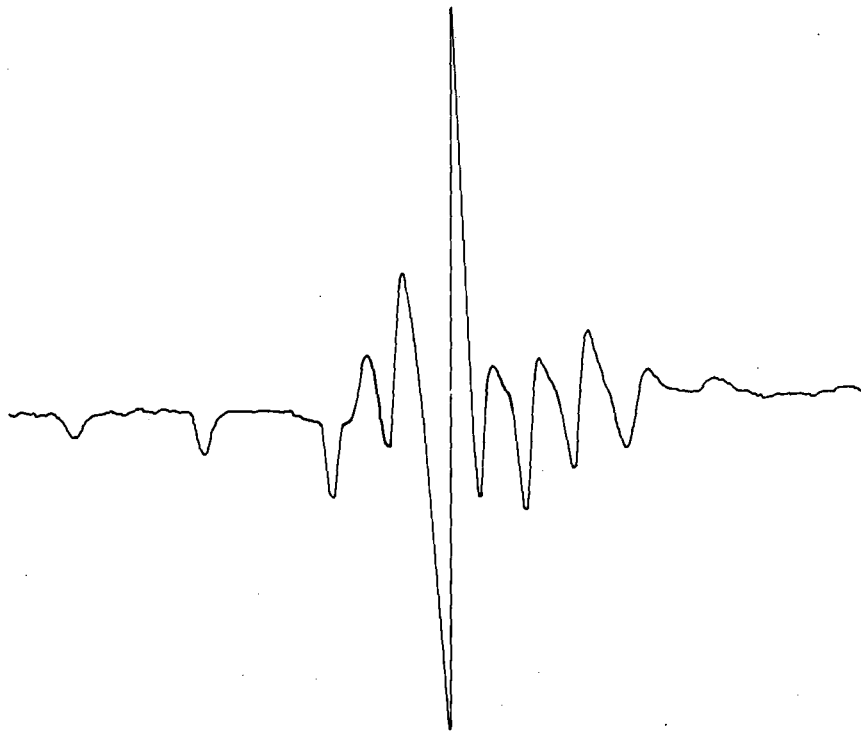


Fig. 26. Spin resonance of Cu(II) N-Methyl salicylaldimine in toluene.



MU-9691

Fig. 27. Spin resonance of glass containing  $V_2O_3$ .

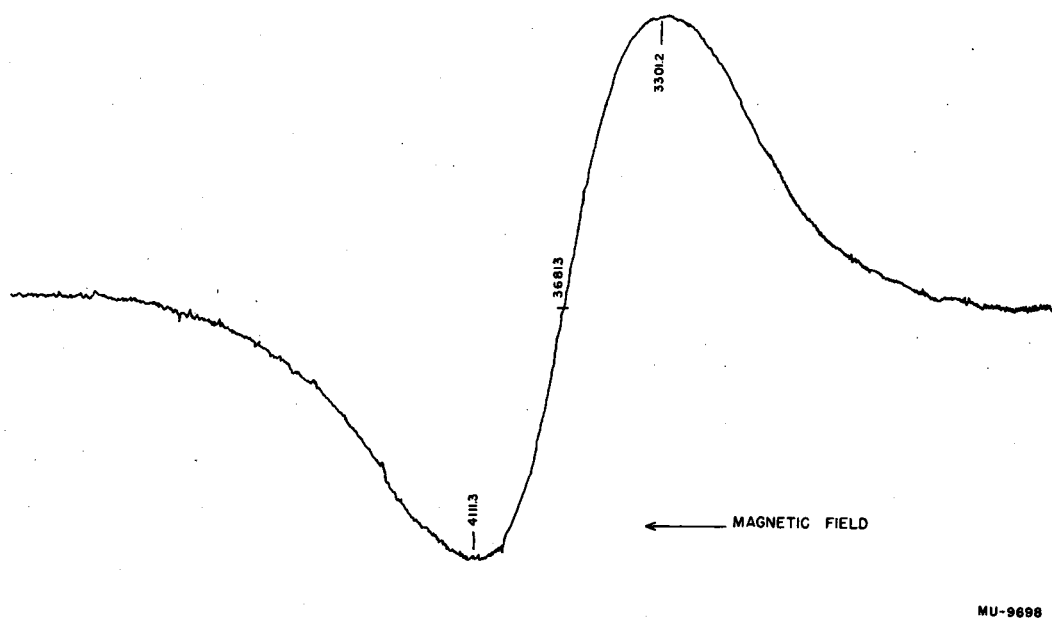


Fig. 28. Spin resonance of VO(II) bis-acetylacetonate--powder.



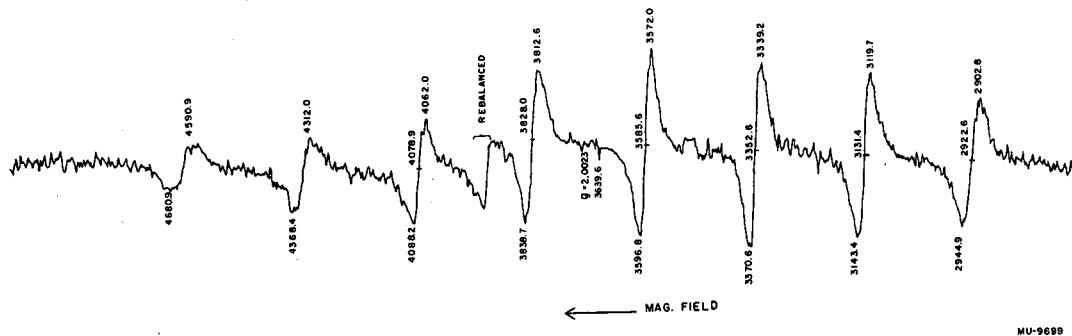


Fig. 29. Spin resonance of vanadyl salicylaldehyde ethylenediimine in toluene.

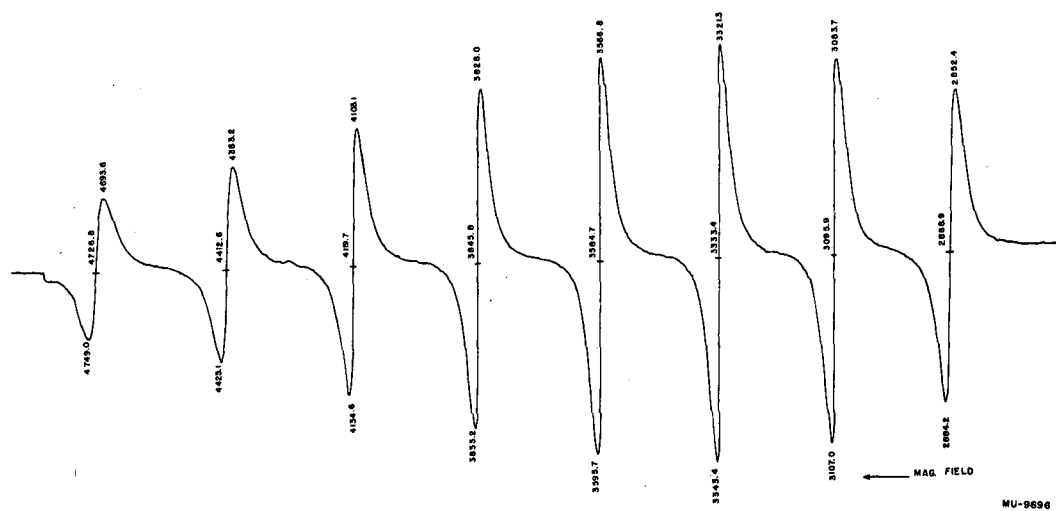


Fig. 30. Spin resonance of vanadyl acetylacetonate in toluene.

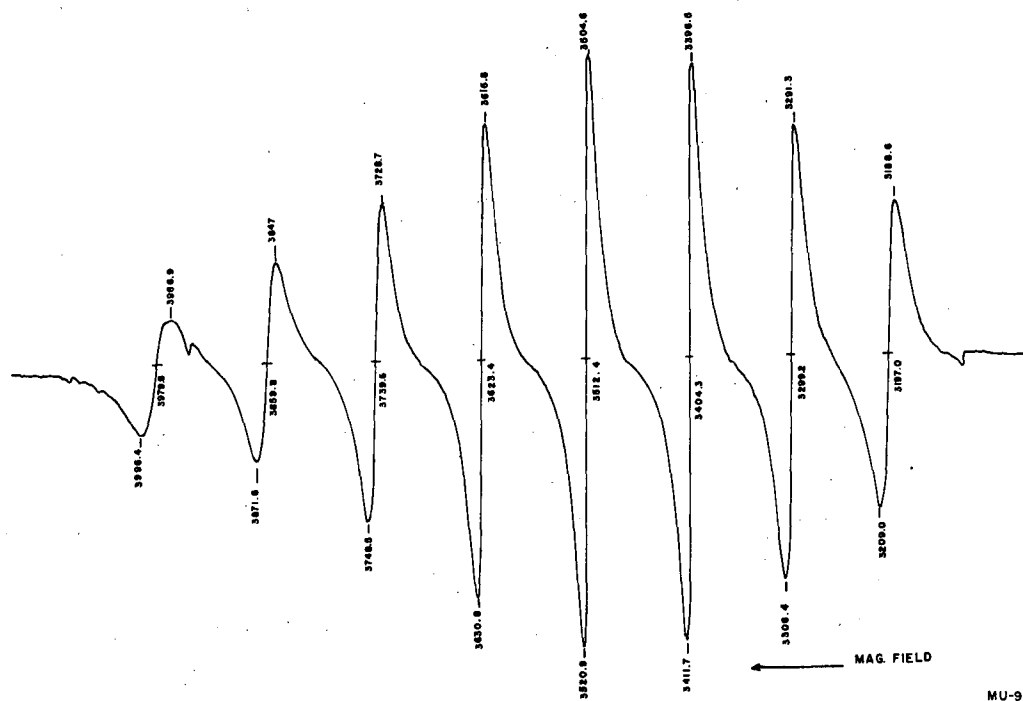


Fig. 31. Spin resonance of vanadyl acetylacetonate in de-aerated dioxane.

patterns of solutions of cupric chelates will not be discussed here. (Dr. McGarvey<sup>23, 37</sup> has studied solution resonance spectra of cupric acetylacetonate and cupric 3-ethylacetylacetonate in detail.) We mention only that the four bands which seem to appear in each curve are very probably caused by the four magnetic states of copper's nucleus, which has spin  $3/2$ .

The vanadium compound spectra presented in Figs. 27, 28, 29, 30, and 31 offer further proof that the chemical nature of the environment of the metal ion may be studied by way of the paramagnetic resonance method. Figures 29 and 30 show resonances for vanadyl salicylaldehyde ethylene diimine and vanadyl acetylacetonate, respectively. The Schiff base chelate shows a resonance pattern qualitatively quite similar to that of the diketone chelate, but the eight nuclear hyperfine lines are spaced closer together for the Schiff base derivative. Figures 30 and 31 illustrate an effect of environment for a given chelate, vanadyl bisacetylacetonate. Figure 30 shows the resonance pattern of a toluene solution, which is observed to be stable. Its color is quite similar to that of the chelate crystals--blue. However, if one dissolves the crystals in deaerated dioxane (dried over sodium blocks) they yield a green solution, which over a few hours precipitates most of the vanadium as a gray-green solid. The green solution gives rise to the resonance shown in Fig. 31. One can see that the medium has changed the envelope of the derivative curve (the envelope now peaks at the fourth rather than at the third line from the left) as well as the spacing between lines (the spacing is now a little less than for the toluene solution) and the width of some of the lines (the first two lines to the left are not so well resolved as they were for the toluene solution). Just what the chemical effects are and what their magnetic results should be we cannot say until more data concerning both the chemistry and magnetism of vanadyl acetylacetonate have been collected.

The nuclear spin of  $V^{51}$  is  $7/2$ . There are then eight possible nuclear magnetic states corresponding to  $m_I = 7/2, 5/2, 3/2, 1/2, -1/2, -3/2, -5/2, \text{ and } -7/2$ . These must be responsible for the separation of the vanadium resonance into eight lines. If the spin and nuclear moments are taken as interacting by an I-S interaction, one may derive a formula for the positions of the resonance lines of the

form  $g H = a - b m_I + b' m_I^2$ , where  $a$ ,  $b$ , and  $b'$  are constants. Figure 32 illustrates that this relationship does apply to the spacing of the hyperfine lines in vanadyl acetylacetonate in toluene and in dioxane. The dioxane point that seems to be in disagreement with a linear function of separation between lines is from a point on the resonance curve where line position was hard to measure because of low absorption intensity; accordingly we do not feel that it spoils the linearity of the graph.

None of the theories that we have seen for hyperfine splitting in such compounds as the vanadium chelates allows for variation of integrated absorption intensity with the nuclear magnetic state. We have measured the areas under the absorption curves, assuming that for a given spectrum each line can be represented by the same kind of function--Gaussian, Lorentzian, etc. The results are shown in Fig. 33. The intensities do not seem to be the same for all eight lines. We cannot state at the present time whether the discrepancy is a property of the system or whether it may be due to our assumption that all lines are of the same functional form. In any case, the problem is an interesting one and deserves further study. Very similar results in the resonance of inorganic vanadium salts have been obtained by other workers.<sup>72</sup>

As a final illustration of the chemical effect in paramagnetic resonance, we mention the spectra of  $V_2O_3$  dissolved in glass, Fig. 27, and the resonance found in vanadium-containing petroleum residues, Fig. 24. The two resonance patterns are remarkably similar; they are almost identical if the residue is studied not in solution but in its natural state. One might guess that the vanadium in the residue is in the +3 oxidation state and that for that reason its spectrum resembles that of the glass. If this is true, it illustrates a remarkable sort of analysis for oxidation state, since there would be no known chemical method for determining the oxidation state of the metal in its tarry surroundings.

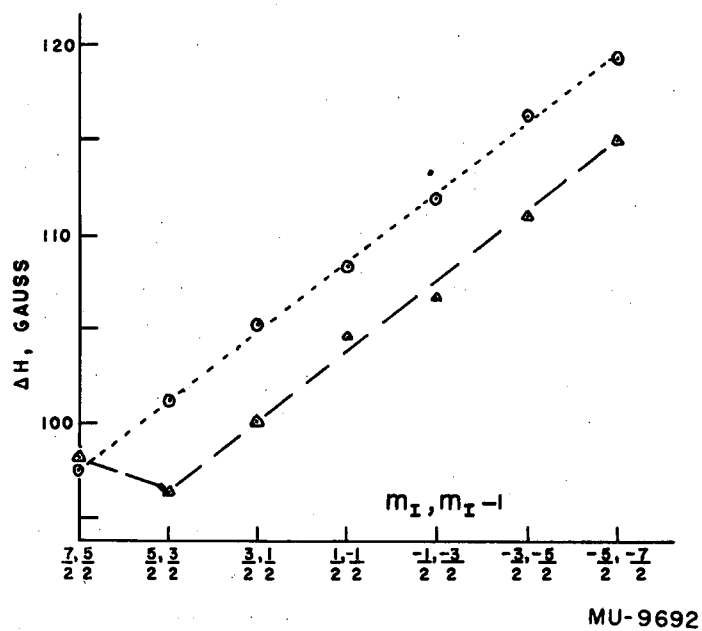
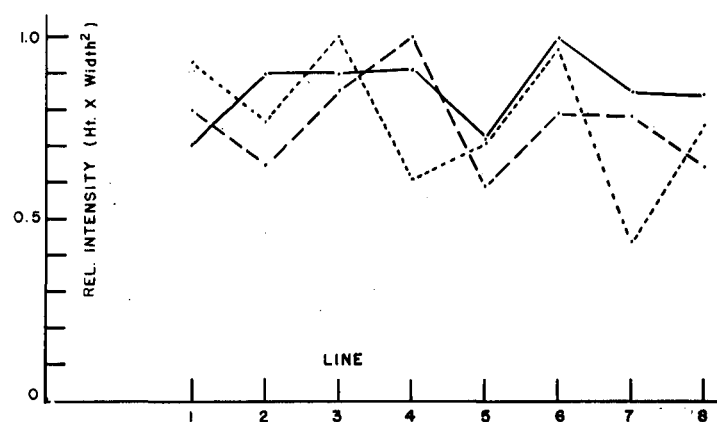


Fig. 32. Spacing between hyperfine lines of nuclear mag. quantum Nos.  $m_I, m_I - 1$  for vanadyl acetylacetonate in ----- toluene, - - - - dioxane.



MU-9695

Fig. 33. Relative intensities of the 8 hyperfine lines for spin resonance of vanadyl acetylacetonate in ----- dioxane, ——— toluene - - - dioxane, de-aerated.

## V. METAL-METAL BONDING: NICKEL (II) BISDIMETHYLGLYOXIME

### Introduction

The investigation reported in this section was touched off by our noticing the results of an X-ray-diffraction structure determination by Godycki and Rundle<sup>62, 63</sup> for a set of metal dimethylglyoximes. The particular compounds studied by those workers were Pd(II)(DMG)<sub>2</sub>, Pt(II)(DMG)<sub>2</sub>, Ni(II)(DMG)<sub>2</sub>, and Au(DMG)<sub>2</sub><sup>+</sup>AuCl<sub>2</sub><sup>-</sup>. All these are flat chelate molecules with the very special feature that their crystals are formed of layers of molecules stacked so that there are metal-metal chains through the crystal. Rundle gives the metal-metal distance for the four DMG chelates studied as 3.26 Å. We were intrigued by the possibility that for such an arrangement the crystal might behave like a one-dimensional metal, with semiconducting or photoconductive properties, and that it might display such characteristics as optical transitions belonging to the special intermolecular metal-metal interactions. Accordingly, we set out to test Ni(DMG)<sub>2</sub> for evidences of the above properties. Also, we attempted to find other Ni(II) chelates that might be metal-metal linked in their crystals. A record of these trials follows.

### Experimental

#### Preparations

Ni(DMG)<sub>2</sub>. To a water solution of nickel acetate was added an alcoholic solution of dimethylglyoxime. The brick-red precipitate was washed repeatedly with water and alcohol and was desiccated in vacuo. Its recrystallization required a special technique, as it is extremely insoluble in most solvents. The following method proved very satisfactory: An Erlenmeyer flask containing toluene (100 cc) was fitted with a Soxhlet extractor. The Soxhlet was in turn fitted with a condenser so arranged that refluxing toluene would fall from the condenser lip directly into the porous cup of the extractor. Into the cup was placed the Ni(DMG)<sub>2</sub> to be recrystallized. The flask was heated on a hotplate for a period of



a week, during which time refluxing solvent was continuously cycling through the solid chelate, dissolving minute quantities of it, and carrying it into the boiling toluene, from which it crystallized in very fine shiny needles, deep red in color. Various other recrystallization procedures and solvents were tried, but none was so satisfactory as the ones just described. Considerable effort was expended in an attempt to obtain large single crystals, but to no avail; although crystals could be obtained that were more than an inch in their longest dimension, none were grown whose other two dimensions exceeded a small fraction of a millimeter. Among methods tried were slow and rapid cooling of hot less-than-saturated toluene, pyridine, chloroform, and nitrobenzene solutions; slow (several weeks' time) evaporation of solvent from such solutions at room temperature, and digestion of crystals made by the continuous extraction method in the solvents mentioned above at steam-bath temperature. The latter procedure was better than the others.

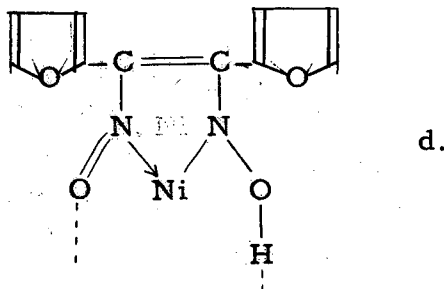
Anal. Calcd. for  $\text{NiC}_8\text{H}_{14}\text{O}_4\text{N}_4$ . C, 33.26; H, 4.88; N, 19.40. Found, C, 33.61, H, 4.78; N, 19.59.

2-Nitroso-1-Naphthol Ni(II). 2-Nitroso-1-naphthol dissolved in methanol was added to the same molar quantity of nickel acetate dissolved in 50 cc  $\text{H}_2\text{O}$ . There resulted a dark chocolate-red precipitate which appeared amorphous in character. It was washed repeatedly with water and sparingly with cold acetone and was allowed to dry. It was shaken with hot  $\text{CCl}_4$  to remove organic materials, filtered, and washed with i-pentane. The dry product is a very intense brownish red and dissolves easily in toluene, chloroform, and acetone to give red solutions. It precipitates from its solutions in these solvents if large amounts of i-octane are added. Because of its gelatinous or gluey nature, it was impossible to crystallize nicely; the best that could be done was to dissolve it in chloroform and precipitate it out with octane. Adsorption of foreign matter upon the finely divided precipitate was likely responsible for its poor analysis.

Anal. Calcd. for  $\text{C}_{20}\text{H}_{12}\text{O}_4\text{N}_2\text{Ni}$ . C; 59.6; H, 3.0; N, 6.95. Found, C, 58.9; H, 4.29; N, 5.40.

Phenanthrene quinone monoxime. This substance was prepared by the reaction of phenanthroquinone with hydroxylamine in 1:1 molar ratio. The reactants were suspended in a mixture of ethanol and chloroform, 15:2.5 parts by volume. The mixture was refluxed for an hour and cooled; the precipitate was recrystallized from boiling ethanol.

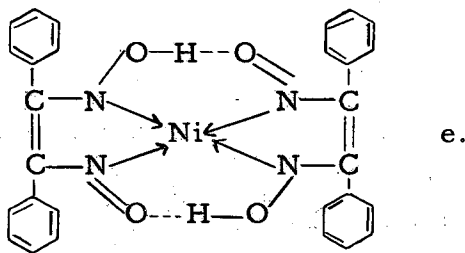
Ni(II) bis- $\alpha$ -Furildioxime. To 50 cc of ethanol containing



1 g (1/220 mol) of  $\alpha$ -furyl dioxime was added 4.5 ml of 0.05 M aq. nickel acetate. A red precipitate appeared immediately. It was filtered and washed well with water, then with small amounts of methanol. Finally, the material was washed well with *i*-octane and dried. Yield, 0.6 g. = 55%.

Anal. Calcd. for  $\text{NiC}_{20}\text{H}_{14}\text{O}_8\text{N}_4$ . C, 48.3; H, 2.84; N, 11.27. Found, C, 47.76; H, 2.97; N, 11.34.

Ni(II) bis- $\alpha$ -Benzildioxime. To a few cc of 0.05 M aq.



nickel acetate was added somewhat less than the equivalent quantity of  $\alpha$ -benzil dioxime. When a drop of acetone was added to start solution of the dioxime, a red-orange precipitate was formed. It was filtered off and washed successively with water, methanol, pentane, and *i*-octane. The dried crystals were red-orange; they streaked yellow on white porous filter paper.

Anal. Calcd. for  $\text{NiC}_{28}\text{H}_{22}\text{O}_4\text{N}_4$ . C, 62.39; H, 4.11, N, 10.39. Found, C, 62.87; H, 4.30; N, 10.54.

### Spot Tests

While searching for Ni(II) chelates of the same type as Ni(DMG)<sub>2</sub>, we made a few quick tests to determine what reagents like DMG might give Ni(II) chelates with color properties similar to that of Ni(DMG)<sub>2</sub> itself: deep red color in the solid state, but yellow or orange in solution in organic solvents. In each case several drops of nickel acetate solution in water were put on the test plate, a few grains of prospective chelating agent were added, and a drop of 50% ethanol was added to aid in solubilizing the agent. The results follow:

- a. Phenyl glyoxime. Orange precipitate.
- b. α-Furil dioxime. Dark red precipitate.
- c. α-Benzil dioxime. Deep orange-red precipitate.
- d. α-Benzil monoxime. Green precipitate.
- e. o-Dihydroxybenzene. No precipitate.
- f. 2-Phenyl glyoxal 1-oxime. Dark green precipitate.
- g. Acetylacetone dioxime. Complexes the Ni<sup>++</sup> to give beautiful azure solution, but no precipitate.
- h. 2-Nitroso-1-naphthol. Intense chocolate-red precipitate.
- i. 1-Nitroso-2-naphthol. Dirty green solution.
- j. 2,3-Hexanedione-3-oxime. Brown oil.
- k. 2,3-Octanedione-3-oxime. Brown oil.
- l. Nitroguanidine, NH<sub>2</sub>C(=NH)NHNO<sub>2</sub>. No reaction.
- m. Nitrosoguanidine, NH<sub>2</sub>C(=NH)NHNO. Red precipitate appears as soon as a little sodium carbonate is added.

None of the solids isolated from the above reactions showed the desired color change between the solid state and solution in chloroform.

### Optical Spectra

Spectra in the visible and ultraviolet regions were taken with a prototype of the Beckman DK recording spectrophotometer. Speed was in each case medium or slow. For the solution spectra, gain setting was normal (ca 35) and slit width was in the region of 0.01 mm. For the suspension spectra the gain control was set at a high value-- between 150 and 300--in order that small slit width might be realized.

All spectra were scanned from low to high wave lengths. Charts were marked with a few reference points of wave length as indicated in other sections of this report. Immediately prior to a spectral run a base line was run with solvent in both cells. For all the measurements reported in this section the 1P21 photomultiplier detector was used. Signal-to-noise ratios for the spectra shown were satisfactory, being < 1% peak-to-peak.

Spectral samples were prepared as follows: Ni(II) salicylaldehyde ethylenediimine, Ni(II) bis-salicylalimine, Ni(II) bisdimethylglyoxime, and the product of reaction of nickel acetate with nitrosoguanidine were weighed and added to sufficient toluene to make up  $10^{-3}$  molar solutions. Our primary aim was not to measure extinction coefficients with accuracy but to observe the general character of the principal absorption bands. Consequently, turbidity in the solutions, even that caused by undissolved solute, was removed by filtration. Therefore, extinction coefficients reported here must be regarded as merely approximate. The solution spectra were taken with both sample solution and reference solvent in 1 cm path silica cells.

Solids to be examined were treated in a variety of ways so that they might be made into fine suspensions. The nitrosoguanidine product was ground with a little water in an agate mortar intermittently for a period of two hours. A portion containing 10 mg of solid was added to 9 ml of water and the suspension was further dispersed by sonic vibration. Ni(II) bis-salicylalimine, 6 mg, was ground in the same way and was added to 20 ml of water. A little laboratory detergent was added and the resulting suspension sonicated. The solid was found to remain in suspension for a period of several days if detergent was present; only a few hours if there was no detergent. Ni(II) salicylaldehyde ethylenediimine was prepared for suspension spectrum in just the same way. Ni(DMG)<sub>2</sub> was prepared for suspension measurements in several ways. Aqueous suspensions were made as described above, with detergent and without. Also, the suspensions were used for spectral measurement and were then filtered through hard filter paper. The colloidal filtrates always yielded spectra of just the same character as did the parent suspensions containing the coarser particles. Neither absorption peak positions nor band widths appeared to be affected by

the state of subdivision within the limits of our tests, although peak intensities were affected. Other samples of  $\text{Ni}(\text{DMG})_2$  were ground and sonicated in isopropanol. Yet another was prepared as a 4% mull in perfluorokerosene; 250  $\mu\text{l}$  was added to 10 ml of carbon tetrachloride and the emulsion was used for spectral tests without being sonicated. We found that even with sonication and vigorous grinding, a good suspension of the chelate in carbon tetrachloride could not be obtained unless the oil were present as an emulsifier. In each case the spectrum of the suspension was obtained by the method described by Shibata et al.<sup>65</sup> The suspension was placed in a 1-cm silica cell as close to the detector as possible. Against the cell face nearest the detector was placed an opal glass plate which served as a secondary light emitter. The same arrangement was used in the reference beam, except that the cell there was filled with plain suspension medium (including emulsifying agents when they were used in the suspension). The relative positions of sample and reference cells were adjusted so that with suspension medium in both, the recorder would trace a good 100% line--comparable to that obtained when the opal glasses were removed. This procedure was necessary with the Beckman DK spectrophotometer for the reason that the light in the reference channel, after it has passed through the reference cell, must be offset by two mirrors to bring it into coincidence with the path of the sample beam, which passes directly into the detector. Such an arrangement places the reference cell with its secondary light emitter too far away from the detector, compared with the sample cell and emitter, if the two cells are set opposite each other in the cell compartment. The sample cell with emitter must be moved away from the detector until the effective fraction of secondarily emitted light received by the detector is the same for both sample and reference emitters.

The spectra so obtained are shown in Figs. 34 and 35. Results of spectral measurements on compounds other than  $\text{Ni}(\text{DMG})_2$  are not shown; their suspension and solution spectra were quite similar. Of course, it must be understood that the extinction coefficients, as we have stated already, may on an absolute basis, be inaccurate. The two spectra of water suspensions given in Figs. 34 and 35 differ in that the  $\text{Ni}(\text{II})(\text{DMG})_2$  samples were synthesized at different times; the sample

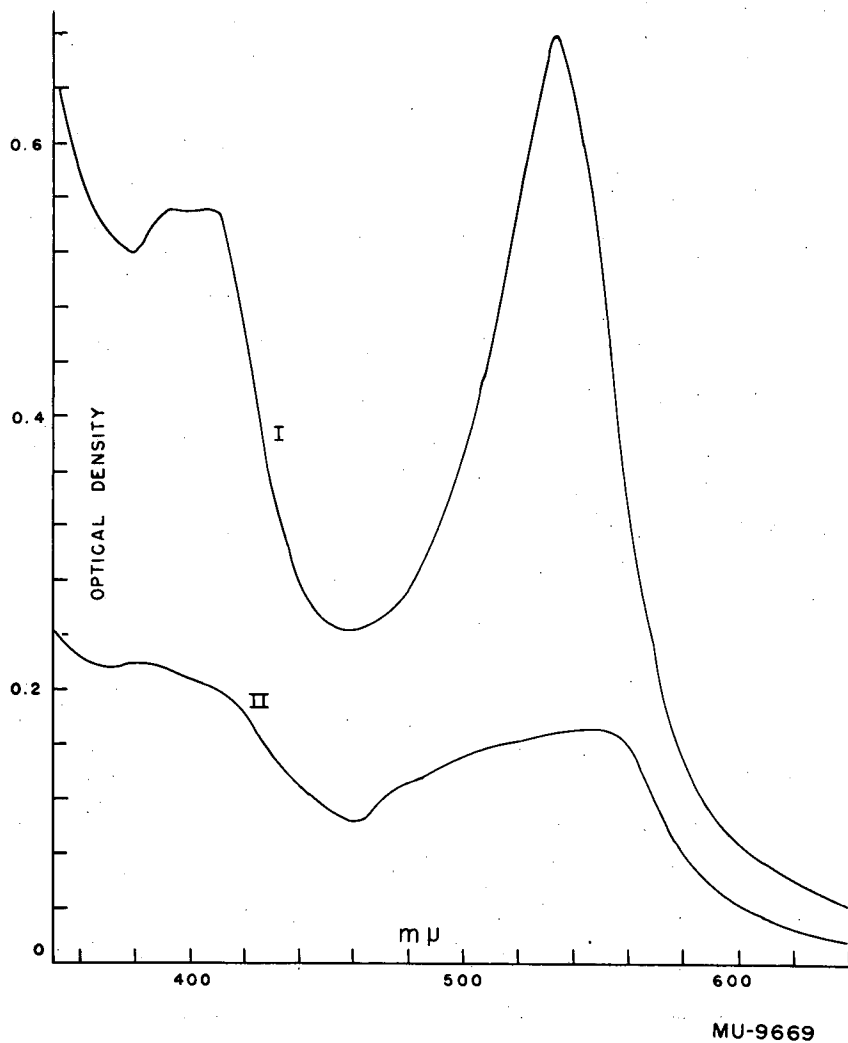


Fig. 34. Visible absorption spectra of Ni(II) bis-dimethylglyoxime suspensions  $10^{-3}$  M, 1 cm path. I. in  $H_2O$  or  $i - C_3H_7OH$ . II. in  $CCl_4$ , emulsified with 1 drop oil.

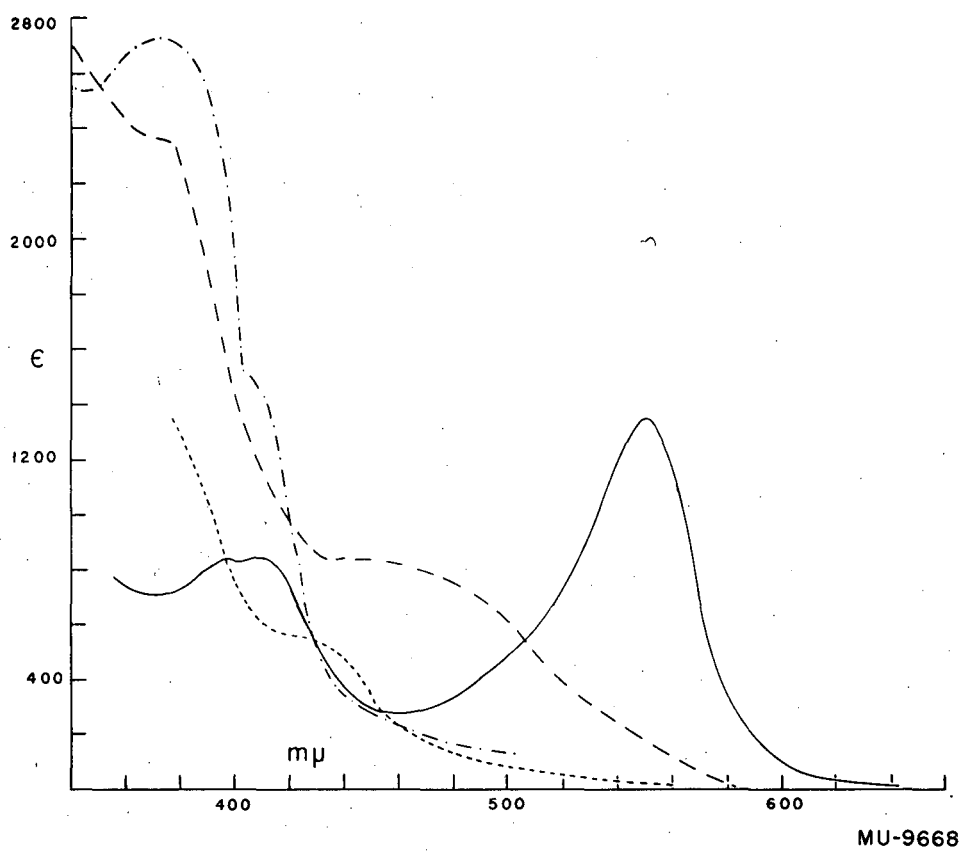


Fig. 35. Visible absorption spectra of Ni(II) bis-dimethylglyoxime, ——— solid, fine sonicated susp. in H<sub>2</sub>O, - - - solution in pyridine, - - - - solution in xylene, - · - · solution in chloroform (K. Sone, 1953).

for the latter figure was a very finely divided material with fluorescent brilliant rose sheen, while that for the first figure was ground from large, well-formed crystals. Apparently the process of grinding the crystals was not so efficient as the direct precipitation of the substance in a finely divided state, since the apparent molar extinction values are about twice as great for the naturally fine-grained as for the hand-powdered sample.

#### Attempts to Measure Electrical Conductivity

We hoped to find, in  $\text{Ni}(\text{DMG})_2$  crystals, evidence for either semiconductivity or photoconductivity, or for both. Since we expected electrical transmission to be in one crystal direction, along the -Ni-Ni-chains, we desired single crystals. However, as we have noted, large crystals could not be grown. Having to make the best of measurements with very fine crystals only, we used the following arrangement: A number of fine crystals about 1 mm long were bridged across a 0.5-mm gap between two mercury drops. Two wires made contact with the mercury and led to the measuring device--a vacuum tube volt-ohmmeter or Megger high-resistance measuring outfit. The equipment was not elegant, but did allow the setting of some limits on the electrical conductivity of the crystals. Resistance readings were taken for the small crystals and also for a large disc (1 mm thickness between contacts; contacts over about  $1 \text{ cm}^2$  area on each side) made by eight tons of hydraulic press pressure upon  $\text{Ni}(\text{DMG})_2$  powder. The experiments were done at normal room lighting as well as with an RSP2 photospot placed a few inches from the sample. With the resistance-measuring devices available to us, we could measure resistances up to  $10^{11}$  ohms. None of the samples we tried, under any conditions, showed  $< 10^{11}$  ohms resistivity; from sample sizes we estimate the specific conductivity of the samples plus contact junctions to be  $< 10^{-12} \text{ ohm}^{-1} \text{ cm}^{-1}$ .

#### Discussion

Examination of the spectra shows very clearly the presence of an absorption band at 550 m $\mu$ , peculiar to the crystalline state of  $\text{Ni}(\text{DMG})_2$ . This effect has been qualitatively observed by Feigl,<sup>66</sup> who



noticed that while suspensions and colloidal preparations of  $\text{Ni}(\text{DMG})_2$  were red, solutions in chloroform, etc., were yellow. Without being aware that Feigl had noticed the effect, we observed it and noted also that a streak test establishes the color of the chloroform solutions of all the  $\text{Ni}(\text{II})$  chelates mentioned in this section and many more besides-- with the notable exception of  $\text{Ni}(\text{DMG})_2$ , which yields a deep red streak. The persistent deep red of the solid is of course due to the strong green absorption band. Our solid-suspension spectra with water as dispersion medium agree quite well with those of Sone,<sup>67</sup> whose results we noticed shortly after the completion of our spectral measurements. So far as we know, there are no reports of spectra for suspensions in media other than water. Our results show that the suspension medium must actually play a role in the electronic transition or transitions responsible for the green absorption band. The character of the band is obviously quite different for carbon tetrachloride as medium from that for hydroxylated media. It seems possible, in view of the -Ni-Ni- chain structure, that the 550-m $\mu$  absorption may arise from transitions involving a periodic wave function or crystal orbital extending the length of the crystallite and that for small crystallites; then, the manner in which the -Ni-Ni- chain is terminated may be important. On the other hand, it may be that the important effect of the particular dispersion medium is interaction with the organic surfaces of the crystallites. If we have measured light absorption only in the outer layer or two of crystal, primarily, then such interaction may affect the transition sufficiently to be observed in the changing character of the solid-unique absorption band. The latter explanation does not depend upon involvement of the -Ni-Ni- chain through an entire crystallite in the electronic transition, while the former one does. Whether we have observed the former or the latter or both effects we cannot say.

The failure to observe semiconductivity or photoconductivity requires little comment other than some remarks about the lack of conclusiveness inherent in the measurements. One cannot tell from the results whether or not the -Ni-Ni- chains behave as semi- or photoconductors. The fact that no significant conduction was apparent may only mean that there was imperfect conduction from chain to chain. Indeed, one would surely think it highly improbable that within a

macroscopic crystal there would be a large fraction of the -Ni-Ni-chains perfectly unbroken from one end of the crystal to the other, or that there would be a large fraction unbroken save for conduction-aiding impurities. Very likely there was effective insulation even within crystallites, or at least between crystallites as well as between the solid and the mercury pool contacts. Inclusion of air in the pressed disc undoubtedly introduced additional detrimental factors.

Finally, we remark upon our inability to find other Ni(II) chelates displaying visible absorption bands characteristic of the solid only. Since we examined a number of chelating agents that differ but little from dimethylglyoxime, except for molecular size, we suppose that for Ni(II) chelates of those agents, -Ni-Ni-chains do not exist because of packing considerations. Examination of models shows that it would be very difficult, for most of the molecules studied, to pack the Ni atoms in a chain, as close as 3.3 Å, without interference between groups of the organic parts of the chelate molecules.

## VI. NEAR-INFRARED SPECTRA OF ALCOHOLS

During a program of testing our prototype of the Beckman Model DK recording spectrophotometer in the near-infrared range, we purified a series of alcohols and observed their spectra in the range 0.7 to 2.0 microns. The aliphatic alcohols should provide near-infrared spectra very rich in detail, as they have hydroxyl groups which should be detected at three positions within the above frequency range--the first three overtones of the -O-H stretch frequency--as well as carbon-hydrogen, carbon-carbon, and hydrogen-bonded hydroxyl linkages. Indeed, our observations bore out this expectation. In the following paragraphs are to be found the purification procedures used, instrumental conditions, the spectra obtained, and a brief discussion of the spectra, including suggestions regarding future research and analytical possibilities.

### Purification of Alcohols

Ethanol. 120 ml was dried over  $\text{MgSO}_4$  and filtered into a 250-ml ground-joint flask fitted with reflux condenser and drying tube. Sodium metal (2 g) was added in small pieces through the condenser and was allowed to react with the alcohol. The diethyl phthalate (22 ml), previously dried over  $\text{MgSO}_4$ , was added. After two hours of reflux, the mixture was distilled. A small starting fraction was discarded; then collection was begun at  $77.0^\circ \text{C}$  (uncorr) and ended, after collection of 75 ml, at  $77.2^\circ \text{C}$ . No rubber connections were used in the apparatus; silicone grease only was used (sparingly) for the ground joints.

n-Propanol. This was dried by boiling with its own bulk of Drierite. After filtration of the cooled alcohol, a little more Drierite was added and distillation was begun. About 25% of the distillate was discarded as the low-boiling fraction ( $89^\circ$ - $95^\circ \text{C}$ ). Collection was from  $95^\circ$ - $96^\circ \text{C}$  (uncorr).

n-Butanol. 70 ml (ca 0.8 mol) was purified as was the ethanol. Instead of diethyl phthalate, 15 ml dibutyl phthalate was used; sodium was cut

to 0.8 g. A small fraction, bp  $109^{\circ}$ - $111^{\circ}$  C, was discarded. Collection of the distillate from  $111^{\circ}$ - $113.5^{\circ}$  C, about 60 ml in all. The bulk of it came off between  $112^{\circ}$  and  $113^{\circ}$  C.

n-Pentanol. 130 ml Baker's Analyzed n-Amyl Alcohol was refluxed with 1.3 g Na plus 20 ml n-amyl butyrate, EK No. 2362, bp  $185^{\circ}$  C. Distillation yielded a fraction between  $135^{\circ}$  and  $136.5^{\circ}$  C, which was discarded, and one which was collected between  $136.5^{\circ}$  and  $137^{\circ}$  C, ca 90 ml.

n-Undecanol. 100 ml stood several days over anhydrous  $MgSO_4$  and was then filtered and allowed to stand over anhydrous  $K_2CO_3$ . The starting material, EK No. 4844, was somewhat yellow. It was distilled under vacuum, gauge reading 25 mm, at  $139^{\circ}$ - $140^{\circ}$  C (uncorr).

n-Hexanol. 20 ml Kahlbaum hexanol was stored over anhydrous  $CaSO_4$ . The alcohol was filtered off and was fractionally distilled in semimicro equipment. All distillate boiling lower than  $148^{\circ}$  C was discarded; the collected fraction boiled over a  $1^{\circ}$  range, between  $148^{\circ}$  and  $150^{\circ}$  C (uncorr).

n-Heptanol. 100 g EK No. 381 stood two weeks over anhydrous  $CaSO_4$ . The supernatant yielded upon distillation a forerun,  $40^{\circ}$  to  $83^{\circ}$  C (ca 20 ml), discarded; a middle run,  $83.2^{\circ}$  to  $84.2^{\circ}$  C (ca 50 to 60 ml), retained; and higher-boiling components,  $84.2^{\circ}$  to  $94^{\circ}$  C (ca 25 ml), discarded.

The Remaining Alcohols Studied. These were not purified, except that they were allowed to stand over anhydrous  $CaSO_4$ . Their sources are listed: i-Propanol, Eastman Spectro Grade; sec-Butanol, EK No. 943; t-Butanol, BKH Co.; i-Amyl Alcohol, Baker and Adamson No. 1195; Methanol, Baker's Analyzed Absolute Methanol; Cyclohexanol, EK No. 703; t-Amyl Alcohol, Matheson No. 2234.

#### Instrumental Conditions

The lead sulfide detector of the Beckman DK spectrophotometer was used throughout the study range of 0.7 to 2.0 microns. Measurements of alcohol spectra were made at various times, under a variety

of conditions of instrument repair (or disrepair), signal-to-noise ratio, and instrument-development history. Consequently, a general set of experimental conditions cannot be given except for the following: Scanning was at "slow" or "medium" speed in every case. The time constant was set at 1. Sweep was always in the direction of increasing wave length. Chart speed was either 2 or 4 inches per minute. During the earliest of the measurements wave lengths were marked by the setting of a reference point thus: one manually activated the recorder pen to blip as one saw the desired wave length pass under the hairline by flipping the sample beam shutter. Then marking rulers and tapes supplied by Beckman Co. were used to supply the rest of the marks. But later tests showed that these rulers and tapes showed only a general family resemblance to actual wave-length drive travel; hence a rapid method of marking wave lengths manually directly on the spectrum recording was needed. Accordingly, the latest curves were obtained by the following device: A microswitch was connected across the sample signal channel. As the operator saw the desired wave lengths pass under the hairline, he flicked the switch; temporary grounding of the sample signal caused a very sharp displacement of the pen. Since coordination of the eye and hand was very easy with this arrangement, and since wave lengths could be reproducibly marked at very close intervals, the method was adjudged satisfactory. We would recommend, however, that the switch, instead of shorting the sample signal, be connected with a small battery across the sample signal channel. This improvement would overcome the only real difficulty inherent in the shorting method--i. e., its insensitivity and slowness of response at low sample transmissions.

### Spectral Measurements

In every case silica cells were used. Three types were employed: (1) 1-cm-square stoppered cells supplied by Pyrocell Co., (2) 10-cm cylindrical cells supplied by Beckman Co., and (3) 0.5-mm cells made by cementing U-shaped lead spacers of proper thickness between two optically flat quartz plates.

Cells were cleaned with concentrated sulfuric acid, washed with distilled water, and allowed to dry. Alcohols to be studied as

pure liquids were introduced into one cell and run vs a blank cell or vs an optically flat quartz plate. (The latter method was found better, as it required each beam to pass just two air-quartz interfaces, whereas an empty cell has four such interfaces in the light path.) One-molar solutions of alcohols in Eastman spectro grade carbon tetrachloride were made up by volume and run vs the same carbon tetrachloride in a matched cell. Some of the spectra were taken during a period when the double-beam feature of the spectrophotometer could not be used. Manual spectra, taken by running plots of signal output successively for a cell filled with solvent and with solution, were found quite satisfactory; as a matter of fact, much higher sensitivity could be attained and better instrument stability was noted for such runs than for double-beam runs.

### Results and Discussion

Figures 36 to 56 show spectra obtained in this study. Each figure is self-explanatory. Figure 36 shows survey spectra, over the range four to fourteen thousand wavenumbers, of the pure alcohols methanol, ethanol, iso-propanol, and tert-butanol and of tert-amylol, 1.0 molar in carbon tetrachloride. One important feature of these spectra is immediately evident: no two are even qualitatively identical. While the general appearance of all is the same, each alcohol exhibits a sufficiently unique spectrum to permit its identification by its near-infrared absorption pattern. The advantages of this region over the normal infrared "fingerprint region" are obvious. One works with glass or quartz cells rather than the fussy salt plates; quantitative work is much easier and its results much more certain than in the low-frequency range; and reliable spectra may be obtained very rapidly--the Beckman DK allows one to obtain spectra over the given range in just a few minutes each. While it is true that the near-infrared extinction coefficients are much lower than those in the normal infrared, very small samples may still be examined in capillary microcells of long path length, available commercially at the present time. Among the survey spectra of Fig. 36, the dilute t-amylol is of special interest, for it shows three strong bands that are missing or very weak in the

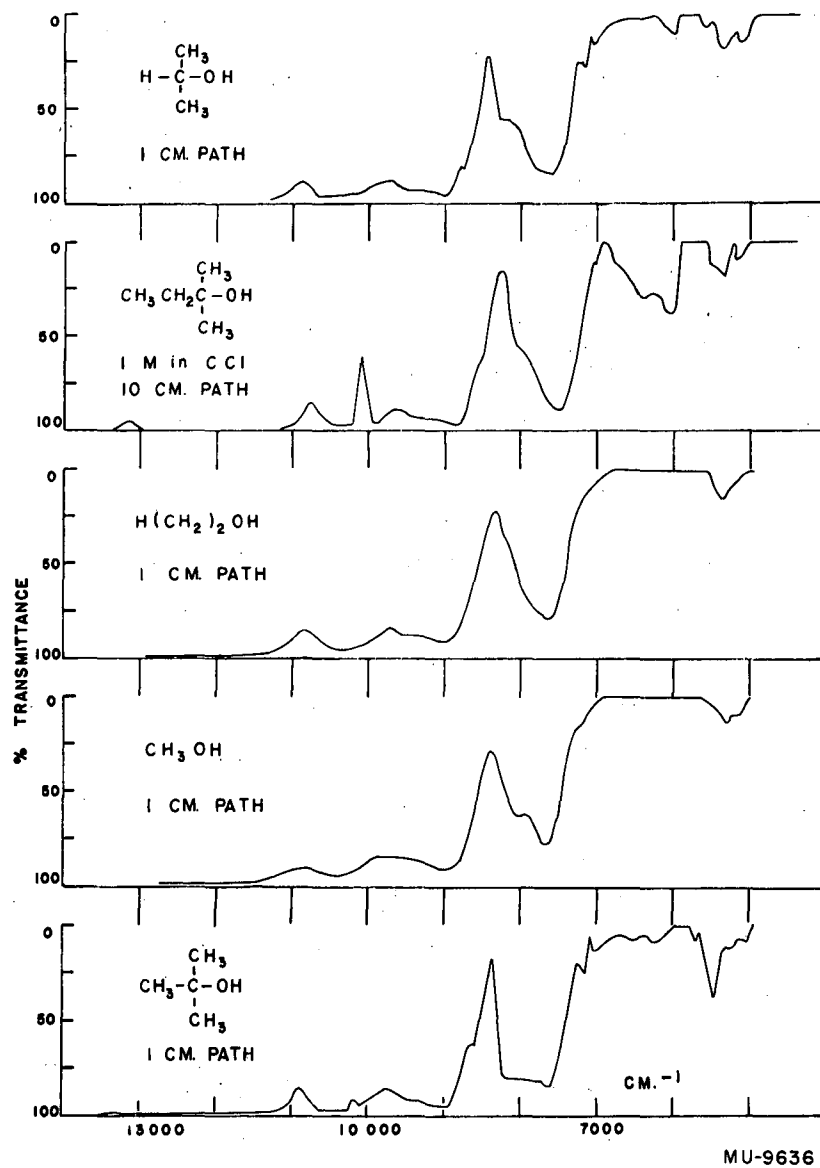


Fig. 36. Near-infrared spectra of alcohols.

pure alcohol spectra--namely, the three harmonics of the -O-H stretch frequency, at 6900, 10,100, and 13,160 wavenumbers, approximately. Furthermore, we have found that these bands occur in the spectra of all the alcohols when diluted with carbon tetrachloride. Close inspection of the remaining four spectra in Fig. 36 shows that such hydroxyl bands are also exhibited by the pure alcohol t-butanol, but with diminished intensity. It seems clear that we are observing the non-hydrogen-bonded hydroxyl groups and that we are seeing the effect of steric hindrance in preventing association of the tertiary alcohol. These general effects have been observed and utilized by other workers,<sup>69, 70, 71, 72</sup> (although usually with the expenditure of a great deal of effort and time because photographic or other laborious techniques were required).

We have investigated the effects just mentioned by means of the second harmonic of the hydroxyl stretch, at about  $10,200\text{ cm}^{-1}$ . Spectra, over a small range about this frequency, of a number of alcohols diluted to 1.0 molar in  $\text{CCl}_4$  are shown in Figs. 37 to 42. The extinction coefficients for the free (non-hydrogen-bonded) hydroxyl bands of these alcohols seem to fall into groups depending upon the steric hindrance to intermolecular hydrogen bonding. The primary alcohols methanol, ethanol, butanol, pentanol, and benzylol all have maximum extinction coefficients for that band lying between  $1.28 \times 10^{-2}$  and  $1.5 \times 10^{-2}$ ; cyclohexanol is in a class by itself with extinction maximum of  $1.70 \times 10^{-2}$ ; sec-butanol has the higher value of  $1.90 \times 10^{-2}$ , while the two tertiary alcohols studied, t-amyl and t-butyl, have values of  $2.43$  and  $2.38 \times 10^{-2}$ , respectively. Thus the primary, secondary, and tertiary alcohols are clearly distinguished. It is interesting to note that cyclohexyl alcohol, though formally a secondary one, seems to be intermediate between the ordinary primary and secondary alcohols in its steric hindrance to intermolecular association. This is to be expected, since the secondary carbon atoms here are tied back into the cyclohexane ring and so should not interfere with the hydroxyl association so readily. The study of the second harmonic of the hydroxyl stretch band might be of considerable value in studying steric hindrance in less well-known or predictable compounds.



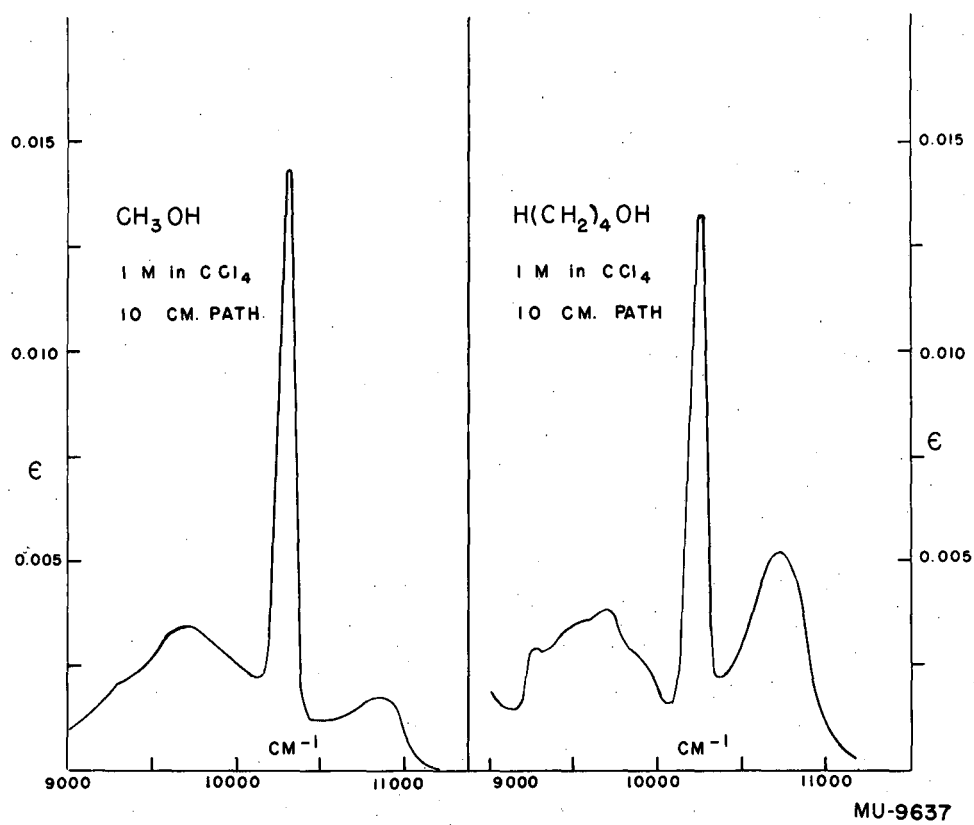


Fig. 37. Near-infrared spectra of alcohols diluted with  $\text{CCl}_4$ .

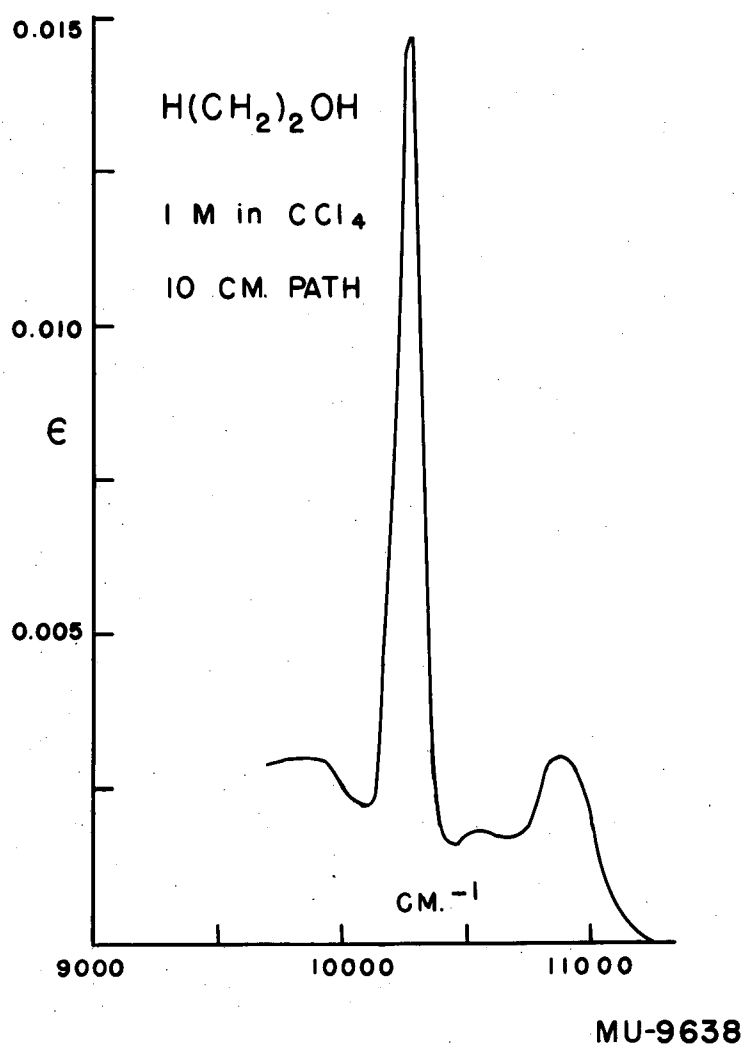


Fig. 38. Near-infrared spectrum of ethanol diluted with CCl<sub>4</sub>.

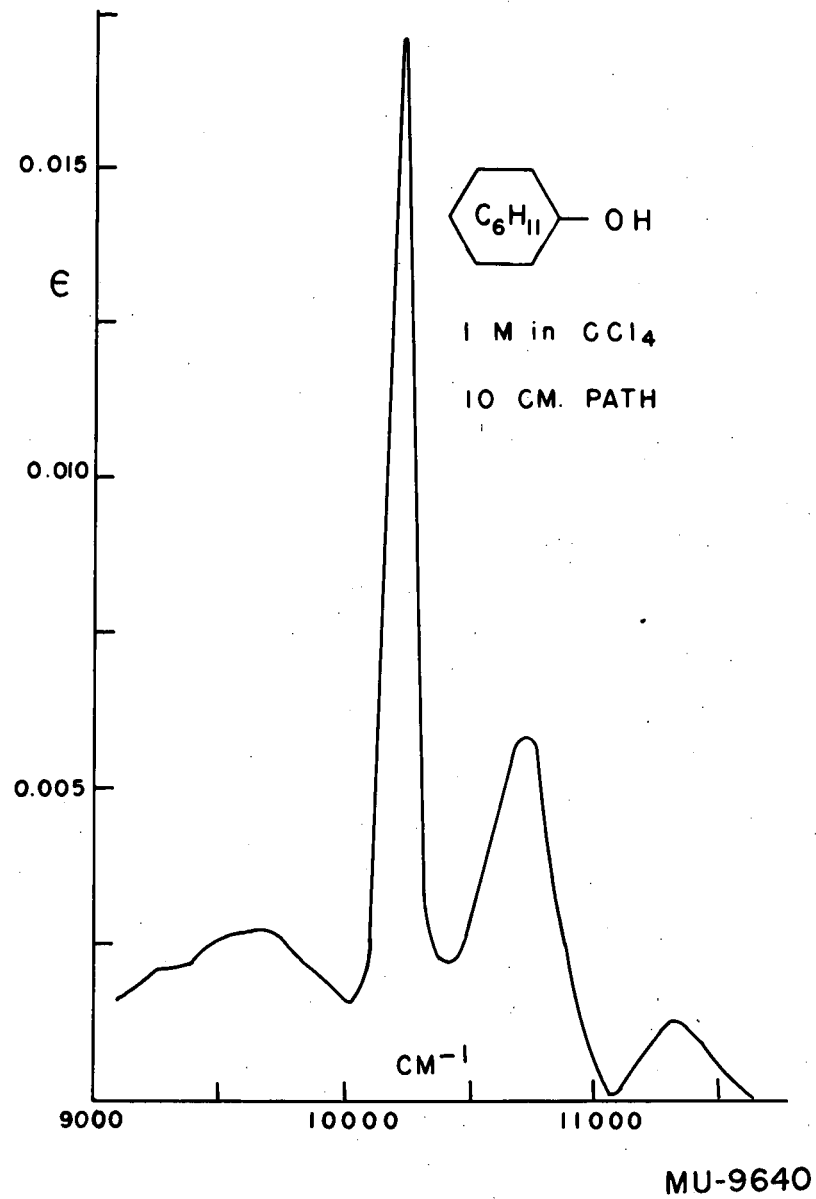


Fig. 39. Near-infrared spectrum of cyclohexanol diluted with  $\text{CCl}_4$ .

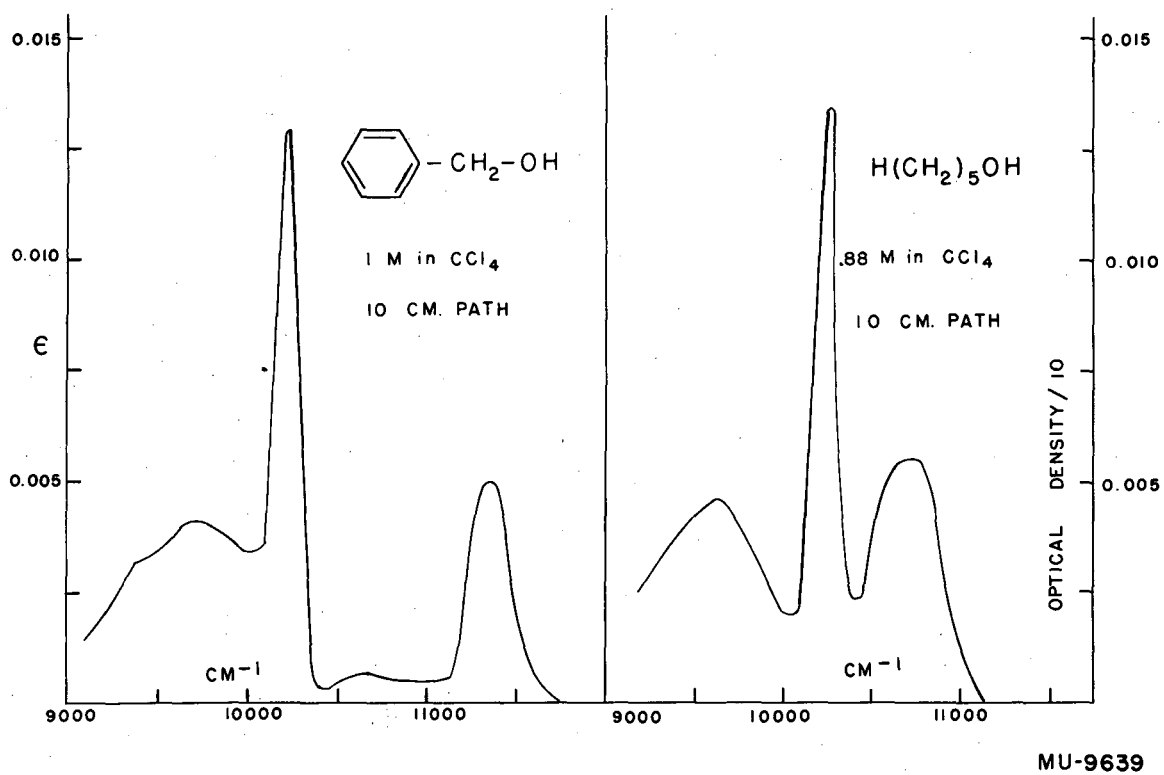


Fig. 40. Near-infrared spectra of two alcohols diluted with  $\text{CCl}_4$ .

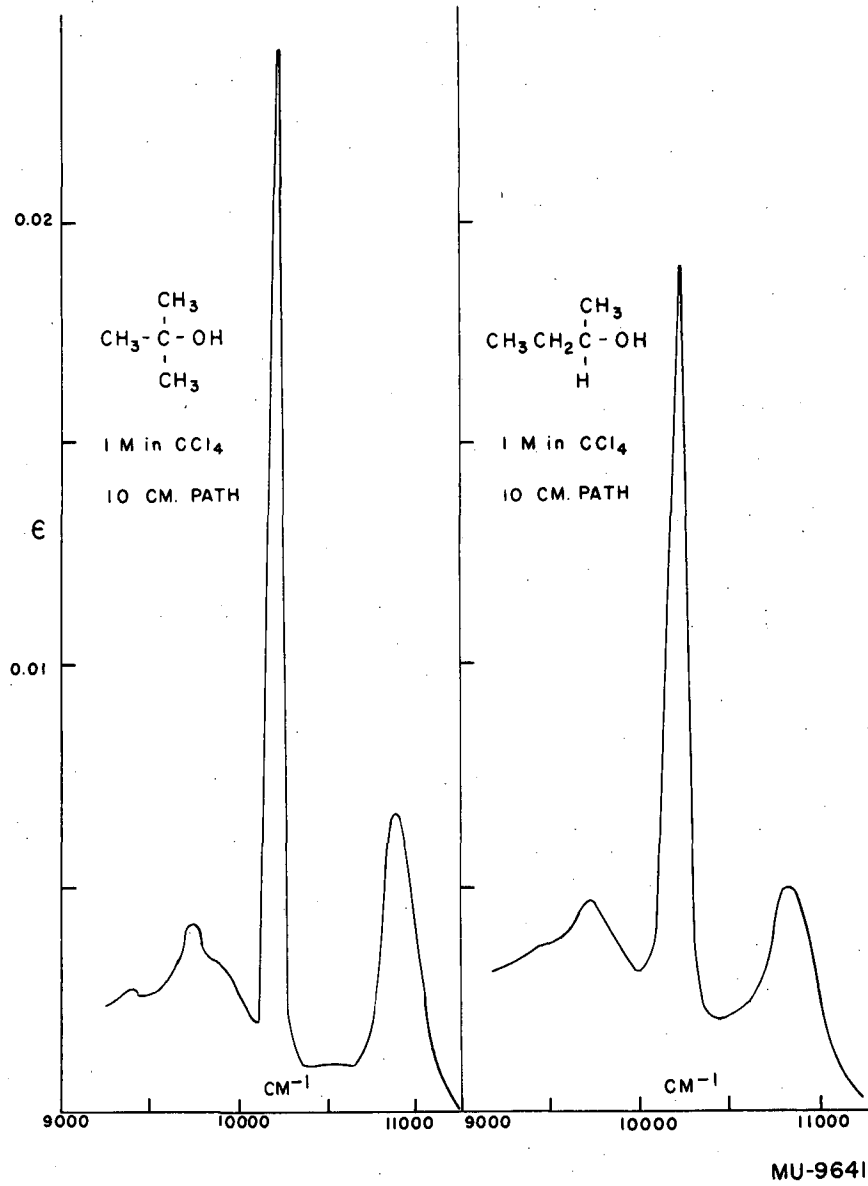


Fig. 41. Near-infrared spectra of two alcohols diluted with  $\text{CCl}_4$ .

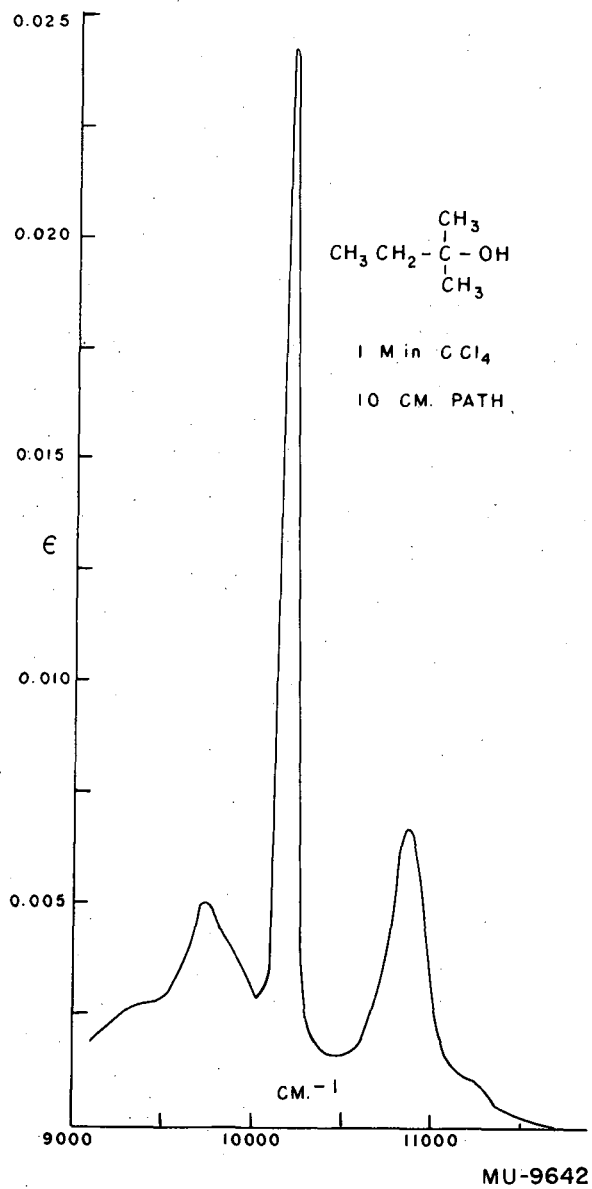


Fig. 42. Near-infrared spectrum of t-amylol diluted with CCl<sub>4</sub>.

Figures 43 and 44 present measurements of the pentanol spectrum, in the  $5000$  to  $9000\text{ cm}^{-1}$  range for two conditions, both with the same amount of alcohol in the light path: (1) a 1-molar solution in  $\text{CCl}_4$ , and (2) the pure alcohol. Figures 45 and 46 present the same measurements for t-amylol. Here the free hydroxyl stretch is seen as the first harmonic, at about  $7000\text{ cm}^{-1}$ . By examination of this band in all four figures, one can state that (1) hydroxyl association is much greater both in pure and in diluted condition for the primary than the tertiary alcohol, (2) both primary and tertiary alcohols show some free hydroxyl groups even in the pure liquid, (3) association of the hydroxyl groups is a steeper function of concentration for the primary than for the tertiary alcohol (on the basis of relative intensities the t-amylol in pure liquid phase has about six times as many free hydroxyl groups per unit volume as does the n-amylol, while at 1-molar the factor is down to about 1.5) (4) there seems to be a weak band at ca  $5200\text{ cm}^{-1}$  which has the same behavior as do the free -O-H bands--namely, higher intensity in the tertiary than in the primary alcohol and extinction coefficient which increases with dilution-- (5) there is broad absorption between  $6000$  and  $7000\text{ cm}^{-1}$  which is stronger for the primary than for the secondary alcohol and whose extinction value decreases upon dilution of the alcohol, and (6) absorption is very nearly independent of concentration in the regions  $5400$  to  $6000\text{ cm}^{-1}$  and  $8000$  to  $8500\text{ cm}^{-1}$ .

For observation (4) of the preceding paragraph we have no ready explanation. Very likely the band observed is a combination of free hydroxyl stretch with some other motion in the molecule. It is a weak band, just as one might expect for many of the combination bands. The other observations permit more certain explanations. The first and second of these require no comment. The third must certainly be the case, since both tertiary and primary alcohols approach the same degree of dissociation--none--in the limit of infinite dilution, but very different degrees of dissociation in the opposite limit--pure phase. (One cannot ascribe differences between the two alcohols in pure state to an actual difference in concentration since their densities are very nearly equal.) Observation (5) seems to indicate absorption due to hydrogen-bonded hydroxyl linkages, while the bands noted in observation (6) must be due to the hydrocarbon parts of the alcohols.

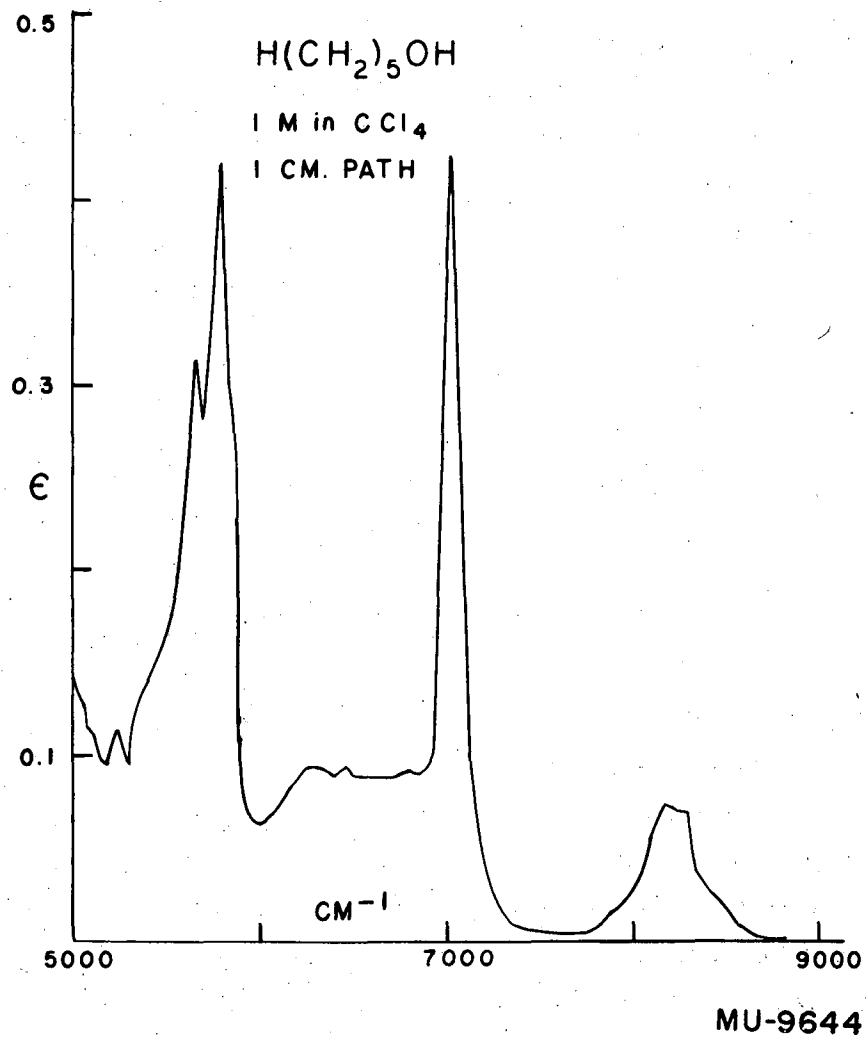


Fig. 43. Near-infrared spectrum of pentanol diluted with CCl<sub>4</sub>.



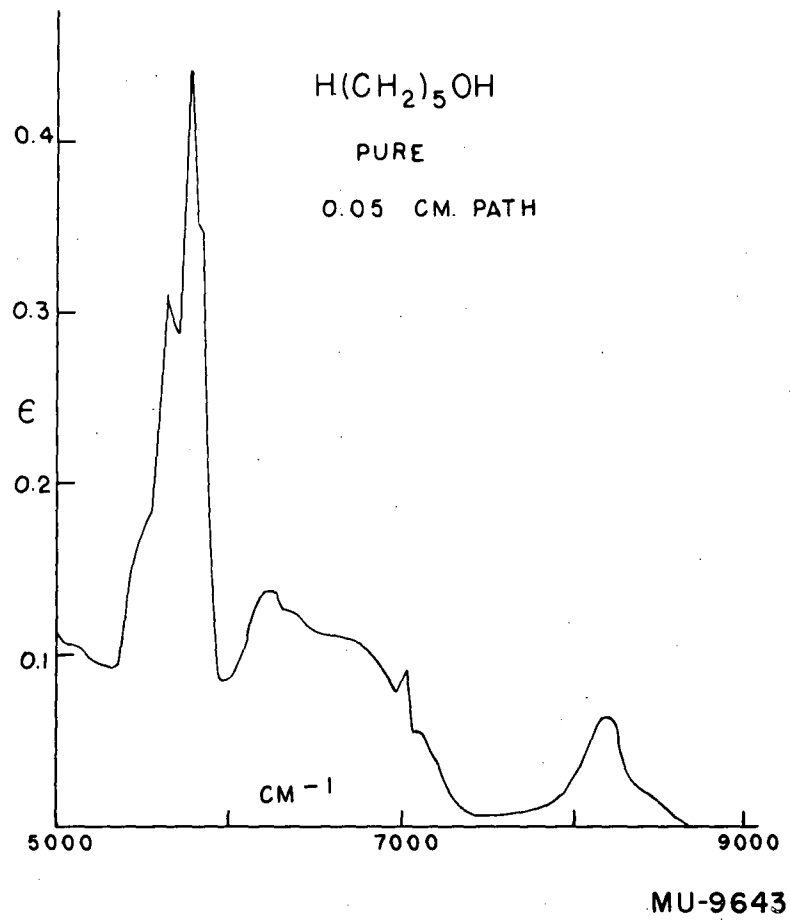


Fig. 44. Near-infrared spectrum of pure pentanol.

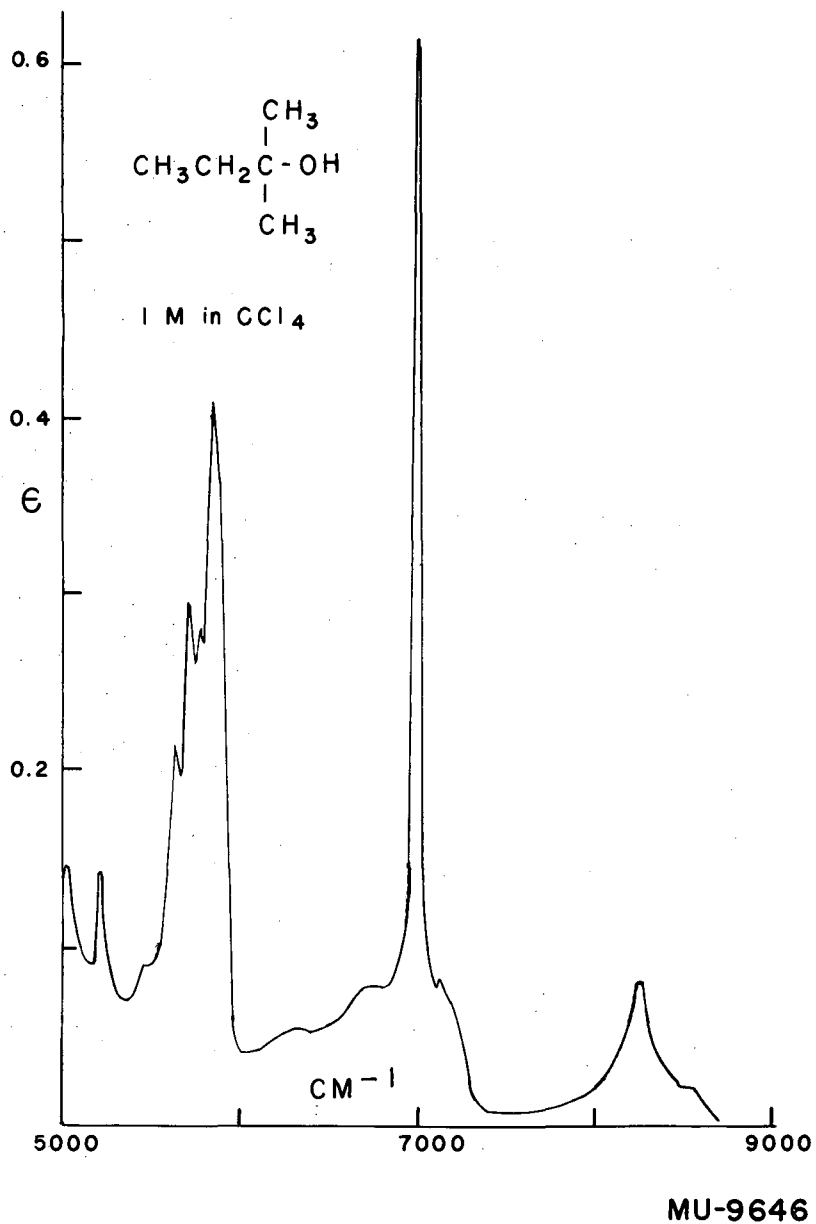


Fig. 45. Near-infrared spectrum of t-amylol diluted with CCl<sub>4</sub>.

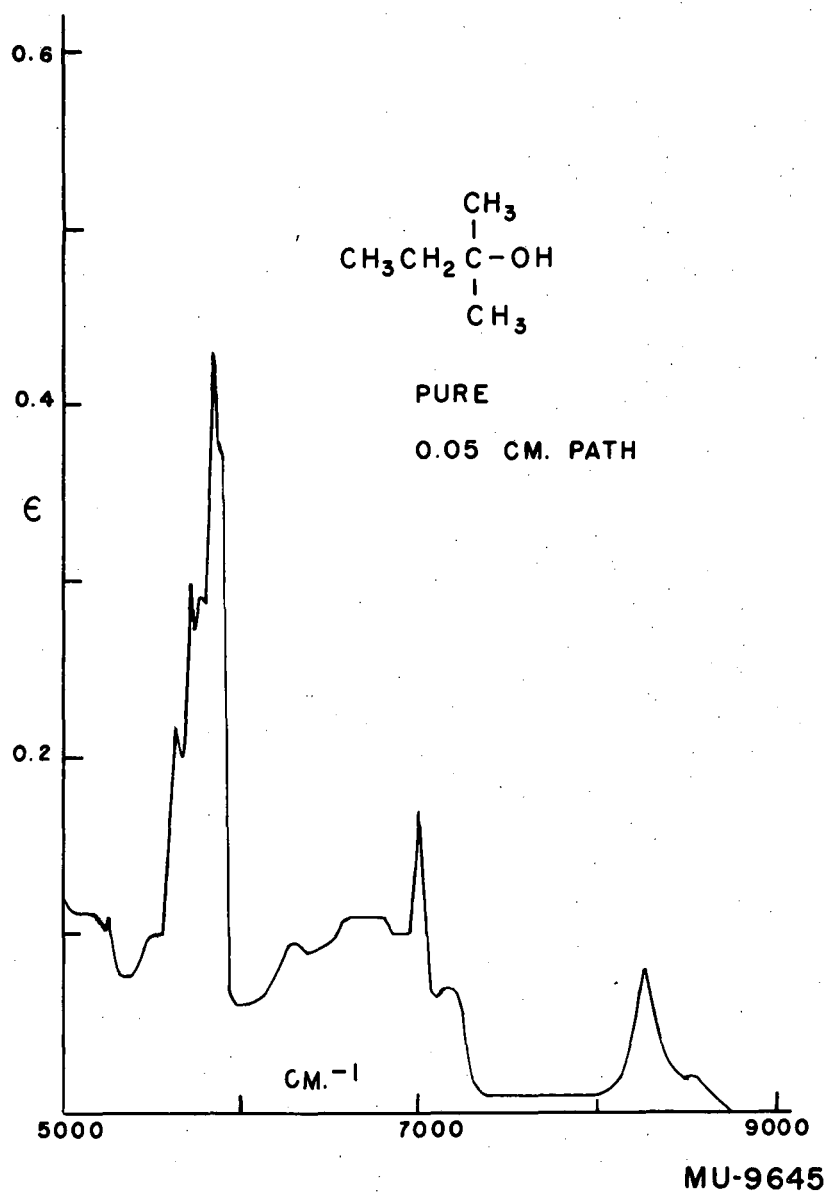


Fig. 46. Near-infrared spectrum of pure t-amylol.

Of the remaining figures, Figs. 47 to 54 show the near-infrared spectra in the range 6500 to 11,500  $\text{cm}^{-1}$  of a number of straight-chain aliphatic alcohols, while Figs. 55 and 56 give detailed views of these same spectra in the range 9000 to 12,500  $\text{cm}^{-1}$ . Certain features of these spectra are worth noting. First, one sees that the free hydroxyl band evident at 7000  $\text{cm}^{-1}$  increases in intensity with increasing hydrocarbon chain length even though the actual number of hydroxyl groups per unit volume decreases. This effect must be caused by the diluting effect of the hydrocarbon chain; obviously, an extremely long-chain alcohol even in the pure state will be a dilute hydrocarbon solution insofar as the hydroxyl groups are concerned. Second, the hydrocarbon frequencies about 8500  $\text{cm}^{-1}$  show interesting behavior. In ethanol, there are clearly two bands there, one at ca 8350 and the other about 8600, the first much less intense than the second. As more methylene groups are put into the hydrocarbon chain, the first band seems to increase in intensity; the second, to decrease. It appears that at a carbon chain length of four the two bands are of about equal intensity; at five the second band has become subsidiary to the first. Further along in the series (the six-carbon alcohol is unfortunately missing from our series) the second band can no longer be seen, while the first, still at 8400  $\text{cm}^{-1}$ , now increases in intensity quite regularly with increasing chain length. It seems likely that some of these two bands, the second is due to a special  $-\text{CH}_3$  frequency, which is inherently more intense than the other but which is very weak in the pure long-chain molecules simply because of the dilution effect, and that the first band is due to general  $-\text{CH}_2$  and C-C frequency, which becomes stronger as chain length is increased because the longer-chain alcohols have greater concentrations of those groups (in their pure liquid phases).

Finally, we shall describe a possible study for which the spectra presented in this section might serve as pilot material. We propose that one might measure attractive dispersion forces between long-chain hydrocarbons by utilizing the association-sensitive hydroxyl stretch bands in the near infrared. The experiments would be as follows: One would start with a series of long-chain alcohols,  $\text{H}(\text{CH}_2)_n\text{OH}$ . For each, one would also need the same alcohols with varying numbers of hydrogens replaced by bulky groups. For each straight-chain alcohol

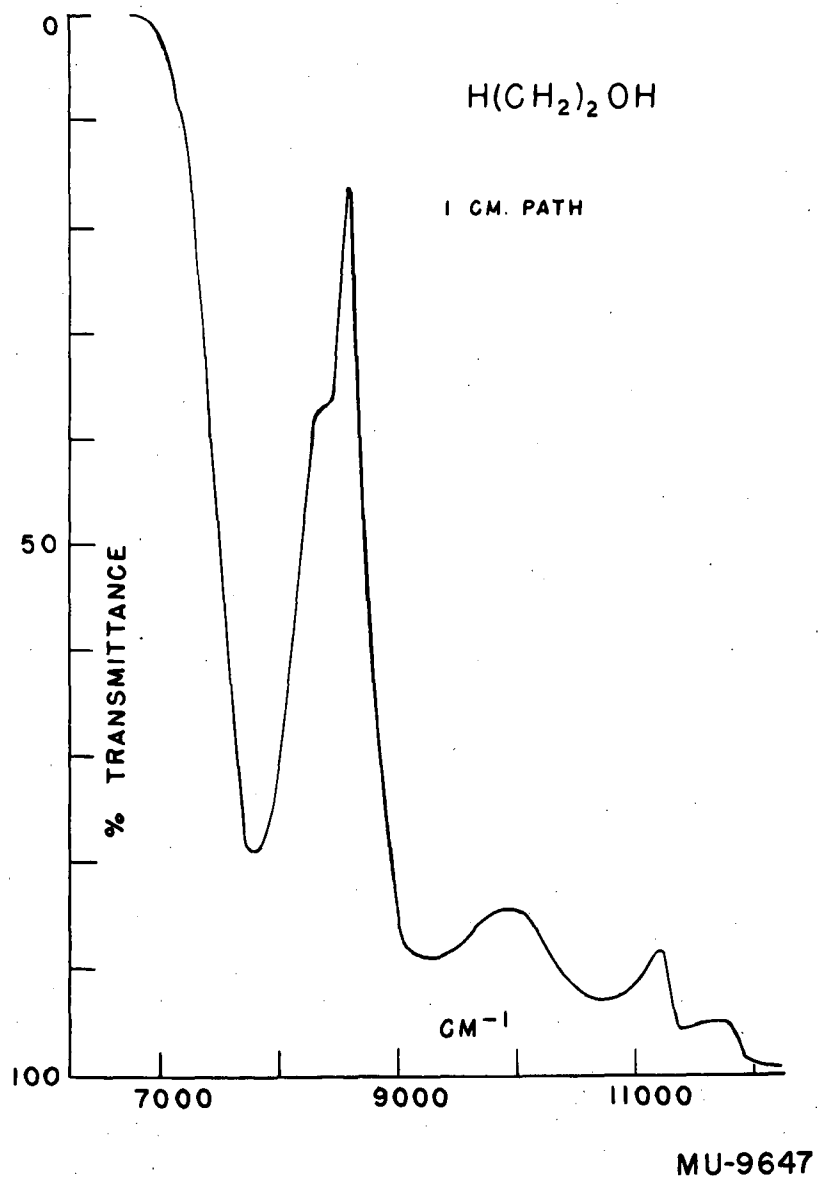


Fig. 47. Near-infrared spectrum of undiluted ethanol.

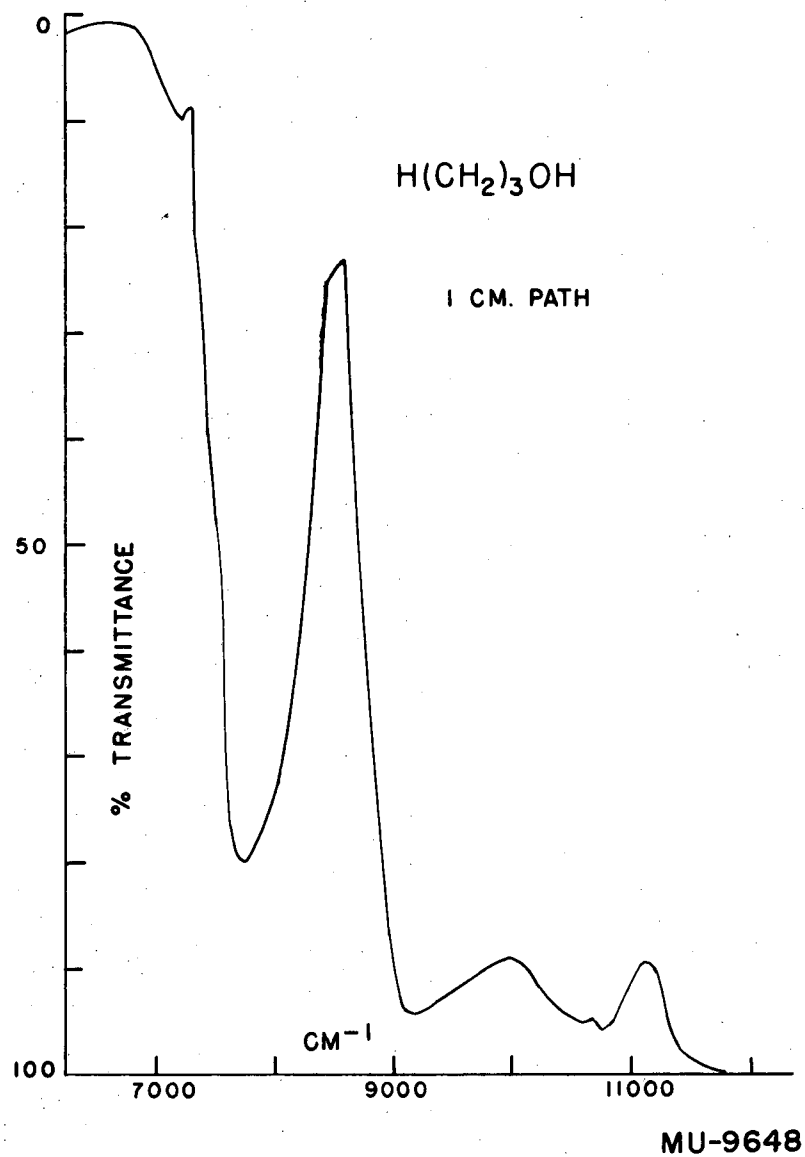


Fig. 48. Near-infrared spectrum of undiluted propanol.

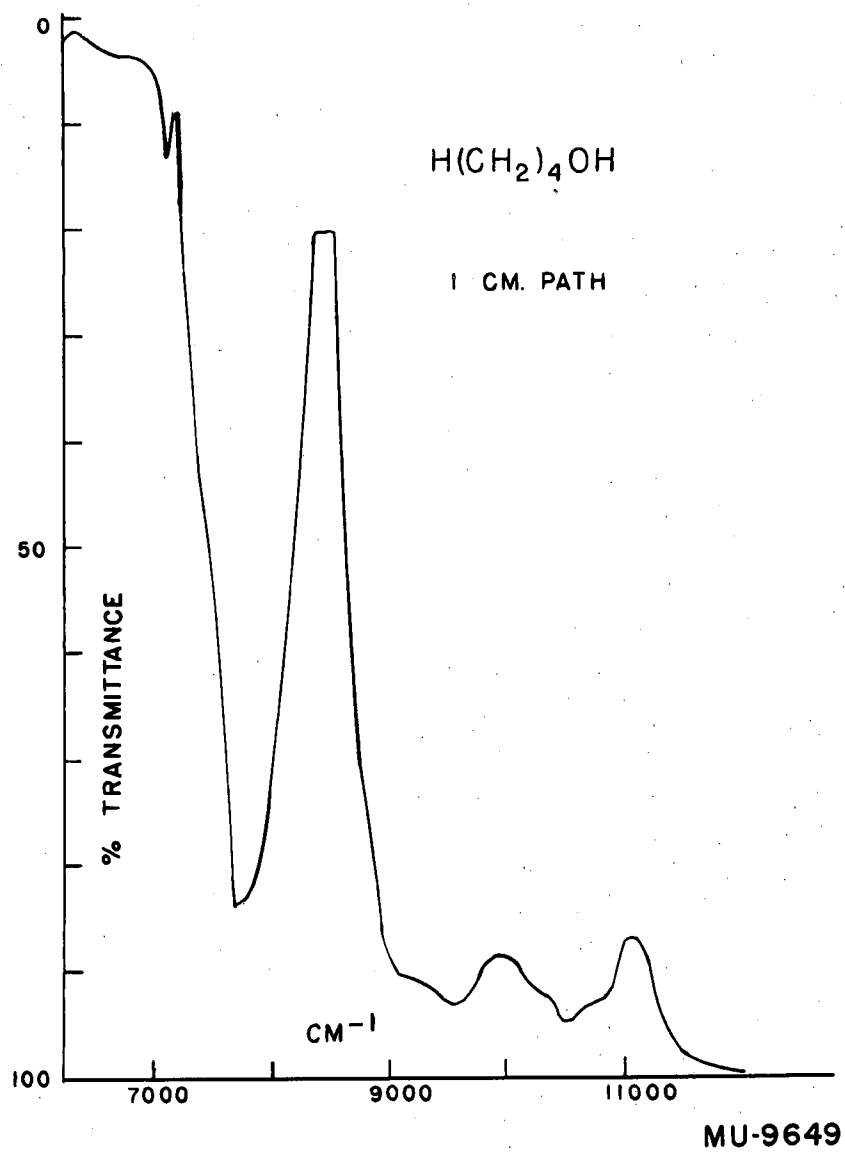


Fig. 49. Near-infrared spectrum of undiluted butanol.

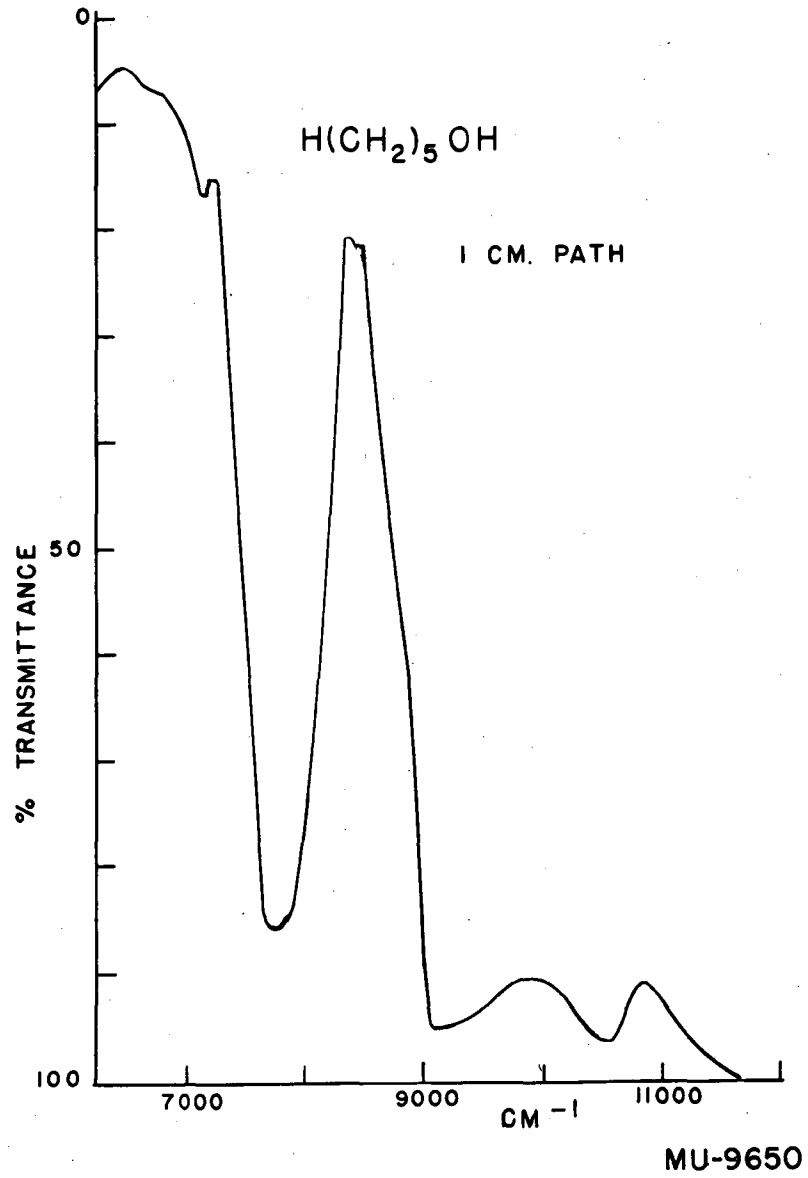


Fig. 50. Near-infrared spectrum of undiluted pentanol.



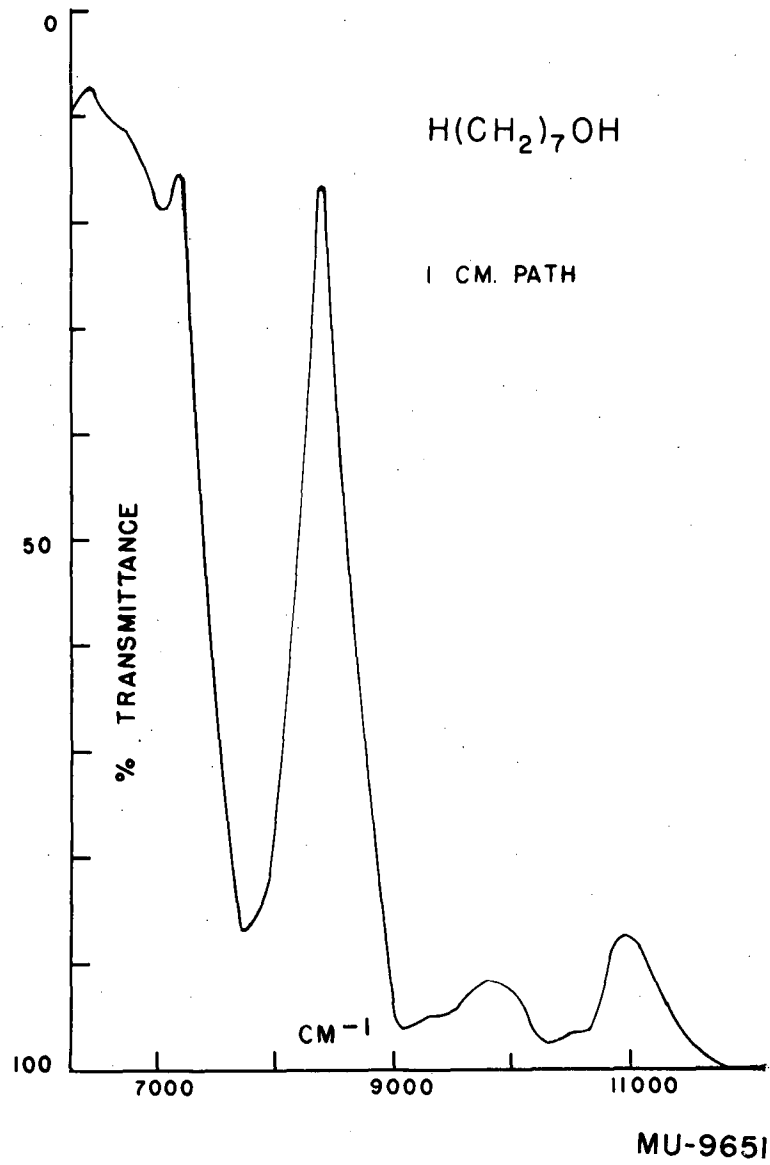


Fig. 51. Near-infrared spectrum of undiluted heptanol.

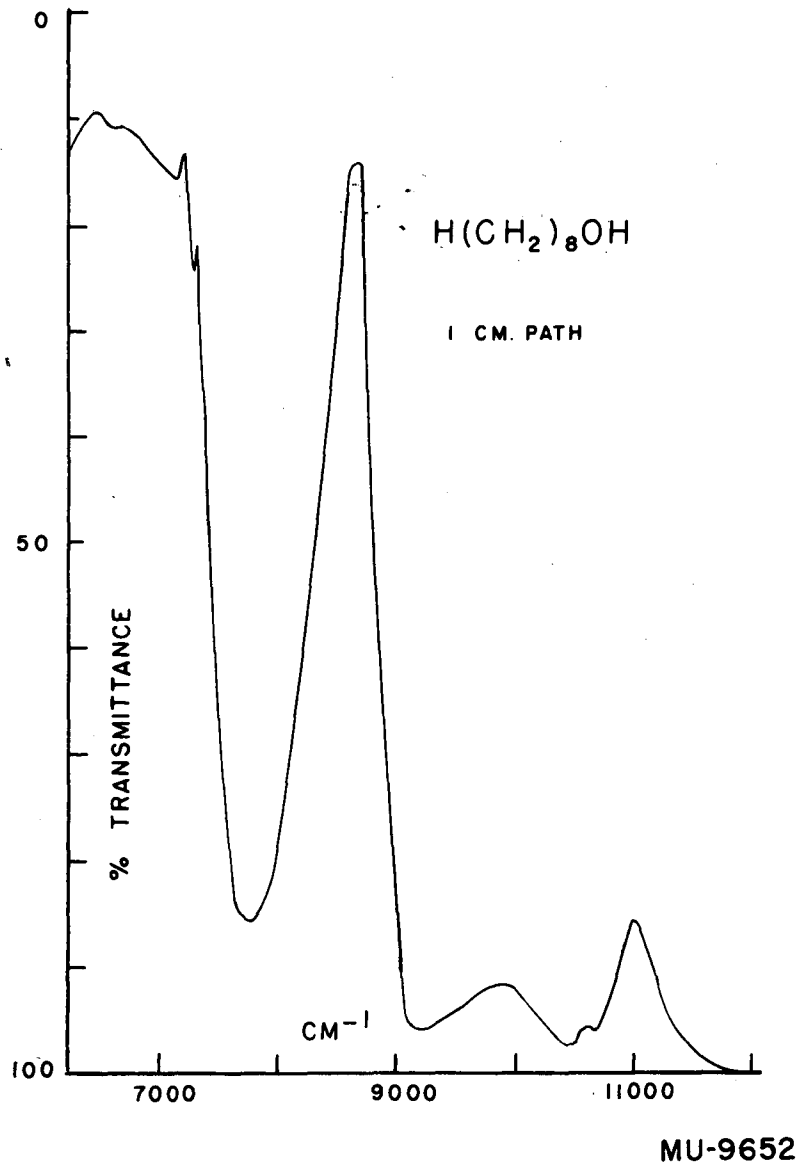


Fig. 52. Near-infrared spectrum of undiluted octanol.

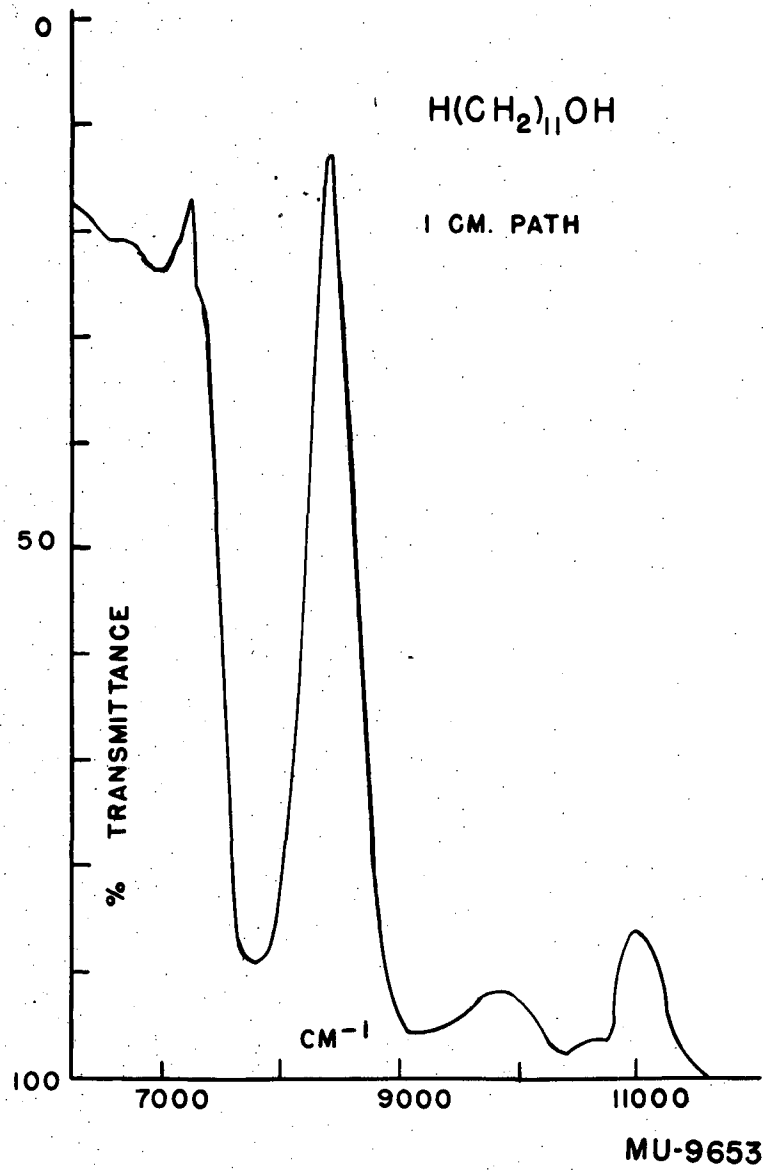


Fig. 53. Near-infrared spectrum of undiluted undecanol.

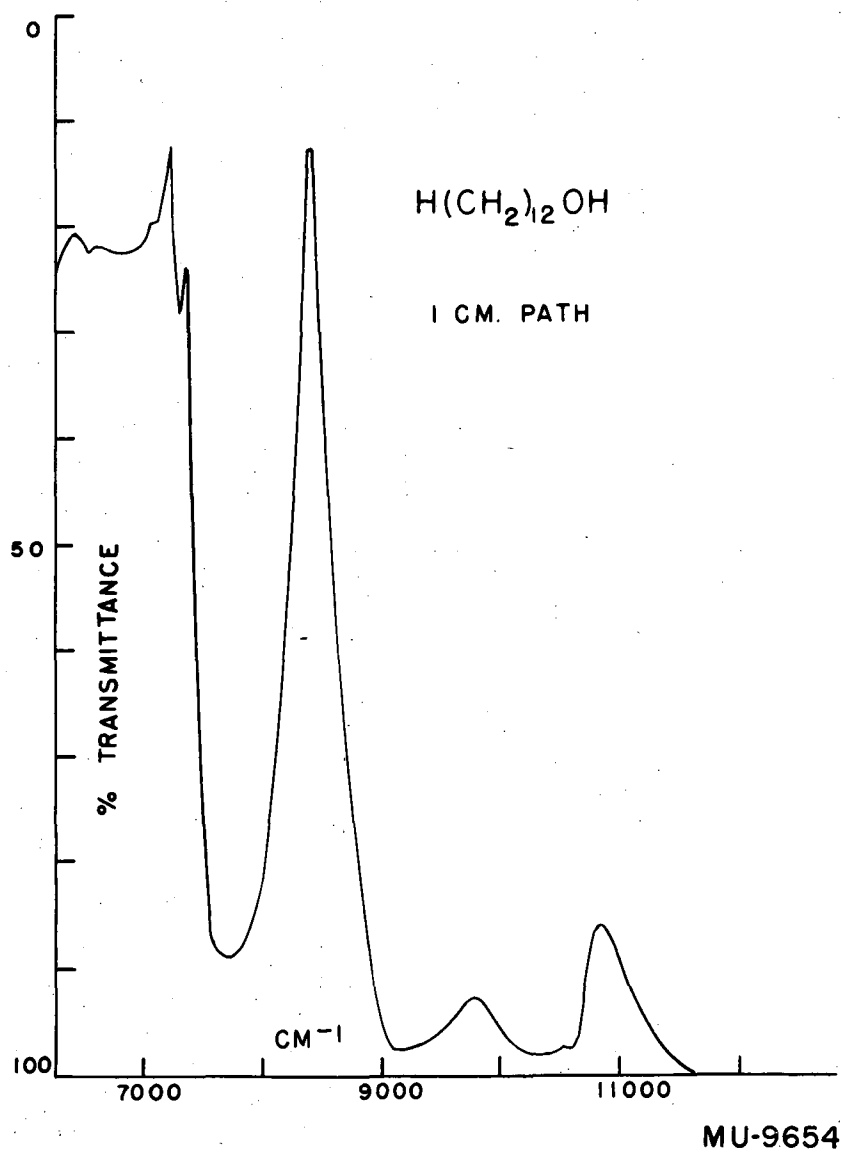


Fig. 54. Near-infrared spectrum of undiluted dodecanol.

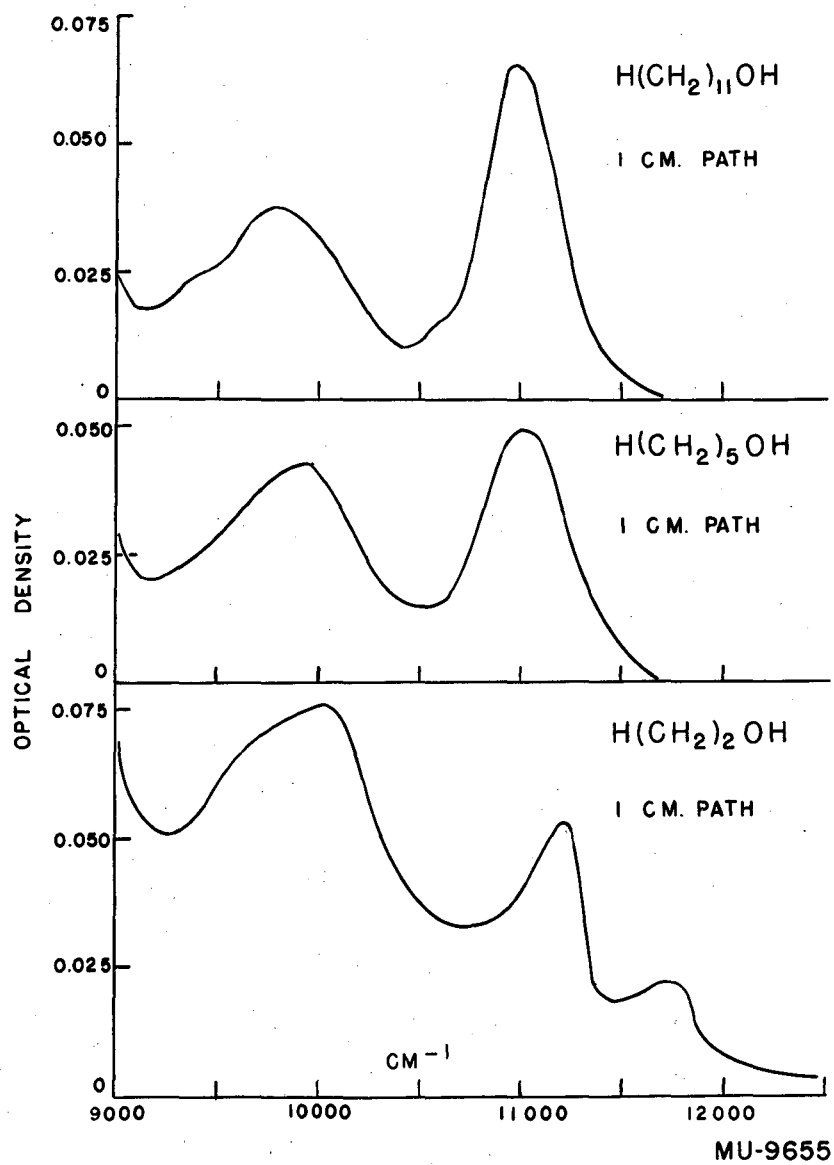


Fig. 55. Comparison of near-infrared spectra of three related alcohols.

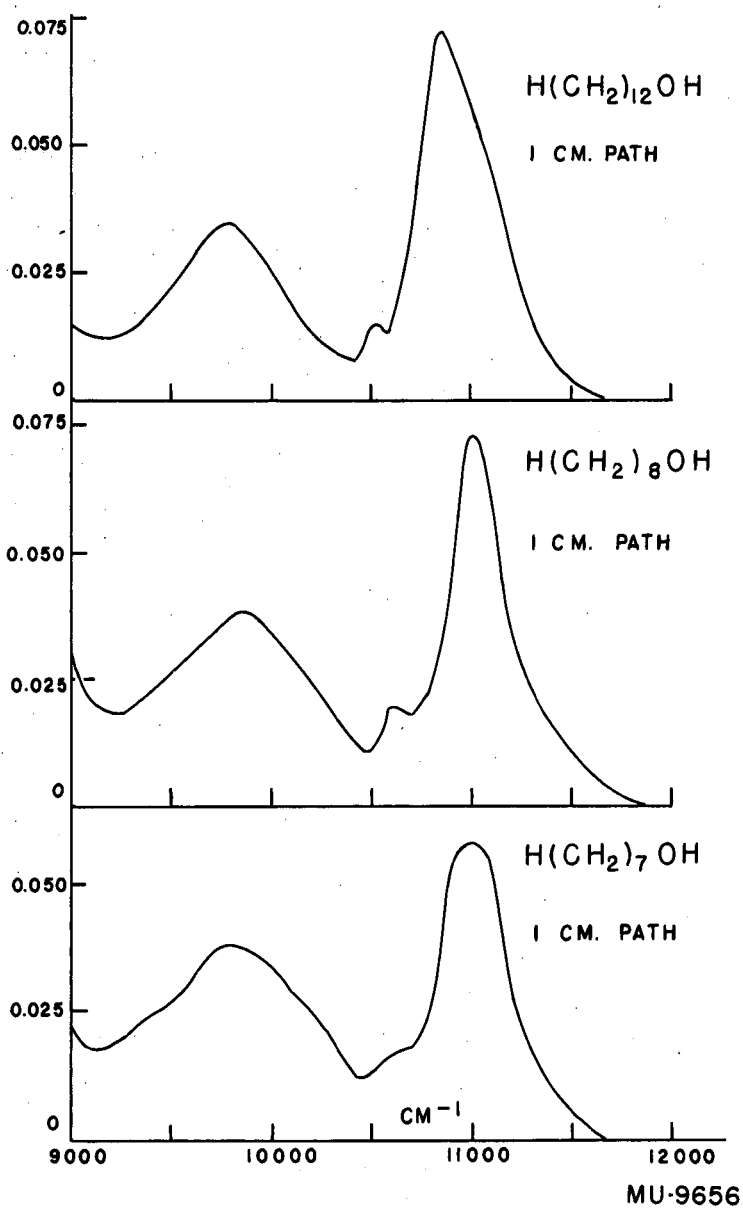


Fig. 56. Comparison of near-infrared spectra of three related alcohols.

and its bristly derivatives, the bimolecular association constant would have to be found by study of the intensities of the free -O-H bands for  $\text{CCl}_4$  solutions of varying concentration. If the dispersion forces were noticeably contributing to the association energy, for each  $n$  one would find smaller and smaller association constants as the molecule was made progressively more bristly. Some measure of interference,  $Q$ , with intermolecular attraction possibility due to dispersion forces could be defined for the bristly chains. Then one could plot, for each  $n$ ,  $\ln(K_{\text{straight}}/K_{\text{bristly}})$  vs  $(1/Q)$ ; extrapolation of this curve to zero should yield  $\ln(K_{\text{disp. + H-bond}}) - \ln(K_{\text{H-bond only}})$ . In this way one might be able to separate the attraction due to dispersion forces from that due to hydrogen-bonding energy alone. By making the measurements over a temperature range, one could then find the enthalpy and entropy of attraction between hydrocarbon chains. Further, by extrapolating the measurements to high  $n$ , one might remove the effects of the hydroxyl groups. The chief difficulty with the study, experimentally, would be the degree of precision to which the measurements of hydroxyl band intensities would have to be made and the necessity for separating out from those absorptions that part contributed by neighboring bands. It is possible that these difficulties could be really prohibitive; if not, then the proposed study should yield some useful information about dispersion forces between long hydrocarbon chains.

## ACKNOWLEDGMENT

It has been an inspiration to work under the expert guidance of Professor Melvin Calvin. I feel extremely fortunate to have been directed, in this era of intense specialization, by one whose outlook and interests are broad and whose emphasis in research is toward the solution of a problem by every possible means rather than upon the application of a technique to any available problem.

Some of the experimental work reported here was performed jointly by me and Prof. Arthur E. Martell of Clark University (Part I); some by Dr. Harry Weaver, of Varian Associates, and me (Part IV). To both of these I am indeed grateful.

Many useful discussions with various members of the Chemistry Department and of the Radiation Laboratory's Bio-Organic Group greatly aided this work. To all of them I extend my sincere thanks.

I thank the National Science Foundation for granting me fellowships during 1953-54 and 1954-55, during which time much of the work here described was carried out.

The assistance rendered by my wife, Geneva, has been immeasurable. Not only has she worked with me steadily in the preparation of this thesis, but she has also contributed much of value to the theoretical work reported in it. The Gaussian analyses of Part II are in large measure her doing; she has worked over with me most of the material presented in Parts II and III. My appreciation of all she has done is beyond expression.

This work was done in part under the auspices of the U. S. Atomic Energy Commission.



REFERENCES

1. A. Gillam and E. S. Stern, "An Introduction to Electronic Absorption Spectra in Organic Chemistry," Edward Arnold, London, 1954.
2. J. D. Park, H. A. Brown, and J. R. Lacher, *J. Am. Chem. Soc.* 75, 4753 (1953).
3. L. J. Bellamy and L. Beecher, *J. Chem. Soc.* 1954, 4487.
4. A. Combes, *Comp. rend.* 105, 868 (1887).
5. L. Claisen and E. Ehrhardt, *Ber. deut. chem. Ges.* 22, 1009 (1889).
6. H. Ley, *Ber. deut. chem. Ges.* 47, 2948 (1915).
7. A. Henne, M. Newman, L. Quill, and R. Staniforth, *J. Am. Chem. Soc.* 69, 1819 (1947).
8. J. Reid and M. Calvin, *J. Am. Chem. Soc.* 72, 2948 (1950).
9. M. Calvin and K. Wilson, *J. Am. Chem. Soc.* 67, 2005 (1945).
10. R. N. Haszeldine, W. K. Musgrave, F. Smith, and L. M. Turton, *J. Chem. Soc.* 1951, 609.
11. G. E. Utzinger, *Helv. Chim. Acta* 35, 1359 (1952).
12. R. Morton and W. Rasney, *J. Chem. Soc.* 1926, 707.
13. A. Henne, *J. Am. Chem. Soc.* 75, 991 (1953).
14. G. T. Morgan and H. W. Moss, *J. Chem. Soc.* 105, 189 (1914).
15. K. H. Meyer, *Ber. deut. chem. Ges.* 45, 2843 (1912).
16. H. E. Acly and H. S. French, *J. Am. Chem. Soc.* 49, 847 (1927).
17. O. Holmes, (Ph. D. Thesis), University of California, 1955.
18. L. E. Orgel, *J. Chem. Soc.* 1952, 4756.
19. J. Lecompte, *Discussions Faraday Soc.* 1950, No. 9, 125.
20. C. Duval, R. Freymann, and J. Lecompte, *Bull. Soc. Chim. France* 1952, 106.
21. C. J. Ballhausen, *Dan. Mat. Fys. Medd.* 29, No. 4 (1954).
22. J. Bjerrum, C. J. Ballhausen, and C. K. Jørgensen, *Acta Chem. Scand.* 8, 1275 (1954).
23. B. R. McGarvey, private discussions.
24. F. E. Ilse and H. Hartmann, *Z. Physik. Chem.* 197, 239 (1951).
25. F. E. Ilse and H. Hartmann, *Z. Naturforschg.* 6a, 751 (1951).
26. L. J. Bellamy and R. F. Branch, *J. Chem. Soc.* 1954, 4491.

27. H. Koyama, Y. Saito, and H. Kuroya, J. Inst. Polytechnics, Osaka City University C4, 43 (1953).
28. C. K. Jørgensen, Acta Chem. Scand. 8, 1495 (1954).
29. D. R. Hartree and W. Hartree, Proc. Roy. Soc. London 157, 490 (1936).
30. K. S. Pitzer, private discussion.
31. L. Pauling, "Nature of the Chemical Bond", Cornell University Press, Ithaca, New York, 1940.
32. A. E. Martell and M. Calvin, "Metal Chelate Compounds", Prentice-Hall, New York, 1952.
33. J. Owen, Proc. Roy. Soc. London 227A, 183 (1955).
34. C. A. Beevers and H. Lipson, Proc. Roy. Soc. London 146A, 570 (1934).
35. R. Connick, private discussions.
36. G. Seeley, Ph. D. Thesis, University of California, 1954.
37. B. R. McGarvey, in preparation for J. Phys. Chem. (1955).
38. A. Speiser, "Die Theorie der Gruppen", Dover, New York, 1943.
39. H. Margenau and G. M. Murphy, "The Mathematics of Physics and Chemistry", D. van Nostrand, New York, 1945, Chs. V-VI.
40. H. Eyring, J. Walter, and G. E. Kimball, "Quantum Chemistry", John Wiley and Sons, New York, 1944.
41. K. S. Pitzer, "Quantum Chemistry", Prentice-Hall, New York, 1953, especially Appendix 6.
42. Y. K. Syrkin and M. E. Dyatkina, "Structures of Molecules and the Chemical Bond", Interscience Publishers, New York, 1950 (translated from the Russian by M. A. Partridge and D. O. Jordan).
43. G. Herzberg, "Molecular Spectra and Molecular Structure II. Infrared and Raman Spectra of Polyatomic Molecules", D. van Nostrand, New York, 1945, Chs. I, II.
44. C. A. Coulson, "Valence", Clarendon Press, Oxford, 1952.
45. J. C. Slater, "Quantum Theory of Matter", McGraw-Hill, New York, 1951.
46. Landolt-Bornstein "Zahlenwerte", 6. Aufl., 1 Band 3. Teil pp. 367-8.
47. Ibid., 1. Teil p. 211.

48. W. H. Kleiner, *J. Chem. Phys.* 20, 1784 (1952).
49. R. L. Mooney, *Phys. Rev.* 55, 557 (1939).
50. H. H. Jaffe, *J. Chem. Phys.* 20, 279 (1952).
51. G. B. Bonino and M. Rolla, *Atti Accad. Nazl. Lincei, Classe Sci. Fis., Mat. e Nat.* 4, 25 (1948).
52. K. Fukui, T. Yonezawa, C. Nagaka and H. Shingu, *J. Chem. Phys.* 22, 1433 (1953).
53. J. G. M. Brenner and W. C. G. Brenner, *J. Chem. Soc.* 1950, 2335.
54. Landolt-Bornstein "Zahlenwerte", 6 Aufl., 1 Band, 2 Teil.
55. G. E. K. Branch and M. Calvin, "The Theory of Organic Chemistry", Prentice-Hall, New York, 1945, Chs. V, VI.
57. H. Bethe, *Ann. Phys.* [5], 3, 133 (1929).
58. B. Bleaney and K. W. H. Stevens, *Repts. Progr. Phys.* 16, 108 (1953).
59. P. A. M. Dirac, "Principles of Quantum Mechanics", Clarendon Press, Oxford, especially pp. 181-4, 149-66.
60. E. U. Condon and G. H. Shortley, "Theory of Atomic Spectra", University Press, Cambridge, 1953.
61. G. Herzberg, "Atomic Spectra and Atomic Structure", Dover, New York, 1944.
62. L. E. Godycki and R. E. Rundle, *Acta Cryst.* 6, 487 (1953).
63. R. E. Rundle, *J. Am. Chem. Soc.* 76, 3101 (1954).
64. S. Yamada, *Bull. Chem. Soc. Japan* 24, 125 (1951).
65. K. Shibata, A. A. Benson, and M. Calvin, *Biochim. et Biophys. Acta* 15, 461 (1954).
66. F. Fiegl, "Chemistry of the Specific, Selective and Sensitive Reactions", Academic Press, New York, 1949.
67. K. Sone, *J. Am. Chem. Soc.* 75, 5207 (1953).
68. M. Cohn and J. Townsend, *Nature* 173, 1090 (1954).
69. J. Kreuzer, *Z. Physik*, 118, 325 (1941).
70. R. Freymann, *Compt. rend.* 204, 41 (1937).
71. E. L. Kinsey and J. W. Ellis, *J. Chem. Phys.* 5, 399 (1937).
72. R. M. Badger and S. H. Bauer, *J. Chem. Phys.* 4, 749 (1936).
73. G. E. Pake and R. Sands, private discussions.